Quality Assessment and Control System for Armourstones

By the use of simple testing tools

J. Spoelstra

Technische Universiteit Delft

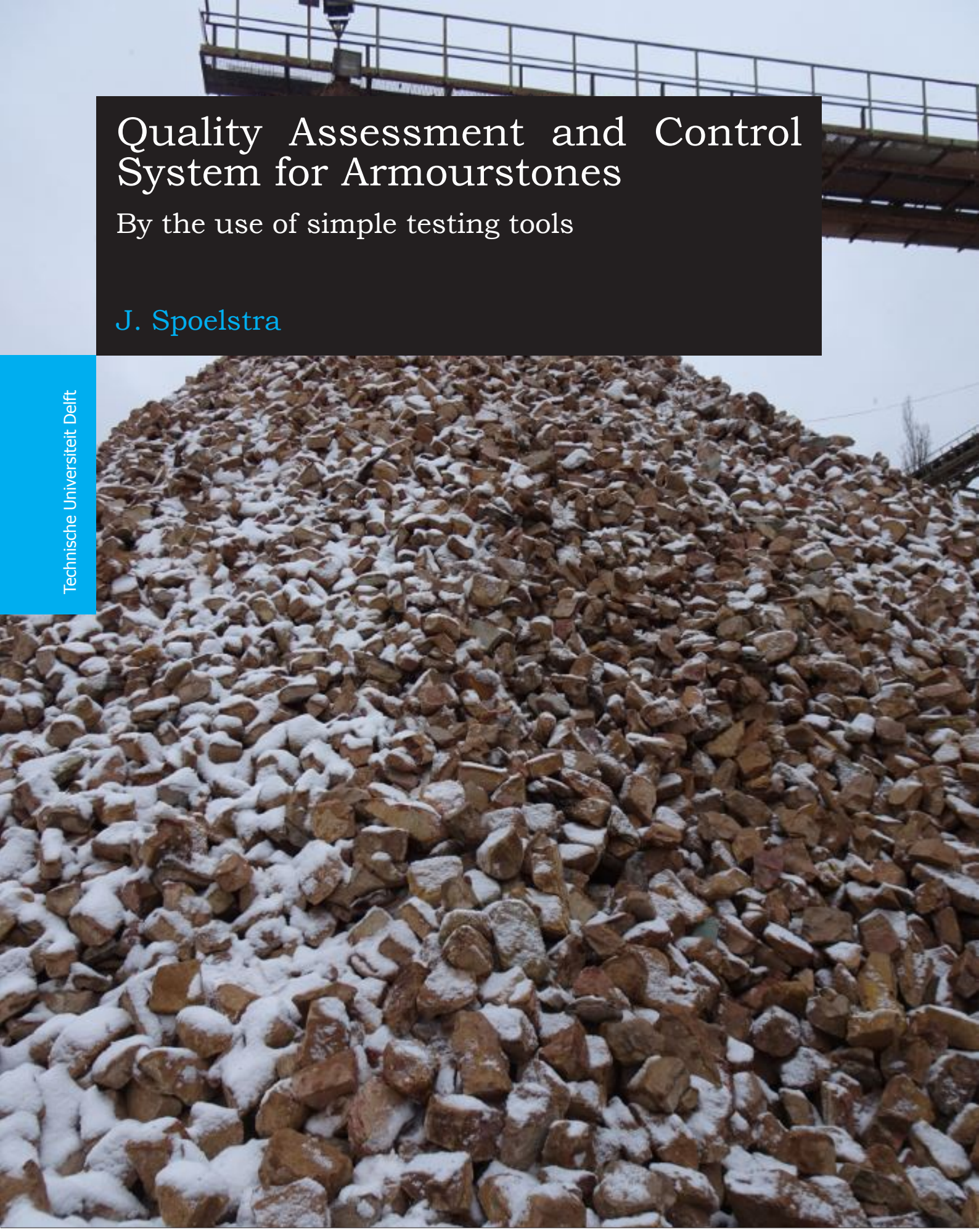

TU Delft Delft University of Technology

Challenge the future

Quality Assessment and Control System for Armourstones

By the use of simple testing tools

by

J. Spoelstra

in partial fulfillment of the requirements for the degree of

Master of Science
in Applied Earth Sciences

at the Delft University of Technology
To be defended publicly on January 29th, 2020 at 14:00

Student number: 4360109

Supervisor:	D. J. M. Ngan-Tillard	
Thesis committee:	A. A. M. Dieudonné,	TU Delft
	P. N. W. Verhoef,	TU Delft
	H. A. Abels,	TU Delft
	U. Wezenberg,	Boskalis

TU Delft Delft University of Technology

Preface

This report presents my MSc thesis research and provides insights and details about the contribution to the quality assessment and control system for armourstones. My interest into rock mechanics and engineering geology and the interest of Boskalis' Rock Department in armourstone durability issues observed during a few of their projects, provided the base of the research topic. This report is for anyone interested in new and existing methods to contribute to the quality assessment and quality control of armourstones.

I want to give a special thanks to Peter Verhoef, who has assisted me with his knowledge and skill in both academic and constructors perspective during my MSc thesis. Special thanks to Udo Wezenberg as well for his support, expertise in armourstones durability and assistance during the quarry visits. I would like to thank the remaining committee members Dominique Ngan-Tillard, Anne-Catherine Dieudonné and Hemmo Abels for their feedback, suggestions and help during this master thesis. Last but not least, thank you to my family and friends for supporting me throughout the past months working on this MSc thesis.

J. Spoelstra
Delft, January 2020

Abstract

Several waterway protection structures in the Netherlands dealt with rapid degrading armourstone after construction. This suggests that the current selection procedure of armourstones is not flawless to all degradation mechanisms, especially in dynamic environments. In this work armourstone is meant to include all rock that is used in river, coastal and offshore constructions, including rip rap and rock fill. Armourstones are in the Netherlands selected by their CE marking, which lists the description of the armourstone product and information on regulated characteristics. These characteristics are tested according to the European standard EN 13381-1&2:2002, which specifies the properties of aggregate acquired by processing natural materials for use as armourstone. This research is executed to provide a contribution in the quality control and assessment of armourstone and rock fill to ensure proper handling and installation in coastal and waterway protection structures.

The research started with a durability investigation according to the standard EN 133831&2:2002 on sampled sandstones and limestones that will be used in a submarin trench backfill, to check the regulated armourstone characteristics. Next, a petrographic analysis under the microscope was performed on methylene blue (MB) stained thin rock sections to investigate the presence of deleterious constituents and structures. This analysis was followed by extensive index testing to investigate the applicability of simple testing tools in a durability investigation. These tools include the Brazilian tensile strength (BTS) test, an indirect tensile strength test, the Equotip test, a surface hardness tester that records the surface rebound of an impact body, and the MB adsorption and staining test. MB is a dye that colours constituents with an excess in negative electric charges.

The tests according to EN 13383-1&2:2002 suggested that the sampled armourstone bulk satisfies the required durability parameters and no evidence was found that indicates rapid degradation during the engineering lifetime. Nevertheless, variability in the armourstone pieces was spotted and some individual rock pieces approached or exceeded minimum durability requirements.

The BTS test revealed considerable variation in tensile strength, a key parameter to assess degradation, between armourstone blocks and within a single block when a similar orientation of the bedding was maintained. Moreover, the orientation of the bedding in the sandstone had large influence on the tensile strength, where the values obtained perpendicular on the bedding were twice as high than parallel to the bedding.

Single impact method (SIM) Equotip measurements on rough, untreated aggregate surfaces were consistent. The rebounds correlated to visual features like grain size, cracks, surface roughness and degree of weathering within handheld specimens. Equotip measurements on the rock cores and sawn surfaces obtained higher mean rebound values and smaller standard deviations. The mean and standard deviation are considered most suitable to be used in a durability investigation. The repeated impact method (RIM) by the Equotip was not successful to indicate the degree of weathering of single hand specimens. The mean Equotip values on the aggregate correlated well to the water absorption when divided into proper density and size classes. The mean rebounds on the cores distinguished well between weathered and intact cores when saturated, and correlate well to the unconfined compressive strength (UCS) values. Furthermore, the Equotip mean rebound value related to the BTS value when performed on isotropic rock disks.

The MB adsorption test and MB staining of the thin sections indicated the presence of localised spots and laminae rich in clay or organic matter. The staining of sawn aggregate surfaces agreed with some of the deleterious structures in the thin sections, yet was not consistent throughout the tested rock pieces and varied between the dark coloured limestone and light coloured sandstone.

The Equotip test, BTS test and MB adsorption test are quick, easy and cheap methods to obtain more understanding in variability and rock behaviour which are not necessarily captured by the standard laboratory tests according to EN 13383-1&2:2002. The simple index tests should always be accompanied by the standard laboratory tests to provide a proper reference and understanding. Detailed mechanical durability tests, like the slaking test or wet-dry cyclic tests, should be performed when the durability assessment indicates a high amount of deleterious minerals and structures, to identify the amount of degradation caused by swelling behaviour of these minerals.

Contents

1 Introduction **1**
1.1 General Overview . . . 1
1.2 Aim of the Research . . . 2
1.3 Research Methodology . . . 3
1.4 Thesis Outline . . . 4

2 Literature Review **5**
2.1 Durability Assessment within The Netherlands . . . 5
2.2 Weathering Processes in a Marine Environment . . . 6
2.2.1 Abrasion . . . 6
2.2.2 Salt Crystallisation . . . 8
2.2.3 Swelling Clay Minerals . . . 8
2.3 Degradation model . . . 11
2.4 Petrographic Evaluation . . . 14
2.5 Equotip . . . 14
2.5.1 Rebound value and UCS . . . 14
2.5.2 Detection of Weathering by Equotip . . . 17
2.5.3 Surface Roughness . . . 18
2.5.4 Data Evaluation . . . 19
2.6 Rock Strength . . . 19
2.6.1 Unconfined Compressive Strength . . . 19
2.6.2 Tensile Strength . . . 22
2.7 Conclusion . . . 23

3 Durability Assessment **25**

4 Sample Acquisition **29**
4.1 Geological Setting of Quarries . . . 29
4.2 Sample Description . . . 33
4.3 Grading . . . 34
4.4 Summary . . . 42

5 Petrographic Analysis **43**
5.1 When should a Petrographic Analysis be Performed . . . 43
5.2 Soundness Analysis . . . 44
5.3 Discussion & Conclusion . . . 47

6 Micro-Deval **49**
6.1 Micro-Deval Test . . . 49
6.1.1 Test Method . . . 49
6.1.2 Results and Discussion . . . 49
6.2 Micro-Deval Method . . . 51
6.2.1 Method . . . 51
6.2.2 Results and Discussion . . . 53
6.3 Conclusion . . . 54

7 Rock Density and Water Absorption **55**
7.1 Determination of Density and Water Absorption . . . 55
7.2 Results of Density and WA Measurement . . . 55
7.2.1 Aggregate . . . 55
7.2.2 Rock Cores . . . 56

7.3 Correlation Density and Water Absorption . . . 56
7.4 Discussion . . . 59
7.5 Conclusion . . . 59

8 Armourstone Strength **61**
8.1 UCS test . . . 61
8.1.1 Core Description . . . 62
8.1.2 Failure Mode . . . 63
8.1.3 Influence of Bedding Orientation on UCS . . . 66
8.2 Brazilian Tensile Strength . . . 71
8.2.1 Test Method . . . 71
8.2.2 Results and Discussion . . . 72
8.3 Conclusion . . . 74

9 Equotip **77**
9.1 Test Method . . . 77
9.2 Statistic Analysis of SIM Measurements . . . 78
9.2.1 Aggregate Samples . . . 78
9.2.2 Core Samples . . . 89
9.3 Correctness of Equotip Measurements . . . 90
9.4 RIM Measurement . . . 92
9.5 Relation between L-value and Water Absorption . . . 97
9.6 Equotip and UCS . . . 100
9.7 Acoustic Velocity and Equotip . . . 103
9.8 Equotip and BTS . . . 103
9.9 Discussion and Conclusion . . . 105

10 Methylene Blue **109**
10.1 Methylene Blue Adsorption . . . 109
10.1.1 Test Method . . . 109
10.1.2 Results and Discussion . . . 110
10.2 Methylene Blue Staining . . . 111
10.2.1 Test Method . . . 113
10.2.2 Results and Discussion . . . 113
10.3 Determination of Clay Mineral . . . 118
10.4 Discussion . . . 119
10.5 Conclusion . . . 120

11 Discussion **121**

12 Conclusion **125**

13 Recommendations **129**

Bibliography **131**

A Petrographic Analysis **137**
A.1 Sandstone . . . 137
A.2 Limestone . . . 150

B MCWI and Parameters for MDE Method **165**

C Density and WA **167**

D Magnesium Sulfate Soundness **169**

E Photos of Intact and Crushed Rock Cores **171**

F Strength Test Results **179**

G Relation UCS and L-value **183**

H Equotip Data Histograms **187**

I Equotip T-test Results **201**

J Relation L-value and WA **207**

K Equotip Core Data **215**

L Photos of Aggregate Pieces **219**

1

Introduction

1.1. General Overview

Armourstones are rocks used in coastal and waterway structures. For example, armourstones are used in breakwaters for the protection of coastal regions or in the cover protection of offshore cables. Such man-made structures are designed with an engineering lifetime, which is the time the structure should perform its function within the specified parameters of the design. Consequently, the armourstones used in the structure should retain their desirable properties over the engineering life. The ability to hold these properties is known as durability. A poor durability of armourstones results in premature degradation, and the designed construction risks losing its engineering function. Degradation is the rock weathering during the time span from construction time until the end of the engineering lifetime of the structure. When the degradation of armourstone is noticed in early stages, repair works can be executed, which can be expensive as large rock masses can be involved. If the degradation remain unnoticed, the construction may loose its engineering function. Accordingly, a proper durability assessment is beneficial for preventing structural failure and reducing the amount of repair works by selecting durable rocks.

Armourstones are purchased by contractors from stone suppliers. The suppliers collect the stones at several quarries to satisfy the demand, which can be in-house or third parties. The armourstones are accepted by the contractor based on the Conformité Européenne (CE) marking. The CE marking is required for rocks to be sold as armourstones according to the European guidelines and lists the description of the armourstone product and information on regulated characteristics. These rock characteristics are tested according to the European standard EN 13383-1&2:2002 (EN 13383-1, 2002; EN 13383-2, 2002). The first part of this standard contains the armourstone specifications and the second part lists the test methods. The standard specifies the properties of aggregate obtained by processing natural, manufactured or recycled materials, and mixtures of these materials, for use as armourstone. The thrust on the CE mark is high within the Netherlands and rocks are purchased when the armourstone characteristics listed on the CE marking satisfy the engineering parameters.

Several projects within the Netherlands experienced rapid armourstone degradation within a few years after construction, despite the CE marking claiming durable rock characteristics of the armourstones. This suggests that the current armourstone selection procedure in the Netherlands has a few drawbacks and shortcomings regarding the durability of armourstone. Boskalis, a leading global dredging and offshore contractor and maritime services provider, experienced problems with armourstones at the Wilhelmina channel in Tilburg, the Netherlands. Armourstones close to the waterline degraded rapidly after construction and replacement works were required. Daan Heineke from the Dutch ministry of infrastructure and water management highlighted during a conference in Aberdeen multiple projects with rapid degradation of armourstones in the Netherlands. Details about most of these projects and degradation of the armourstones are not known as the projects belong to various contractors. An investigation of Verhoef and Wezenberg (2018) reviewed the durability of armourstone and the purchase procedure of armourstone from Boskalis Nederland. They concluded that the contractor has very limited knowledge about the origin of the armourstones due to the purchase system via stone suppliers and that purchased products may contain rocks with a low

durability. Important features like variability in rock quality and the processing method of the armourstone are not captured within a CE marking and therefore not known by the contractors. The armourstones are directly placed in the construction from the quarry without extra quality checks, due to the high thrust in the CE marking.

There are several disadvantages to only use the CE marking with standard test results. Firstly, armourstones are natural products, therefore contain variability within their properties. Due to the relative small sample sizes used for the testing procedures (EN 13383-1, 2002), there is little knowledge about the variability within a quarry with respect to certain rock properties. The rocks tested for the CE are selected by the quarry themselves and may not be representative for all production faces. There may be a variation in rock type and/or variation within a rock type. Secondly, some of the standard test procedures used in EN 13383-1&2:2002 can be adapted to be more representative for the in-situ conditions. Finally, some rock parameters are completely disregarded by the European standard that may considerably influence the armourstone durability as reported by CIRIA/CUR/CETMEF (2007). Chapter 3 of the Rock Manual (CIRIA/CUR/CETMEF, 2007) provides an elaborate presentation on the guidance in selecting armourstone material properties for the use in the design of waterway and coastal protection structures. Section 3.2 to 3.11 of the manual target quarried rock, the type of material investigated during this research.

Thus, the current procedure for the acquisition and handling of armourstones is not a sound procedure for all constructions. Unnoticed degradation mechanisms in combination with a dynamic environment have already resulted in rapid degradation of armourstones.

1.2. Aim of the Research

The current durability assessment is not sound to all degradation mechanisms for every construction environment, resulting in premature degradation of armourstones. Goal of the thesis research will therefore be: to contribute to the design of a quality assessment and quality control system for armourstone rock that ensures a workable and sound procedure for the acquisition and proper handling and placement in coastal and waterway protection structures.

The thesis is performed in co-operation with Boskalis. For their project 'Borssele Export Cables' a submarine rock backfill is required. Two gradings, 5-40kg and 32-56mm, are obtained from quarries in Germany and Belgium and will be used to create an armour and filter layer respectively. Initial descriptions of the rock types (presence of shales and greywacke) and the environment of the project (intertidal zone) are ringing the alarm bells with respect to potential durability issues. The armourstone durability will be investigated for this project.

The beforementioned issues/cases show the necessity of the study described in this thesis, of which the research question calls;
Can simple index test successfully contribute to the design of a quality assessment and quality control system for armourstone rock that ensures a workable and sound procedure for the acquisition and proper handling and placement in coastal and waterway protection structures?

The focus lies on simple testing tools, since these can be performed quickly without major additional costs next to the durability assessment according to EN 13383-1&2:2002. The simple testing tools include the Brazilian tensile strength (BTS) test, Equotip test, methylene blue (MB) adsorption test, and MB staining. The BTS test is an indirect tensile strength test which breaks small rock disk with a compressive force (ISRM, 1978). The BTS test device used during this research has a hydraulic hand pump to create the compressive force on the rock disk.

The Equotip is a small device that shoots an impact body with a tungsten carbide tip towards a rebound surface. The Equotip can be used on rock surfaces (Meulenkamp and Grima, 1999; Verwaal and Mulder, 1993), although originally designed to be a hardness tester for metal surfaces. The tip rebounds after impact, which is measured by the device and translated into a rebound value known as the L-value. There are various Equotip tip types. The Equotip type C and D are used during this research, which differ in impact force. The type C tip has an impact of 3 newton millimetre (Nmm) and the type D tip has an impact of 11 Nmm.

The methylene blue adsorption test is used to indicate the presence of clay minerals and organic content in crushed rock material. Methylene blue is a dye that stains clay and organic particles by a chemical reaction due to an excess in negative electric charges in these clay and organic particles

(Chiappone et al., 2004). During the adsorption test a titration with MB solution is performed on an aggregate mixture diluted in distilled water, until the chemical reaction (cation exchange) is completed. The end of the chemical reaction is indicated by a blue halo when a spot of the test solution is dropped on filter paper.

The MB staining is performed on thin sections of 30 µm thick and on sawn surfaces. The staining will highlight the deleterious constituents and reveal possible concentrated structures of these constituents (Voskuilen and Verhoef, 2003).

During this MSc thesis research several sub-questions will be investigated regarding the simple testing tools. They are listed below with an explanation of interest.

- Can reliable Equotip measurements be taken on irregular, untreated, small aggregate samples?
  Equotip measurements on the untreated aggregate surface include the weathered outer surface of the rocks, which is missed by measurements on rock cores and/or sawn surfaces. The Equotip rebound values on the untreated surface could relate to the degree of weathering, which is an important factor in a durability assessment.
- Are previous correlations between Equotip and unconfined compressive strength (UCS) valid for saturated samples?
  The UCS is determined according to EN 1926 (1999). This standard prescribes that the cores should be saturated during testing. Previous correlations between the mean Equotip rebound value and UCS value were determined on dry cores. These correlations can be used to predict the UCS of the rock cores based on their mean rebound value. However, for armourstones these trends need to be validated in a saturated condition since these rock will be saturated when placed in construction.
- Can the water absorption (WA) of armourstones be derived from Equotip measurements?
  The water absorption is an indicator of the in-service durability and indicates resistance to cyclic stresses like freeze and thaw. Moreover, the water absorption influences the apparent density of the armourstone when placed in the construction. The Equotip could indicate the in-service durability as well if it is capable to prospect WA values.
- Does the Equotip correlate to Brazilian tensile strength?
  The tensile strength is an interesting parameter for a durability investigation, because several degradation mechanisms, like degradation by salt crystallisation or slaking, are tensile failure of the rock matrix. A prediction of the BTS by the Equotip could reduce the amount of BTS measurements to indicate the behaviour of the armourstone during tensile failure.
- Is the Equotip capable of showing the weathering degree of single rock pieces, and what statistical analysis suits the Equotip data best for a weatherability study?
  The degree of weathering influences the degradation rate of armourstones. A consequent analysis by the Equotip on degree of weathering could indicate the rate of detoriation. The statistical analysis on the Equotip data influences the results, since they set the impact of outliers like weak and/or strong features in the rock matrix.
- What is the influence of the stress orientation with respect to the bedding within an anisotropic rock sample on the strength values?
  The bedding within armourstones influences the UCS and BTS values when the major stress is applied from various directions. The minimal strength values are limiting the rock's resistance when placed in waterway protection structures. Thus, influence of the bedding on the strength values is important to be considered for the durability analysis.
- Is Methylene Blue surface staining capable of showing deleterious clay structures?
  The preparation and staining of thin sections is not required if staining of the sawn surfaces properly reveals the presence of deleterious minerals and structures. This will reduce costs and experience required to indicate the presence of the deleterious constituents and structures.

1.3. Research Methodology

In order to obtain the general characteristics of the rocks and a 'standard' durability estimate, a selection of the laboratory tests according to EN 13383-1&2:2002 will be executed. These tests will also be

used as reference material for the forthcoming tests. The following tests will be performed on the armourstone samples for a basic durability analysis, where the corresponding testing standards are in between the parenthesis;

- Apparent mass density (EN 13383-2 Clause 8)
- Water absorption (EN 13383-2 Clause 8)
- Micro-Deval (EN 13383-1 Clause 5, EN 1097-1 Clause 7)
- $MgSO_4$ Soundness(EN 13383-1 Clause 5, EN 1367-2 Clause 8)
- Methylene blue adsorption (EN 933-3, Verhoef 1992)
- UCS (EN 1926)

Next to these tests, the following tests will be performed to obtain more and detailed rock characteristics;

- Petrographic analysis (EN 13383-1 Appendix C)
- Methylene blue staining
- Brazilian Tensile Strength test (ISRM 1978b, ASTM D3967-81)
- Equotip testing (Aoki and Matsukura (2007); Verwaal and Mulder (1993))

The petrographic analysis will be performed to understand the behaviour of rocks during the mentioned laboratory tests. The MB staining is performed in an attempt to highlight deleterious clay structures within the rock matrix. The Brazilian tensile strength is neglected within EN 13383-1&2:2002, yet is assumed to be the limiting strength that needs to be considered for several degradation mechanisms. The Equotip will be performed using several methods in order to obtain an insight in the rock variability. Its results will be compared to the other laboratory test in an effort to understand its contribution in an armourstone durability check.

1.4. Thesis Outline

The report starts with a literature review in chapter 2, where the methods, results, and conclusions of relevant preceeding research are discussed. The next chapter contains a poster that provides a suggested workflow to acquire armourstone that satisfies the durability requirements. This is a general introduction into the topic of armourstone durability. The collected samples are discussed in chapter 4. Chapter 5 discusses the importance of a petrographic analysis and presents deleterious constituents and structures found within some of the aggregate pieces. Next, the rock parameters are discussed, which are obtained according to EN 13383-1&2:2002. Chapter 6 presents the results of the micro-Deval test and provides a prediction of the armourstone degradation according to the micro-Deval (MDE) method. Next, chapter 7 lists the water absorption and density of the rock pieces. The results of the strength tests are described in chapter 8. The last chapters will show the application of simple testing tools for a durability assessment. Chapter 9 discusses the use of the Equotip for a durability estimate and chapter, 10, shows the use of methylene blue in a durability investigation. The discussion is elaborated in chapter 11 and the conclusions of the research are discussed in chapter 12. The final chapter contains recommendations on the quality assessment and quality control system of armourstones based on the results obtained during this research.

2

Literature Review

The literature study will focus on the major degradation mechanisms to which armourstones in waterway and coastal protection structures are exposed. These mechanisms will be related to the armourstone resistance tests included in the standard EN 13383-1:2002 and additional resistance tests. A variety of rock parameters, partly included within EN 13383-1:2002, will be discussed together with their impact on the rock durability. The importance and applicability of simple index test to assess the deterioration and to contribute to a durability investigation will be examined. Furthermore, the impact of anisotropy on the resistance against degradation will be explored.

2.1. Durability Assessment within The Netherlands

In current practise the properties of armourstones are determined according to the European standard EN 13383-1&2:2002. Several rock properties are stated in this standard and involve; geometrical requirements, physical requirements, chemical requirements and durability requirements. The geometrical requirements include; grading and shape, the physical requirements; particle density, resistance to breakage and resistance to wear, and the durability requirements; water absorption, resistance to freezing and salt crystallisation, and Sonnenbrand. Part 1 of the standard contains the specification of each property and part 2 the test methods. Every single property contains several categories that state the requirements to be met during testing. For example water absorption has category $WA_{0,5}$, corresponding to an average absorption of $\leq$0,5%. Engineering experience is required in order to select the appropriate category that will ensure a suitable rock for the engineering structure. CIRIA/CUR/CETMEF (2007) published table 3.12, see table 3.1 in this report, that divides the range of test values into excellent, good, marginal and poor. Assigning the corresponding range to every test value by means of this table, estimates the durability of the armourstone. A major drawback is that the table does not take the design of the engineering structure and its site conditions into account. The degradation model by Latham et al. (2006), which will be discussed in section 2.2.3, does take the design and site conditions into consideration. The European standard does not include all tests to define rock properties listed by CIRIA/CUR/CETMEF (2007). For example, the petrographic analysis and methylene blue absorption are not included within EN 13383-1:2002. In this way the presence of deleterious clay minerals or micro-textures can be missed, both negatively affecting the durability of armourstone, while the mechanical tests from EN 13383-2:2002 may indicate that the armourstone properties are satisfactory for the structure (Pieters et al., 1992). The tensile strength is not included within the EN 13383-1:2002 as well. The tensile strength plays a crucial role in the resistance to various weathering processes, like slaking and crystallisation in rock pores, which will discussed in section 2.2.2. The swelling of deleterious structures in the rock matrix and growth of crystals in the pore spaces will result in tensile failure of the rock matrix.

The products of the armourstone quarries are tested on all properties stated in EN 13383-1:2002 by external laboratories. The test results are transferred to the corresponding categories and then listed on the CE form. In addition to the CE form is the declaration of performance (DoP), a certificate produced by the quarry itself to show that their product is suitable to be used as armourstone. The

disadvantage of both forms is that variability within the quarry is not captured. The test samples are provided by the quarry and can be representable for the entire quarry by proper selection. Nevertheless a quarry can select only the fresh and durable rocks to be tested, resulting in misleading information on the forms. Therefore, providing both forms is no guarantee for a durable armourstone.

Nicholson (2001) states a proper durability assessment should be executed with the specific weathering conditions of the construction in mind. This statement is well in place for the situation within the Netherlands, since this is currently neglected within the European standard.

2.2. Weathering Processes in a Marine Environment

Jenny (1941) identified weathering is a function of the parent material, climate, organisms, topography, humanity, and time. During the weathering process the parent material with primary minerals and original structure is transformed into fragmented particles with loss of primary structure and arise of secondary minerals. Rock weathering is coherent to the climate, as the weathering grade depends on the contact with air and water (Waltham, 2002). In general the grain size, strength and bulk density of the rock decrease with increasing weathering grade.

Weathering has an influence on the mechanical properties of rock. A considerable amount of literature has been published on this influence. Kee (2010) investigated the degradation of armourstones in the Middle-East by comparing test results before placements of the armourstone in breakwater and test results after some years in service. He observed that water absorption increases over time and strength decreases. Latham et al. (2006) predicts the reduction in average mass of armourstone after a certain amount of years in construction based on rock properties and site aggressiveness. One of the models uses abrasion rates from the micro-Deval test to predict the mass loss and the other model uses a rating system including multiple rock properties, from quarry characteristics to laboratory testing results. Gonzalez and Scherer (2004) studied the damage due to wetting and drying cycles of swelling inhibitors in rocks and noticed that during the cycli the tensile strength of the rock was reached. This process is called slaking and noticed by multiple studies (Dunn and Hudec, 1966; Erguler and Ulusay, 2009; Pieters, 1992; Sebastián et al., 2008; Singh et al., 2005). In an investigation into salt crystallisation, Jefferson (1993) found that salt crystallisation is one of the strongest weathering processes.

Weathering processes can be split up in three categories; mechanical weathering, chemical weathering, and biological weathering. Mechanical weathering is the physical break-down of rocks, while there is no change in chemical composition. During chemical weathering there is an action of chemical agents on the rock, consequently breaking down the minerals and transformation into new compounds. Biological weathering is mechanical and chemical weathering induced by plants or bacteria. The weathering mechanisms are coherent. For example, decrease in particle by mechanical or biological weathering increases the effectiveness of chemical attack on a rock, resulting from the increase in surface area.

Most weathering reactions are very slow due to their slow kinetics and take over the engineering time to occur. However, there are weathering reactions that can occur within the engineering time of a structure (Pieters et al., 1992). An example is the degradation by secondary minerals. They can be present in rocks considered fresh, due to slow weathering over geological time span, since the quarried rock is close to the surface. In an engineering structure as a breakwater these secondary minerals can have detrimental effects, even if they are only present in very small quantities. These aggressive degradation mechanisms are within the scope of this research, because they occur within engineering time. The degradation mechanisms, that will be focused on, are discussed next.

2.2.1. Abrasion

Abrasion is the weathering of a rock surface due to friction between rocks and sediment caused by grinding against each other. Some examples of abrasion mechanisms are the friction by sand particles or the impact of larger clasts against the armourstone surface, as a result reducing the surface roughness (Feal-Pérez and Blanco-Chao, 2013). It is a considerable factor influencing the durability of an armourstone in marine conditions (Acir and Kiliç, 2012; Feal-Pérez and Blanco-Chao, 2013). Abrasion results in a loss of the armourstone engineering performance. In marine environments abrasion is a function of sea wave impact and time. The loss of mass by abrasion is inversely related to the armourstone's weight, owing to the decrease in exposed area of the rock with

increasing mass (Acir and Kiliç, 2012). The boundaries and pores between grains represent weaknesses in the rock structure, at which failure of rocks generally takes place (Kahraman and Gunaydin, 2007).

According to Acir and Kiliç (2012) the current method of lab testing to assess the resistance against abrasion, as stated by CIRIA/CUR/CETMEF (2007), is not comparable to the in-situ construction conditions as sea water is absent in the test setup. The suggested test setup applies only one rock piece hang by a wire in the drum of a slake durability test apparatus, to avoid contact with the inner walls. The drum is for 50 % filled with brackish sea water instead of tap water. By rotating the drum with this setup, the rock is subjected to long-term coastal conditions. Still, the method proposed by Acir and Kiliç (2012) is doubtful to represent the in-situ conditions, because no sediment load is used in the test. Consequently, there is only a simulation of wave impact and the abrasion by suspended particles is neglected. In the micro-Deval and Los Angeles abrasion test the friction is simulated by the addition of steel balls to the rotating drums. Nevertheless, Acir and Kiliç (2012) showed that the transition to sea water increases the abrasion impact compared to fresh water and thus should be taken into account for a durability estimation.

Various studies have assessed empirical relations between abrasion and other rock properties. These can be promising since abrasion tests, although simple, can be costly and protracted. Kahraman and Gunaydin (2007) showed the interdependence between the abrasion loss by Los Angeles test with the point load and Schmidt hammer value, presented in figure 2.1. The abrasion resistance can in this way be determined more favourable regarding time and money. Conforming to the coefficient of determination (R^2) for the two models, the point load is more suitable to estimate the abrasion loss. In an attempt to improve the model the data was again analysed, but this time separated into two porosity classes; (1) with a porosity below 1 % and (2) with a porosity above 1 %. The models achieved by regression analyses show a better fit with a R^2 of 0.81 and 0.77 for the two classes respectively, compared to a R^2 of 0.72 for the full porosity range. The alternative of the Los Angeles test is the micro-Deval test. Both correlate to each other, consequently there probably exists a good match between the micro-Deval value and point load as well. Important to realise is that the correlation between LA value and point load can be varying with rock type according to the results from Ballivy and Dayre (1984), who showed that the correlation between LA value and UCS is not constant for a variety of limestones. In addition, the research of Cargill and Shakoor (1990) resulted in a non-linear relation between the UCS and the Los Angeles abrasion loss divided by the dry rock density. The dry density of the rock in the relation already suggest the correlation is rock type dependent.

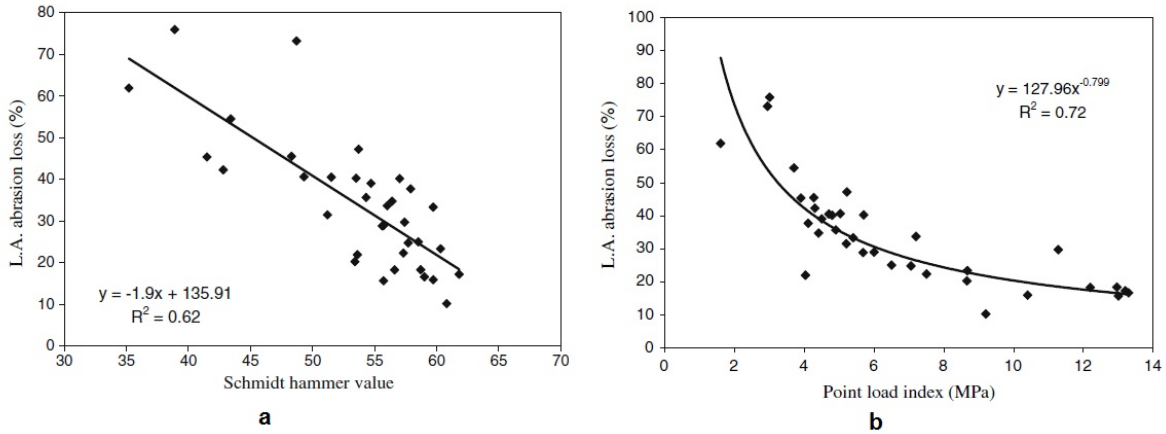

Figure 2.1: Abrasion loss versus (a) Schmidt hammer value and (b) Point load index after Kahraman and Gunaydin (2007).

The surface roughness of armourstone induced by abrasion is highly dependent on the rock properties, mainly on type, structure, size and hardness of the minerals (Feal-Pérez and Blanco-Chao, 2013). For example, micas are highly flexible as a result of the cleavage and no fracture which makes them hard to erode by abrasion. In case that brittle rocks are exposed to a high, abrupt loading, a lot of fractures can be created with serious size. This indicates that care should be taken with the

correlation or prediction of abrasion resistance of armourstone with simple testing tools. Generalising the observations to all rock types could be superficial.

2.2.2. Salt Crystallisation

Salt crystallisation in the pores of rocks is a severe weathering process, especially in arid environments with high temperatures exceeding 30°C. Most severe form of decay is pressure crystallisation, whose intensity depends on the pore size and salinity of the water. Salt can enter rocks in solution by complete submersion and by means of capillary rise, which is called the wick effect. Difference in weight loss due to salt crystallisation between the two processes depends on the petrographic properties, porous media and degree of coherence. The crystallisation of salt results in a loss of the coherence between the grains and the matrix in a rock. Benavente et al. (2001) executed a salt crystallisation test my immersing samples for 10% in a saline solution. They observed that in the capillary zone salt crystallisation is highly developed, because of the high evaporation rates. Consequently, weight loss of rock material mainly occurs in the capillary zone. For this reason testing armourstone for resistance against salt crystallisation by capillary forces seems essential. In the capillary zone even a low weight loss can produce a lot of damage. The process will mainly occur in tidal zones, where the stress on rocks is already high due to the mave loading. Cylindrical samples fell apart quickly during a salt immersion test as a result of the pressure crystallisation, therefore can be used as an intensive durability test (Benavente et al., 2001). 'The granular disintegration actively occurs at the surface and in the outermost layer by removing the matrix materials and/or reducing intergranular bonding due to salt weathering' (Aoki and Matsukura, 2007). The salt crystallisation by capillary raise test is not included in EN 13383-1:2002.

The pore size and structure are a considerable factor within the resistance against salt crystallisation. Benavente et al. (2001) divided the pore size in three classes; macro, with pore sizes from 2500 μm and fluid flow driven by gravity; meso, with pore sizes between 0.1-2500 μm and fluid flow driven by capillary forces; and micro, with pore sizes below 0.1 μm and fluid flow driven by adsorption forces. In the case of microporosity, fluid flow can be limited by air bubbles in the pores. Additional experiments have shown that rocks with a high volume of pores with a radius of <1 mm are easily affected by salt crystallisation (Sebastián et al., 2008). The crystallisation pressure is decreasing with increasing pore size. The specific surface area (SSA) of a rock is the surface area of voids per unit mass of a porous material. The SSA value is negatively correlated to the pore size, thus a high SSA value indicates a relative high area of the rock material will be decayed by salt crystallisation (Benavente et al., 2004). Therefore, a rock with micro- and mesoporosity will be most sensitive to pressure crystallisation. Based on these results, the aggressiveness of salt crystallisation seems to reduce as it advances, since the pore size is increased by the stress induced by the growth of salt crystals. Yet, the crystallisation greatly reduces the decayed rock strength as well and thus the increase in pore size does not slow the degradation process down. Moreover, Benavente et al. (2004) claim a material that absorbs more water facilitates several decay mechanisms. As a result a rock with higher porosity is more vulnerable to decay.

Benavente et al. (2004) proposed a new petrographical durability estimator (PDE), which shows the material resistance for various crystalline pressures. The PDE is an estimator that is based on the pore structure and material strength. As would be expected, there is a strong correlation between weight loss after salt crystallisation and the petrophysical durability estimator with respect to compressive strength. However, the best correlation in the petrophysical durability estimator is produced when expressed in terms of flexural strength. Tensile strength can be considered as the resistance of stone to salt crystallisation and flexural strength is an indirect measurement of the tensile strength of the material. Figure 2.2 shows the results obtained by Benavente et al. (2004) and displays the correlation between the PDE and weight loss by salt crystallisation. The estimator saves a lot of time compared to the cyclic salt crystallisation test and supplies a quick durability assessment.

2.2.3. Swelling Clay Minerals

Clay minerals are deleterious materials and can result in degradation of a rock upon wetting and drying due to their swelling behaviour, referred to as slaking (Gonzalez and Scherer, 2004; Pieters, 1992). Clays with high swelling potential, such as smectites, have an intercrystalline swelling mechanism and are referred to as swelling clays. In between the crystal layers clay minerals absorb and exchange water and cations, thereupon causing severe swelling. Another, less intense,

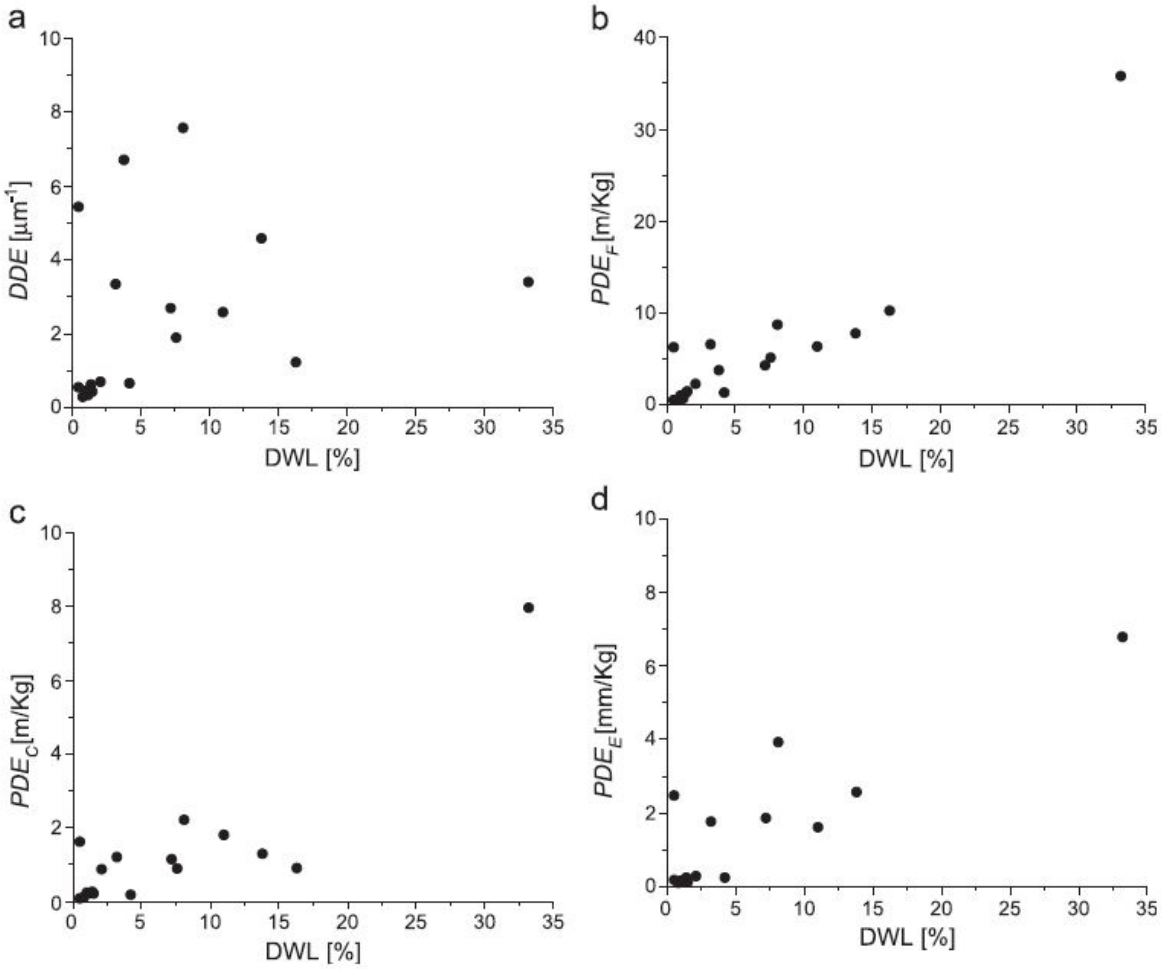

Figure 2.2: Correlation between the percentage of dry weight loss by salt crystallisation (DWL) and (a) the durability dimensional estimator (DDE) and the petrophysical durability estimator respectively expressed in terms of (b) flexural strength (PDE_F), (c) uniaxial compressive strength (PDE_c) and (d) Young's dynamic modulus (PDE_E) after Benavente et al. (2004).

mechanism is the osmotic swelling due to a concentration difference in ions within the clay and rock pores. Both swelling mechanisms are visually explained in figure 2.3. Gonzalez and Scherer (2004) highlighted the damage caused by swelling clay minerals is constraint to the outside of the rock. The outside zone is most vulnerable to wetting and drying, as it takes less time to saturate the outer layers of a rock. Contraction of the rock surface during the drying period can exceed the tensile strength of the rock, henceforth forming cracks. Also flakes can be created as a result of the mechanical stress between wet rock parts and the dry areas behind (Sebastián et al., 2008). The occurrence of active clay minerals within a rock can affect its durability (Dunn and Hudec, 1966; Gonzalez and Scherer, 2004; Pieters, 1992; Pieters et al., 1992; Sebastián et al., 2008).

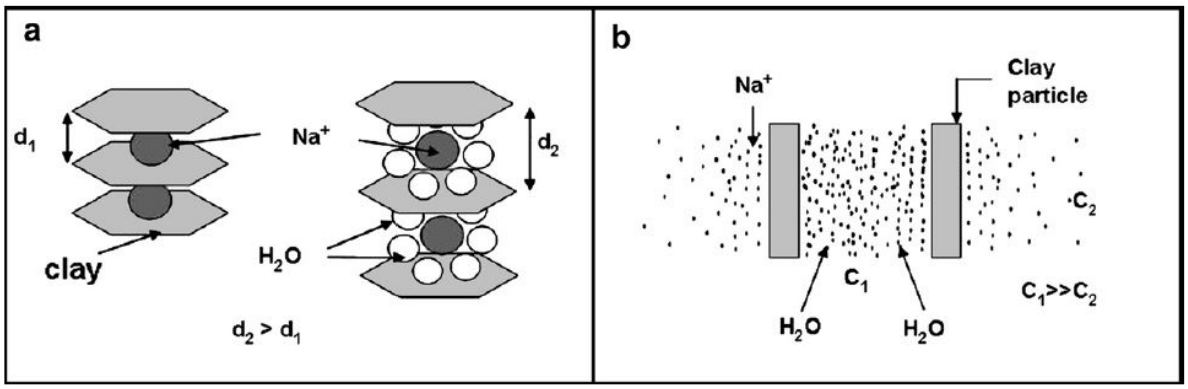

Figure 2.3: Process of (a) intercrystalline swelling and (b) osmotic swelling of clay minerals after Sebastián et al. (2008). D is the spacial spacing of the clays, d_1 before hydration and d_2 after hydration. C is the concentration of Na ions, C_1 is the Na concentration between clay layers and C_2 the Na concentration in the pore water. The process depicted in subfigure a occurs in the clay particle indicated in subfigure b.

Gonzalez and Scherer (2004) present an elastic analysis, neglecting viscoelastic behaviour, of the stress in the rock surface plane during swelling and shrinking. Maximum stresses by swelling occur when the swelling layer is relative very thin to the dry volume, such that the expansion is repressed by the dry volume. The obtained stress σ_s is expressed in equation 2.1 where; E_{wet} is the Young's modulus of the wet rock, v_{wet} is the Poisson's ration of the wet rock and ε_s is the free swelling strain. The stress is compressive (σ_s is negative) and damage occurs when the compressive strength is exceeded. Defects in the rock structure can result in buckling of the surface. As the rock dries the exterior shrinks, resulting in tension due to resistance of the dry bulk volume. The tensile stress parallel to the drying surface is stated by equation 2.2 where; E_{dry} is the Young's modulus of the dry rock and v_{dry} is the Poisson's ratio of the dry rock. Damage occurs in this case when the tensile strength of the rock is exceeded. Tensile strength of rocks is generally lower than compressive strength. Consequently, rocks will damage during the drying cycles. Yet, damage during wetting cycles cannot be excluded. By back analysing the damaged samples it was concluded that the damage could not only have taken place during the drying stage and thus additional damage was caused during the wetting stages. Equation 2.1 and 2.2 do not take into account the relaxation ability of the rocks.

$$\sigma_s = -\frac{E_{wet}\,\varepsilon_s}{1 - v_{wet}} \tag{2.1}$$

$$\sigma_s = \frac{E_{dry}\,\varepsilon_s}{1 - v_{dry}} \tag{2.2}$$

It was noticed by Gonzalez and Scherer (2004) that the ability of rocks to relax, can reduce the damage induced by swelling processes, such as swelling clay minerals. They also tested the influence of swelling inhibitors applied by surface treatment on the swelling behaviour of architectural rocks. Although the results were satisfactory, surface treatment of armourstone seems not economically favourable, because large bulk volumes are involved.

The degradation caused by swelling clays is not only a function of the type and amount of clay minerals, but as well their distribution within the rock matrix. Dunn and Hudec (1966) demonstrated with their research that concentration and orientation of the clay minerals have a large influence on the

durability of a rock. They observed that rocks with homogeneously distributed clay minerals, up to 30% of the total mass, were resistant against cyclic wetting and drying, while rocks with minor amounts, though aligned along bedding planes, suffered considerable damage. Furthermore, the alignment of clay minerals increases the capillary action of the rock potentially increasing the swelling effect and generation of flakes (Sebastián et al., 2008). Given these points, both the amount of swelling clays and their structure within the rock should be researched during a durability analysis. As long as the clay minerals cannot be reached by water within the rock there is no risk on swelling. The swelling clay minerals only exhibit their swelling behaviour as the pore fluids can reach them. Sebastián et al. (2008) detected that rocks with a high open porosity, by pores and fissures between 10 and 50 µm in access size, exhibit more mechanical weakening. This open porosity range may be detected with simple testing equipment and is definitely observed during a petrographic analysis.

2.3. Degradation model

The degradation of in-service armourstone occurs most of the time due to the reaction of the engineering environment with the deleterious minerals or micro-structures present in the rock (Latham et al., 2006; Pieters et al., 1992). Thus, the durability of the armourstone is a function of both intrinsic rock properties and the site conditions. There are a number of studies that suggest that both the intrinsic rock properties and the construction environment are important. For example, Latham (1991) noticed the degradation rate may be evenly influenced between the site aggressiveness and the armourstone properties. In table 2.1 the environmental and rock property criteria for the applicable armourstone criteria are listed. As highlighted by Van der Meer (1987), the armourstone bulkiness is the main element for structural importance and for the armour stability the mass of the rock block is the most important parameter. Consequently, most degradation models prospect a mass loss over time. A well known degradation model is the model proposed by Latham (1991). He used a mill abrasion test to obtain the rock fabric strength k_s. Next, he considered 9 factors that influence the degradation rate. Every factor is assigned a weight for a certain environment, after which they are all multiplied to one factor X that describes the site aggressiveness. The individual factors are listed below;

- X_1: Blocksize
- X_2: Grading
- X_3: Initial shape
- X_4: Incident wave height
- X_5: Zone of structure
- X_6: Meteorological climate
- X_7: Water-borne attrition agents
- X_8: Concentration of wave attack
- X_9: Mobility of armour in design concept

Besides the intrinsic properties, Latham (1991) reported that degradation of armourstone is substantially sped up by: (1) climate cyclic stresses, (2) an abrasive attack by shingle, and (3) the mobility of the armour blocks. It is questionable if the use of only the abrasion mill test provides a good basis for the mass loss curve over time. Different rock types will react differently to for example salt crystallisation due to their strength and pore structure. These differences between rock types are not covered within the factors of the site aggressiveness and the test result of the abrasion mill test.

Parallel to the research of Latham (1991), Lienhart (1998) also developed a degradation model. Both researchers worked together and published their latest updates in Latham et al. (2006). The degradation models discussed by Latham et al. (2006) are models that produce a prospected rate of degradation that counts on rock properties and loading intensity, referred to as site aggressiveness. They describe two models; (1) the micro-Deval model and (2) the armourstone quality designation (AQD). Also some updates are proposed for the factors mentioned by Latham (1991). For X_6 the

Table 2.1: A completed rating sheet for the armourstone quality designation after Lienhart (1998)

(a)	(b)				(c)	(d)	(e)
Criteria	Quality rating				Rating value	Weighting	Weighted rating
	Excellent	Good	Marginal	Poor			
	(=4)	(=3)	(=2)	(=1)	Average	%	{(c)× (d)} / mean of (d)
Lithological classification		✓			3	58	2.12
Regional in-situ stress			✓		2	73	1.78
Weathering grade		✓			3	73	2.67
Discontinuity analysis		✓			3	95	3.48
Groundwater condition			✓		2	73	1.78
Production method				✓	1	95	1.16
Rock block quality			✓		2	80	1.95
Set-aside		✓			3	73	2.67
Petrographic evaluation			✓		2	95	2.32
1 Block integrity test				✓	1.5	90	1.65
Block Integrity visual			✓				
2 Mass density		✓			3	80	2.93
Water absorption		✓					
Microporosity/total porosity		✓					
Methylene blue absorption		✓					
3 Compressive strength			✓		1.67	88	1.79
Schmidt impact index			✓				
Sonic velocity				✓			
4 Point Load strength			✓		2.67	88	2.87
Fracture toughness		✓					
L A Abrasion		✓					
5 Micro-Deval			✓		2	88	2.15
6 Freeze–thaw loss		✓			3.67	80	3.58
$MgSO_4$ soundness	✓						
Wet–dry loss	✓						
					Sum	1229	34.9
					n	15	15
					Mean	81.9	2.33

Note 1: This sheet includes 15 factors (9 field, 6 laboratory) hence overall rating or Armourstone Quality Designation, AQD is mean of column (e) based on all 15 factors. If no data are available for one or more factors, AQD should be based on the number of included factors. A complete and balanced set of data is ideal.

Note 2: In addition to engineering geology indicators, each boxed grouping of tests 1 to 6, generates one average rating value in column (c) from one or more suggested tests. They refer to 1: resistance to Major Breakage, 2: mineral fabric physical quality, 3: resistance to Minor Breakage (compressive), 4: resistance to Minor Breakage (tensile, dynamic), 5: resistance to wear (shear and attrition), 6: resistance to in-service weathering.

Note 3: test results and field assessments can be used to generate continuously varying ratings from 0.5 to 4.5 rather than using integer values. Similarly AQD results can vary from 0.5 to 4.5.

meteorological climate weathering intensity (MCWI) of Lienhart (2003) is used.

• Micro-Deval method (MDE)
The micro-Deval method is comparable to the method described by Latham (1991) and makes use of the abrasion by the micro-Deval mill. The method seems to be relevant for the degradation process by attrition and surface grinding processes. Yet, the authors claim that by interaction of the different factors all principal degradation mechanisms are covered. Due to the lack of multiple laboratory tests this is statement is questionable. The MDE method is performed in the following manner; first the micro-Deval value is transformed to a k_s, which relates to the resistance against abrasion, by equation 2.3 where M_{DE} is the micro-Deval value. Next the mass loss M/M_0 versus time is plotted by equation 2.4 where; t is the time in 1000's of revolutions, M_0 is the initial mass of the armourstone and M is the mass of the armourstone at time t. After the mass loss is determined the equivalent wear time factor X is calculated to transfer the time from equation 2.4 to an engineering time in the construction. X is determined by multiplying all site aggressiveness parameters mentioned before as shown in equation 2.5. Finally, the time in 1000's of revolutions is transferred to a time in construction by multiplying the t from equation 2.4 by X from equation 2.5. The result is a mass loss curve M/M_0 against the service lifetime.

$$k_s = 4.12 \cdot 10^{-5} \cdot {M_{DE}}^{1.485} \tag{2.3}$$

$$M/M_0 = 0.05 \cdot e^{-30\,k_s\,t} + 0.95 \cdot e^{-k_s\,t} \tag{2.4}$$

$$X = X_1 \cdot X_2 \cdot X_3 \cdot X_4 \cdot X_5 \cdot X_6 \cdot X_7 \cdot X_8 \cdot X_9 \tag{2.5}$$

• Armourstone quality designation (AQD)
The armourstone quality designation (AQD) is closely related to the method reported by Lienhart (1998). The AQD is dependent on laboratory test results and quarry analysis. The criteria are all assigned a quality rating from 1 to 4, poor to excellent respectively. An average rating is obtained for criteria that rely on more laboratory tests. For every criteria a weighting is assigned, which is a way to assign the major and minor criteria for the durability assessment. The rating and weight result in the weighted rating. The mean of the weighted ratings for all criteria is considered the AQD. An example of the AQD calculation and a list of all criteria can be seen in table 2.1. The categories determined within the quarry can already result in a good indication of the armourstone durability relative to other faces and highlight the variability within a quarry (Lienhart, 1998). During the AQD method the AQD is converted to k_s by equation 2.6, which represents the intrinsic resistance to mass loss of the quarry source. Again, the mass loss is calculated by equation 2.4 and the equivalent wear time factor by equation 2.5. By multiplying the time in the mass loss curve with the wear time factor the mass loss per year in construction is obtained, similar to the MDE method.

$$k_s = 0.032 \cdot AQD^{-2.0} \tag{2.6}$$

Latham et al. (2006) eventually conclude that the AQD method uses more relevant parameters compared to the MDE method, hence is an appealing method. Nevertheless, the MDE method is probably better calibrated as the abrasion test results were compared to related historical cases. The AQD method is prefered in this study because of all the parameters taken into account both in the quarry and laboratory.

In practise the degradation rate will increase after time, while the laboratory test show a constant or decreasing degradation rate. Consequently, Latham et al. (2006) propose that between 10% and 50% mass loss an increased degradation rate may be more sensible. Also, deterioration rates for several degradation mechanisms can vary abrupt for a short period followed by a period with a low degradation rate. Some examples are salt crystallisation and burst by freeze-thaw (Latham et al., 2006). These are important factors in order to predict a mass loss in time. Nevertheless, in a study to assign durable rocks the exact degradation curve is not required. The emphasis lies on the fact that the rock durability must exceed the engineering lifetime. In that case average degradation rates over the engineering life are sufficient.

2.4. Petrographic Evaluation

Petrographic examination is a meaningful tool to be used for a durability assessment, owing to the detailed view in rock properties that are compatible with the capability of armourstone. Benavente et al. (2004) concluded that a petrophysical estimator, based on strength and pore structure, strongly correlates to salt weathering of rocks. Likewise, small amounts of secondary minerals with detrimental effects need to be investigated by petrographic analyses for the purpose to indicate swelling potential during wetting (Pieters, 1992; Pieters et al., 1992). The orientation and distribution of clay minerals can be observed by means of petrographic analysis when the thin section are stained with methylene blue (MB). The research of Dunn and Hudec (1966) demonstrated that the distribution and alignment of clay minerals is extremely important for the slaking magnitude. Furthermore, petrographic features like mineral content, mineral orientation, grain shape, grain contacts and micro-structures relate to the behaviour of rocks during strength testing (Pieters, 1992; Tavallali and Vervoort, 2010). For example, a larger grain size lowers the strength of the rock, because cracks can propagate more easily. The shear strength of rock decreases with increasing roundness, due to the lack of interlocking grains. Furthermore, the bonds between the grains are stronger when the grain boundary area is larger. Moreover, the presence of joints and cracks in rock lessen the strength and durability of a rock. Instead, infilling of these empty spaces may better the strength and durability. A preferred orientation of grain shape causes anisotropy in the rock's strength. Together with a wide range of minerals inside the rock, it is impossible to average behaviour over the rock since the composition can change. Feal-Pérez and Blanco-Chao (2013) highlighted the significance of rock properties, such as mineral content and structure, for prospecting abrasion resistance.

The results of the referred research show that the detailed view on the rock matrix by petrographic analysis correlates to many mechanical degradation mechanisms. So, a petrographic characterisation is crucial in a proper durability assessment of armourstone. This statement is confirmed by Pieters et al. (1992).

2.5. Equotip

The Equotip is a small test device that shoots an impact body with a spherical tungsten carbide tip of 3 mm diameter by a spring force towards an impact surface. The impact body rebounds upon hitting the surface. The impact velocity and rebound velocity are determined from an induced current by the impact body as it moves through a coil within the apparatus. The produced voltage is corresponding to the velocity of the impact body. The impact and rebound velocity are expressed in the rebound value (L) by equation 2.7 where; V_{impact} is the impact velocity and $V_{rebound}$ is the rebound velocity. The Equotip was originally designed to test the hardness of metals and detect hair cracks within the metal structure. However, due to the low impact force of the Equotip a large range of soft to hard rocks can be tested as well, without the creation of major damage to the rock surface (Aoki and Matsukura, 2007). The rebound of the impact body is a result of the elasticity of the rock surface, which correlates to the rock strength (Aoki and Matsukura, 2008).

The Equotip can be used with a variety of tips; D for standard surfaces, DC and DL for inaccessible areas, G for cast and forgings, C for smaller parts, s for ultra durable metals and E for very hard surfaces. In this study the type C and type D will be used, which have an impact of 3 and 11 Nmm respectively. Thus, the type C has a lower impact energy and is specially designed for surface hardened components, coatings and thin or impact-sensitive parts. The type D is designed for the majority of testing applications.

Much of the research on the application of the Equotip on rock focuses on identifying and evaluating the relation between rebound value and UCS.

2.5.1. Rebound value and UCS

Verwaal and Mulder (1993) found a relation between Equotip L value and the UCS of rock, for limestones, granites, sandstones and man-made gypsum. They suggest the Equotip is a convenient piece of equipment to estimate the UCS. Their result is presented in figure 2.4. There is scatter in the data, but overall the UCS increases with increasing rebound value. Nevertheless, curve fitting for separate rock types, or ranges within a rock type, could result in a better fit. An example is the study by Aoki and Matsukura (2008) which obtained a better fit by dividing the data in several rebound classes and transformed the data to porosity classes. The scatter in data reduces and the prediction

of the UCS is more accurate. However, the exponential trend over the entire porosity range is neglected in this way. The separated relations are almost linear and only fit within the predetermined range. Outside this range the prediction is way off. The exponential fit can be observed as well when analysing the entire point cloud. To determine a quick UCS value taking the entire porosity range into account is easier, since the porosity of a test sample does not need to be obtained. When the UCS is determined within a porosity range and the actual porosity turns to be outside of this range, the UCS approximation will deviate more from the actual UCS compared to the estimation covering the entire porosity. This phenomena can be observed in figure 2.6.

$$L = \frac{V_{rebound}}{V_{impact}} \cdot 1000 \tag{2.7}$$

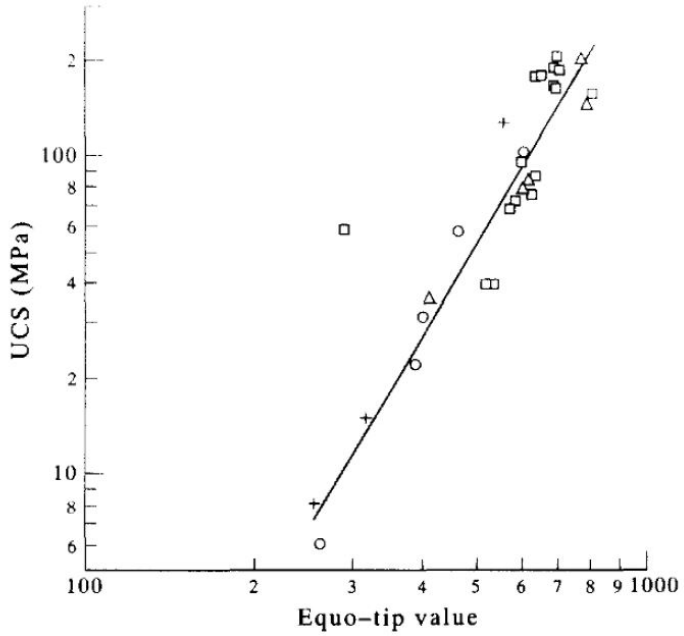

Figure 2.4: Correlation between UCS and Equotip value after Verwaal and Mulder (1993)

Aoki and Matsukura (2008) performed the single impact method (SIM), similar to Verwaal and Mulder (1993). In combination with the data of Verwaal and Mulder (1993) they observed likewise the increase in UCS with increasing rebound value, despite a large data scatter. Yet, this time the scatter is observed for rocks within the same porosity range. For this reason this scatter is a result of the difference in the measurement scale according to their investigation. The Equotip measurement is limited to a very narrow area, while the UCS measures the strength of an entire core. As a result, more rock defects, like micro-cracks or veins, may be involved in a UCS measurement. By taking the average rebound value from measurements over a complete specimem, by regular spacing, a reliable UCS value can be obtained (Verhoef, 2010). One of the largest influencing properties on data scatter is the porosity. Therefore, Aoki and Matsukura (2008) separated the data into three rebound value ranges as discussed before. Their result is given in figure 2.5 and shows that the UCS does depend on both porosity and rebound value. The relation for the UCS and porosity between the three rebound ranges is obtained by means of a multiple regression model and given in equation 2.8 where; L_s is the average rebound value and n the porosity expressed in %.

$$UCS = 0.079\, e^{-0.039n}\, L_s^{1.1} \tag{2.8}$$

Figure 2.6 displays the variation between the results obtained by several studies. As can be seen is there a big spread between the different estimations. The scatter between the estimations increases with increasing UCS, which suggests that the relationship between UCS and L value is less accurate for stronger rocks. This is confirmed by the data points collected in the several studies, which deviate more from the trend for the stronger rocks. The corresponding relations are summarised in table 2.2.

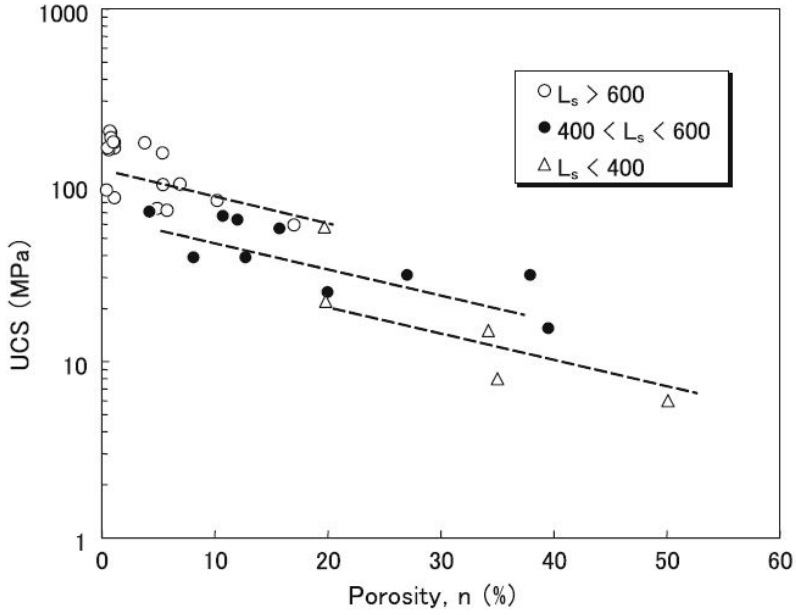

Figure 2.5: Correlation between UCS and L values for three ranges after Aoki and Matsukura (2008)

All studies made use of the type D tip. When the curves for the porosity classes are neglected and only the curve for the porous limestone of Kee (2010) is used, the curves are closely aligned. The curves together contain several rock types. From the figure can be concluded that there probably is one close estimation for the UCS from the Equotip rebound value that covers all rock types. Although, there is a limit towards the rock types the correlation can extend. For example, rocks with a very high porosity are not appropriate as no successful rebound can be measured (Verhoef, 2010). To obtain a proper measurement the entire specimen should be covered by a regular measurement grid, since only a sample of adequately size will truly represent the strength of the rock (Verhoef, 2010; Wilhelm et al., 2016). The difference in measurement grid is possibly the reason for the deviation of the curve from Aoki and Matsukura (2007); Verwaal and Mulder (1993). Both studies took the average of only 10 impacts and Verwaal and Mulder (1993) only took the measurements at the flat ends of the rock cores impact. The other studies performed more measurements and also took readings along the length of the rock cores. All studies took the Equotip measurements vertically downwards on the samples to consistently include acceleration of the tip by gravity.

Table 2.2: Multiple correlations between UCS and Equotip

Correlation	Rock types	Reference
$UCS = 4.906 \cdot 10^{-7} \cdot L^{2.974}$	Sandstone, Limestone, Dolomite, Granite and Granodiorite	Verhoef (2010)
$UCS = 2.205 \cdot e^{0.006\,L}$	Crystalline Limestone	Kee (2010)
$UCS = 1.668 \cdot e^{0.0064\,L}$	Porous Crystalline Limestone	Kee (2010)
$UCS = 1.1123 \cdot e^{0.0078\,L}$	Calcarenite	Kee (2010)
$UCS = 8 \cdot 10^{-6} \cdot L^{2.5}$	Sandstone, Limestone, Granite and man-made Gypsum	Aoki and Matsukura (2008); Verwaal and Mulder (1993)
$UCS = 547.19 \cdot e^{0.005\,L}$	Shale, slab section	Lee (2015)
$UCS = 311.16 \cdot e^{0.0058\,L}$	Shale, butt section	Lee (2015)

Hujer et al. (2014) relate the rebound value to a UCS value estimated by scratch test and obtained

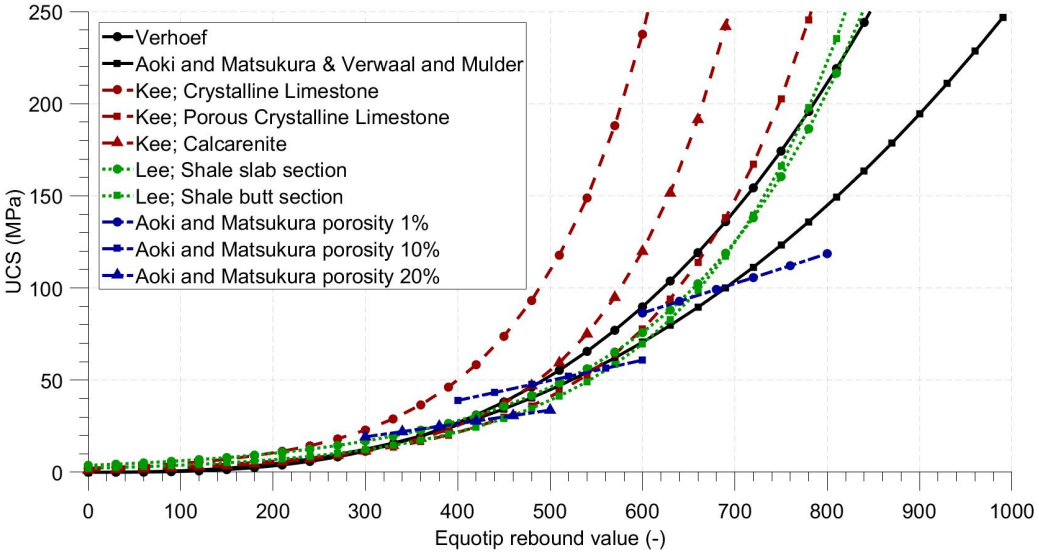

Figure 2.6: Relationship between Equotip rebound value and UCS from different studies

a clear relation. This seems legit since both the Equotip and scratch test reflect the hardness of the rock surface. As a result of the obvious correlation, they suggest to calibrate Equotip measurements with the scratch test.

A single regression equation to relate the L value to UCS is the simplest approach for practise, since it is quick and no additional measurements need to be taken to obtain other required rock parameters, such as porosity. The Equotip is a great tool to show variation of rock strength within a specimen and average value is a good approximation for UCS (Aoki and Matsukura, 2007; Verhoef, 2010; Viles et al., 2011; Wilhelm et al., 2016).

2.5.2. Detection of Weathering by Equotip

Besides the estimation of the UCS, the weathering state of a rock can be estimated as well from Equotip measurements. Weathered surfaces will result in a lower rebound value compared to unweathered surfaces, since weathering is recognisable in the surface zone by changing rock properties (Aoki and Matsukura, 2007; Coombes et al., 2013; Wilhelm et al., 2016). As a result of the very low impact energy, the Equotip is able to only measure the rebound of a very thin surface layer (Aoki and Matsukura, 2007; Coombes et al., 2013). Consequently, the first measurement taken during the RIM stands for the rebound of the weathered material when the outer surface is weathered.

Next to the discussed single impact method (SIM), Aoki and Matsukura (2008) proposed a new testing method; the repeated impact method (RIM). This method takes 20 successive Equotip measurements at the same spot. With the RIM they observed that the rebound value increases gradually with increasing number of impacts until it starts to oscillate around a constant value, as shown in figure 2.7. This increase results from the hardening of the rock surface at the impact point, due to the formation of a micro compression zone below the Equotip point. The repeated impact method shows the elastic properties of the rock surface and subsurface (Wilhelm et al., 2016). From the combination of SIM and RIM Aoki and Matsukura (2008) developed the k-value, which is the ratio between L_{max}, the mean of the three highest L values of the RIM, and L_s, the mean of 10 single impact rebound values both measured on the surface of small rock blocks with sides of about 10 cm. They perceived that the k-value is constant for a certain rock type. Once the k-value is established for a rock type, the mean single impact of a fresh rock surface can be estimated from the L_{max} measured at the weathered surface. The difference between L_s for the fresh and weathered surface is an indication of the degree of weathering of a rock. The drawback is that a fresh surface is needed in order to establish the k-value. Aoki and Matsukura (2008) do not match the rise in rebound value directly to the degree of weathering. It seems likely that the development of rebound value contains details about the degree of weathering and depth of weathering as well, as they point out it is

influenced by the looseness of the rock surface, consolidation of mineral grains and compaction due to the repeated Equotip impacts. This development will probably evolve differently in weathered zones compared to fresh zones. Another remark is the sample size used for the determination of L_s, which can be too little. The ISRM suggests at least 20 measurements, while Viles et al. (2011) suggest a sample size over 50 readings for some cases. Wilhelm et al. (2016) concluded at least 45 rebound values were required in order to discriminate all their tested rock types. They state that the amount of measurements is dependent on the rock type, but that 45 readings give an high enough confidence level. When many SIM measurements are taken, a weathering grade can potential be estimated from the spread in data. The spread gives an indication of the homogeneity of the rock surface (Verhoef, 2010). During weathering the homogeneity is expected to decrease, since the rebound value for weak parts in the rock surface decreases more quickly than for stronger parts. Thus the variation in Equotip data increases as weathering proceeds (Wilhelm et al., 2016). Therefore, a higher spread in rebound values indicates a higher degree of weathering. Measurements of a similar, non-weathered rock piece are required to validate this claim. Finally, the Equotip is showed to be a useful tool to monitor the weathering of armourstone in service (Coombes et al., 2013; Kee, 2010). Coombes et al. (2013) researched weathering of limestones, granites and concrete blocks placed in a breakwater by Equotip measurements. The results show a variation in rebound value after a short exposure to the marine conditions. The hardness of the limestones reduced after 8 months and even more after 20 months, the granite did not show much variation and the concrete increased in hardness over time. These findings suggest that the Equotip is a tool capable to relate weathering processes that operate at micro scale to the geomechanical properties important to the durability of armourstone in the intertidal zone. A low L value expresses a weathered, porous, or soft surface, while a high value suggests a less weathered surface.

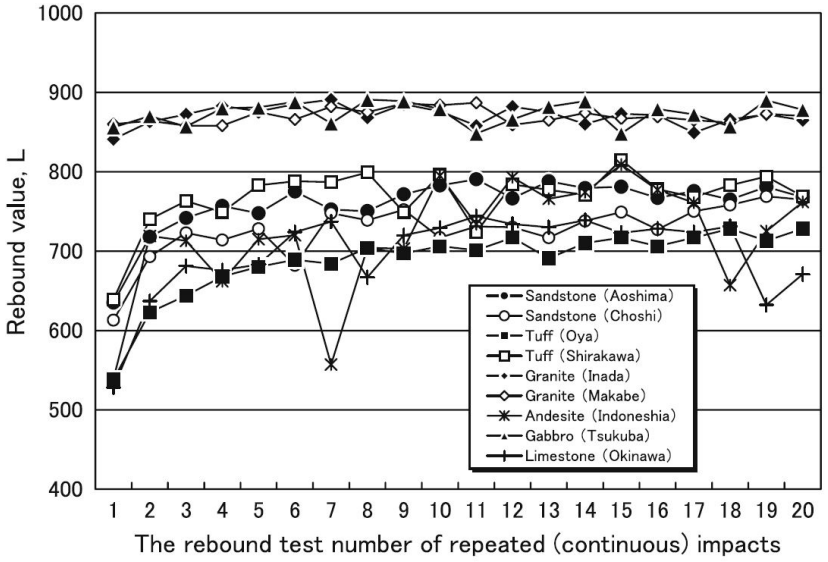

Figure 2.7: Variation in Equotip rebound value with number of measurements at the same spot after Aoki and Matsukura (2008)

2.5.3. Surface Roughness

The procedure in data acquisition by Equotip is important in order to obtain reliable results. Several studies investigated the influence of a sample surface roughness on the rebound value. Grinding the rock with a grinding stone before testing is satisfactory to obtain a test surface on rocks with extreme roughness. However, Feal-Pérez and Blanco-Chao (2013) claim that Equotip measurements are very sensitive to surface roughness. Otherwise, Okawa et al. (1999) conclude that the smaller scale surface roughness, for instance polishing the surface with sandpaper or using the sawn surface, does not affect the Equotip rebound value. The surface irregularities lower the impact energy of the impact body, because the irregularities are frequently crushed by the tip before the actual surface is measured (Viles et al., 2011). Wilhelm et al. (2016) suggests the surface roughness is an indication of weathering for several samples with comparable surface textures prior to the weathering influence. The surface

roughness and weathering are closely related, yet probably rock properties that influence rebound value differently for different rock types.

The influence of the surface roughness is a questionable item and several studies do not agree weather a rebound surface should be smoothed or not. The application of the Equotip data in a durability assessment seems important concerning the appropriate sample preparation. The studies discussed up till now do not all have the similar goal. For determining the UCS of a rock, the rough surface caused by weathering is not an interesting feature and can thus be removed. In addition it can even disturb the measurements with low rebound values, underestimating the UCS. Contrary, surface roughness can be an important indicator of the weathering stage when the weathering grade of the rock needs to be studied.

2.5.4. Data Evaluation

Wilhelm et al. (2016) provides a clear insight in the evaluation of Equotip data. First of all, Equotip rebound values generally show a non-normal distribution resulting from outliers. Outliers should not be removed from the data, because they are expected to be inherent to the natural rock properties. For this reason robust statistic analysis, such as median and median absolute deviation (MAD), should be used, given that they are less influenced by divergence due to the natural variability of rocks. Additionally, a separate study on the outliers or a more sensitive analysis, such as standard deviation, could reveal the surface weathering obtained during a SIM study. Most research on the correlation with UCS use the mean of multiple L values, distributed over the sample, to predict the UCS value.

2.6. Rock Strength

The rock strength is an intuitive indication of durability. Generally rocks with a high strength are considered durable. There is a large number of published studies (Goudie, 1999; Nicholson, 2001; Valdeon et al., 1996; Zezza, 1990) which describe that rocks with a high compressive strength and Young's modulus have a lengthy durability. In addition Benavente et al. (2004) obtained a good estimation on resistance against salt weathering with a petrographic durability estimator, based on porosity and strength, and Kahraman and Gunaydin (2007) acquired a prediction of the abrasion resistance based on the point load test. Most of the studies refer to the compressive strength, which is also one of the categories stated in the European standard EN 13383-1:2002. But, most of the weathering mechanisms described before are a result of tensile failure within the rock material. Tensile strength of rocks is not present in the current standard En 13383-1:2002 and not referred to by many papers.

2.6.1. Unconfined Compressive Strength

A common expression of rock strength is by means of unconfined compressive strength. The compressive strength of a rock is the highest stress it can resist when loading axially. The UCs is measured by compressing a cored sample between two end plates with a constant strain or stress rate. The measured strength relies on several factors.

First of all, the current European standard for armourstone EN13383 specifies cores of 50 mm diameter with a length to diameter ratio (L/D) of 1. The cores can be of different size with respect to core diameter and L/D. The size of the cores has influence on the strength value obtained with the UCS test (Brown and Hoek, 1980; Hawkins, 1998; John, 1972). Samples with a larger diameter have a higher chance of flaws within the rock structure and a lower UCS is expected. The L/D of the core has effect on the stress distribution within the sample and consequently the UCS value. The test results of any core size can be corrected to a standard size. Brown and Hoek (1980) established an equation that returns the UCS value of a core with any diameter to a strength value that would be obtained with a 50 mm core diameter. Their result is showed by equation 2.9 and figure 2.8. ASTM D2938-82 corrects for the L/D ratio instead of the diameter and returns an obtained UCS value to a strength value of a core with a L/D of 2, conform equation 2.10. In addition is the influence of L/D ratio on UCS value visualised in figure 2.9. Turk and Dearman (1986) created a correction equation that takes both the diameter and L/D into account, presented in equation 2.11. With this equation the UCS is transformed to a value for a core size with a diameter of 50 mm and a L/D of 2.

$$UCS_{50} = UCS_m \left(\frac{D}{50} \right)^{0.18} \tag{2.9}$$

$$UCS_{corr} = \frac{UCS_m}{0.88 + 0.24 \left(\frac{D}{L} \right)} \tag{2.10}$$

$$UCS_{50} = UCS_m \left(\frac{D^{0.18}}{1.754 + 0.535 \left(\frac{D}{L} \right)} \right) \tag{2.11}$$

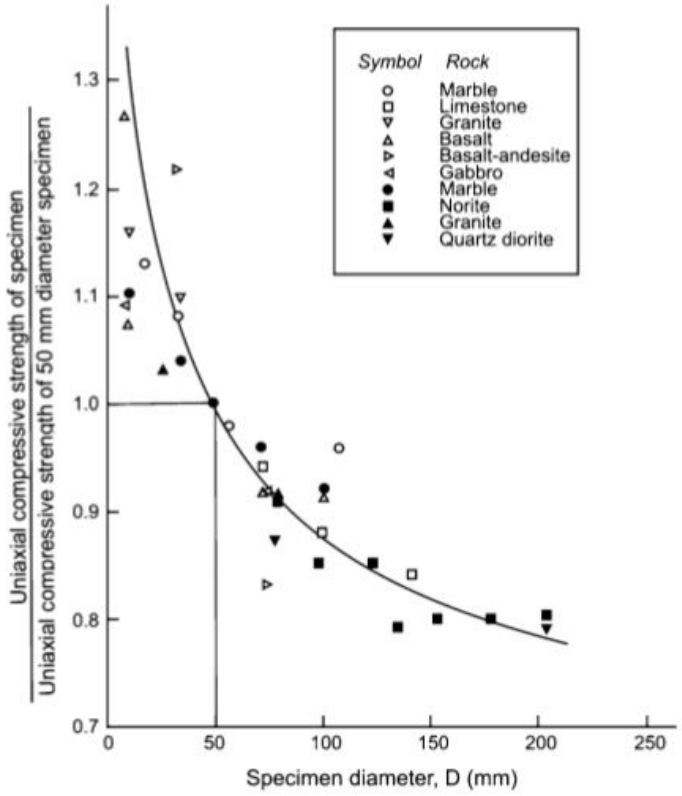

Figure 2.8: Relation between UCS and core diameter after Brown and Hoek (1980)

Next, the conditions in which a sample is tested to obtain the UCS value is critical to measure the correct strength. In the case of a durability investigation the lowest possible compressive strength is most interesting. In general rocks are to a great extent weaker in wet conditions (Palmstrom, 1995). The influence of moisture content on the compressive strength can be significant for certain rock types. Colback and Wiid (1965) detected a reduction of about 50% in strength for saturated quartzitic sandstone and shale. Burshtein (1969) examined the influence of moisture content on the strength of sandstone and observed a reduction in compressive strength of 50% by an increase in moisture content of 4%. Moreover, he spotted a greater reduction in the tensile strength. With a rise of 1.5% in moisture content the tensile strength lessened to one third of its dry value. The reduction was also observed for argillite, yet less extreme. This proposes that the influence on moisture content is dependent on rock type. This is confirmed by Broch (1979), who concluded that the influence of moisture content on strength reduction increases with rising amount of dark minerals, e.g. amphiboles, biotite and pyroxenes, and for increasing anisotropy. Additionally he observed that the greatest reduction of strength occurs within water contents below 25%. Van Eeckhout (1976) investigated the mechanism behind the strength reduction of coal mine shales and concluded that it is caused by expansion and contraction, which lengthens internal cracking, and decrease of fracture energy with increasing moisture

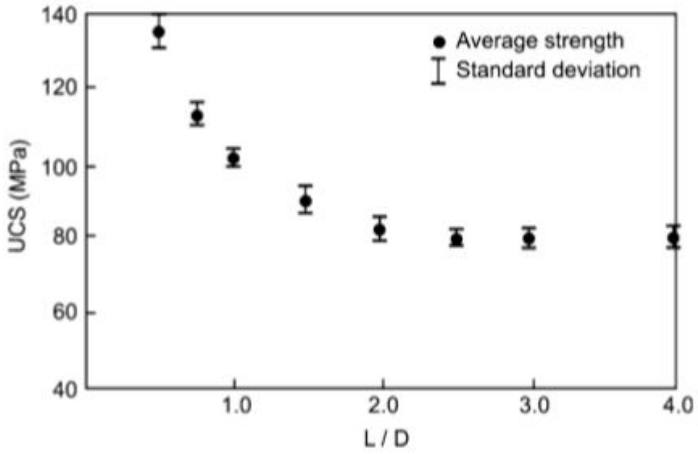

Figure 2.9: Relation between UCS and L/D ratio after John (1972)

content. From this can be concluded that the strength testing conditions should represent the in service conditions and moisture content is a major factor influencing rock strength.

Finally, the orientation of the test sample in the apparatus has an effect if the sample is anisotropic. Anisotropy is common in sedimentary and metamorphic rocks. During strength testing of anisotropic rocks different failure mechanisms have been observed. Tien and Kuo (2001) created a new failure criterion holding two different failure modes for transversely isotropic rocks: (1) a sliding mode in which failure occurs mainly along the discontinuities in the sample, and (2) a non-sliding mode where failure propagates through the rock matrix and the material strength dominates. The orientation of the anisotropy is indicated by angle β. If $\beta$is 0, the layering or schistosity is perpendicular to the compression axes and if $\beta$is 90 parallel. The sliding mode is mainly observed within the β range of 20-50°by evaluating previous research data with the new failure criterion. In this range the minimal compression strength is present, usually around 30-45°. The maximum is often found if $\beta$is 0 or 90°. The predictions obtained with the proposed failure criterion exhibit the three types of anisotropy, namely U type, shoulder type and undulatory type as defined previously by Ramamurthy (1993). Figure 2.10 shows the three types of anisotropy.

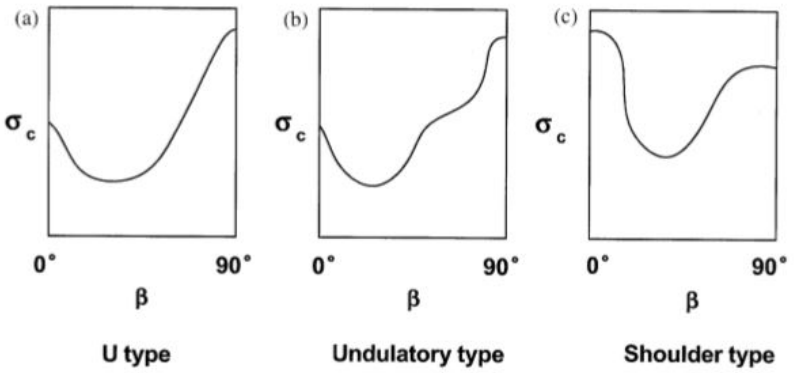

Figure 2.10: UCS versus β after Ramamurthy (1993)

A lot of research has been executed on the correlation between the UCS and Young's modulus with other material properties. A first UCS estimate can be made by a field identification with a geological hammer. Amount of blows, rebound and sound give a first indication of the hardness of the rock. This estimate can be assisted by the strength index obtained with a point load test. Table 2.3 lists the field observations, strength index and UCS recommended by the International Society for Rock Mechanics (ISRM, 1985).

Next to this, the UCS can easily be estimated, using diagrams showing the interrelationship between rock properties. The best known diagram is the relationship between UCS and E_{50} by Deere and Miller

Table 2.3: Determination of uniaxial compressive strength by hand held accessories after Briševac et al. (2016)

Grade	Description	UCS	$I_{s(50)}$	Field identification	Rock types
R6	Extremely strong rock	>250	> 10	Specimen can only be pull apart by a geological hammer	fresh basalt, chert, diabase, gneiss, granite, and quartzite
R5	Very strong rock	100 - 200	4 - 10	Specimen requires many blows of geological hammer to fracture it.	amphibiolite, sandstone, basalt, gabbro, gneiss, granodiorite, limestone, marble, rhyolite, and tuff
R4	Strong rock	50 - 100	2 - 4	Specimen requires more than one blow by geological hammer to fracture it.	limestone, marble, sandstone, and schist
R3	Medium strong rock	25 - 50	1 - 2	Cannot be scraped or peeled with a pocket knife; specimen can be fractured with a single firm blow of a geological hammer.	phyllite, schist, siltstone
R2	Weak rock	5 - 25	-	Can be peeled by a pocket knife with difficulty; shallow indentations made by firm blow with a point of geological hammer.	chalk, rock salt, claystone, marl, siltstone, schist
R1	Weak rok	1 - 5	-	Crumbles under firm blows with point of geological hammer; can be peeled by pocket knife	highly weathered or altered rock, schist
R0	Extremely weak rock	0,25 - 1	-	Indented by thumbnail.	stiff fault gouge
UCS – uniaxial compressive strength [MPa]; $I_{s(50)}$ – strength index [MPa]					

(1966). Such diagrams are only valid for certain rock types or even a range within a rock type.

Additionally to the diagrams, simple regression equations can be applied to estimate the UCS and E values of certain rock types. In these equations UCS and E are dependent variables that depend on other rock properties, the independent variables. These equations are again only valid for certain rock types. Some examples of simple regression equations with porosity as independent variable are listed in table 2.4. It is observed that exponential regression equations are more accurate in determining the UCS and E than linear ones (Briševac et al., 2016). An exception are metamorphic rocks. For these rock types linear regression equations result in a better fit. Although the simple regression equations are easy to use, their dependence on a particular rock type or range within a rock type makes them less convenient.

Multiple regression equations are advanced from the simple regression equations, which use multiple independent variables to predict a dependent variable. Equation 2.12 shows the general form of a multiple regression equation where; Y is the dependent variable, X is the independent variable, B is the contribution of the independent variable and ε is the random error. However, sometimes parameters are used as independent variables, which are not independent (Briševac et al., 2016). For example density and porosity can not be claimed to be independent from each other. Consequently, the correctness of some multiple regression is uncertain and one should always consider is the independent variables are really independent.

New advancements are complex computer models that make use of neural network to estimate UCS and E. Estimates made by these models are the most accurate (Briševac et al., 2016). Nevertheless, a big data cloud for calibration is required before the models give a close approximation.

To conclude, simple techniques of determining the UCS and E are accurate enough in the preliminary stage of design.

$$Y = \mathrm{B}_0 + \mathrm{B}_1 X_1 + \mathrm{B}_2 X_2 + \ldots + \mathrm{B}_k X_k + \varepsilon \tag{2.12}$$

It is now well believed that fracture of brittle solids during uniaxial compression involves nucleation of tensile microcracks from inhomogeneities or flaws within the rock sample, which eventually merge to lead to axial splitting (Huang et al., 2002). The stable growth of these microcracks starts at the onset of dilatancy during uniaxial compression. Therefore, tensile strength is a considerable rock parameter and will be discussed next.

2.6.2. Tensile Strength

It must be highlighted that the amount of research on tensile strength in a durability investigation is considerably less than on uniaxial compressive strength. The UCS is by many engineers considered as

Table 2.4: Uniaxial regression equations with porosity after Briševac et al. (2016)

Equation	Type of rock	Authors
UCS = 183 - 16,55 n	granite	Turgul and Zarif, 1999. [5]
UCS = 74,4 e $^{-0,04\,n}$	sandstone	Palchik, 1999. [6]
E = 10,10 - 0,109 n	porous rocks	Leite and Ferland, 2001. [7]
UCS = 210,1 e$^{-0,821\,n}$ E = 37,9 e$^{-0,863\,n}$	shale, claystone, siltstone	Lashkaripour, 2002. [8]
UCS = 273,1 e $^{-0,076\,n}$	porous chalk	Palchik and Hatzor, 2004. [9]
UCS = 195,0 e $^{-0,21\,n}$	sandstone	Tugrul, 2004. [10]
UCS - unconfined compressive strength [MPa]; E - elastic modulus [GPa]; n - porosity [%]		

the most important rock parameter and probably therefore the amount of research is excessive. Yet, the tensile strength can easily be determined on irregular samples by the point load or on rock disks by the Brazilian tensile strength (BTS) test and relates to many of the discussed degradation mechanisms. Moreover, many of degradation mechanisms, such as degradation by salt crystallisation and slaking, are tensile failure of the rock material. Rocks fail more easily in tensile mode, since the tensile strength of a rock can be an order of magnitude lower than the compressive strength of the same rock. According to Xu et al. (1988), the BTS test is most in favour since the testing procedure and sample preparation are easy and cheap, and is capable of giving a good measure of uniaxial tensile strength. Tavallali and Vervoort (2010) investigated the influence of layer orientation on the tensile rock strength by the Brazilian tensile test. During the test the sample can fail in shear, in tension or in a combination of the both. It was observed that different types of cracks appear during failure, depending on the orientation of the lamination. Fractures propagating through the intact rock material are abundant and fracturing occurs mostly in the centre region of the sample up to a 50° angle between the compression axis and the layer orientation. Fracturing along the laminations, referred to as 'layer activation', gets dominant as this angle increases. The transition from central failure to layer activation occurs when the laminations are in the range of 45-60° with respect to the plates of the test apparatus. Tavallali and Vervoort concluded that as the angle between the laminations and the plates of the Brazilian tensile test device increase, the fracture length and BTS decrease. In addition results showed that there may be a relation between the fracture length within the sample and the BTS. A longer total fracture length corresponds to a higher strength. The tensile strength correlates stronger to the total fracture length than to the inclination of the laminations, so difference in BTS is small for samples with a similar fracture pattern.

2.7. Conclusion

The literature review resulted in understanding about the variety in degradation processes resulting in degradation of armourstones and the importance of construction climate. Not all investigated degradation mechanisms are well captured within the laboratory tests suggested by the standard EN 13383-1:2002.

The importance of tensile strength is neglected within the standard. Yet, several studies have shown that the tensile strength is the limiting strength value considering several degradation mechanisms. Expansion forces by for example swelling of clay seams or crystal growth in the rock pore spaces results in tensile failure through the rock matrix. The tensile strength of rock disks can easily be approached by the indirect Brazilian tensile strength test.

The BTS test is one of the simple testing tools that are needed to investigate the rock behaviour during deterioration and prospect degradation rates. The salt crystallisation by capillary rise test is a simple test which provides aggressive degradation that exceeds degradation observed during the magnesium sulfate soundness test. The Equotip test is simple, cheap and quick to perform, and several studies found relations to rock parameters, such as the UCS, and relations to the deterioration of armourstone. The Equotip is a simple testing tool that is easy to be included into a durability investigation.

The anisotropic arrangements of minerals has great influence on the UCS and BTS. Moreover, swelling behaviour of aligned clay minerals easily results into armourstone degradation when exposed to wet-dry cyclic tests. Execution of laboratory test with various orientations of the laminations into the test setup highlights the influence of the laminations on the minimal armourstone resistance against degradation.

3

Durability Assessment

Both rock properties and engineering conditions must be taken into account during a durability assessment. Figure 3.1 shows a poster created to show the steps to think about and an advised selection procedure during the purchase of armourstones, to reduce the risk on rocks that do not satisfy the durability requirements once in place. The poster is divided into four sections, that each highlights a different aspect during the procedure of acquiring adequate armourstones. Each section will be discussed individually next.

The environmental factors impacting the engineering structure should be determined first before considering the rock parameters. This can be seen in the first section of the poster. The location of the structure determines the stress applied by the environment on the armourstones. For example, deep water constructions, like a scour protection for offshore foundations, are in a constant environment. The main stress applied on the rocks is the force by the ocean currents at these deeper parts, which is relative constant throughout the year. However, the stress is greatly increased when moving towards the tidal zone. Tidal fluctuations, action of waves, temperature fluctuations, evaporation and scour by placing anchors and ship propellers all play a role in this zone. As more processes get involved impacting the armourstone, more stress is applied on the armourstones and thus a higher demand must be set on the durability requirements. Engineering structures may exist in several of the zones and not be limited to one. For example a backfill of a submarine trench will have rocks in deep waters, the tidal zone, wave runup zone and dry zone. Consequently, rocks in one part of the construction are imposed to a greater stress and require a higher durability. Furthermore, armourstone can have a different function within a structure. The trench backfill mentioned before consists of an armour and a filter layer. The filter layer is designed for the hydrodynamic stability, while the armour layer must protect against the strong environmental impacts. This results in different durability requirements for the armourstones. To summarise, the environment of the engineering structure and the function of the armourstone within the structure determine the environmental stress it has to sustain during the lifetime of the construction.

The rock materials are discussed in the second section of the poster. This section is a brief description with some examples of favourable and unfavourable rock characteristics. For example a high density is desirable. A high density only is not a guarantee for a durable rock, but it indicates that the porosity of a rock is probably low and the rock contains stronger minerals. A low degree of weathering is favourable, because the amount of weak, secondary minerals and weak planes within the rock's structure increase upon weathering. This reduces the resistance against the imposed environmental stress. The Rock Manual (CIRIA/CUR/CETMEF, 2007) contains many rock parameters and their influence on the durability of armourstone. Table 3.12 within the Rock Manual is an extensive sheet with rock characteristics divided into 4 classes; poor, marginal, good and excellent. The table is here shown in table 3.1. The table provides a good guideline for the estimation of rock durability. However, the table does not apply for a specific purpose or structure as mentioned in the top of the table and only specifies the rock characteristics. A selection of the criteria from table 3.1 are incorporated in the British standard BS EN13383-1&2.

The third section addresses the importance of combining the environmental conditions, function in the engineering structure and the rock parameters. The appropriate rock characteristics can be

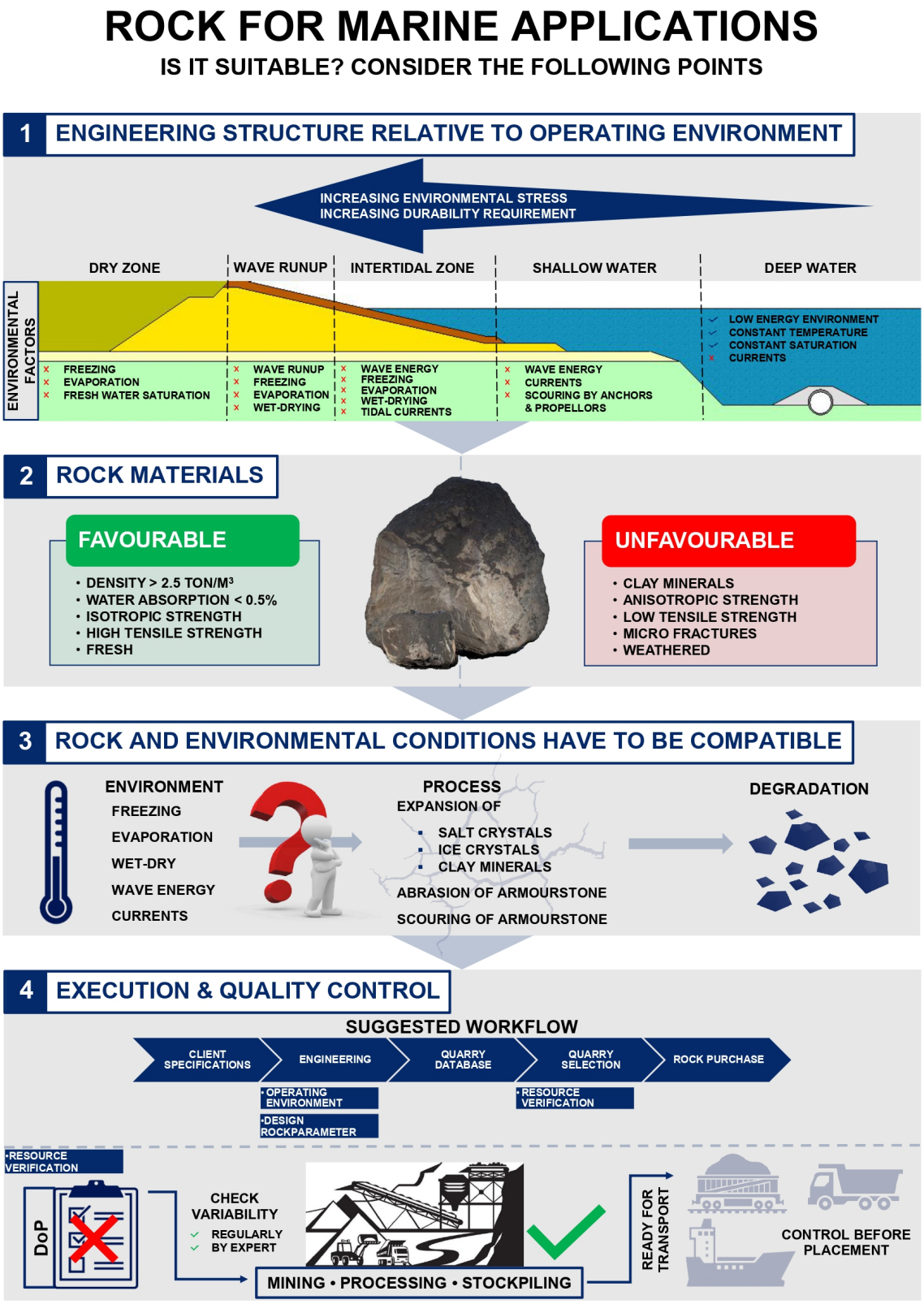

Figure 3.1: Suitability of rock for marine applications. Poster created by Udo Wezenberg and Jelle Spoelstra. The four steps indicate in chronological order the points that need to be considered during the acquisition of durable armourstone.

Table 3.1: Table 3.12 from chapter 3 of the Rock Manual (CIRIA/CUR/CETMEF, 2007). The table contains several criteria that can be considered during a durability assessment. Each criteria is divided in four ranges; (1) Excellent, (2) good, (3) marginal and (4) poor. These ranges indicate the risk on degradation for the specific property.

	Quality and durability guide (not intended for specification purposes)					
	Criteria	Reference	Excellent	Good	Marginal	Poor
Laboratory Tests	Petrographic evaluation	Trained petrographer	**	**	**	**
	Mass density, ρ_{rock} (t/m³)	EN 13383-2:2002	> 2.7	2.5–2.7	2.3–2.5	< 2.3
	Water absorption (%)	EN 13383-2:2002	< 0.5	0.5–2.0	2.0–6.0	> 6.0
	Microporosity/total porosity (%)	Lienhart (2003)	< 2	2–6	6–20	> 20
	Methylene blue adsorption (g/100g)	Verhoef (1992)	< 0.4	0.4–0.7	0.7–1.0	1.0
	Compressive strength (MPa)	EN 1926:1999	> 120	120–80	80–60	< 60
	Schmidt impact index (% rebound)	ISRM (1988)	> 60	50–60	40–50	< 40
	Sonic velocity (km/s)	EN 14579:2004	> 6	4.5–6	3–4.5	< 3
	Point load strength (MPa)	ISRM (1985)	> 8	4–8	1.5–4	< 1.5
	Fracture toughness (MPa.m$^{1/2}$)	ISRM (1988)	> 1.7	1.0–1.7	0.6–1.0	< 0.6
	Indirect tensile (Brazilian) strength (MPa)	ASTM D3967-95a (2004) ISRM (1978)	> 10	5–10	2–5	< 2
	Los Angeles (% loss)	EN 1097-2:1998	< 15	15–25	25–35	> 35
	Micro-Deval (% loss)	EN 1097-1:1996	< 10	10–20	20–30	> 30
	$MgSO_4$ soundness (% loss)	EN 1367	< 2	2–10	10–30	> 30
	Freeze-thaw (% loss)	EN 13383-2:2002	< 0.5	0.5–1	1.0–2	> 2
	Sonic velocity reduced by freeze-thaw (% change) ***	Section 3.8.6	< 5	5–15	15–30	> 30
	Wet-dry (% loss)	ASTM D5313-04	< 0.5	0.5–1	1.0–2	> 2

Note

* breakage rate, B_u, may be estimated visually by counting without weighing or derived accurately by weighing, see Section 3.8.5.1

** no criteria established, see Section 3.3.2

*** provisional criteria needing confirmation from further research

**** D_{i80} = 80 per cent passing *in situ* block size.

selected when the environmental stress applied on the engineering construction is known, in order to reach the desired durability. Each environmental factor will result in a mechanisms exerting stress on the armourstone. These processes apply to certain rock characteristics. This can be illustrated briefly by discussing the construction of a breakwater. Tidal action, wave impact, abrasion, saturation and evaporation all have impact on the breakwater. Each of these mechanisms influences several rock parameters that determine the resistance against the applied stress. For example the evaporation of salt sea water may induce the growth of salt crystals within the rock pore space. The crystal growth depends on the porosity, pore size and connectivity of the pores, while the resistance of the rock to withstand the crystal pressure depends on the tensile strength of the rock. Thus, these rock properties

should be taken into account during the durability estimate regarding the evaporation of salt water. This process should be repeated for all mechanisms to obtain the suitable set of required rock parameters for the construction.

The fourth section highlights the quality control within the quarries to make sure the required armourstone rock properties discussed before are met. Current quality control within quarries is validated by the CE mark and declaration of performance (DoP). The armourstones are tested according to EN13383-1&2 for both documents. However, this does not include variability within the quarries and time. The variability within a quarry should be known for a proper durability assessment. The CE mark suggest a quarry is a factory with a constant product. Nonetheless, quarries are no factories and the products they deliver, change in properties depending on location within the quarry and advancements in time. During quarry visits, this variability can be discovered and the rock parameters can be determined for all applicable rock types present. In addition, the production line and stockpiles should be examined to see how the flows of rock with different properties and durability are separated and handled. These separated rock flows can be examined individually to see if they satisfy the durability requirements set for the engineering construction. In this way the variability within rock properties is known and can carefully be managed to satisfy the rock parameters required to ensure a durability the survives the project lifetime.

4

Sample Acquisition

A quarry visit of two days was executed in January 2019 in order to select appropriate samples for the research. The goal of the visit was to check the production and rock quality of the armourstone within the quarries, which is going to be used as a backfill for a submarine cable trench. The location of the quarries and the project location of Borselle Export Cables are depicted in figure 4.1. Rock samples were collected at each quarry in order to check the rock quality by means of laboratory testing.

4.1. Geological Setting of Quarries

The first quarry visited, was the Hartsteinwerke in Trechtinghausen, Germany. The rock deposits in the quarry originate from the early Devonian, a period from $\pm$393 to $\pm$417 million years ago, and were deposited in a shallow marine to coastal environment. The Devonian is characterised by a dynamic period with several sea level fluctuations. During the Devonian and later Carboniferous two cycles of transgression and regression took place in Northwestern Europe. The changing sea level creates a sequence of alternating rock types on top of each other. During a transgression cycle the sea level rises and the deposited sediments get finer, when a similar geographic location is maintained. As a result, the rock type will gradually change from conglomerate to sandstone to shale to limestone as the sea level rise proceeds. The cycle is reversed during regression. The sequence of alternating coarseness is clearly observed within the Hartsteinwerke, where the rock formation contains a layered structure of altering sandstone, quartzite and shale in a variety of thicknesses. The alternation of sedimentary layers is described in detail by Douw (2009). The layered structure is influenced by the Hercynian orogeny, a phase of mountain-building during the Late Paleozoic. The collision of Gondwana and Euramerika, two former continental plates, creates a compressive force which folds and faults the original straight, layered structure of the sedimentary rock formations. Within the quarry this is observed as a large fold, thrust belt, a system of minor folds and faults and by the low grade metamorphism of the rocks (Douw, 2009). A geological map of the area around the Hartsteinwerke is presented in figure 4.2. The present formations in the area of the Hartsteinwerke are listed in table 4.1. The effect of the change in sea level is clearly visible in the geological map. Adjacent formations of conglomerate, sandstone and slate can be observed on the map. The influence of the Hercynian orogeny can be observed in the cross-section in figure 4.3 where many low angle thrust faults are visible. The presence of the folds and faults result in a large variability in rock type and rock quality on a scale of 10's of meters within the quarry and forms a complex geology within the Hartsteinwerke. The rocks from this quarry are in the report referred to as sandstone to keep the reference clear and simple.

Carrière des Limites was visited after the Hartsteinwerke. The quarry is located in the south of Belgium close to the city Rochefort. The rocks in this quarry originate from the middle and late Devonian. The geology of Belgium is described by Boulvain and Vandenberghe (2018) and is shortly summarised in this section, specified to the area of the in total three quarries visited in Belgium. The southern part of Belgium was subjected to a sea level rise during the middle Devonian (Givetian-Frasnian) $\pm$388 to $\pm$372 million years ago. Barrier reefs formed in the Ardennes, with extensive layered limestones behind barrier islands. These type of limestones are encountered in Carrieère des Limites. During the late Devonian (Famennian) regression took place and marks the

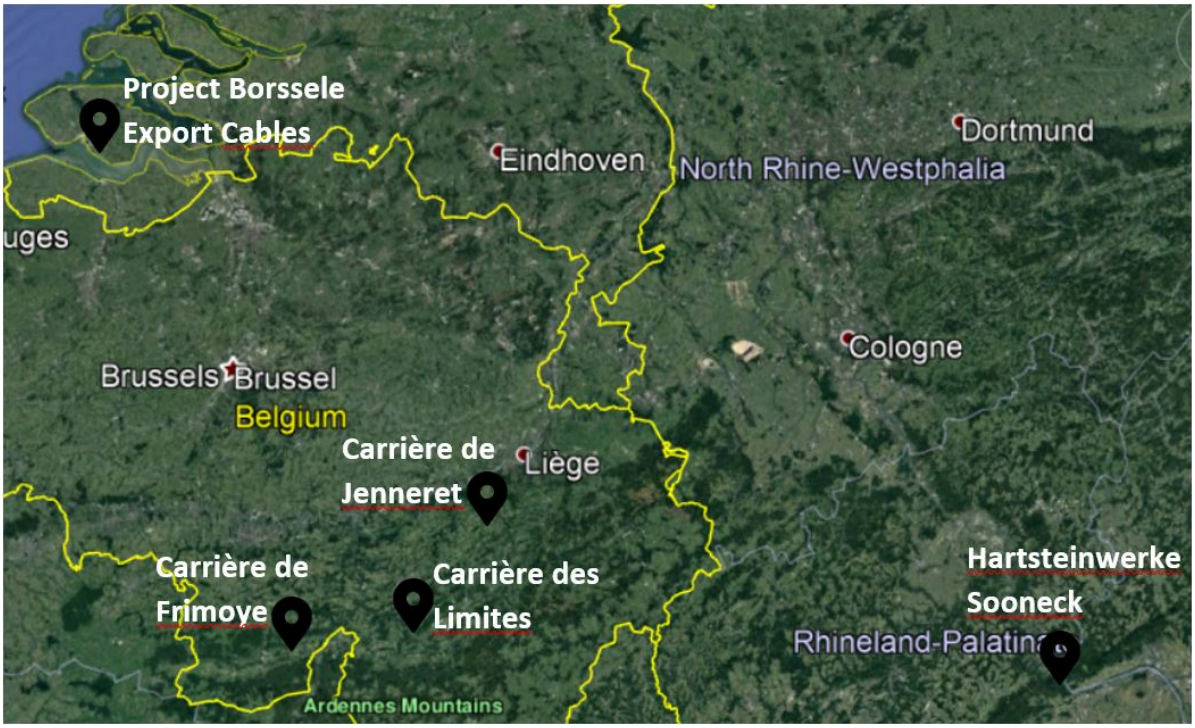

Figure 4.1: Locations of the visited quarries (Google Earth, 2019). The Hartsteinwerke is located 50 km west of Frankfurt, Germany. Carrière des Limites is close the the city Rochefort, Belgium. Carrière de Jenneret is located 25 km south of Liege, Belgium. Carrière de Frimoye is located 35 km south of Charleroi, Belgium

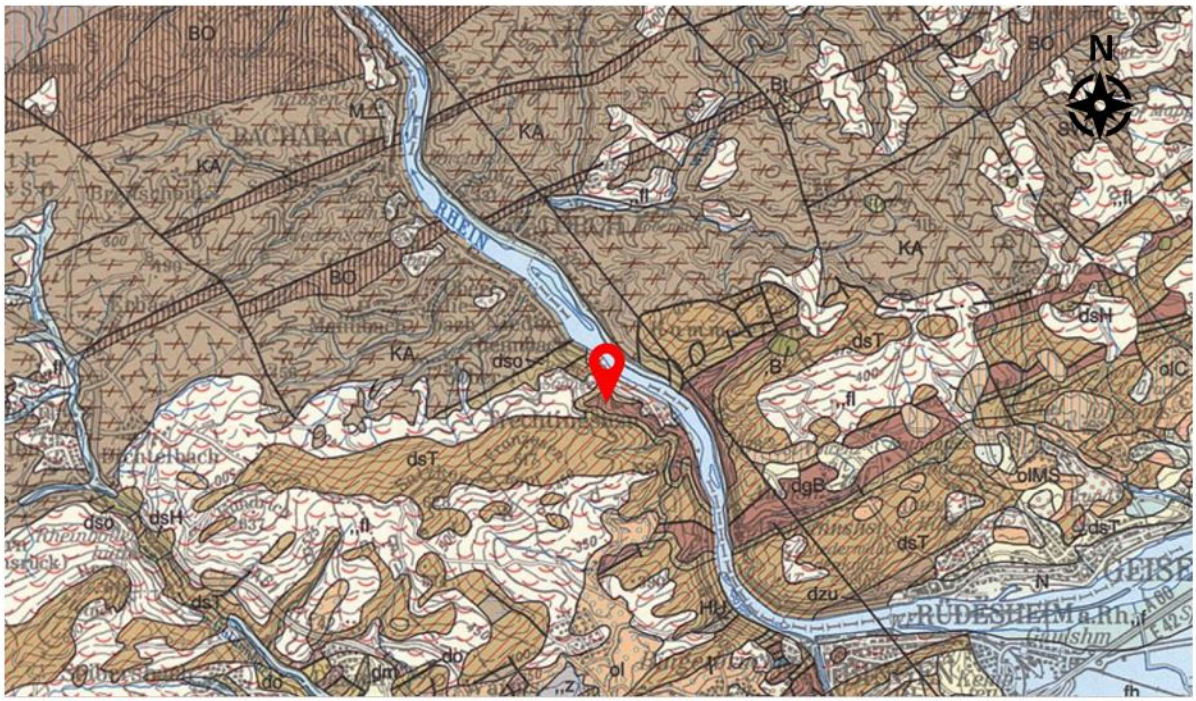

Figure 4.2: Geological map of the area around the Hartsteinwerke, which is located at the red mark (Franke and Anderle, 2001). The straight black line oblique through the centre of the chart corresponds to a cross-section, depicted in figure 4.3. The cross-section extends outside the displayed range of the geological map.

Table 4.1: Legend with description of the geological units present in the area of the Harsteinwerke in the geological map shown in figure 4.2.

Abbreviation	Geological Period		Description depositional environment	Rock/Soil Type	Formation thickness
„fl	Pleistocene		Fluvial deposit	Silt, clayey sand, and gravel	-
dso	Devonian	Upper Siegen/Ulmen	Marine deposit	Slate (black), and Quartzite (white)	ca. 200m
dsT	Devonian	Middle and Upper Siegen	Marine deposit	• Top formation: Quartzite (white) • Bottom formation: Massive Slate (black, grey), and a single Slate (green-grey, red)	Up to 1000m
dgB	Devonian	Gedinne	Estuarine deposit	Slate (red, green), Quartzite Sandstone (red, green, white-grey), and Conglomerate	420-950m

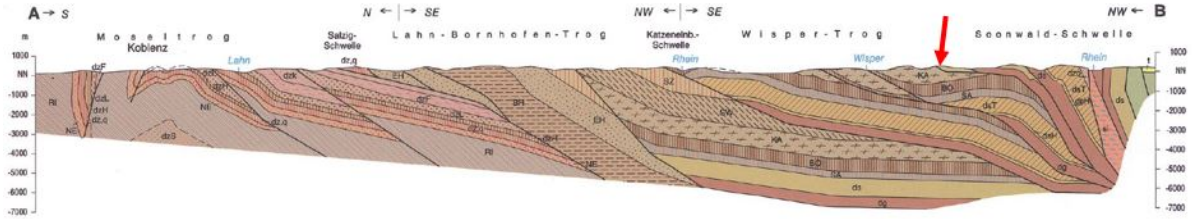

Figure 4.3: Geological cross-section over the area of the Hartsteinwerke (Franke and Anderle, 2001). The location of the Hartsteinwerke is highlighted by the red arrow.

lowest sea level during the Devonian. Consequently, the rock formations shift towards shale and sandstone. Although, only the extensive layered limestones are observed in Carrière des Limites. The geology of Belgium is depicted in figure 4.4 together with the location of Carrière des Limites. The geological map highlights a compression axis from southeast to northwest, resulting from the Hercynian orogeny. The mountain-building era resulted in a sequence of folds in southern Belgium. One of these structures is the synclinorium of Dinant. This is an elongated folding structure which shows an alternation of several anti- and synclines. Carrière des Limites is located in the synclinorium of Dinant, depicted in figure 4.5. The extensive limestones in Carrière des Limites result in a homogeneous armourstone product. The rocks from this quarry are in the report referred to as limestone (Lim).

The rock formations present in Carrière de Jenneret originate from the early Carboniferous (Dinantien) $\pm$359 to $\pm$331 million years ago. These formations consist of limestones, resulting from marine deposits, placed during a period of transgression. A cut off of the basin from the oceans provided anaerobe circumstances and consequently formations of black limestones, because the organic materials are preserved within the rock. The formations are compressed due to the Hercynian orogeny. The compression axis runs roughly from southeast to northwest as shown in figure 4.4. The quarry is also located in the synclinorium of Dinant as can be seen in the cross-section in figure 4.6. Three formations surface within the quarry; the formation of Martinrive, the formation of Longpré and the formation of Terwagne (Roelen, 2017). The formation of Martinrive is a fine grained, black limestone with concentrations of chert nodules and crinoids. Locally the limestone is dolomized. The formation has a thickness of 25 to 30 m. The formation of Longpré contains two distinctive layers. The bottom part is characterised by massive dark limestones. The upper part consists of thick, light grey oölite. The total formation has a thickness of 70-100 m. Finally, the formation of Terwagne consists of a lower dolomite with a fine, grey to black limestone on top. The formation has a thickness of $\pm$ 100 m. The rocks from this quarry are in the report referred to as limestone (Jen).

Carrière de Frimoye was visited during another visit in April 2019. The rock formations are situated

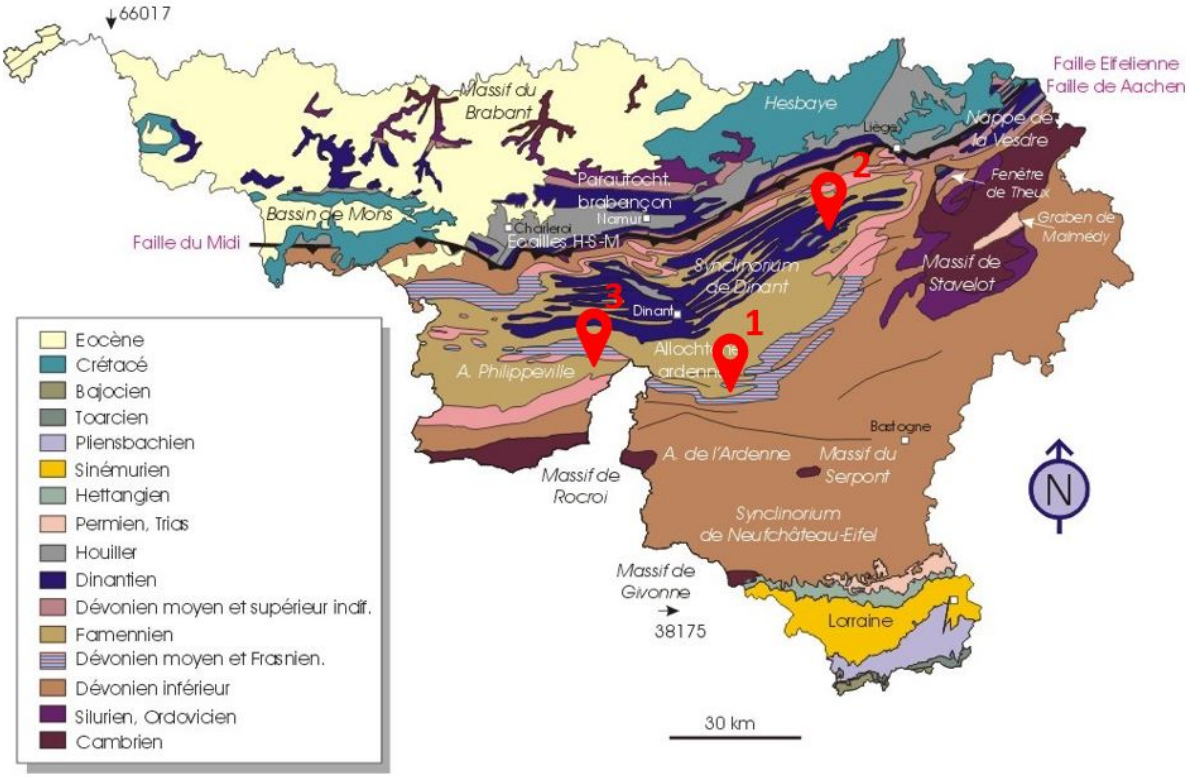

Figure 4.4: Geological map of Belgium after Boulvain and Vandenberghe (2018). The red marks show the location of the quarries visited where; pin 1 is Carrière des Limites, pin 2 is Carrière de Jenneret and pin 3 is Carrière de Frimoye.

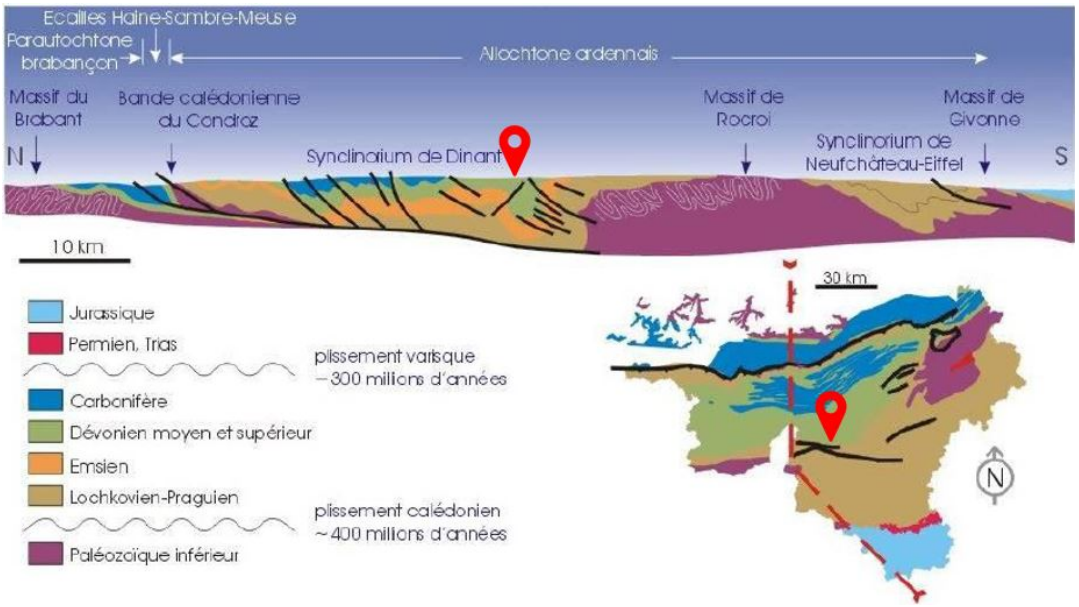

Figure 4.5: Geological cross-section of the area close to Carrière des Limites, which is highlighted by the red pin (Boulvain and Vandenberghe, 2018).

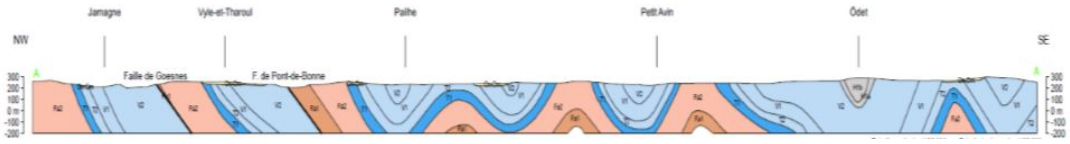

Figure 4.6: Geological cross-section of the area close to Carrière de Jenneret, approximately 14 km west of the quarry (Roelen, 2017). Since the cross-section is parallel to the compression axis of the folds, the cross-section is almost similar to the location of the quarry.

on the same geological structure as Carrière des Limites and Carrière de Jenneret, because this quarry is located in the south of the same synclinorium. The rocks in Carrière de Frimoye have their origin in the middle Devonian (Givetian-Eifelien) $\pm$393 to $\pm$383 million years ago and are mainly limestones. The rock formations originate from approximately the same time frame as the ones mined in Carrière des Limites. The rocks from this quarry are in the report referred to as limestone (Fri).

4.2. Sample Description

The samples from the Hartsteinwerke, Carrière des Limites and Carrière de Jenneret are obtained during the quarry visit. The variability within the armourstone product for project Borselle Export Cables delivered by the visited quarries is covered within the samples. The samples were collected at the exploration faces that will provide the armourstone or at the stockpiles that store temporarily the product for the project. The samples from Carrière de Frimoye were send afterwards.

Aggregate Samples

Four aggregate bags with a total weight of 55.50 $\pm$0.55 kg were collected at the Hartsteinwerke. The aggregate was sampled from the conveyor belt towards the stockpile, sampling the full cross-section of the conveyor belt. The aggregate bags show a mixture of rock pieces changing in colour, structure and degree of weathering as shown in figure 4.7. About 6% of the pieces within each aggregate bags display clear anisotropy, considered to be weaker aggregate pieces. For example a few fragments of chlorite are present. Figure 4.8 presents a selection of these weak lumps.

Three bags of limestone aggregate were sampled from the stockpile in Carrière des Limites. The total sampled weight is 51.25 $\pm$0.15 kg. Within the aggregate sample only small differences can be observed in the rock matrix with the naked eye. The aggregate can be separated into mudstone, wackestone and packstone according to the Dunham's classification. Figure 4.9 displays several pieces tested during this research which originate from Carrière des Limites.

2 bags of aggregate samples with a total weight of 22.30 $\pm$0.1 kg were collected at Carrière de Jenneret. One of the exploration faces of the quarry can be seen in figure 4.12. The depicted exploration face is used to produce armourstone. Other faces within the quarry are mainly used for dimension stone. The aggregate was collected from the stockpile, due to the snow present in the quarry. A few of the pieces contain weathered parts. Breaking the aggregate into small particles resulted in the observation of recrystallised limestone. The selection of the sampled pieces is presented in figure 4.10.

Block Samples

11 block samples were collected with a total weight of 136.85 $\pm$0.55 kg at the Hartsteinwerke. The blocks were obtained from 3 exploration faces, which causes variation between the block samples. 3 of the blocks originate from the face shown in figure 4.11. A shear zone runs through this face. The 3 blocks from this face show a clear layered structure (bedding) and foliation parallel to slightly oblique to the bedding as a result of the shear force. The other blocks show no clear layering and look homogeneous. In all blocks quartz veins are present. Rock cores were drilled from the blocks in the laboratory. The cores in group 1 are drilled from the blocks obtained at the face in figure 4.11 and show a clear bedding and foliation. Group 2 is drilled from the blocks sampled at the other two exploration faces and are homogeneous, dark red cores. A more detailed description of the cores will be given later in the report. Photographs of the cores are listed in Appendix L.

10 block samples were collected from the stockpile at Carrière des Limites with a total weight of 194.40 $\pm$0.5 kg. The exploration face, that was in use during the visit is depicted in figure 4.12. Due to the high amounts of snows during the visit, blocks could not be samples at the face itself. The

Figure 4.7: Example sandstone aggregate pieces from the Hartsteinwerke. The pieces show a variety in colour and degree of weathering to the naked eye. The colours include, light brownish yellow, brownish, light brownish grey and reddish brown.

block samples look all similar, show no major fractures and are homogeneous at the naked eye. Calcite veins are present in most of the blocks. Several cores are drilled from the rock blocks and displayed in Appendix L as well.

From Carrière de Frimoye 12 small block samples were received by post. The exploration face is displayed in figure 4.12. 2 of the blocks show a slightly higher degree of weathering. Most of the blocks present clear calcite veins. Overall, the blocks looked similar at the naked eye. Again the cores can be observed in Appendix L.

4.3. Grading

Armourstones are produced in certain gradings, which are classes that describe the size for armourstones. The production of armourstones always results in a range of sizes due to the fractures in the rock mass and the breaking of blocks by the excavation method. The excavated material is broken and sieved into specific sizes. The size opening of the sieves determines the range of particle sizes within the end product. The size is important for the hydrodynamic stability of marine structures, but has an influence on the durability as well. There are three type of gradings according to the British standard EN 13383; heavy, light and coarse gradings. Heavy gradings consist of large size armourstones used for armour layers and are usually handled individually. Table 4.2 shows the grading requirements from EN 13383, which is a copy of table 3.5 from CIRIA/CUR/CETMEF (2007). For project Borselle Export Cables two gradings are used. One grading is used as filter layer and the other for the armour layer. The filter layer is composed of fine granular material to prevent the underlying material to be piped or washed out by hydraulic forces. The armour layer contains larger rock blocks and is used to protect a structure mainly against hydraulic forces such as wave impact, weathering agents like growth of salt crystals, and additional forces.

The grading requirements include the ELL (Extreme Lower Limit), NLL (Nominal Lower Limit), NUL (Nominal Upper Limit), EUL (Extreme Upper Limit) and M_{em} (effective mean mass). The ELL is the mass below which no more than 5 percent passing by mass is permitted, the NLL is the mass below

Figure 4.8: The photograph presents some anisotropic samples from the sandstone aggregate showing weak planes. All pieces have a clear lamination, resulting in their flaky shape. Many of the pieces split along the weak planes when squeezed between two fingers.

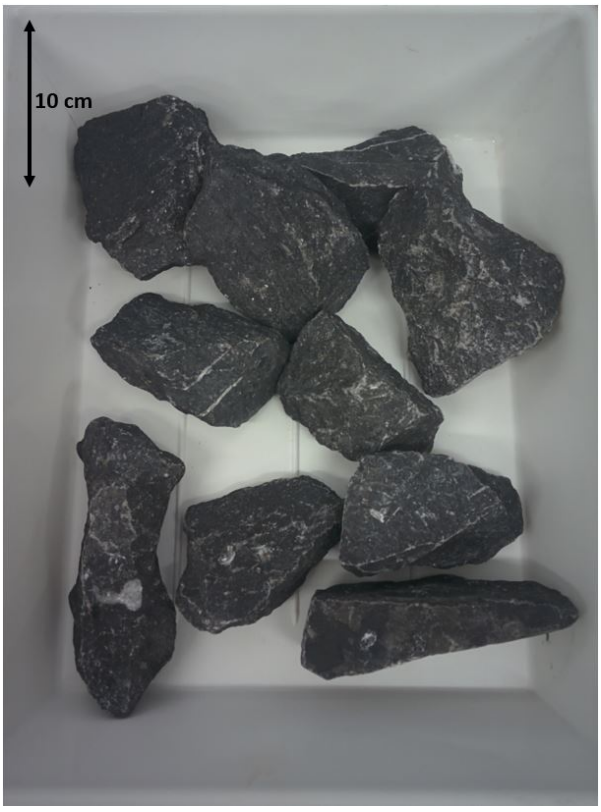

Figure 4.9: Example limestone (Lim) aggregate pieces from Carrière des Limites. The pieces have a similar appearance to the naked eye, except their shape. All pieces are dark grey and have a rough surface. Some of the pieces contain recrystallised bioclasts and/or calcite veins.

Figure 4.10: Example limestone (Jen) aggregate pieces from Carrière de Jenneret. The samples are covered in mud.

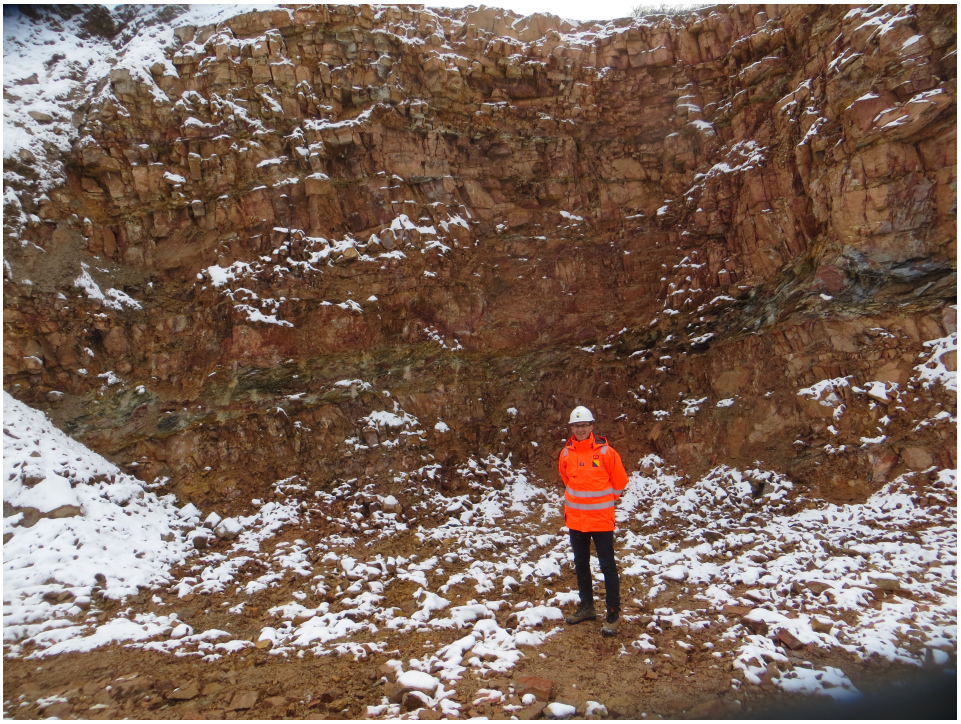

(a)

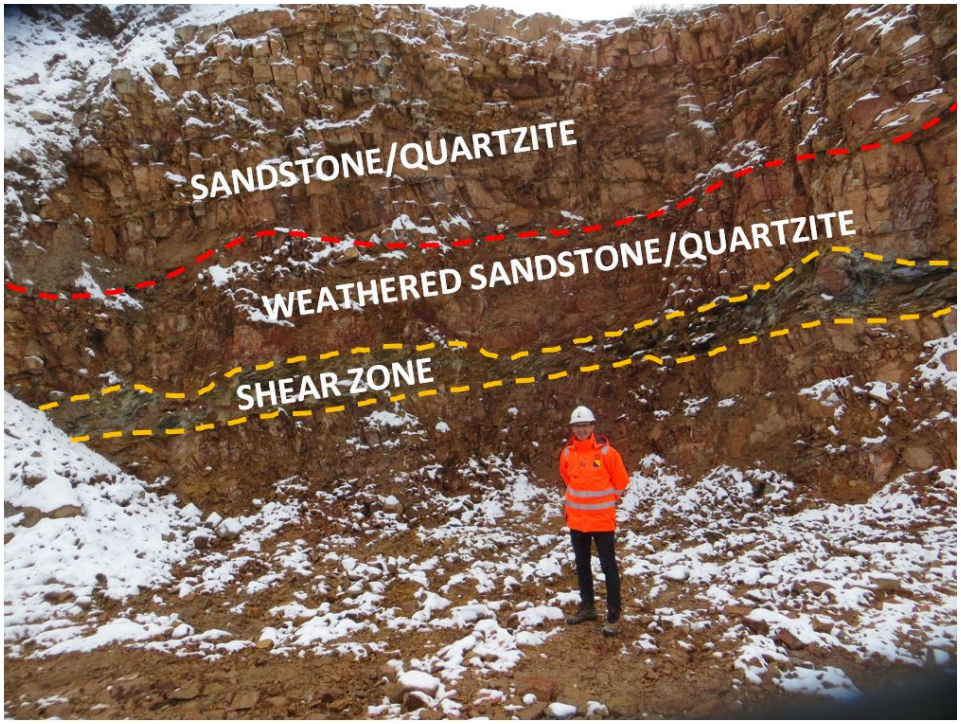

(b)

Figure 4.11: One of the exploration faces within the Hartsteinwerke. 4 block samples are sampled at this location from the rock pile of a blast round. (a) shows the exploration face and (b) highlights the shear zone within the face and the weathered rock parts. The photograph is taken towards the southwest.

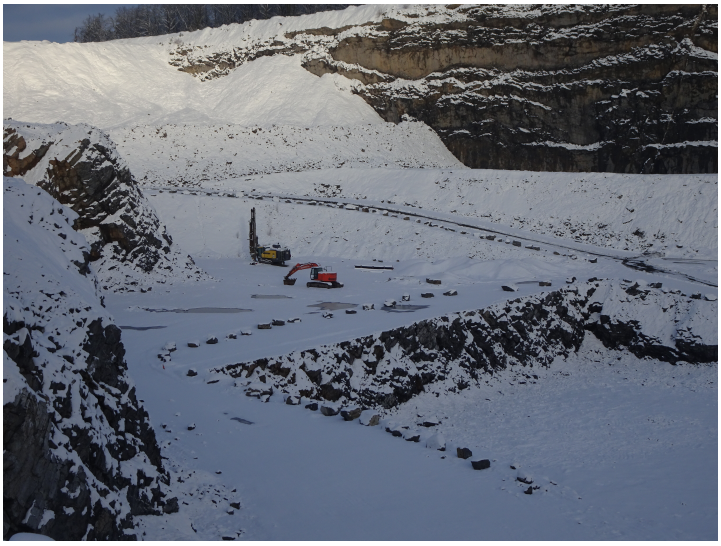

(a) Exploration face in Carrière des Limites.

(b) Exploration face in Carrière de Jenneret.

(c) Exploration face in Carrière de Frimoye.

Figure 4.12: The figure displays the exploration faces (during the visit) of the remaining three quarries. The snow during the first visit limits the view on the exploration faces. The face in Carrière des Limites could not be reached up close due to the high amounts of snow. (a) shows the exploration face of Carrière des Limites (photograph taken towards the northwest from the southern boundary of the quarry), (b) presents the exploration face of Carrière de Jenneret (photograph taken towards the east of the most northern exploration face) and (c) displays the exploration face of Carrière de Frimoye (photograph taken towards the northwest of the northern exploration face).

Table 4.2: Table 3.5 from chapter 3 of the Rock Manual (CIRIA/CUR/CETMEF, 2007) showing the standard grading requirements. These requirements are listed in EN 13383-1:2002 as well.

	Class designation	ELL	NLL	NUL	EUL	M_{em}	
Heavy	Passing requirements kg	< 5% kg	< 10% kg	> 70% kg	> 97% kg	lower limit kg	upper limit kg
	10 000–15 000	6500	10 000	15 000	22 500	12 000	13 000
	6000–10 000	4000	6000	10 000	15 000	7500	8500
	3000–6000	2000	3000	6000	9000	4200	4800
	1000–3000	700	1000	3000	4500	1700	2100
	300–1000	200	300	1000	1500	540	690

	Class designation	ELL	NLL	NUL	EUL	M_{em}	
Light	Passing requirements kg	< 2% kg	< 10% kg	> 70% kg	> 97% kg	lower limit kg	upper limit kg
	60–300	30	60	300	450	120	190
	10–60	2	10	60	120	20	35
	40–200	15	40	200	300	80	120
	5–40	1.5	5	40	80	10	20
	15–300 *	3	15	300	450	45	135

	Class designation	ELL	NLL	NUL	EUL	
Coarse	Passing requirements mm	< 5% mm	< 15% mm	> 90% mm	> 98% mm	< 50% mm
	45/125	22.4	45	125	180	63
	63/180	31.5	63	180	250	90
	90/250	45	90	250	360	125
	45/180 **	22.4	45	180	250	63
	90/180 ***	45	90 ***	180 ***	250	NA

which no more than 10 percent passing by mass is permitted, the NUL is the mass below which no less than 70 percent passing my mass is permitted and the EUL is the mass below which no less than 97 percent passing by mass is permitted. The M_{em} is the mean mass excluding the fragments within a grading. Fragments are considered to be all rock pieces below the ELL. The M_{em} is the bulk mass divided by the number of rock pieces when the fragments are removed beforehand. This number should not be confused with the M_{50}, which is the mass of the theoretical block for which half of the mass of the sample is lighter. Thus, this mass represents the mean mass taking the fragments into account. Theoretically the M_{em} and M_{50} are related based on numerous measurements during various projects in the past (CIRIA/CUR/CETMEF, 2007). The relation is expressed in equation 4.1 and relies on the M_{85} and M_{15}. These are the masses in a grading at which 85 and 15% of the rock pieces have a

lower mass respectively. The equation can be expressed in the NUL and NLL, when using theoretical, idealised curves as shown in equation 4.2.

$$\frac{M_{50}}{M_{em}} = 0.860\left(\frac{M_{85}}{M_{15}}\right)^{0.296} \tag{4.1}$$

$$\frac{M_{50}}{M_{em}} = 0.860\left(\frac{NUL}{NLL}\right)^{0.201} \tag{4.2}$$

The grading requirements from table 4.2 can be expressed in a theoretical grading curve using the inverse Rosin-Rammler equation expressed in equation 4.3 where; y is the fraction passing value, M_y is the corresponding mass and n_{RRM} is the uniformity index. This index describes the steepness of the grading curve according to equation 4.4. A grading curve is a cumulative curve that shows the percentage of rock pieces that pass below a specific size. It visually displays the size of the aggregate pieces in the grading and shows whether the grading has a narrow or wide distribution. The narrow distribution contains mainly aggregate pieces of one size, while a wide distribution is a mix of various sized rock pieces. The armour layer for Borssele Export Cables is a 5-40 kg light material grading. The theoretical grading curve is presented in figure 4.13. The grading requirements from EN 13383 are represented by the coloured bars. The filter layer for Borselle Export Cables is a 32-56 mm grading. This is no standard grading expressed in table 4.2. Instead, the EN 13242 is consulted which is the European standard for aggregates used in hydraulic constructions. Table 2 in this standard determines the grading requirements for the specific 32-56 mm grading for category G_c 80-20. The results are listed in table 4.3. The theoretical size distribution curve, computed with the inverse Rosin-Rammler curve, is presented in figure 4.14. Again, the coloured bars indicate the grading requirements according to the standard.

Table 4.3: Curve limitations to satisfy the sieving curve for Category GC 80-20.

Category GC 80-20	Size (mm)	% passing by mass maximum	% passing by mass minimum
2 D	112	100	100
1.4 D	78.4	100	98
D	56	99	80
d	32	20	0
d/2	16	5	0

$$M_y = M50 \cdot \left(\frac{ln(1-y)}{ln\left(\frac{1}{2}\right)}\right)^{\frac{1}{n_{RRM}}} \tag{4.3}$$

$$n_{RRM} = \frac{log\left(\frac{ln(1-y_{NUL})}{ln(1-y_{NLL})}\right)}{log\left(\frac{NUL}{NLL}\right)} \tag{4.4}$$

There is one major difference between the two distributions of the armour and filter layer. The curve of the armour grading 4-50 kg in figure 4.13 is a mass distribution while the curve of filter grading 32-56 mm in figure 4.14 is a size distribution. For computational purposes the size must be transformed to a mass or the other way around. The relation between mass and particle diameter is stated in equation 4.5 where; ρ_{app} is the apparent density and D_n the dimension of the equivalent cube (CIRIA/CUR/CETMEF, 2007). In other words, the mass of the aggregate is transformed to a perfect cube with sides of length D_n and an apparent density of ρ_{app}. However, the equivalent cube dimension should be corrected to an aggregate piece diameter. Research from Laan (1981) resulted in a factor of 0.84 to convert the equivalent cube dimension into an aggregate piece diameter (D), according to equation 4.6. The grading curves are required for the micro-Deval method, which is going to be discussed in chapter 6.

$$D_{n50} = (M_{50}/\rho_{app})^{\frac{1}{3}} \tag{4.5}$$

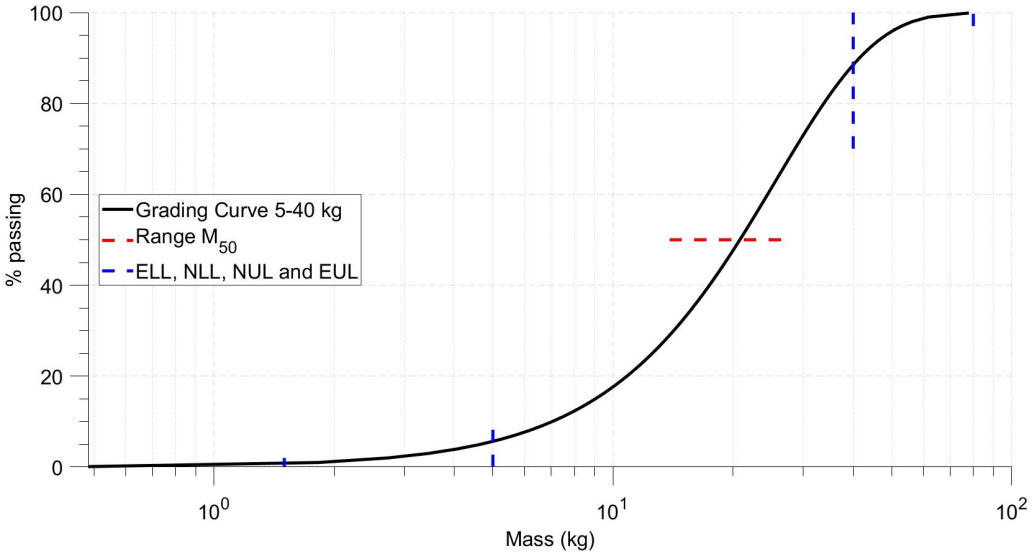

Figure 4.13: Roslin-Rammler curve for the 5-40 kg grading. The coloured bars show the grading requirements set by the EN 13383-1:2002. The reguirements are listed in table 4.2 as well.

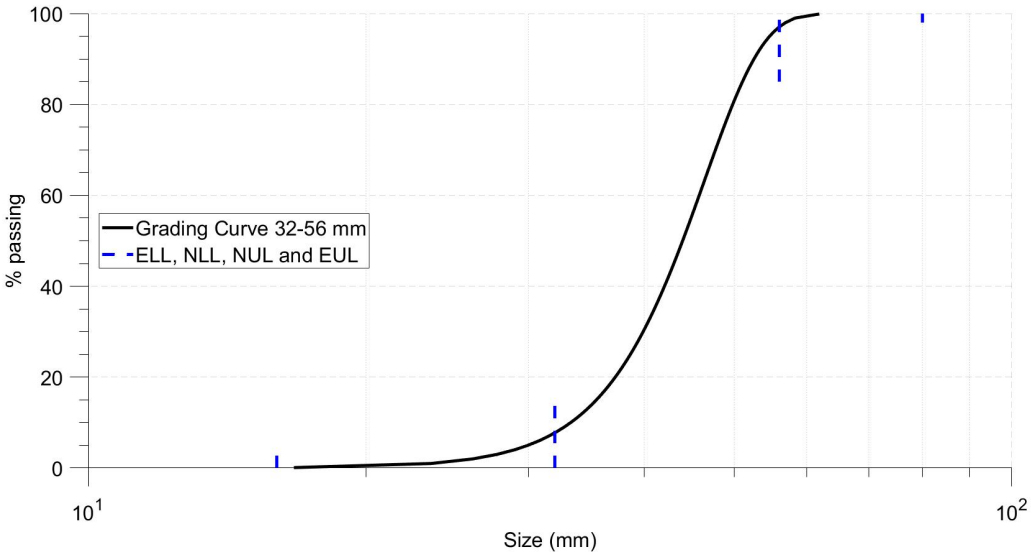

Figure 4.14: Roslin-Rammler curve for the 5-40 kg grading. The coloured bars show the grading requirements set by the EN 13242:2003. The requirements are listed in table 4.3.

Table 4.4: Summary of all collected rock blocks and aggregate available for testing.

Quarry	Hartsteinwerke	Carriere des Limites	Carriere de Jenneret	Carriere de Frimoye
Rock type	Sandstone	Limestone	Limestone	Limestone
Aggregate available for testing	• 55.5 kg aggregate 32-56 mm grading (stockpile) • 11 rock blocks (exploration face)	• 51.3 kg aggregate 32-56 mm grading (stockpile) • 10 rock blocks 5-40 kg grading (stockpile)	22.3 kg aggregate 32-56 mm grading (stockpile)	12 rock blocks

$$D_n = 0.84D \tag{4.6}$$

4.4. Summary

The quarry visits were executed to ensure that the quarries are capable to deliver the requested amount of durable armourstone for project Borselle Export Cables. A quarry inspection should contain the following points to examine the availability of armoustone with the desirable quality. The exploration faces should be inspected to assess the presence of complex geological structures, like folds and faults, which indicate the regional in-situ stress. Moreover, observations in the variability in rock type, variation in degree of weathering, presence of discontinuities and groundwater conditions reveal signals of a variety in armourstone durability between the exploration faces. A desk study before the visit can assist by studying the geological maps and geological history of the area around the quarry. The processing of the blasted rock blocks needs attention during the visit as well. The use of equipment and transport flow of the armourstone need to be understood after a visit. The breaking, sieving and stockpiling of the armourstone should be monitored. Focus should be laid on how rocks with different durability, as a result of natural variation within the quarry, are separated during process flow and how rocks with a too low durability are excluded from the final product. The stockpile areas should be visited to ensure separation of the various products and protect the armourstone against for example streams of water that run down the slopes. Investigate the testing equipment and testing method performed by the quarry, which they use to guarantee an armourstone product of reasonably constant quality. Finally, the quarry must be able to provide the tonnage of armourstone requested in the expected time frame. All sampled armourstone blocks and aggregate available for testing are listed in table 4.4.

The sampled rock blocks and aggregate pieces will be used in this research for several tests. A petrographic analysis into deleterious minerals and structures is going to be discussed in chapter 5 and Appendix A. The method and results of the micro-Deval test will be discussed in chapter 6. The water absorption and density of tens of sandstone and limestone aggregate pieces are going to be determined in chapter 7. The UCS and BTS of the sampled rock blocks will be tested in chapter 8. The Equotip measurements are going to be performed in chapter 9 and the methylene blue adsorption test and methylene blue staining will be listed in chapter 10.

Not all tests listed in EN 13383-1:2002 and the Latham model (Latham, 1991) are executed during this research. The resistance to freezing and testing is not tested. The test is not executed because the resistance to salt crystallisation was tested with the magnesium sulfate ($MgSO_4$) soundness test, see Appendix D. This test provides resistance against the crystallisation within the rock pores and therefore indicates resistance against ice crystallisation as well. Moreover, the $MgSO_4$ soundness test takes less time to perform than a freeze-thaw test. No Sonnenbrand test was executed, because the selected rock pieces for this research do not originate from volcanic rock sources. No fracture toughness test (Franklin et al., 1988) was performed, since the combination of UCS test, BTS test (both performed with various orientations to the anisotropy) and Equotip testing, whose rebound is influenced by the presence of cracks, indicate the behaviour of the present fractures within the armourstone when exposed to increasing stress levels. Moreover, the fracture toughness test is difficult to perform.

5

Petrographic Analysis

A petrographic analysis examines and evaluates optical properties and micro-structural characteristics of rocks using a microscope. It provides a detailed view on the mineral content, internal weathering and textural features within the armourstone. A petrographic analysis gives an understanding of the processes subjected to the rock in time, like sedimentary structures and diagenesis. The analysis is a great tool to identify possibly deleterious structures and constituents. So, a soundness analysis can be performed based on the observations made during the petrographic analysis. The petrographic analysis of this research is performed with assistance of three books; (1) Adams and MacKenzie (1999), (2) Adams et al. (1984) and (3) MacKenzie et al. (2017). These books contain photographs of thin sections from various rock types with explanations about for example the mineral content, micro-structures and possible geological processes that influenced the development of the rock structure.

Thin sections are prepared from the sandstone, limestone (Lim) and limestone (Jen) aggregate. The thin sections are approximately 30 µm thick, uncoated and are stained with Methylene Blue to highlight the active swelling clay minerals. The petrographic observations will be used to understand the behaviour of the rocks during the laboratory tests and to provide a soundness analysis of the rock pieces. The coding of the samples start with HA, LA or JA, which stands for aggregate from the Harsteinwerke, Carrière des Limites and Carrière de Jenneret respectively. The number refers to a specific aggregate piece.

5.1. When should a Petrographic Analysis be Performed

A petrographic analysis is a very useful and detailed medium to obtain understanding about the durability of an armourstone when no additional rock properties are known. For example, it provides an insight into deleterious constituents and structures that have a great influence on the decay of the armourstone's engineering parameters during the in-service life. Nevertheless, the analysis does not give a full understanding of strength, resistance to abrasion and other rock parameters. Therefore, the petrographic analysis should always be accompanied by the durability test as stated within the BS EN 13383-1&2:2002.

Nonetheless, the inverse can be the case. All rock properties tested according to the standard EN 13383-1&2:2002 are known. Is a petrographic analysis still required? The lab tests can be well suited to the engineering conditions, but they do not prospect behaviour of the armourstone in great detail. The result is a number which is classified as excellent, good, marginal or poor. In contrast, the petrographic analysis makes it possible to prospect of the deterioration of the armourstone. The combination of both provides a detailed view in potential degradation and strength classification. The behaviour of armourstones can be understood and estimated with the help of a petrographic analysis when the armourstones are subjected to environmental conditions that vary from the laboratory testing conditions. A petrographic analysis should especially be performed when a quarry shows complex geological structures. The pressure and temperature changes forming these complex structures may alter the minerals within the rocks and change the internal structure of the rock, by processes such as diagenesis, metamorphism and weathering. For example minerals reorientate perpendicular to the principal stress direction during deformation and metamorphism, resulting in anisotropic properties. In

addition secondary minerals can form during weathering by the break down of primary minerals and rock fragments, like micas and chlorite, causing weak concentrations within the rock matrix. Feldspar minerals and micas may have been decayed into non-swelling clay minerals such as kaolinite and illite. Although, these clay minerals have no swelling behaviour, they are weaker than the source minerals and consequently reduce the rock strength and resistance to environmental stresses such as abrasion. The concentrations of these minerals and degree of anisotropy greatly depend on the grade of metamorphism and how much the rocks are affected by weathering. This can very on a metre scale within a quarry. This variability may be not well captured within the standard testing methods, so a petrographic analysis of the mineral composition and geological structures present gives a good indication.

5.2. Soundness Analysis

The important features regarding the durability of the armourstone are evaluated within the thin sections. The observations during the petrographic analysis focus on; mineral content, grain size, grain contacts, grain shape, sorting, homogeneity, porosity, stylolites and MB adsorption. A detailed description of the thin sections is listed in Appendix A. Here some examples will be discussed that could negatively impact the durability of the armourstone.

Figure 5.1 shows a sandstone aggregate sample from the Hartsteinwerke that has been exposed to deformation at a low grade of metamorphism. This has resulted in a preferential orientation of the elongated quartz grains, which can be recognised by the double extinction colours black and white in crossed polar light in figure 5.1b. Micas, which are the elongated grains with the very bright extinctions colours, are orientated in the same direction. Additionally, a system of iron hydroxide filled cracks, the dark lines with red/brownish tints on the edges, run parallel to this direction. These features result in anisotropic rock properties. The UCS and BTS may be considerably lower parallel to the orientation and higher perpendicular. Additionally, the iron hydroxide in combination with the micas and chlorite indicate internal weathering, weakening the rock material. The low amount of contacts between the grains in between the crack filled iron hydroxide and the increase in amount of micas could reduce the resistance against abrasion as well in these domains.

Figure 5.2 displays a coloured concentration due to the MB staining on the thin section of limestone sample LA 1. The dark blue colour could indicate the presence of active clay minerals. The colouring is concentrated to the area around a stylolite, which is a concentration of insoluble material gathered during pressure dissolution within the rock. It cannot be determined if the clay is a swelling clay based on the petrographic analysis only, yet should be combined with the MB adsorption test. The quantity of clay can be estimated within the thin section and the activity by the adsorption test. The activity of an individual clay fraction can be determined by combining the two, which is specific for each clay type. In this way the type of clay mineral can be obtained, which will be presented in chapter 10. A swelling clay, like smectite, concentrated along the stylolite could be deleterious. A stylolite may be a weak plane within the rock's structure, depending on the crystallisation. A poorly crystallised stylolite is a weak plane within the rock matrix, while the strength of a well crystallised stylolite can be similar to the strength of the rock matrix. Repeated swelling of clay minerals around the stylolite, for example during wetting-drying cycles, could result in splitting of the aggregate piece along the stylolite, assuming the clay minerals have swelling behaviour and the stylolite is poorly crystallised.

Figure 5.3 shows pore spaces within limestone (Jen) sample JA 6 because of dissolution of bioclasts. The dissolution results in relative big pore spaces, exceeding 500 µm in diameter, within the sample. The presence of such pores has an effect on the rock's durability, especially when a sample contains high amounts of dissolved bioclasts. The pore spaces provide chambers for the growth of crystals, for example ice crystals during freezing and salt crystals during evaporation. These crystals exert a pressure on the rock matrix. The size of the pores has influence on the crystallisation pressures as described by Benavente et al. (2007) and large free draining pores are not deleterious. The pores within sample JA 6 are not considered large according to the sizes set by Benavente et al. (2007) and are not free draining. However, the pore spaces seem to be completely closed off and cannot be reached by the water. Therefore the pores within JA 6 probably provide no risk on high crystallisation pressures. Nevertheless, if water could reach into these pores, for example through micro porosity, degradation of the limestone sample could be accelerated.

Cracks within a sample could reduce the durability of the rock. An example is presented in figure

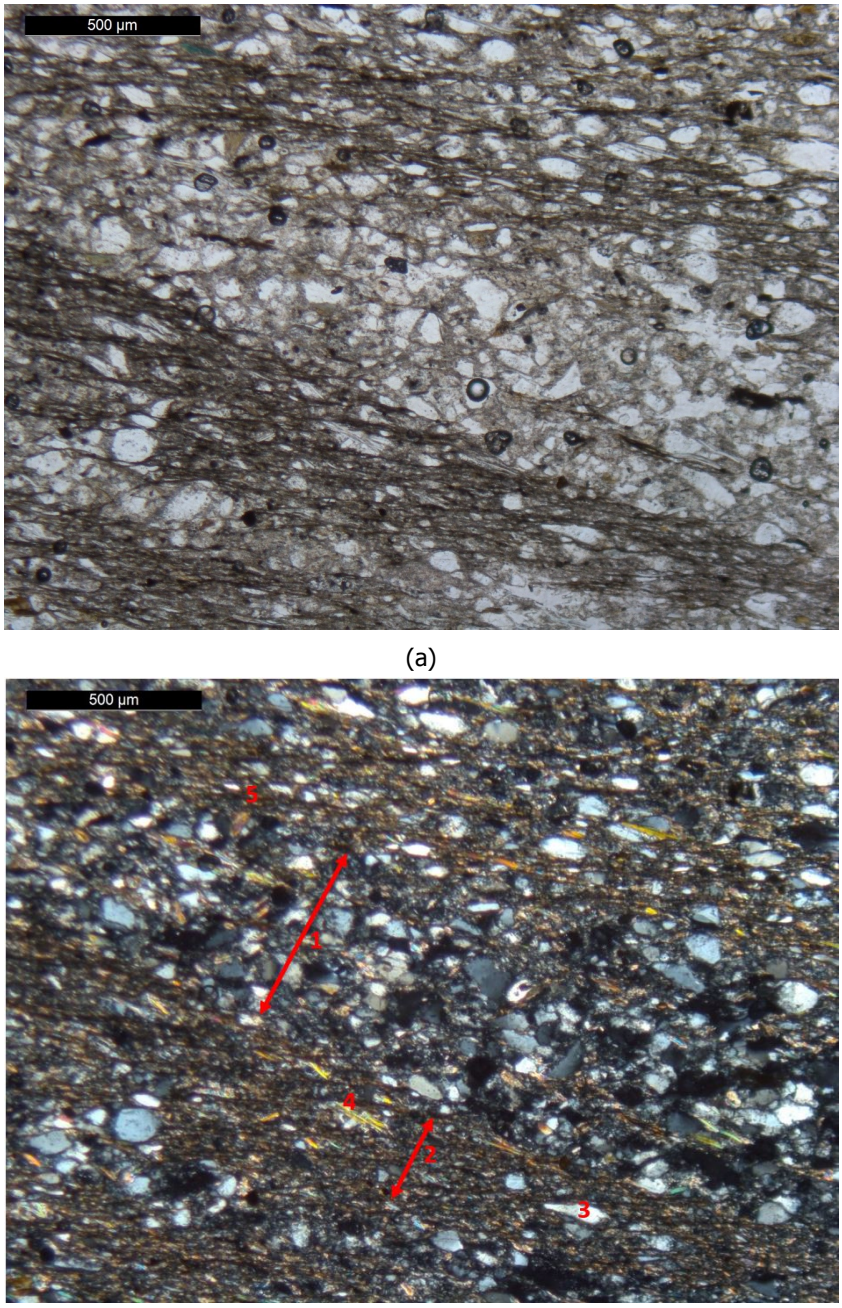

Figure 5.1: Microscopic photograph of sandstone aggregate sample HA 53 from the Hartsteinwerke; (a) taken with plane polarised light and (b) taken with crossed polarised light. The arrows 1 and 2 cross two distinctive domains in the thin section, interpreted to be two sedimentary layers. The domain indicated by arrow 1 contains a high density of quartz grains indicated by the white and black extinction colours under crossed polarised light. The domain pointed by arrow 2 consists of small quartz grains, a higher content of micas and a system of iron hydroxide filled cracks. Point 3 shows an example of a larger elongated quartz grain. The elongated quartz grains are abundant in this thin section, yet most are smaller than the one indicated by number 3. Number 4 is near a group of micas recognisable by their bright extinction colour and elongated shape. Number 5 is on top of a slightly bigger iron hydroxide filled crack which is black in the centre and has red/brownish tint along the its edges.

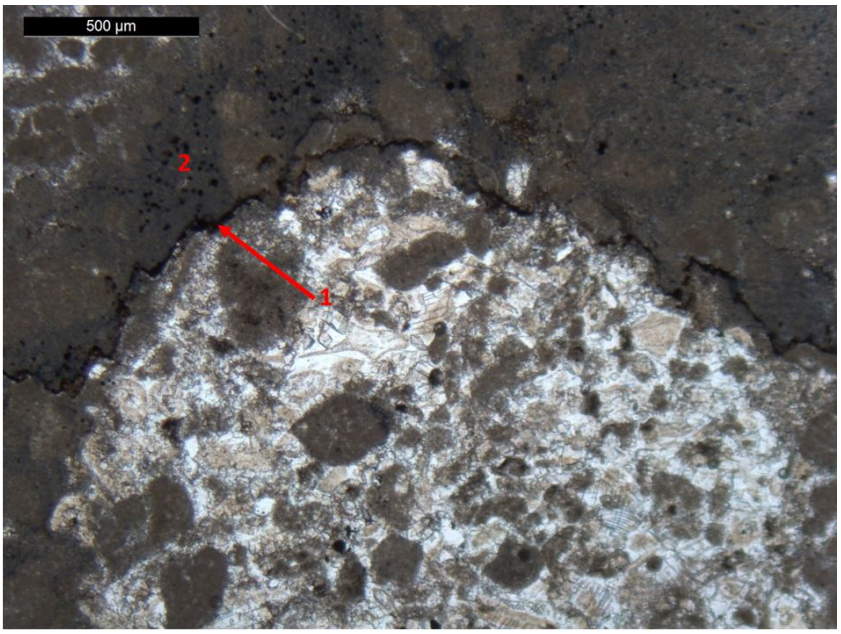

Figure 5.2: Stylolite within limestone sample LA 1 originating from Carrière des Limites. The matrix around the stylolite is coloured blue by the staining with Methylene Blue. Arrow 1 points to the stylolite, which is the boundary between the micrite matrix above and the recrystallised calcite matrix below. Number 2 indicates the blue colour by MB staining of the thin section. The colouring is present in the fine micrite matrix around the stylolite and concentrations of opaque minerals above the stylolite.

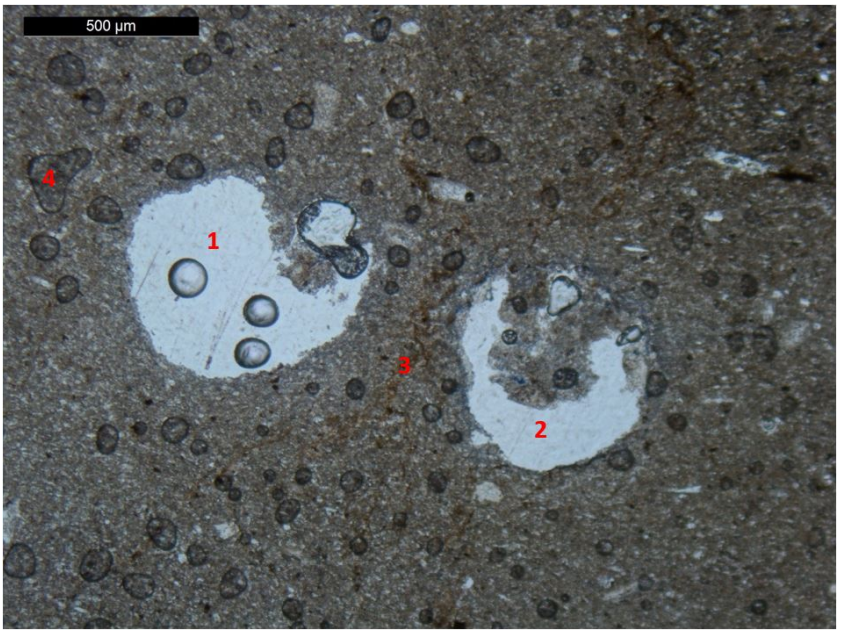

Figure 5.3: Dissolved bioclasts leaving a pore space within limestone sample JA 6 from Carrière de Jenneret. Numbers 1 and 2 are in the pore spaces left by dissolution of bioclasts. Number 3 is on top of iron hydroxide with a red/brownish colour. Some bubbles, as can bee seen at number 4, are present within the thin section. This are small air bubbles within the epoxy of the thin section.

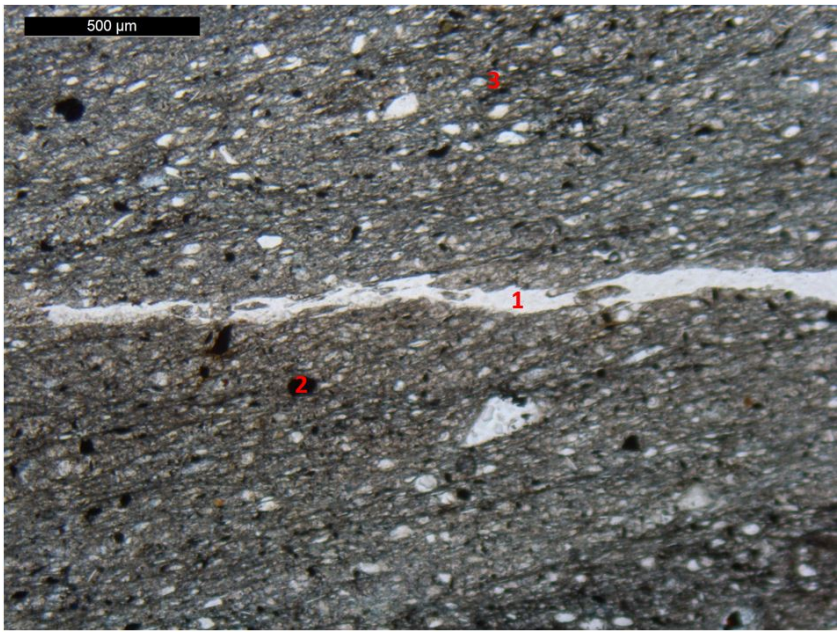

Figure 5.4: Crack within sandstone sample HA 41 from the Hartsteinwerke. The cracks is pointed out by number 1. Some opaque minerals are present in the thin section of HA 41 as well. An example is indicated by number 2. Some iron hydroxide around these opaque minerals is present as can be seen at number 3.

5.4, which is a crack within sandstone sample HA 41. Water inflow through the rock will reduce the material strength and may increases the speed of internal weathering. The crack in sample HA 41 is approximately 80 µm thick and 3 mm long. Only one crack is seen within the thin section. Tiny cracks can grow and connect when exposed to stress, reducing the rock strength. The sample's durability can be greatly influenced by the cracks if more of them are present within the entire sample.

Elongated fragments, such as bivalves, can be aligned along the orientation of the bedding during deposition as can be seen in figure 5.5. The rock could split more easily along the bedding when cementation between the particles is not well developed. The bioclasts in sample LA 2 are fully recrystallised, which makes crystallisation of e.g. salt crystals impossible within the fragments. Tensile forces could be aligned normal to the bedding by crystallisation in pore spaces of partly to fully disolved bioclasts. Consequently, the sample may fail easily along the bedding in tensile fashion.

5.3. Discussion & Conclusion

Some of the analysed thin sections are expected to perform less in function compared to other tested rock pieces. Several of the sandstone samples contain an anisotropic structure, secondary minerals and presence of iron hydroxide as shown in figure 5.1. The anisotropy and secondary minerals, due to the low grade metamorphism, may result in a weaker characteristic and more rapid degradation in construction. Some of the limestones are anisotropic due to the alignment of bioclasts along the former direction of the bedding, while others have pore spaces resulting from dissolution of the bioclasts. Both features can influence the durability of the armourstone, depending on for example the bonding of the cement to the bioclast fragments. None of the thin sections studied during the petrographic analysis have a high porosity. Present pores within the rock matrix are enclosed by cement and seem to be non reachable, so permeability is even lower. The amount of cracks within the thin sections is very low and limited to tiny, isolated cracks in a few of the samples. Overall, most of the samples are expected to have a proper characteristics to sustain the engineering lifetime. Only, the durability of the weathered, anisotropic sandstone samples is questionable.

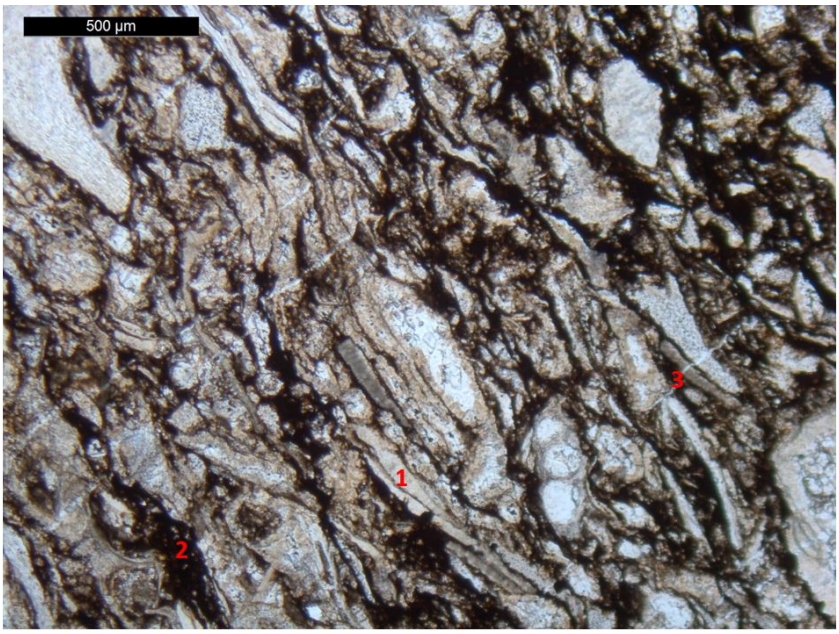

Figure 5.5: Alignment of bioclasts in the thin section of limestone sample LA 2 originating from Carrière des Limites. The elongated bioclast are closely packed and orientated in a similar direction as presented by number 1. Many of the bioclasts are tiny shell fragments, which is the case at 1. Spaces between the bioclast fragments are mainly filled with iron hydroxide, recognised by the dark colour and red/brownish tint along the edges. Number 2 presents an example of the iron hydroxide. A system of tiny recrystallised cracks runs perpendicular to the bioclasts in the thin section. One of these recrystallised cracks crosses number 3.

6

Micro-Deval

6.1. Micro-Deval Test

6.1.1. Test Method

The micro-Deval test is executed according to EN 1097-1 (1996) and indicates the resistance against abrasion. To prepare the test samples, aggregate particles are crushed with a jaw crusher and sieved to fall within the 10-14 mm range. The 10-14 mm range is then sieved on a 12 mm sieve in order to create a 500 g sample of which $\pm$35% passes the 12 mm sieve. The weight of the sample and the fraction that passes the 12 mm sieve are listed in table 6.1. This sample is loaded in a drum together with 5 kg of steel balls and 2.5 L of water. Two of these drums are prepared and loaded into the micro-Deval apparatus, depicted in figure 6.1. The apparatus rotates the drums, which results in an impact force from the steel balls onto the aggregate particles. Consequently, small chips break off the surface, grinding the edges of the rock particles. The drums are rotated for 12000 rotations at a speed of 100 rotations per minute, after which the material is sieved on a 1.6 and 8 mm sieve. The material retained on the sieves is weighted and referred to as m. The micro-Deval coefficient is calculated according to equation 6.1.

$$M_{DE} = \frac{500 - m}{5} \tag{6.1}$$

6.1.2. Results and Discussion

The results from the micro-Deval test are listed in table 6.2. The total lost weight consists of all rock material passing the 1.6 mm sieve. The micro-Deval coefficients of the sandstone drums are the same for both drums, although the distribution between the two sieves is different. For the second drum a larger amount is retained on the 1.6 mm sieve, yet a smaller amount on the 8 mm sieve. Larger chips broke of the rock fragments in the second drum, resulting in a higher catch on the 1.6 mm drum. For the limestone (Lim) a similar trend is observed, however this time the amount of particles from drum 1 retrieved on the 1.6 mm sieve is larger and on the 8 mm sieve lower. The total lost weight for the limestone (Lim) is larger than the total lost weight for the sandstone. Consequently, the M_{DE} coefficient is higher for the limestone (Lim). The amount of material caught by the 1.6 mm sieve is almost identical for the third sample, the limestone (Jen), but more material is left on the 8 mm sieve for drum 2. Consequently, there is a small difference between the micro-Deval coefficients of the two drums. The total lost weight of the limestone (Jen) is only slightly higher than of the sandstone with a difference of 5-10 g. As a result, the micro-Deval coefficient of the limestone (Jen) is almost identical to the coefficient of the sandstone.

The abrasion rate is controlled by the weakening influence of water on clay minerals rather than breakage along fresh surfaces within the mineral fabric (Latham, 1993). Thus, the amount of clay minerals within the sample mainly determines the abrasion loss. The amount of clay minerals is investigated with the petrographic analysis and methylene blue adsorption test on the aggregate. The micro-Deval results agree with the observations of the petrographic analysis and results obtained with the MB adsorption test, which will be discussed in chapter 10. About 95% of the sandstone aggregate

Figure 6.1: The micro-Deval apparatus. The apparatus contains two rotating drums, referred to as drum 1 and drum 2 in table 6.1 and 6.2, that run simultaneously during the test.

Table 6.1: Weights and grading of samples at start of micro-Deval Test. The aggregate that is inserted into the drums needs to satisfy a certain size distribution according to EN 1097-1:1996. Therefore, the 12 mm sieve is placed on top of the 10 mm sieve and below the 14 mm sieve. In this way it is controlled that an amount of ±30-40% of the ±500 g aggregate (10-14 mm) passes the 12 mm sieve.

Sample	Drum	Retained on 10 mm sieve	Retained on 12 mm sieve	Total Weight	% passing 12 mm sieve
Sandstone	1	175.19 g	326.16 g	501.22 g	35.0 %
	2	175.06 g	324.91 g	499.97 g	34.9 %
Limestone (Lim)	1	175.86 g	324.96 g	500.82 g	35.1 %
	2	174.60 g	325.18 g	499.78 g	34.9 %
Limestone (Jen)	1	174.96 g	324.60 g	499.56 g	35.0 %
	2	174.88 g	325.20 g	500.08 g	35.0 %

is the strong quartzite seen in the thin section presented in figure A.10. The high quartz content, interlocked contacts between the grains and very low amount of clay result in a high resistance against abrasion. Furthermore, the MB adsorption is low with a V_B of 0.22 g/100g clay. The clay content within the limestone (Lim) is higher than within the sandstone. Concentrations of clay increase the material loss during abrasion and are mainly concentrated around stylolites within the limestone (Lim), as seen during the petrographic analysis. In addition, the MB adsorption is higher for the limestone (Lim) with a V_B of 0.35 g/100g clay. Based on these observations the micro-Deval coefficient is expected to be higher for the limestone (Lim), which is the case. The limestone (Jen) has a micro-Deval coefficient close to the sandstone. The thin section of the limestone (Jen) shows no indication of concentrations of clay minerals. The MB adsorption test obtained a V_B of 0.15 g/100g clay. As a result a lower micro-Deval coefficient is expected for the limestone (Jen) than for the limestone (Lim), which is validated. The amount of clay minerals, according to the MB adsorption test, is lower for the limestone (Jen) than for the sandstone. However, the micro-Deval coefficient is slightly higher than for the sandstone. This is expected to be caused by the difference within the rock fabric. The limestone contains a higher amount of fine cement, which is recrystallised carbonate mud. The recrystallised cement has more defects than the strong interlocked quartz grains within the sandstone. Consequently, the micro-Deval loss increases for the limestone (Jen). The decrease in clay content and increase in defects within the rock's matrix result in an almost similar MD coefficient.

Table 6.2: Results of the micro-Deval tests and the M_{DE} coefficient. The micro-Deval coefficient is the mass loss percentage of the material that has passed the 1.6 mm sieve after 12000 revolutions in the micro-Deval apparatus.

Sample	Drum	Retained on 1.6 mm sieve	Retained on 8 mm sieve	Total Weight Retained (1.6 mm + 8 mm)	M_{DE}
Sandstone	1	3.62 g	427.50 g	431.12 g	14 %
	2	9.78 g	419.76 g	429.54 g	14 %
Limestone (Lim)	1	16.54 g	369.28 g	385.82 g	23 %
	2	11.62 g	374.39 g	386.01 g	23 %
Limestone (Jen)	1	4.73 g	416.81 g	421.54 g	16 %
	2	4.11 g	420.93 g	425.04 g	15 %

6.2. Micro-Deval Method

6.2.1. Method

The MDE method is a degradation model, described in chapter 2 section 2.3, that uses the M_{DE} coefficient to create a mass loss curve. Figure 6.2 displays the curves obtained with the MDE model for the sandstone, limestone (Lim) and limestone (Jen). The x-axis shows the time in 1000s of revolutions within the micro-Deval apparatus while the y-axis shows the mass loss relative to M_0, which is the initial mass of the aggregate piece before exposed to abrasion. A higher micro-Deval coefficient results in a more rapid decrease in mass following the MDE method. This is clearly visible for the tested aggregates, as the curve of the limestone (Lim) shows a rapid decline in the early stages compared to the sandstone and limestone (Jen). The limits of the four categories, poor, marginal, good and excellent, set by Lienhart (1998) are displayed as well. Both the sandstone and limestone (Jen) fall within the good category, while the limestone (Lim) falls within the marginal category. The plot in figure 6.2 can be evolved into a time scale with the years in construction. This is done by multiplying the x-axis with factor X, which is a product of the factors X_1 to X_9. The factors are all listed in table B.2 in Appendix B. The time scale will be scaled according to the construction environment at the project location of Borselle Export Cables. The trench backfill consists of a 32-56 mm sandstone filter layer and a 5-40 kg limestone armour layer. Several of the parameters X_1 to X_9 change with grading or rock type. Therefore, the factor X will vary between the sandstone filter layer compared to the limestone armour layer. In addition, some of the parameters depend on the location/function within the construction. So, several factors X will be computed to transfer the mass loss curve in 1000s of rotations to years in construction for the applicable combinations. The factor is not calculated for the limestone (Jen), since the quarry supplying these rocks is disregarded for project Borselle Export cables. Thus, these rocks will not be used in the construction.

The first parameter X_1 describes the effect of the size of the armourstone. The effect is given by equation 6.2. The size of the armourstone has an influence on its durability. Larger blocks have a smaller surface compared to multiple smaller blocks. The rock block is less vulnerable to certain types of erosion, like abrasion due to the lower surface area. The M_{50} for the armour layer is 0.015 tonnes and $0.13 \cdot 10^{-3}$ tonnes for the filter layer. The corresponding ratings are 0.12 and 0.025.

$$Rating = 0.5 \cdot (M_{50})^{\frac{1}{3}} \tag{6.2}$$

The next parameter is the grading factor X_2. The rating is based on the ratio between the M_{85} and M_{15}, which are the masses at a passing rate of 85 and 15% in the sieving curve respectively, and is stated in equation 6.3. A high ratio between the two represents a wide or well graded grading. Contrarily, a low ratio indicates a narrow graded grading. The grading has effect on the packing and porosity of bulk-placed materials and on the behaviour such as filtering and piping. The M_{85} and M_{15} are 48 kg and 8.7 kg for the limestone. The ratio between diameters is used for the sandstone, because the diameter ratio is the same as the weight ratio as a result of the theoretical conversion (see chapter 4 section Grading). The D_{85} is 51 mm and the D_{15} is 35.5 mm. Consequently, the score is 1.76 for the limestone (Lim) 5-40 kg grading and 1.13 for the sandstone 32-56 mm grading, resulting in a rating of 1.0 and 1.2 respectively.

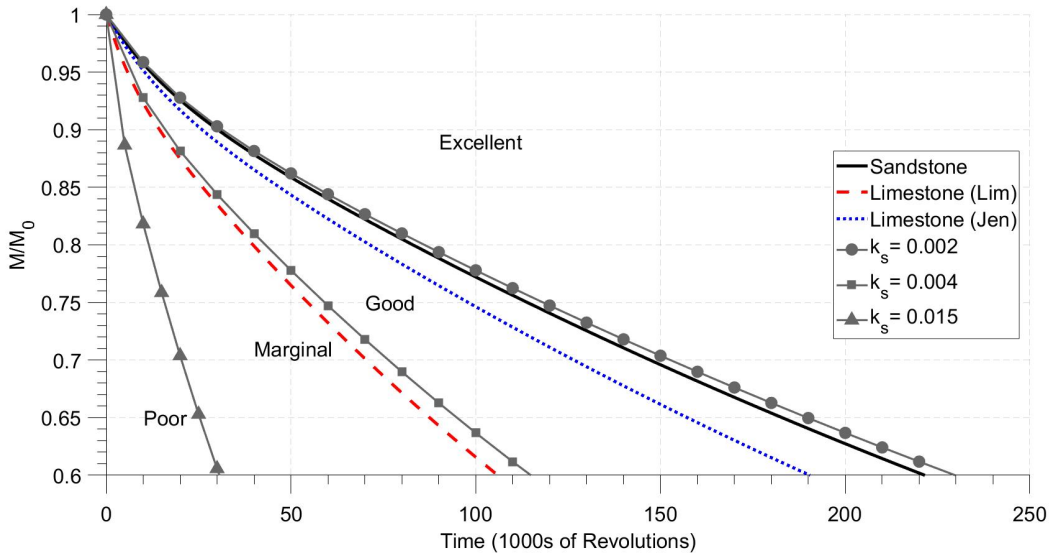

Figure 6.2: The mass loss curve of the sandstone, limestone (Lim) and limestone (Jen) aggregate based on the MDE method. The grey lines represent the boundaries set by Lienhart (1998), dividing the range into the four durability classes; poor, marginal, good and excellent. k_s is the rock fabric strength depending on the micro-Deval coefficient according to equation 2.3. The sandstone and limestone (Jen) fall within the good category, while the limestone (Lim) falls within the marginal category.

$$Score = \left(\frac{M_{85}}{M_{15}}\right)^{\frac{1}{3}} \tag{6.3}$$

The third parameter X_3 takes the angularity of the armourstone into account. The angularity of the block influences the interlocking of the pieces of armourstone into each other. The higher the angularity of the rock piece the better the interlocking between the armourstones. The 5-40 kg limestone armour blocks are blocky, while the 32-56 mm sandstone aggregate is angular. The corresponding ratings are 1.1 for the armour layer and 1.0 for the filter layer.

The parameter X_4 is a rating influenced by the significant wave height and the drop test breakage index (I_{M50}) and describes the impact of waves on the armourstone. The significant wave height is the mean wave height of the highest third of the present waves. The height is measured from crest to trough, which are the highest and lowest point of a wave. The significant wave height varies with location and time, but overall show the historical data of the ministry of infrastructure and water management a significant wave height below 4 m for the North Sea close to Borselle. The I_{M50} is not determined for the armourstones used in Borssele due to their relative small size. Therefore, an estimate is made on the I_{M50}. Most physical properties of the sandstone and limestone fall within the excellent or good class (Latham et al., 2006). So, the I_{M50} is selected to fall within the good category of 2-5%. This results in a rating of 2.6 for parameter X_4.

The fifth parameter X_5 describes the impact of the zone within the construction. As discussed before, the environmental stress on armourstones varies with location in the construction. For the trench backfill in Borssele multiple zones are of interest, since the trench runs from a offshore wind farm to the coast. Consequently, the armourstone will be used in a supra-tidal, inter-tidal and submerged zone. The climate in Borselle is temperate, resulting in a rating of 8, 1 and 10 for the three zones respectively.

The next parameter X_6 takes more climate factors into account, the MCWI index of Lienhart (2003). The MCWI is computed according to equation 6.4 where; a is the range between the mean maximum and mean minimum temperature, b is the mean annual temperature, c is the mean number of days with a temperature above 0 °C, d is the mean number of days with a temperature equal to or below 0 °C, e is the range between the extreme minimum and maximum temperature, f is the mean number of days with a precipitation above 0.25 mm, g is the annual precipitation in cm and h is the total normal degree-days with a base temperature of 18 °C. The weather data of the KNMI weather station

Table 6.3: Parameters X_1 to X_9 and final conversion factor X for the MDE method. The parameters and conversion factor vary for the rock type, because the sandstone is a filter layer and the limestone is an armour layer. Consequently the environmental stress exposed to the rock types differs. The parameters and conversion factor vary for the different regions (e.g. supra-tidal and inter-tidal) as well, again as a variation in the exposed stress to the armourstone.

Parameter	Limestone 5-40 kg Armour Layer			Sandstone 32-56 mm Filter Layer		
Zone	Supra-tidal	Inter-tidal	Always Submerged	Supra-tidal	Inter-tidal	Always Submerged
X_1	0.12	0.12	0.12	0.025	0.025	0.025
X_2	1	1	1	1.2	1.2	1.2
X_3	1.1	1.1	1.1	1	1	1
X_4	2.6	2.6	2.6	2.6	2.6	2.6
X_5	8	1	10	8	1	10
X_6	1.4	1.4	1.4	1	1	1
X_7	1	1	1	1	1	1
X_8	1.8	1.8	1.8	1.8	1.8	1.8
X_9	2	2	1.5	2	2	1.5
X	13.84	1.73	12.97	2.25	0.28	2.11

Vlissingen of the year 2018 are used to compute the MCWI at this location. The MCWI at Vlissingen is only 0.74. The values of the factors a to h can be found in table B.1 in Appendix B. The water absorption is 0.24% for the limestone (Lim) and 0.79% for the sandstone. As a result the rating for X_6 is 1.4 for the limestone and 1.0 for the sandstone.

$$MCWI = \frac{a}{b} \cdot \frac{d}{365} \cdot \frac{e}{c} \cdot \frac{g \cdot h}{f} \tag{6.4}$$

The parameter X_7 is a rating for the water-borne attrition agents, which influence the impact of erosion by abrasion. Within the North-Sea close to Vlissingen this is mainly sand by erosion of the channel towards the harbour of Antwerp. The corresponding rating is 1.0.

The eighth parameter X_8 is about the concentration of the wave attack in the tidal zone. The tidal range of the North Sea is throughout the year between 2.0 and 6.0 m, considering the data of the ministry of infrastructure and water management. The slope angle of the tidal flat at the connecting point of the submarine cable to land is really low and is below 1:3.0. Consequently, the rating for X_8 is 1.8.

Finally, the last parameter X_9 describes the mobility of the armour rock within the construction. This parameter is only applicable to the limestone (Lim) for the design of Borselle Export Cables, because only the limestone (Lim) will be used as armour layer. The D_{n50} for the limestone armour blocks is 0.20 m. The relative buoyant density (Δ) is approximately 2.0, using a density of 1027 kg/m^3 for the sea water. The ΔD_{n50} value is 0.4 m for the limestone (Lim). The significant wave height is, as discussed before below 4 m. However, in this case there is a division between the trench close to the coast and the trench in open sea. The significant wave height in the coastal zone does not exceed 1 m, while it does in open sea. Consequently, the rating of X_9 is 2.0 for the trench backfill close to the coast and 1.5 for the backfill further from the coast.

Now, all the parameters can be multiplied to find the final factor X to convert the time scale from 1000s of revolutions to in-service engineering time (years). The parameters and factor X for the limestone 5-40 kg armour and sandstone 32-56 mm filter in the supra-tidal, inter-tidal and submerged zone are all displayed in table 6.3. It should be noted that the calibration reliability is not similar for all parameters as can be seen in table B.2 in Appendix B. This influences the accuracy of the degradation prediction. However the largest parameter influence is for the rock fabric strength (k_s), which has an excellent calibration reliability and is accurately determined during this research. The poorest calibration reliability is for parameter X_7 about the water-borne attrition agents. Yet, this parameters has not a large influence on the final degradation curve.

6.2.2. Results and Discussion

The mass loss curves of the sandstone and limestone (Lim) during the in-service engineering time are plotted in figure 6.3. The figure highlights the distinct difference between the two rock types and the zones within the construction. The mass loss in the inter-tidal zone is more aggressive compared to the other two zones as a result of the high environmental stress in this zone. In addition, the

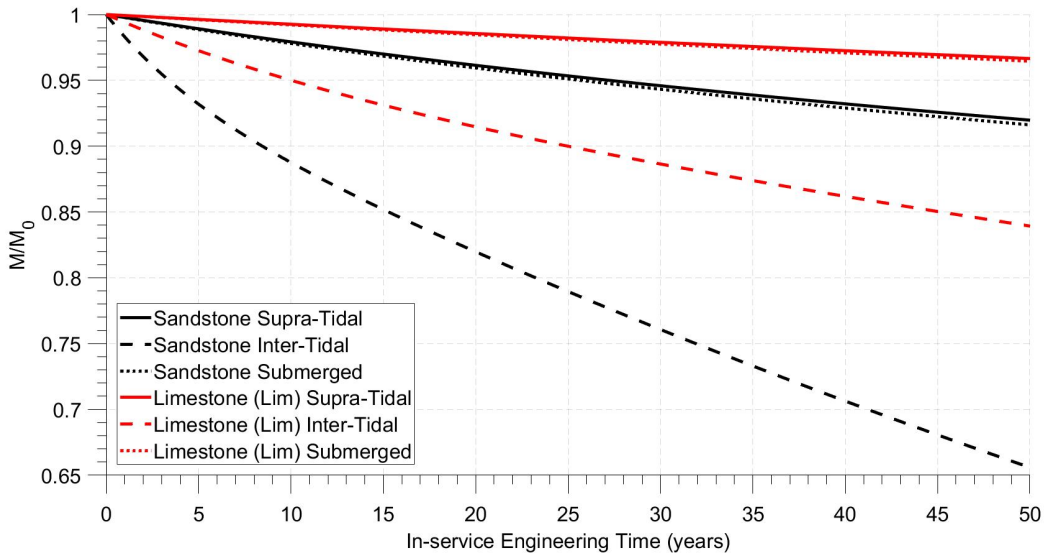

Figure 6.3: The mass loss curve of the sandstone and limestone (Lim) aggregate based on the MDE method for the in-service engineering time. The degradation rate of the sandstone is now faster than for the limestone (Lim) compared to figure 6.3 due to the conversion factor X.

sandstone aggregate degrades faster than the limestone armourstones. In figure 6.2 this was not the case and the limestone (Lim) degraded faster than the sandstone based on the M_{DE} coefficient. The divergence in predictions is a result of the factor X. However, the sandstone will presumably not degrade that fast in function. The factor X of the MDE method is computed for a rock type that is solely in the design. Two rock types with a different function are present at project Borssele Export Cables, to be specific the limestone 5-40 kg armour layer and the sandstone 32-56 mm filter layer. The smaller size of the sandstone aggregate results in a more rapid degradation according to the micro-Deval method. Nevertheless, this sandstone filter layer is protected by the limestone armour layer in the construction reducing the environmental stress on the sandstone. The sandstone will degrade slower in construction than prospected by the MDE method. In addition, the calibration reliability is not equal for all parameters incorporated in factor X, therefore increasing the uncertainty of the prediction. Nevertheless, the most certain parameter k_s has the highest calibration reliability. Finally, Latham et al. (2006) already indicated the incorrect approach of the linear degradation rate, which is actually believed to be non-linear.

6.3. Conclusion

The micro-Deval test indicates the least resistance against abrasion for the limestone (Lim). The micro-Deval coefficient of the sandstone and limestone (Jen) fall within the excellent category of CIRIA/CUR/CETMEF (2007). The MDE method is not suitable for the design of Borselle Export Cables, which contains two layers of armourstone with different functions. Nevertheless, an indication is obtained for the degradation rate in the various environments of the project. The most rapid degradation is expected in the inter-tidal zone, while degradation is estimated to be slow in the submerged and supra-tidal zone.

7

Rock Density and Water Absorption

7.1. Determination of Density and Water Absorption

Rock density and water absorption (WA) are valuable rock properties concerning the durability requirements of armourstone as discussed in chapter 2. Rock density is in this case the apparent mass density (ρ_{app}) in g/cm^3. This is the mass density of a rock sample that may have its connected pores filled with water. It is mainly influenced by the real density, the mass density of the mineral components within the rock fabric, the voids in the rock fabric and the degree of saturation (CIRIA/CUR/CETMEF, 2007).

The density and WA were determined on 40 aggregate samples from the Hartsteinwerke, on 10 aggregate samples from Carrière des Limites and on 10 aggregate samples from Carrière de Jenneret, according to EN 13383-2 (2002) Clause 8. On the aggregate from the Hartsteinwerke 40 measurements were executed instead of 10, since aggregate from this quarry showed more variability between the individual rock pieces. The tested aggregate pieces were all between 150 and 450 g when dried in the oven. The density was calculated according to equation 7.1 where; M_1 is the mass of the saturated and surface dried test portion, M_2 is the apparent mass in water of the saturated test portion, M_3 is the mass of the oven-dried test portion and ρ_w is the density of water at 25°C. The density calculation is based on Archimedes' principle for a fully submerged object. The gap between M_1 and M_2 is equal to the weight of the displaced fluid mass by the aggregate piece. The pieces are submerged in water, of which the density is 997 kg/m$_3$ at 25 °C. From the density and displaced water mass, the sample volume can be calculated. The density of the aggregate piece is determined from this volume and the oven-dry weight. The WA was computed according to equation 7.2 and is the increase in sample mass caused by the absorption of water, relative to the oven-dry sample mass.

$$\rho = \frac{M_3 \cdot \rho_w}{M_1 - M_2} \tag{7.1}$$

$$WA = \frac{M_1 - M_3}{M_3} \cdot 100 \tag{7.2}$$

Additionally, the density and WA were determined on all cores used for the UCS testing, which will be described later on. The density was computed differently in this case. A core is a nearly perfect cylinder, so the volume can be calculated by formula 7.3 where; r is the radius of the core and L the length. The density is determined by dividing the oven-dry core weight by this volume. The WA of the cores was again determined according to equation 7.2.

$$V = \pi r^2 \cdot L \tag{7.3}$$

7.2. Results of Density and WA Measurement

7.2.1. Aggregate

The results of the density and WA measurements on the aggregate samples are listed in table 7.1 and C.1 in Appendix C. Table C.1 presents the density and WA of 30 additional sandstone aggregate pieces,

which were measured in a later stage. The standard deviation and mean value in this table are over all 40 measurements and include the 10 values from table 7.1. The test results show a higher variance for the sandstone from the Hartsteinwerke and limestone from Carrière de Jenneret with respect to the limestone from Carrière des Limites. The sandstone aggregate pieces show a range in density of 2.56 to 2.64 g/cm^3. The pieces with a lower apparent density show higher values for the water absorption. A visual examination of the aggregates clarifies the variation in the data. The photos presented in figure L.1 in Appendix L display differences in the rock fabrics of the aggregate pieces. Some pieces contain larger quartz crystals, while others show a higher amount of platy minerals. Moreover, some samples show a platy structure throughout the full aggregate piece. The porosity and degree of weathering differs as well between the sandstone aggregate pieces. All these features could explain the variety in density and WA of the sandstone aggregate. The mineral content and porosity influence the density, while the rock's structure and porosity determine the WA. The limestone (Jen) aggregate shows reasonably constant values, yet there are two pieces that influence the standard deviation notable. These pieces, number 4 and 6, have low densities compared to the other samples of 2.49 and 2.44 g/cm^3 respectively and high WA values of 2.50 and 2.84%. The low density and high WA can be explained by the higher degree of weathering of the two samples compared to the other ones as can be seen in the photos in figure L.3 in appendix L. A higher degree of weathering increases the amount of secondary minerals with a lower grain density and increases the armourstone's porosity. The aggregate pieces from Carrière des Limites show constant results with a typical density for limestone of $\pm$2.70 g/cm^3. There is some variation within the WA values, however all values are considered low with a WA of below 0.5%. Visual examination on the appearance of the limestone (Lim) aggregate agrees with constant values, since the samples look similar. There is only a small difference in the amount of calcite veins and bioclasts.

7.2.2. Rock Cores

The density and WA of the rock cores are displayed in table 7.2. The sandstone cores can be divided into two groups concerning the density and WA. Group 1 contains the first 7 cores, while the remaining cores belong to group 2. The cores in group 1 show a lower density of 2.38 to 2.51 g/cm^3 and relative high WA of 1.56 to 2.79%. In contrast, the cores in group two show higher densities of 2.53 to 2.61 g/cm^3 and WA values of 0.27 to 0.57%. The increase in density and decrease in WA for the second group is a result of the sampling location within the quarry. The blocks originate from multiple exploration faces within the quarry. Thus, the cores from group 1 and group 2 do not originate from the similar face, resulting in other rock properties. The presence of two distinct groups with different properties result in a larger standard deviation for the sandstone cores with respect to the limestone cores. The limestone (Lim) cores are consistent in density and water absorption, like the aggregate samples. The density ranges from 2.63 to 2.70 g/cm^3 and is with a mean of 2.66 g/cm^3 lower than the measurements on the aggregate sample. The density measurement on the cores is less accurate than the measurement on the aggregate samples, due to the simplified volume measurement. The volume of the cores is not measured by Archimedes principle, but with the radius and length of the core. Nevertheless, the radius and length of the core are not consistent over the sample. A core always deviates slightly from a perfect cylinder, e.g. a change in diameter or small pieces broken of the core edges. A deviation of a tenth of a millimetre already result in a change in density of $\pm$0.01 g/cm^3. The limestone (Lim) cores show very low values for the WA with a maximum of 0.14%. The limestone (Fri) cores show more variation than the limestone (Lim) cores. Some cores are homogeneous, like cores FC1 and FC2. While other cores, such as F12, show recrystallised fossils and some even brown weathering patterns, e.g. sample FC4, FC6 and FC8. The last three samples show a higher WA of 0.64, 0.42 and 0.49 respectively. These higher values can be linked to the higher degree of weathering. Sample FC 2 has a high WA of 1.43%, yet this cannot be explained visually on the sample. The density for the limestone (Fri) cores shows a drop in value for core FC4 and FC8, which is linked to the higher degree of weathering. Yet, sample FC6, that shows a higher degree of weathering and higher WA, has a density of 2.67 g/cm^3 equal to the mean value.

7.3. Correlation Density and Water Absorption

The apparent rock density is a function of the minerals within rock matrix and the volume of the voids present in the rock matrix, assuming the rock is completely dry. When the voids are interconnected and

Table 7.1: Results of density and WA of aggregate samples. M_1 is the mass of the saturated and surface dried test portion, M_2 is the apparent mass in water of the saturated test portion and M_3 is the mass of the oven-dried test portion. Mean density and WA absorption values fall within the good and excellent category from the Rock Manual (CIRIA/CUR/CETMEF, 2007) as listed in table 3.1 for all three rock types.

Sample	Number	M_1 (g)	M_2 (g)	M_3 (g)	ρ (g/cm^3)	WA (%)
Hartsteinwerke	1	190.86	117.50	188.46	2.56	1.27
	2	180.51	112.67	179.36	2.64	0.64
	3	177.77	110.35	176.70	2.61	0.61
	4	209.99	130.87	209.26	2.64	0.35
	5	272.26	168.51	269.96	2.59	0.85
	6	379.22	235.14	375.29	2.60	1.05
	7	178.62	110.30	176.76	2.58	1.05
	8	165.30	102.53	163.88	2.60	0.87
	9	220.34	136.14	218.70	2.59	0.75
	10	246.35	153.24	245.11	2.62	0.51
	Mean	-	-	-	2.60	0.79
	Standard Deviation	-	-	-	0.02	0.28
Carrière des Limites	1	267.82	168.80	266.65	2.68	0.44
	2	240.72	151.64	239.86	2.68	0.36
	3	183.95	116.17	183.78	2.70	0.09
	4	197.87	125.34	197.56	2.72	0.16
	5	165.54	104.66	165.42	2.71	0.07
	6	156.95	99.31	156.59	2.71	0.23
	7	187.77	119.02	186.96	2.71	0.43
	8	177.10	112.00	176.92	2.71	0.10
	9	166.03	105.23	165.56	2.71	0.28
	10	163.40	103.53	162.99	2.71	0.25
	Mean	-	-	-	2.71	0.24
	Standard Deviation	-	-	-	0.01	0.14
Carrière de Jenneret	1	408.38	255.51	406.12	2.65	0.56
	2	274.87	171.08	272.71	2.62	0.79
	3	256.20	160.22	255.40	2.65	0.31
	4	164.45	100.30	160.44	2.49	2.50
	5	385.11	240.50	383.03	2.64	0.54
	6	217.13	131.03	211.14	2.44	2.84
	7	258.68	161.99	257.80	2.66	0.34
	8	211.33	132.44	210.49	2.66	0.40
	9	295.78	184.53	294.67	2.64	0.38
	10	307.44	192.06	306.36	2.65	0.35
	Mean	-	-	-	2.61	0.90
	Standard Deviation	-	-	-	0.08	0.95

reach the rock surface, water inflow is possible. Therefore, a correlation is expected between the rock density and the water absorption. Equation 7.4 shows the relation between bulk density and porosity of a rock sample, where; ρ_b is the bulk density, ρ_d is the particle density and n is the porosity. The porosity is the volume of the voids divided by the total volume. Thus, when a sample is fully saturated the water absorption is linearly related to the porosity. In this case a linear relation is expected between ρ_b and WA. However, when the sample is not fully saturated, due to closed of pore spaces, the relation is not linear anymore. The strength of the correlation will probably depend on the rock type, because the inter-connectivity of pore spaces differs with a variety of rocks. For example extrusive rocks with a vesicular texture are expected to have a very poor linear correlation between density and WA as well. The solidified magma around the gas bubbles forms a structure with a high porosity, but the pores are completely sealed of and do not absorb any water. These features result in a very low density, but

Table 7.2: Results of density and WA of rock cores. M_1 is the mass of the saturated and surface dried test portion and M_3 is the mass of the oven-dried test portion

Sample	Number	M1 (g)	M3 (g)	Length (mm)	Diameter (mm)	ρ (g/cm^3)	WA (%)
Hartsteinwerke	1	130.56	127.22	40.8	40.85	2.38	2.63
	2	129.69	126.17	40.55	40.80	2.38	2.79
	3	139.22	135.77	43.15	40.55	2.44	2.54
	4	141.99	139.80	42.95	40.60	2.51	1.57
	5	125.31	121.97	38.95	40.85	2.39	2.74
	6	129.95	127.96	40.25	40.6	2.46	1.56
	7	125.81	123.77	-	-	-	1.65
	8	142.59	142.15	42.30	40.75	2.58	0.31
	9	142.18	141.64	42.25	41.10	2.53	0.38
	10	139.44	139.02	42.15	40.40	2.57	0.30
	11	142.25	141.44	42.30	40.60	2.58	0.57
	12	140.36	139.64	41.75	40.50	2.60	0.52
	13	141.68	140.87	42.15	40.65	2.58	0.57
	14	139.47	139.09	42.05	40.20	2.61	0.27
	Mean	-	-	-	-	2.51	1.31
	Standard Deviation	-	-	-	-	0.09	1.01
Limites	1	138.05	137.99	40.90	40.25	2.65	0.04
	2	142.73	142.55	41.80	40.45	2.65	0.13
	3	144.51	144.31	42.15	40.15	2.70	0.14
	4	152.73	152.65	43.90	40.90	2.65	0.05
	5	142.18	141.95	41.65	40.15	2.69	0.16
	6	149.83	149.77	42.90	40.65	2.69	0.04
	7	143.73	143.66	42.30	40.50	2.64	0.05
	8	137.46	137.37	39.60	41.00	2.63	0.07
	9	139.43	139.30	40.15	40.65	2.67	0.09
	10	140.38	140.33	41.70	40.30	2.64	0.04
	Mean	-	-	-	-	2.66	0.08
	Standard Deviation	-	-	-	-	0.03	0.05
Frimoye	1	141.84	141.13	41.90	40.25	2.65	0.50
	2	144.04	142.01	42.45	40.05	2.66	1.43
	3	129.77	129.55	39.75	39.20	2.70	0.17
	4	141.34	140.44	42.85	39.95	2.61	0.64
	5	132.30	132.16	40.85	39.00	2.71	0.11
	6	141.37	140.78	41.70	40.10	2.67	0.42
	7	132.30	132.17	40.30	39.50	2.68	0.10
	8	133.08	132.43	41.35	39.45	2.62	0.49
	9	147.66	147.51	43.35	40.30	2.67	0.10
	10	136.91	136.79	40.10	40.25	2.68	0.09
	11	136.47	136.24	40.40	40.10	2.67	0.17
	12	138.77	138.67	40.70	40.15	2.69	0.07
	13	149.16	148.96	43.90	40.40	2.65	0.13
	Mean	-	-	-	-	2.67	0.34
	Standard Deviation	-	-	-	-	0.03	0.38

relative low WA as well.

$$\rho_b = (1 - n) \cdot \rho_d \tag{7.4}$$

Figure 7.1 shows the density and WA of the sandstone and limestone aggregate pieces. The sandstone pieces show a clear exponential trend of the form $y = a \cdot e^{bx}$ between the density and WA. Thus, the sandstone aggregate contains non reachable pores, according to the theory discussed before. Nonetheless, the rock fabric of the sandstone aggregate pieces varies to one another observed during the petrographic analysis. Thus, the nonlinear relation does not proof the presence of closed of pore spaces. The limestone from Carrière de Jenneret shows a very strong linear relation with a coefficient of determination of 0.99. This suggest that the majority of the pores are filled upon saturation. The limestone aggregate from Carrière des Limites is limited to a smaller density and WA range, therefore does not reveal a correlation on itself. Nevertheless, the data points of the limestone

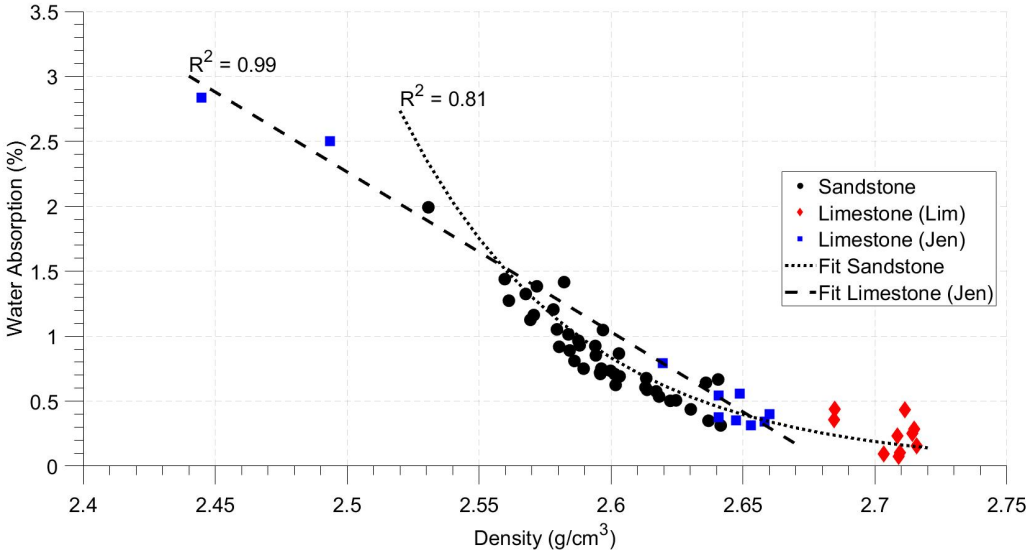

Figure 7.1: Relation between density and WA for the aggregate from the Hartsteinwerke, Carrière des Limites and Carrière de Jenneret. The dotted line shows the exponential regression on the sandstone data. The dashed line shows the linear regression on the limestone (Jen).

(Lim), oscillate around the exponential trend obtained on the sandstone and do not follow the linear trend from the other limestone (Jen). The trends are not universal for all rock types, since the sandstone and limestone (Jen) already align to two distinct curves. The measurements on the cores provide a trend as well visualised in figure 7.2. Yet, the spread between data points is larger as a result of the less accurate density measurement.

7.4. Discussion

The variability in density and WA for the sandstone can be linked to the observations of the petrographic analyses. The sandstone aggregate contains a mix of multiple exploration faces within the quarry. This mix is observed within the thin sections as a sample of quartzite, mica quarzite, sandstone and siltstone. The last three show clear anisotropic features due to the thrust and shear zones within the quarry and a higher amount of secondary minerals. In addition, these pieces contain a higher amount of cement compared to the quartzite. The anisotropy, secondary minerals and higher amount of cement may increase the ease of fluid inflow and decrease the density of the sample. Some of the limestone (Jen) pieces have weathered surfaces. The weathering has probably increased the sample's porosity or permeability as the WA values for these samples are higher. The variety can as well be caused by a slight change in rock fabric, since several limestones surface within the quarry as mentioned in chapter 4. Dissolved bioclasts were observed during the petrographic analysis within a limestone aggregate piece of Carrière de Jenneret. These pore spaces are probably not connected and a sample with these dissolved pore spaces is expected to have a lower density and lower WA, since water cannot reach these empty pore spaces. The data points of the limestone (Jen) display no samples with a relatively low density and WA compared to all other tested aggregate pieces. Therefore, the tested limestone (Jen) aggregate pieces probably contain no to a minor amount of dissolved pore spaces. The limestones (Lim) have similar WA values, with a maximum difference of 0.37%. The differences are expected to be caused by a change in rock matrix. The petrographic analysis distinguished the presence of grainstones, packstones and wackestones in the aggregate mixture of Carrière des Limites, which could explain the small variety in WA values.

7.5. Conclusion

The density and WA test results provide an insight in the variability within the aggregate produced by the quarries. The ten samples for the sandstone already show variation between the pieces, which increases after testing another 30 samples. Thus, the variability is not properly identified within the

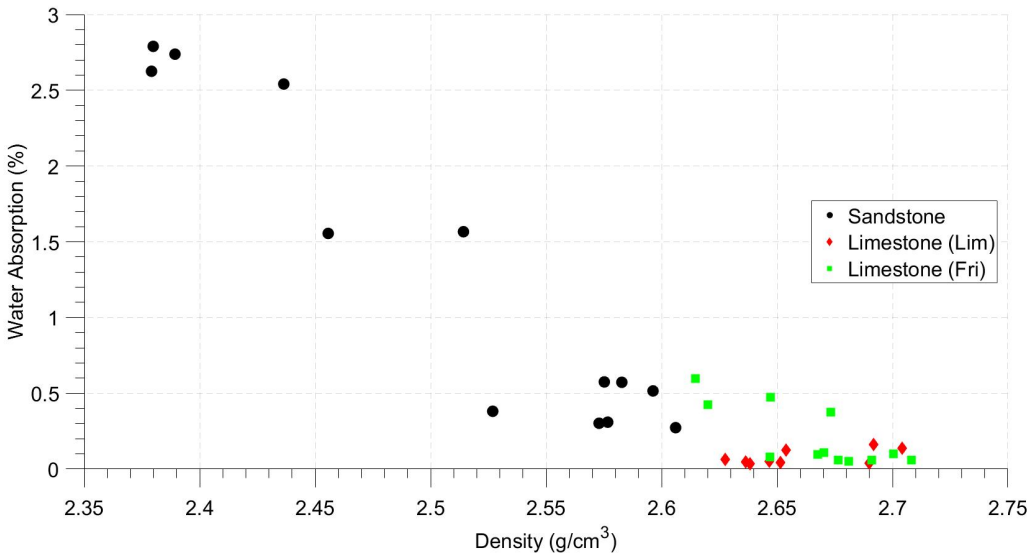

Figure 7.2: Relation between density and WA for the cores from the Hartsteinwerke, Carrière des Limites and Carrière de Frimoye.

first ten samples. The WA values of the limestone (Jen) aggregate have a gap of over 2% as well. The larger variations within the samples can be explained by a visual examination on the rock pieces. Furthermore, the petrographic analysis indicates a more detailed view on features that can explain the difference in WA and density values. The density and WA values correlate well for the tested aggregate pieces and rock cores. The sandstone presents a exponential relation, while the limestone (Jen) displays a linear relation. Thus, the relation is not unique for several rock types.

8

Armourstone Strength

The strength of armourstone is an important parameter with respect to its durability. Two strength tests are performed during this research; the uniaxial compressive strength (UCS) test and the Brazilian tensile strength (BTS) test. The UCS test is included within the standard EN-13383:1&2, however the BTS is not. The BTS test is the first simple index tool described in order to provide the extra insight within the durability characteristics of the tested armourstone. The rock strength has to withstand the stress imposed by the environment from the moment it is placed in the construction until the end of its service life. The environmental stress can be forced in both compression, e.g. attrition, and tension by salt crystallisation, for example.

8.1. UCS test

The cores for the UCS test are extracted from the sampled armourstone blocks, using the drill depicted in figure 8.1. The UCS test is performed on two sets of cores. The first set contains 14 air-dried cores with a length of $\pm$80 mm and a length over diameter ratio (L/D) of 2. 7 cores are sandstone and the 7 remaining cores are limestone (Lim). The second set contains 10 sandstone cores, 10 limestone (Lim) cores and 10 limestone (Fri) cores. The cores have a length of $\pm$40 mm and L/D of 1. These cores are fully saturated during compression. So, two different core sizes are tested during this research, one set with a L/D of 1 in saturated condition and one set with a L/D of 2 in air-dried condition. The UCS test is performed on cores with a L/D of 1 and length of 40 mm, because this is the procedure according to the standards EN 13383-1 (2002) and EN 1926 (1999). However, a L/D of 2 is preferred to obtain more reliable measurements regarding elastic modulus and strength (ASTM, 2001). The stress distribution within the sample during compression is disturbed at the connection between the rock core and end plate of the test apparatus, as this connection is never a perfect fit (Halleux et al., 2015). The disturbance at the cores edges has less influence on the failure within longer samples compared to shorter samples. The faces of all cores are sawn parallel and sanded such that no irregularities can be felt by touch. The end faces are sanded until parallel. The sonic velocities of the core samples are measured before performing the UCS test. The UCS value is measured using the UCS test apparatus displayed in figure 8.2. A core is placed between two pressure plates. The top one is fixed in place and the bottom one is able to move upwards. Next the core is clamped between the two plates by moving the bottom one up until a minor positive pressure of $\pm$0.5 MPa is measured. Next, the UCS test is started by increasing the pressure on the core sample by moving the bottom plate upwards. A strain controlled test with a rate of 0.001 mm/s is performed during this research, in order to develop a controlled failure curve. The strain is monitored by measuring the vertical displacement within the sample using the two pins fixed on the bottom plate. The strain (ε) is calculated according to equation 8.1 where; ΔL is the vertical displacement and L is the length of the core sample. The test is continued until the core sample is not able to withstand the applied force anymore and fails. This is easily determined for cores that fail in brittle mode. These test will display a sudden drop in stress applied on the sample within a small axial strain, indicating failure of the sample. The cores that fail in ductile fashion display a slow drop in stress applied on the sample, which is accompanied by a more rapid increase in axial strain. However, this point is harder to determine because the drop in stress applied on the sample can be the initiation

Figure 8.1: Drill used for the extraction of the rock cores from the blocks sampled at the quarries.

of micro-cracks and not complete failure of the core sample. Therefore, the test was continued for a while after the peak stress to determine if failure occurred. In addition, a close look to the core sample reveals the initiation of a shear fracture over the full sample.

$$\epsilon = \frac{\Delta L}{L} \tag{8.1}$$

8.1.1. Core Description

The cores are labeled with S, L, H, LIM and FRI. S and L are stand for the sandstone and limestone (Lim) cores with a L/D of 2. H, LIM and FRI stand for the sandstone, limestone (Lim) and limestone (Fri) cores with a L/D of 1.

The sandstone cores can be split up into two groups based on their visual appearance. The first group consists of samples H1, H2, H4, H5, H7, S4, S5, S6 and S7, and shows a clear bedding and foliation within the samples as a result of the sedimentary structure and deformation at low grade metamorphism that occurred during the geological history of the area around the Hartsteinwerke. The cores show a layered, alternating beige and pink colour, which is interpreted as the bedding of the sandstone. Core H4 and H7 have less of a pink colour compared to the other samples in group 1 and have developed some minor joints $\pm 20°$ to the vertical plane. During the drilling core HA7 broke along one of these cracks. The cores from group 1 are drilled from the blocks sampled at the face depicted in figure 4.11. The remaining cores H8, H9, H10, H11, H13, H14, S1, S2 and S3 are very solid, homogeneous, dark red cores and originate from the other sampled exploration faces.

The cores obtained from the limestone (Lim) rock blocks look similar. All cores have a grey colour and have a homogeneous rock matrix. The cores show no obvious cracks, expect core LIM9. This core sample has a crack starting at the top of the sample almost running to the bottom. The crack slightly opens when the sample is squeezed between the thumb and index finger. Most of the cores show a number of calcite veins. The cores can be divided into three groups. Group 1 contains no calcite veins, which occupies only core LIM7. The second group contains only a minor amount of thin (< 1mm) calcite veins and take up LIM3, LIM5 and LIM10. The third group contains thicker calcite veins and consists of the remaining cores.

The limestone cores (Fri) vary more in visual appearance than the limestone (Lim) cores. The cores have a grey colour, yet some show some beige stained spots. These spots possibly highlight internal weathering within the rock blocks. The grey colour of the samples is darker than the grey colour of the limestone (Lim) cores. Sample FRI4 and FRI8 display the largest spots with beige staining.

Figure 8.2: UCS apparatus used to compress the rock cores and obtain the UCS value armourstones. Picture taken after a test on the sandstone core.

Furthermore, a small crack runs from the top of FRI4 vertically towards the bottom. The cores FRI 6 and FRI7 show some minor beige stained concentrations. Again calcite veins run through the cores. The cores FRI1, FRI2, FRI3 and FRI10 look similar and are homogeneous limestone cores with a grey colour and no cracks. Sample FRI5 has a concentration of calcite crystals on the edge of the core of approximately 1.5 by 1 cm. The remaining cores contain calcite veins and recrystallised bioclasts. These features are the largest in core FRI12.

Photographs of the intact cores with a L/D of 1 are presented in appendix E in figure E.1, E.4 and E.6 for the sandstone, limestone (Lim) and limestone (Fri) cores respectively.

8.1.2. Failure Mode

There is a variety in the failure mode of the cores during the compressive strength testing. The failure mode can be deducted from the stress-strain curves and the appearance of the sample after failure. First the observations on the sandstone cores will be discussed.

The UCS values for the sandstone are summarised in table 8.1. Nevertheless, the stress-strain curves give more detailed information about the failure mode next to the measured UCS value. These curves can be divided into three parts. The first part is the non-linear part at the low strains, corresponding to the clamping stage of the sample within the UCS apparatus. During this stage micro cracks are closed within the sample. The next stage is the linear elastic behaviour and the third stage the non-linear plastic behaviour until failure of the sample. Five of the cores from the first group of sandstone cores have low UCS values of $\pm$30 MPa. Two failure modes are observed in the group of sandstone cores with a low UCS, despite the minor difference in UCS values. The failure of cores S6 and S7 is brittle shear failure along the bedding plane displayed in figure E.3 in Appendix E. The stress-strain curves in figure 8.5a show an instant drop after reaching the UCS value, indicating a brittle failure. This drop is not observed in the curves of sample H1 and H2 in figure 8.4a. These curve with a slight bend and the stress decreases slowly after failure, while the strain proceeds. The samples failed ductile, which is confirmed by the almost intact cores after failure. The failure mode of sample H5 is between the two cases described before. The curve in figure 8.4a shows no instant drop after failure, yet the photo of the core after failure in figure E.2 in Appendix E presents a shear failure along the bedding. The failure mode is probably between the ductile and brittle mode. The remaining core piece of H5 was able to withstand a large portion of the imposed stress after the shear failure, as a result of the ductile behaviour. Two other cores of group 1, H7 and S5, have slightly higher UCS values of 63.4 and 59 MPa respectively. Sample S5 has a clear shear failure in figure 8.3a, while

Table 8.1: The UCS and E_{50} of the tested rock cores. Samples H1 to H14 are the saturated sandstone cores from the Hartsteinwerke with a L/D of 1. Cores LIM 1 to LIM 10 are the saturated limetsone cores from Carrière des Limites with a L/D of 1. Cores FRI 1 to FRI 13 are the saturated limestone cores from Carrière de Frimoye with a L/D of 1. Samples 1L to 7L are the air-dried limestone cores from Carrière des Limites with a L/D of 2. Samples 1S to 7S are the air-dried sandstone cores from the Hartsteinwerke with a L/D of 2.

Sandstone, L/D of 1, saturated											
Sample	H 1	H 2	H 4	H 5	H 7	H 8	H 9	H 10	H 11	H 13	H 14
UCS (MPa)	31.2	35.7	101.3	28.8	63.4	195.8	260.7	301.9	140.7	197.2	262.5
E_{50} (GPa)	7.2	6.5	23.9	7.6	13.3	37.8	42.6	44.6	32.1	38.2	45.1
		Sandstone, L/D of 2, air-dried									
Sample	1S	2S	3S	4S	5S	6S	7S				
UCS (Mpa)	208	182	206	94	59	28	33				
E_{50} (Gpa)	51.6	49.3	52.1	31.9	18.3	13.3	13.9				
		Limestone (Lim), L/D of 1, saturated									
Sample	LIM 1	LIM 2	LIM 3	LIM 4	LIM 5	LIM 6	LIM 7	LIM 8	LIM 9	LIM 10	
UCS (MPa)	119.1	166.7	173.2	198.1	171.8	192.6	203.4	158.8	184.3	173.7	
E_{50} (GPa)	40	44.3	44.8	46.2	45.4	45.2	47.3	44	43.6	42.5	
		Limestone (Lim), L/D of 2, air-dried									
Sample	1L	2L	3L	4L	5L	6L	7L				
UCS (Mpa)	180	182	182	187	138	172	166				
E_{50} (Gpa)	65.7	69.5	63	60.5	64	66.7	65.3				
		Limestone (Fri), L/D of 1, saturated									
Sample	FRI 1	FRI 3	FRI 5	FRI 6	FRI 7	FRI 8	FRI 9	FRI 10	FRI 11	FRI 13	
UCS (MPa)	62.5	181.4	235.9	163.7	231.3	128.9	156.8	226.6	190	214.1	
E_{50} (GPa)	20	42.3	47.7	44.4	47.9	34.3	44.2	42.4	44.9	43.6	

sample H7 looks almost intact. Yet both samples behave ductile during failure. Core S5 is exposed to major radial strains during failure, as can be seen in figure 8.5b. This is probably due to the ductile rock behaviour during failure, resulting in flexing along the shear fracture. Sample S5 is in the transition zone between ductile and brittle failure. The two remaining cores of the first group, H4 and S4, already have higher UCS values of 101.3 and 140.7 MPa respectively. Core HA 4 shows again the shear failure. Yet, core S4 shows another brittle failure pattern indicated by the steep drop after failure in the stress strain curve. The failed core presents a set of parallel fractures, which have split the core into multiple elongated pieces. The axial splitting of core S4 can be seen in figure 8.3b. The stress-strain drops already in stress value before failure, which is presumably the result of crack growth within the sample. This assumption is emphasised by the cracking sound before failure. The radial strain in figure 8.5b increases considerably with 0.6% during failure of S4, due to the opening of the cracks running vertically through the sample before failure. The cores from the second group all behave in a brittle fashion and have a steep drop in the stress-strain curve after failure. Some of the cores show a clear shear fracture, while others broke into several pieces and contain a combination of parallel fractures or inclined fractures that merge in the centre of the core. The UCS values from this group range from 140 to 300 MPa. The stress-strain curves of the UCS tests on the group 2 sandstone cores are presented in figure 8.4a and 8.5 as well. Photographs of the failed cores from group 2 are listed in figure E.2 and E.3 in Appendix E. The two discussed groups within the sandstone cores can easily be distinguished in both stress-strain curves. The tangent of the curve from the samples of group 1 is much lower as group 2, which corresponds to the difference between the Young's moduli. Some sandstone samples fall between the two groups as discussed before, which probably correspond to another exploration face in the quarry.

The failed limestone (Lim) cores present three failure patterns. These patterns are best observed in the cores with a L/D of 2, which will be discussed first. All cores failed in a brittle mode, as indicated by the steep drop after failure in the stress-strain curve plotted in figure 8.6a. The corresponding UCS values are listed in table 8.1. Some of the cores broke into multiple pieces as shown by core L4 in figure 8.3c. Two of the fractures run through a thin calcite vein, while others run through the rock matrix and connect all cracks together. The crack propagation results in radial strains as can be seen in figure 8.6b. Next, some of the cores splitted in axial fashion as visualised in figure 8.3d. Again the opening

(a) Shear failure along bedding within sandstone core sample S5.

(b) Axial splitting along sandstone core sample S4.

(c) Brittle failure of limestone (Lim) core L4.

(d) Axial splitting of limestone (Lim) core L6.

(e) Failure along the calcite vein present in limestone (Lim) core L5.

(f) Brittle failure of limestone (Fri) core FRI 7. Chips have broken from the core edge and along minor calcite veins.

Figure 8.3: The various failure patterns observed after failure during UCS test of the sandstone and limestone cores. The depicted cores are the air-dried cores with a L/D of 2 except core Fri 7 which is saturated and has a L/D of 1. The failed cores with a L/D of 1 are listed in Appendix E, including the cores of Carrière de Frimoye.

of the crack through the centre in axial direction increases the radial strain. Finally, a few of the cores failed along the calcite veins present within the samples such as core L5 in figure 8.3e. The cores with a L/D of 1 show similar behaviour visualised in figure 8.4b. However, a few samples, like LIM 5 and LIM 10, do not drop suddenly after failure. During failure only a small chip broke of the edge, which can be seen in the photographs in figure E.5 in appendix E. The result is a core piece after failure that still provides resistance close to the UCS value, but will not reach the previous imposed stress anymore. The UCS test results of the limestone (Lim) cores are listed in table F.2 in appendix F. Core LIM 1 does not agree with the observations on the other cores. The obtained UCS value is considerably lower with 119 MPa. The stress-strain curve displays a steep drop at 105 MPa due to crack propagation within the sample. After failure at 119 MPa the stress drops quick for a short period and then stabilises at 110 MPa. The stress is at this value for 0.01% axial strain after which it drops again. This is the result of small chips breaking of the core sample. The low value of LIM1 cannot be explained based on the observations and is probably a result of an internal defect within the rock matrix. The obtained UCS for the cores (L/D of 1), except LIM1, are close with a difference of 44.6 MPa between the minimum and maximum UCS values. Furthermore, the Young's modulus of these cores is comparable as well with a variation of 4.8 GPa between the minimum and maximum value. The result of the air-dried cores with a L/D of 2 show also the close range; 49.0 MPa for the UCS and 9.0 GPa for the elastic modulus. The stress-strain curves have a similar slope, as indicated by the Young's moduli and are only slightly shifted to one another because of the initial stage of clamping the core in place. The limestone (Lim) can be regarded strong with an average UCS value of $\pm$ 170 MPa.

In general, the limestone (Fri) cores failed brittle, except core FRI1. Nonetheless, the recorded UCS values, listed in table 8.1, vary more with respect to the limestone (Lim) cores. The cores released chips of rock, breaking over the length of the core. This is displayed by the stepwise decrease in stress in the stress-strain curve in figure 8.4c. The cores that failed without the release of chips are core samples FRI 3, 7 and 10. The exception, core FRI 1, was almost intact after performing the UCS test and only contained a crack over the sample oriented approximately 30° to the horizontal plane. The average UCS value of the 10 tested cores is 179 MPa. Yet, the UCS value differs 107 MPa between the minimum and maximum value, neglecting FRI 1. Core FRI1 turned out to be internally weathered by breaking the core after the UCS test, which could relate to the lower UCS value and Young's modulus.

Relation Core Dimension

The UCS tests are performed on saturated cores with a diameter of 40 mm and L/D of 1 and on air-dried cores with a diameter of 40 mm and a L/D of 2. Some of the cores with different L/D originate from the same block sample. These results are compared in table 8.2. The obtained strength values are similar between the two dimensions. The results deviate with a maximum of 15 MPa for the limestone (Lim) and only 6 MPa for the sandstone. The UCS values recorded on the cores with a L/D of 1 are higher for all cores except one limestone (Lim) core. The UCS values of the cores with a L/D of 1 can be used to estimate the UCS value for a core with a L/D of 2 according to equation 2.10. The corrected UCS values result in lower values than recorded on the cores with a L/D of 2 themselves. Thus the correction results in a underestimation of the true UCS value. However, it should be noted that the cores with a L/D of 1 are saturated, while the cores with a L/D are dry. Saturation of the core samples reduces the UCS value (Colback and Wiid, 1965; Palmstrom, 1995). So, the underestimate of the air-dried UCS value of the cores with a L/D of 2 by the corrected UCS value from the saturated cores with a L/D of 1 makes sense. Nevertheless, the air-dried cores can contain a small amount of water, which can already lead to significant reduction in strength. The tested cores with a L/D of 1 have a larger spreading in UCS than the cores with a L/D of 2. The spreading is 273 and 84 MPa for the sandstone and limestone (Lim) cores with a L/D of 1, and 180 and 49 MPa for the sandstone and limestone (Lim) cores with a L/D of 2 respectively.

8.1.3. Influence of Bedding Orientation on UCS

Some of the sandstone blocks have an obvious developed bedding as mentioned before. The orientation of this bedding towards the direction of the major deviatoric stress influences the strength (UCS and BTS) value (Tien and Kuo, 2001). Therefore, extra cores are tested to examine the effect of the bedding orientation on the UCS value. The core drilling at various angles towards the bedding turned out to be difficult. The cores broke along the bedding into thin disks and no cores of proper length could be extracted from most blocks. One of the blocks had enough strength along the bedding planes to

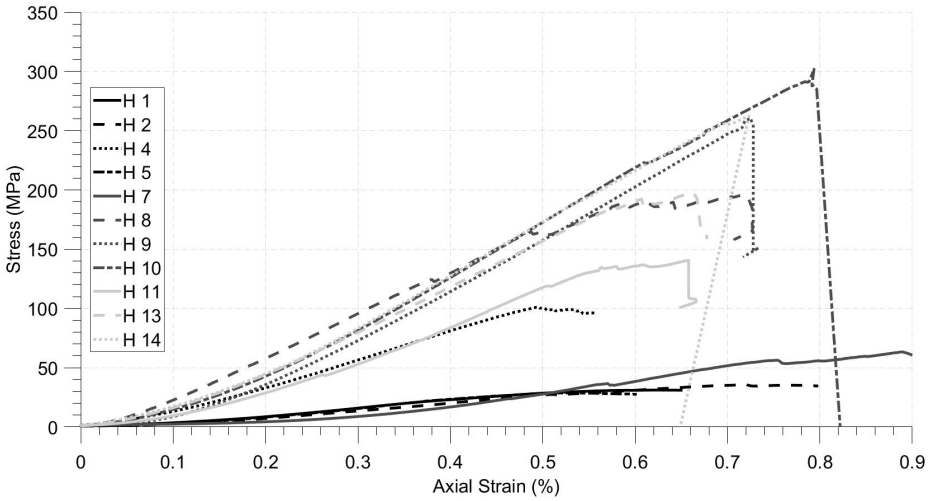

(a)

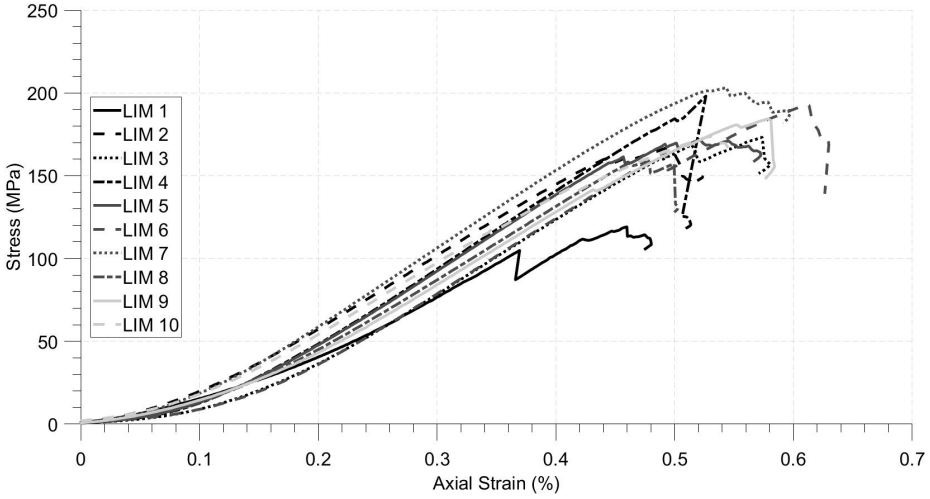

(b)

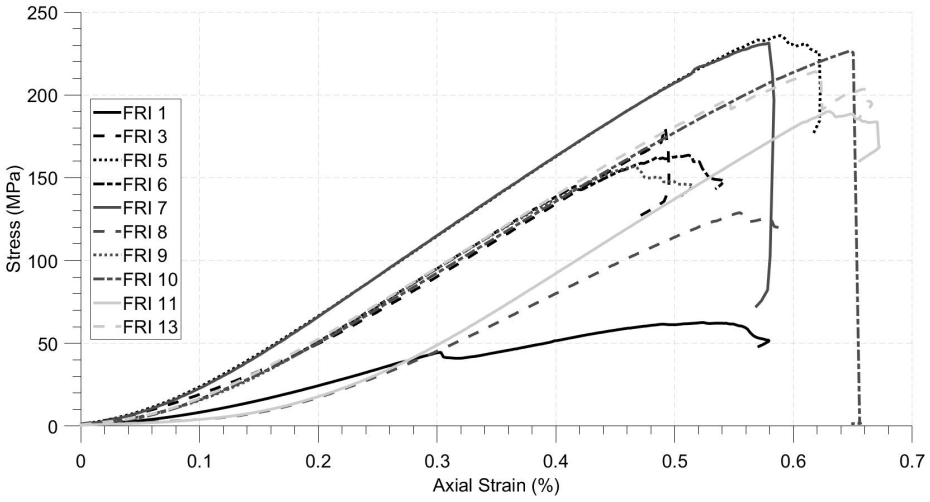

(c)

Figure 8.4: Stress-strain curves obtained during the unconfined compressive strength testing on; (a) sandstone, (b) limestone (Lim) and (c) limestone (Fri) cores with a L/D of 1 in saturated condition.

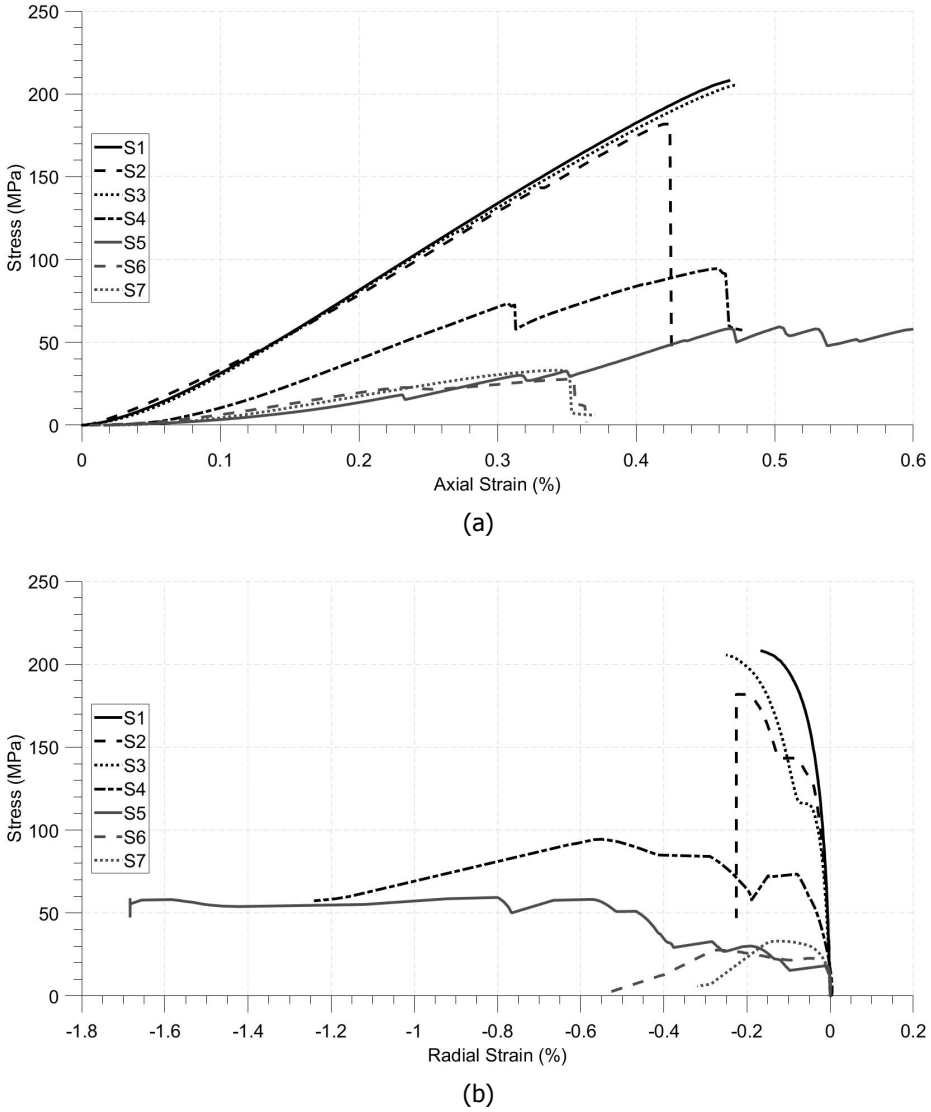

Figure 8.5: Stress-strain curves obtained during the unconfined compressive strength testing on air dried sandstone cores with a L/D of 2; (a) shows the axial strain versus the stress and (b) shows the radial strain versus the stress applied on the cores.

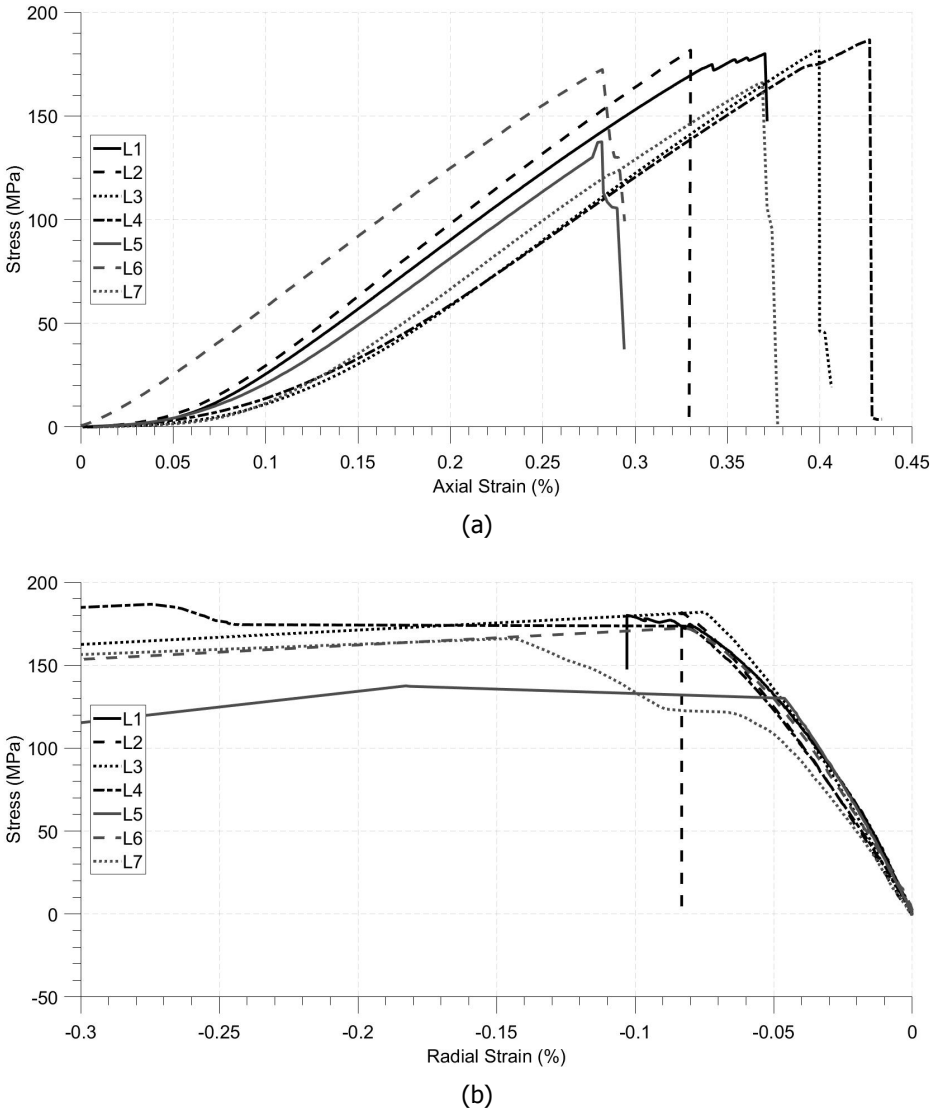

Figure 8.6: Stress-strain curves obtained during the unconfined compressive strength testing on air dried limestone (Lim) cores with a L/D of 2; (a) shows the axial strain versus the stress and (b) shows the radial strain versus the stress applied on the cores.

Table 8.2: Comparison of the UCS and Young's modulus for the cores from similar blocks, yet with different L/D ratio and degree of saturation.

Sample	L/D = 1 (saturated)		L/D = 2 (air-dried)		Corrected to L/D = 2 (saturated)
	UCS (MPa)	E (GPa)	UCS (MPa)	E (GPa)	UCS (MPa)
Limestone	179.3	64.6	171.1	43.6	152.8
	163.3	65.5	178.8	45.5	159.6
Sandstone	76.5	25.1	82.4	18.6	73.5
	30.5	13.6	31.9	7.1	28.5
	198.7	51.0	200.1	38.5	178.7

provide cores of 80 mm length. Nevertheless, this block was not very big so only three cores could be extracted.

The cores have been drilled perpendicular, parallel and at an angle of 30° to the bedding. The UCS values perpendicular, parallel and at an angle of 30 ° are 92.7, 56.5 and 35.0 MPa respectively. The stress-strain curves are presented in figure F.1 in Appendix F. The curves show three different UCS values and three different Young's moduli for the three cores, while they originate from the same source block. All three cores failed ductile, as indicated by the slow drop at failure in the stress-strain curve and almost intact cores after failure presented in figure E.3 in Appendix E. The three UCS values can be used to predict the UCS values that will be obtained at any stress direction to the bedding by the model of Tien and Kuo (2001), discussed in chapter 2.

Multiple triaxial test are required to provide the required parameters in order to apply this model. Yet, the stress direction towards the bedding that results in the lowest UCS value is the main objective of the model in this research. Therefore, not all parameters need to be defined in great detail. The k factor is the ratio between the main deviatoric stress at 0 and 90° to the bedding and is 1.64 for the tested core samples. The deviatoric stress is equal to the UCS value in the test setup, because this is the only stress applied to the core sample. Thus, the k factor is obtained from the measured UCS values. The n factor describes the strength variation for the angles where non-sliding failure occurs, described by the Hoek and Brown failure criterion. The factor n mainly affects the predicted UCS values close to the angles perpendicular to the bedding, where an increase in n decreases the prospected UCS. Furthermore, an increase in n shifts the point where the failure pattern changes from the Mohr-Coulomb to the Hoek and Brown criterion to a lower angle with respect to the bedding.

The Mohr-Coulomb criterion describes the failure along a sliding plane within the core sample, in this case the bedding. Both criteria are transformed by Tien and Kuo (2001) to fit their model. Equation 8.2 is the criterion for the sliding failure where; c_w is the cohesion of the discontinuity (bedding), φ_w is the friction angle of the discontinuity and $S_{1(B)}$ is the major deviatoric stress with angle B to the discontinuity. Equation 8.3 is the criterion for the failure through the rock mass after Tien and Kuo (2001) where; k is the strength ratio between the major deviatoric stresses orientated 0 and 90° to the bedding, n is the transversal anisotropy parameter and B is the angle between the orientation of the discontinuity and the major deviatoric stress direction.

The n factor is hard to determine and relies on the Young's modulus, shear modulus and Poisson's ratio of the rock according to equation 8.4 where; $E_{90°}$ is the Young's modulus perpendicular to the discontinuity, G' is the shear modulus in the plane normal to the discontinuity and v' is the Poisson's ratio for the plane perpendicular to the discontinuity. The Young's modulus and Poisson's ratio are determined by measuring the vertical and radial strain during the UCS tests on the cores perpendicular and parallel to the bedding. The shear modulus can be approached according to equation 8.5. Nonetheless, the n factor will be 1 when the shear modulus is approached theoretically. Therefore, the model will be computed for several n factors ranging from 1 to 4 since the n-value will be in this range according to Tien and Kuo (2001) for most rock types. A n factor between 1 and 1.5 is considered most representable, because the n values fall within this range for rocks with similar material properties, like UCS value and internal friction angle, as the sandstone tested during this research.

The external friction angle and cohesion are the remaining two parameters that need to be determined for the Mohr-Coulomb criterion. The external friction angle is obtained from a field study of van Beusekom (1999). Many tilt tests resulted in an average external friction angle of 35° for the

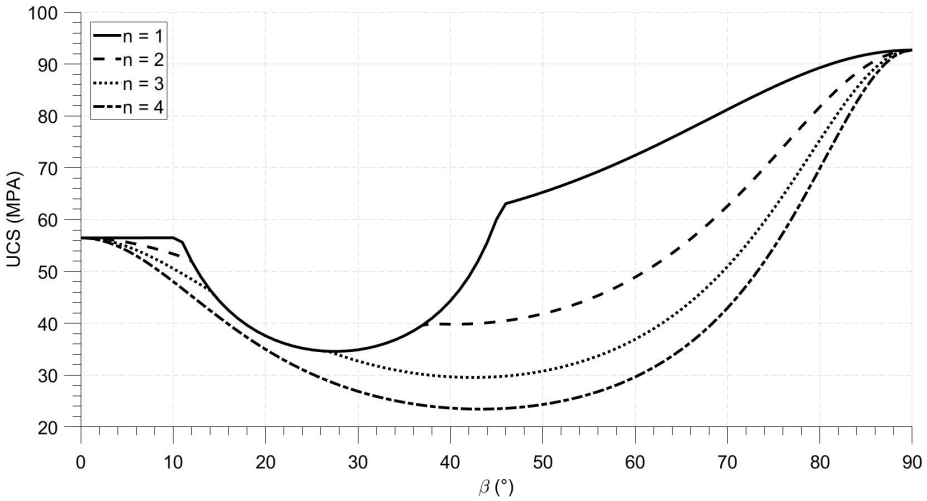

Figure 8.7: The transverse isotropic UCS criterion (Tien and Kuo, 2001) of the tested sandstone samples for various tranversal anisotropy parameter (n). The model is calibrated, for n is 1, to the recorded sandstone UCS values at 0, 30 and 90° to the bedding, where 0° is a perpendicular axial compression to the bedding.

sandstone. The cohesion is obtained by a back analysis with the model of Tien and Kuo (2001) on the UCS value recorded at an angle of 30° to the bedding. The back analysis of the cohesion results in a value of ±9 MPa. The criterion after Tien and Kuo (2001) on the sandstone from the Hartsteinwerke is displayed in figure 8.7 for various n-values. The lowest UCS value is expected when B is about 27-28° for the case that n is between 1 and 2. Yet, the lowest value is prospected at a B of 43° in the case n is equal to 3 or 4. The change in n has a large influence on the UCS value for a higher B. The expected n value, based on literature, is lower than 2 and therefore it can be assumed that the lowest UCS value is at an angle of 27-28° to the bedding.

The parabolic shape of the curve (n=1) represents the Mohr-Coulomb failure criterion and determines in this case the angle at which the UCS value is the lowest. An increase in cohesion or external friction angle narrows the parabolic shape and increases the expected UCS value. The transition from the Mohr-Coulomb to the Hoek and Brown criterion shifts towards a lower B. However, mainly the change in friction angle shifts the point of lowest UCS value to another angle. An increase in friction angle reduces the angle B. The angle at which the lowest UCS value is expected, shifts with 2-3° for this sandstone if the external friction angle turns out to be 5° higher or lower.

$$S_{1(\mathrm{B})} = \frac{2(c_w + \sigma_3 \cdot tan(\phi_w)}{\left(1 - tan(\phi_w) \cdot tan(\mathrm{B})\right) \cdot sin(2\mathrm{B})} \tag{8.2}$$

$$\frac{S_{1(\mathrm{B})}}{S_{1(90°)}} = \frac{k}{cos^4(\mathrm{B}) + k \cdot sin^4(\mathrm{B}) + 2n \cdot sin^2(\mathrm{B}) \cdot cos^2(\mathrm{B})} \tag{8.3}$$

$$n = \frac{E_{90°}}{2G'} - v' \tag{8.4}$$

$$G' = \frac{E'}{2 \cdot (1 + v')} \tag{8.5}$$

8.2. Brazilian Tensile Strength

8.2.1. Test Method

The tensile strength is tested by the Brazilian Tensile Strength (BTS) test according to ISRM (1978). The test is executed on rock disks with a diameter of 40 mm and thickness of 20 mm. 13 sandstone disks are tested and 13 limestone disks, of which 4 originate from Carrière des Limites and 9 from Carrière de Frimoye. Two disks are obtained from one core, indicated by the underscore 1 or 2 at the end of each sample code. The BTS test result is an indirect tensile strength, because a vertical

Table 8.3: Brazilian Tensile Strength test results of the sandstone disks. The last 5 results with the indices ∥, ⊥ and 30° refer to the bedded sandstone disk tested at three angles, parallel, normal and at 30° , to the bedding.

Sample	H3_1	H3_2	H8/11_1	H8/11_2	H6_1	H6_2	H12_1	H12_2	H∥_1	H∥_2	H⊥_1	H⊥_2	H30°_1
σ_t (MPa)	5.7	4.6	14.2	12.4	7.0	4.8	12.8	11.4	3.9	2.2	7.7	8.0	3.3

compressive force is translated to a horizontal tensile force. The tensile strength at the centre of the disk at time of failure is computed according to equation 8.6 where; P is the applied force, R is the radius of the disk and L is the thickness of the disk. The disks are compressed between two flat platens. High contact compressive stresses between the flat plates and rock disk can results in local fracturing before tensile failure that proceed from the disk's circumference towards the tensioned centre (Price, 2008). In this case the recorded tensile strength is not correct and curved platens can overcome these stress concentrations. The tensile strength is an important character regarding the durability of armourstone. Several deterioration mechanisms, like salt crystallisation and swelling of clay minerals, impose a tensile stress on the rock. The block samples tested on their BTS value correspond to the blocks tested on their UCS.

$$\sigma_t = \frac{P}{\pi R L} \tag{8.6}$$

8.2.2. Results and Discussion

The BTS test results of the sandstone are listed in table 8.3. Five of the sandstone disks originate from block sample H7/10 and are tested parallel, normal and at an angle of 30° to the bedding within the sandstone. The remaining eight disks are obtained from four other block samples, corresponding to the ones used for the UCS testing. The BTS values for the samples H8/11_1&2 and H12_1&2 are above 10 MPa and clearly higher than the other sandstone disks. The disks H8/11_1&2 and H12_1&2 belong to the dark red, homogeneous sandstone that has no clear bedding. These disks can be compared to the cores H 8 ,9 ,10, 11, 13 and 14. The BTS results agree with the division in strengths observed during the UCS tests. The BTS test performed with different angles towards the bedding lead to a difference of 5.8 MPa between the disks, while they are drilled from the same source block. The lowest BTS value is observed on the disks tested parallel to the bedding. This results in a tensile stress perpendicular to the bedding, consequently splitting the disk along the bedding, as can be seen in figure 8.8b. The orientation is not perfectly parallel, since the disk twisted slightly during clamping the disk between the plates. The bedding is in the case of the tested sandstone a weak plane within the rock structure and thus the low BTS values make sense. The BTS of H∥_1 is higher than the BTS of H∥_2 because the axial splitting along the bedding is not as smooth, which can be a result of a slight change in rock fabric providing for example a better cohesion between the quartz grains. Furthermore, minor cracks parallel to the splitting surface are noticed before failure of the disk suggesting the resistance along the bedding is slightly higher in sample H∥_1. The BTS of the disk tested at an angle of 30° is with 3.3 MPa comparable to the values parallel to the bedding. The failed disk is presented in figure 8.8c. The failure is still along the bedding, yet this time slightly angled and not perfectly vertical. So, the angle of 30° is still low enough to induce tensile failure along the weak bedding plane and not through the rock matrix. The test results of the disks perpendicular to the bedding acquired values of 7.7 and 8.0 MPa, nearly four times as high. The failed sample in figure 8.8a shows a rough axial split instead of the smooth split along the bedding in the previous discussed samples and agrees with the assumption of failure through the rock mass. The samples H8/11_1&2 and H12_1&2 are homogeneous and show no bedding. Their BTS value is not influenced by the orientation within the apparatus and high compared to the other disks. The specimens have a brittle failure pattern with a concentration of parallel cracks towards the outer edges of the disks. This results in a loss of material at these points as can be seen in figure 8.9. The curves platens should have been used here, since compressive failure was reach at the contact points before tensile failure at the tensioned centre of the disk. From the results on the sandstone disks can be concluded that the tensile strength is greatly influenced by weak structures within the rock matrix. Tensile stresses induced in the sandstone samples showing a bedding will result in tensile failure at low stresses along the bedding plane.

The results of the BTS test on the limestones are presented in table 8.4. The table contains both results for the limestone (Lim) and limestone (Fri), which can be recognised by the L and F in front of the

Table 8.4: Brazilian Tensile Strength test results of the limestone disks.

Sample	L8/10_1	L8/10_2	L7/10_1	L7/10_2	F5/10_1	F5/10_2	F4/10_1	F4/10_2	F2_1	F2_2	F4_1	F4_2	F12_1	F12_2
σ_t (MPa)	6.5	6.7	6.8	7.0	8.0	7.2	6.2	5.8	9.2	8.3	3.2	2.8	9.6	7.8

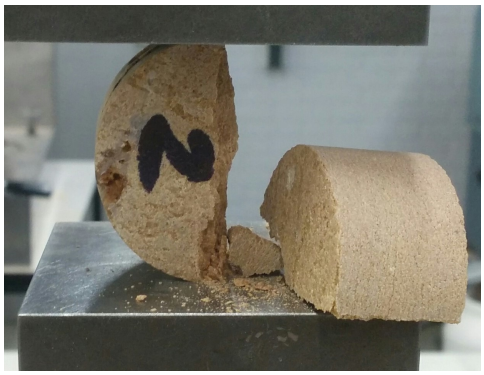

(a)

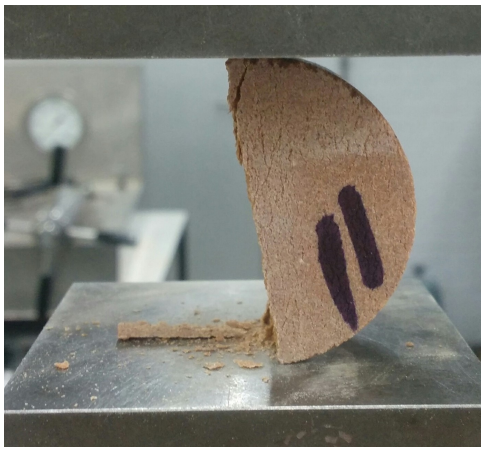

(b)

(c)

Figure 8.8: Selection of the failed sandstone disk specimens after the Brazilian Tensile Strength test; (a) normal to the bedding, (b) parallel to the bedding (slightly tilted 0-10 °) and (c) at an angle of 30° to the bedding.

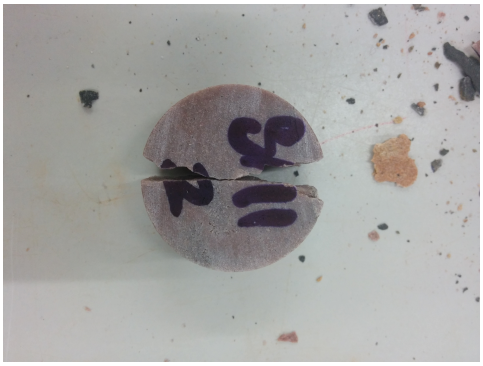

Figure 8.9: Disk 8/11_2 after failure in brittle fashion. The material loss at the contact points of the BTS test apparatus indicate that compressive failure occurred before tensile failure through the tensioned centre. Curved platens should have been used for this disk instead of flat end platens.

sample codes respectively. The BTS values of the limestones do not show the large range observed for the sandstone, however the minimum and maximum BTS still vary $\pm$7 MPa. The BTS of the limestone (Lim) is consistent between 6.5 and 7.0 MPa. Yet, the BTS recorded on the limestone (Fri) ranges from 2.8 to 9.6 MPa. The difference is observed between the blocks and between the two disks from one single block. The largest difference is between the samples from different blocks. For example, the average BTS of F4_1&2 is 3.0 MPa, while the average BTS of F2_1&2 is 8.8 MPa. Samples F4_1&2 give signs of internal weathering, beige stained spots, potentially forming weak planes and failure at a low applied force which is in agreement with the UCS test results. The difference between the disks _1 and _2 is for most limestone (Fri) samples within 1 MPa. This gap can be a result of small changes in rock fabric between the two disks or minor defects such as small cracks. But, it can also be a result of a thin bedding within the limestone. This bedding is not visible by the naked eye, but is present as a result of the sedimentary deposition as observed in the thin section LA 2 by the petrographic analysis. The orientation of the applied force to the bedding has an influence on the BTS. The effect is smaller than for the sandstone, probably because the limestone is fine grained and therefore the bedding planes are not very weak. The samples F12_1&2 show a larger gap of 2 MPa. Both failed disks are visible in figure 8.10. Disk F12_1 in figure 8.10a failed after a few parallel cracks formed and left a rough splitting surface. In contrast, disk F12_2 failed along one tensile crack which is very smooth. This suggests that sample F12_2 failed along the bedding resulting in a lower BTS and F12_1 failed through the rock matrix.

8.3. Conclusion

Both strength tests indicate the variance within the sandstone and influence of the stress direction towards the bedding. Additionally, the three sampling locations of the block samples are reflected by the UCS and BTS test. Halve of the sandstone cores, originating from the shear zone, turn out to be weak and strongly influenced by the bedding. A minimum UCS value of 35 MPa is expected to be obtained at a loading orientation of 27-28° to the bedding for these sandstones. The other halve consists of very strong, homogeneous sandstone with UCS values exceeding 250 MPa. The tested limestones are considered strong with average UCS values of 180 and 170 MPa for ten cores. The limestone (Lim) is very consistent, while the limestone (Fri) varies more. The BTS test results are greatly influenced by the orientation of the bedding to the tensile force axis. This is clearly observed during testing of the sandstone. The difference in smoothness of the splitting surface for the limestone disks indicates the influence of the bedding as well. However, the disks with clear differences were not examined during the petrographic analysis, so the influence of the bedding cannot be confirmed for the limestone pieces. The two sandstone groups distinguished by the UCS test are recognised by the BTS test as well. The limestone (Lim) has a consistent BTS values of 7 MPa, while the limestone (Fri) varies more just like observed during the UCS test. The BTS test proofs to be a simple index test capable of investigating the influence of the weak bedding plane on tensile failure and to recognise variability due to a change in rock structure.

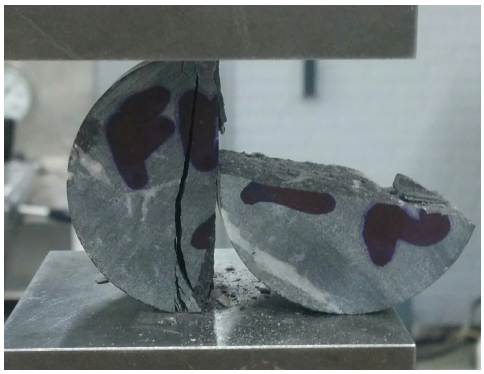

(a)

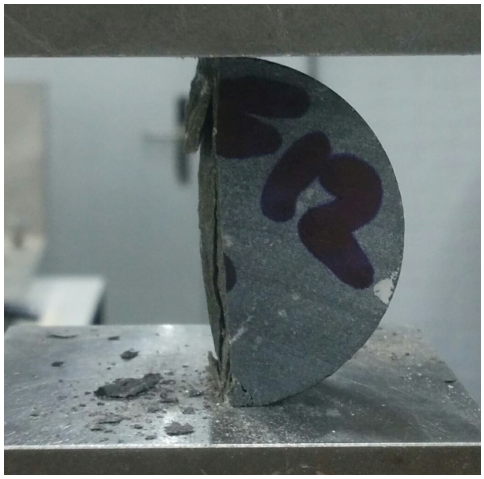

(b)

Figure 8.10: Limestone (Fri) disks after failure during BTS test; (a) sample F12/1 and (b) sample F12/2.

9

Equotip

The rock properties determined according to EN-13383:1&2 give an indication of the armourstone durability. In addition variability within the sandstone and limestone is recognised by tests. The first simple index test, the BTS test, agreed with the observed variation and indicated the influence of the bedding plane within the weak sandstones. This chapter will be investigate of the Equotip agrees with these observations as well and can possibly add valuable information next to these obtained test results.

9.1. Test Method

Equotip measurements are performed on the aggregate samples obtained from the quarry stockpiles. Their surface is not prepared for testing by means of e.g. sawing and sanding, and the pieces are mainly tested in air-dried condition. The measurements are taken on the aggregate's surface with a regular spacing of $\pm$1 cm, far as possible, covering the full sample surface area. The total amount of measurements per sample is close to minimum of 45 as proposed by Wilhelm et al. (2016). Sample shape and surface roughness can limit the regular distribution of Equotip measurements over the surface area. The Equotip is slightly shifted until it properly rebounds, in the case that it is not possible to obtain a rebound at a specific location. The Equotip gives a L-value even when there is no rebound on the rock surface, because the tip rebounces on the support ring that prevents the tip from shooting out of the apparatus. In this case, the L-value for the type D is between 250 and 350. In addition, the Equotip makes an easily distinguished sound when it rebounces on the support ring. Therefore, a mishit is easily distinguished. Both the simple impact method (SIM) and repeated impact method (RIM) are performed on the aggregate pieces. The RIM measurement will be taken once on each aggregate sample, otherwise the high number of measurements makes the method inconvenient. The RIM is tested at the smoothest part of each aggregate piece, that is away from the corners and edges of the sample. The reproducibility of the obtained results will be tested on a few aggregate pieces by performing multiple RIM measurements at different spots.

After these measurements, some aggregate particles are prepared by creating a sawn surface along their length axis. The saw creates a smooth surface over the centre of the aggregate pieces. The Equotip measurements are performed on the sawn surface. This surface is covered with a 1 cm grid spacing as well. The total amount of measurements per sample will be lower compared to the method before, since only a small part of the aggregate surface is tested. Yet, the smoothness of the surface will reduce the scatter in the data caused by the surface roughness of the untreated samples (Wilhelm et al., 2016). Consequently, the lower number of rebound points may be enough to obtain a reliable mean rebound value. The obtained L-values will be compared to the rebound values recorded on the unprepared, rough surfaces.

Next to the aggregate samples, the rock cores are tested with the Equotip as well. Since the cores have a smooth, sawn surface, less measurements are required. In total 22 rebounds are taken per cores, distributed over the core as depicted in figure 9.1. 5 measurements are taken at both flat ends and 12 measurements along 4 lines over the core length, each line made up of three measurements. Only SIM measurements are performed on the rock cores. The cores are tested in oven-dry and

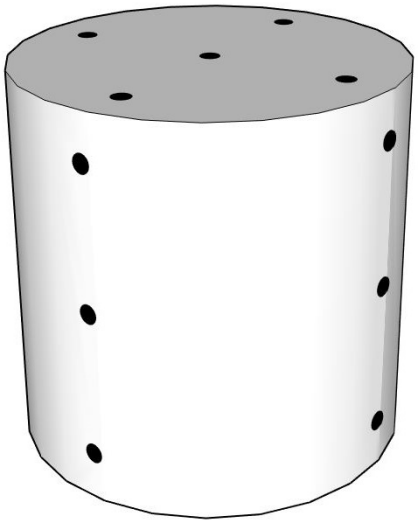

Figure 9.1: Approximate distribution of Equotip measurements over the core volume. The black dots represent the impact points of the Equotip.

saturated condition. The disks used for the BTS test are tested with the Euqotip as well in oven-dry condition.

All Equotip measurements are executed with both the type D and type C tip. There is a slight shift in the measuring grid of the type C tip with regard to the type D tip to prevent a double rebound on a specific spot. Moreover, the Equotip is performed vertically downwards in all cases.

9.2. Statistic Analysis of SIM Measurements

First the Equotip rebound values will be statistically evaluated. The mean, median, standard deviation and MAD are considered to investigate the tested rock pieces and rock cores. Moreover, the student's t-test is performed to compare the different samples to one another.

9.2.1. Aggregate Samples

Histograms

First, the rebound values on the rough aggregate surface are evaluated. The Equotip measurements on the aggregate do, in general, not show a normal distribution. Figure 9.4, 9.6 and 9.8 illustrate a few examples of the Equotip type D distributions of the sandstone, limestone (Lim) and limestone (Jen) aggregate pieces respectively. There is a variety in the histograms as can be seen in those figures. The examples will be discussed one by one. First, the histogram of sandstone aggregate sample HA 20 in figure 9.4a is close to a standard distribution. However, sandstone sample HA 24 shows a deviating distribution with two clear peaks in the frequency away from the mean value in figure 9.4b. The peaks can be explained by the measuring grid of the Equotip measurements. The hardness of the aggregate surface is not constant, but influenced by the mineral content, presence of joints and cracks, presence of stylolites and veins, and the difference in degree of weathering. Consequently, during the measurements with the Equotip, the tip may hit more quartz crystals in the sample HA 24. This results in a peak at the higher rebound values. The samples HA 20 and HA 24 are presented in figure 9.2. There is no big difference between the two samples based on their visual appearance on this scale. The rock structure of the two sample appears to be the same. In addition, there are no big cracks visible in the sample and the degree of weathering seems to be similar. Nevertheless, some differences are observed that can explain the distribution in the rebound values when the pieces are examined by a 10x hand lens. Figure 9.3 shows the hand lens view on the samples HA 20 and HA 24. The rock matrix of HA 24 consists of larger quartz crystals compared to HA 20. The sugar like structure is a typical quartzite structure. The chance that the Equotip hits a quartz crystal in the matrix of HA 24 is therefore larger than for sample HA 20. Hence, the peak at higher rebound values can be explained due to the high hardness of the present quartz crystals. In addition, a few minor cracks run through the sample HA 24. A rebound on or close to such a crack will lower the L-value. So, the minor cracks

may explain the peak at the lower rebound values. Theses features and the 'luck' of hitting them with the standard measuring grid results in a non-normal distribution for sample HA 24. The constant matrix of HA 20 and absence of cracks results in the near normal distribution.

In contrast, the distribution of limestone (Lim) sample LA 5 in figure 9.6a is far from a normal distribution and shows only an increase in frequency upon increase in rebound value. This increase in frequency in histogram translates to a higher amount of rebounds with a high rebound value during the Equotip measurements. The sample has a smooth surface compared to other samples, low degree of weathering and several calcite veins run through the sample. Inspection with the 10x hand lens shows a homogeneous, very fine rock matrix without visible crystals. Some small fossils, mainly shells, are present. The fine, homogeneous matrix and fairly smooth aggregate surface result in high rebound values. No higher rebound values can be obtained, due to a lack of larger, harder crystals within the matrix and low degree of weathering. This explains the peak in the frequency for the highest rebound values. The histogram of limestone (Lim) sample LA 7 in figure 9.6b also displays an increase in frequency for the higher rebound values. Yet, the highest rebound value is not the most frequent hit this time. The only explanation can be given by the slight increase in surface roughness for this sample compared to LA 5, when inspected by the naked eye as can be seen in figure 9.5. Small 'dents' in the rock surface may slightly decrease the impact of the Equotip, reducing the rebound value. Furthermore, calcite veins which are present in equal amount in LA 5 and LA 7 result in their turn into a small amount of lower rebound values.

The limestone (Jen) samples JA 1 and JA 2 are depicted in figure 9.7. Both aggregate samples have two sides with a higher degree of weathering, yet only one of these sides is captured in the pictures. Sample JA 1 increases significantly in surface roughness on one of the weathered sides. The corresponding histograms of the two samples are visualised in figure 9.8. The histogram of JA 1 contains some very low values of below 200. This can be explained by the rough, weathered side that resulted in a poor rebound of the Equotip. The remaining rebound values show a frequency that is close to a normal distribution. The histogram of JA 2 displays two easily distinguishable peaks in the frequency domain. Probably the peak at the lower rebound value of $\pm$500 is obtained at the weathered sides, while the peak at a rebound of $\pm$700 results from the Equotip measurements on the relative fresh sides.

To summarise, there is already variation within the histograms of the Equotip data of 6 aggregate samples. Most histograms deviate from a normal distribution. Yet, the obtained Equotip distributions seem to correlate to textural features and mineral content within the aggregate samples. Therefore, the mean and standard deviation of the distributions can be valuable parameters when considering the rock strength, variation in mineral content, rock structure, degree of weathering and ultimately rock durability. A list of histograms for the tested aggregate samples is displayed in Appendix H, which emphasises the variability within the histograms of the Equotip data. The histograms of the type C tip are listed in the same Appendix. The histograms of the type D and C tip differ per sample, due to the shift in measuring grid. Nevertheless, the shape of the histogram is similar for most samples.

Mean and Standard Deviation

The mean and standard deviation of both type D and C Equotip are visualised in figure 9.9 for a selection of the aggregate pieces. The type C and D tip have similar tungsten carbide tips with a diameter of 3 mm. Yet, the impact energy of the type C is lower and therefore the impact footprint as well. The rebound energy of the type C tip is reflected less deep into the aggregate pieces compared to the type D tip. Consequently, a rebound value obtained by the type C Equotip is more likely to be related to a single feature in the rock matrix and not averaged over a larger volume, as the case for the type D tip. This impact volume is not investigated during this research, but assumed to be below the 1 cm spacing maintained during the SIM measurements. The mean L-value is higher for the type C tip compared to the D tip for most aggregate samples. The difference in rebound value between the two types ranges from 0 to 100 for the sandstone, from 0 to 70 for the limestone (Lim) and from 15 to 75 for the limestone (Jen). Nevertheless, there are samples that show a drop in mean rebound value when using to the type C tip instead of the type D. This is presumably the result of the difference in measuring grid for the type D and type C tip, already observed within the histograms. The Equotip measurements of the two tip types are not performed at the exact same location and consequently a different mean value can be obtained. The difference in mean value between the type D and C is small compared to the standard deviation of the measurements on each sample, which is between 100

(a) (b)

Figure 9.2: Sandstone aggregate samples; (a) sample HA 20 and (b) sample HA 24. The scale is similar for both samples.

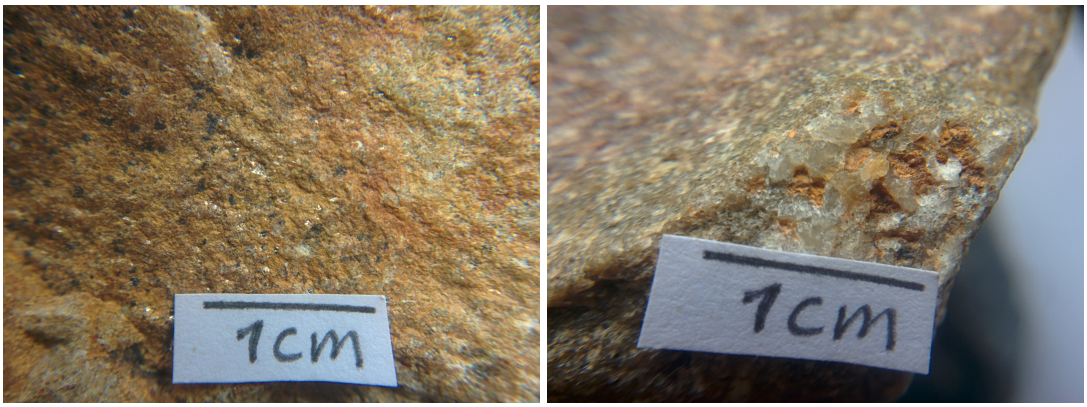

(a) (b)

Figure 9.3: Hand lens view of sandstone aggregate samples; (a) sample HA 20 and (b) sample HA 24.

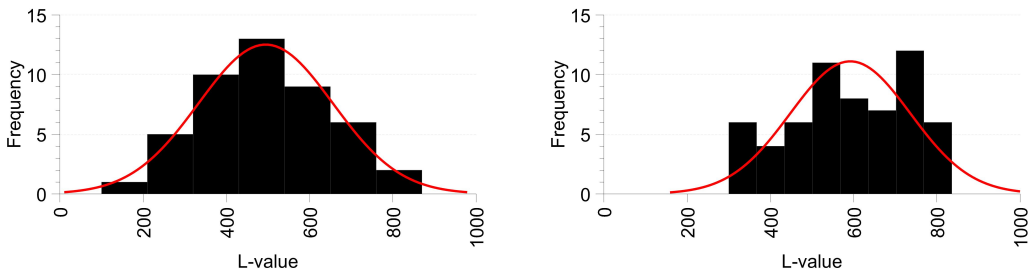

(a) (b)

Figure 9.4: Histograms showing the distribution of the Equotip type D measurements on the sandstone aggregate; (a) sample HA 20 and (b) sample HA 24.

Figure 9.5: Limestone (Lim) aggregate samples; (a) sample LA 5 and (b) sample LA 7. The scale is similar for both samples.

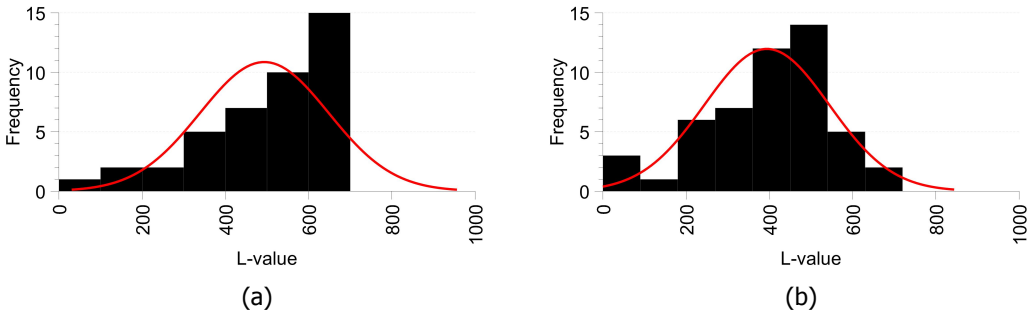

Figure 9.6: Histograms showing the distribution of the Equotip type D measurements on the limestone (Lim) aggregate; (a) sample LA 5 and (b) sample LA 7.

Figure 9.7: Limestone (Jen) aggregate samples; (a) sample JA 1 and (b) sample JA 2. The scale is similar for both samples.

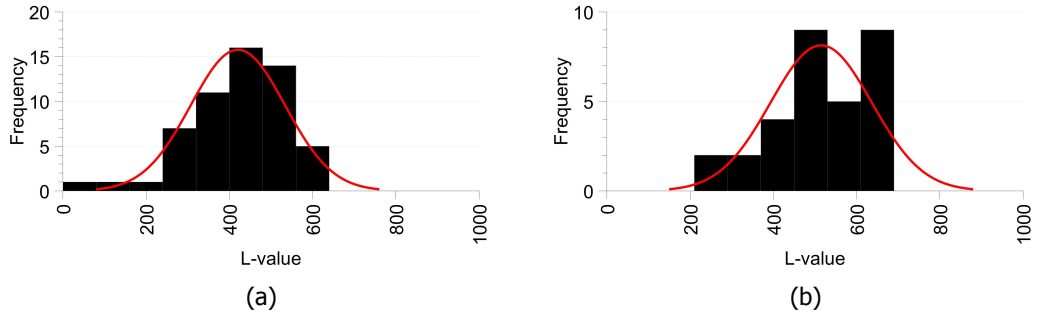

Figure 9.8: Histograms showing the distribution of the Equotip type D measurements on the limestone (Jen) aggregate; (a) sample JA 1 and (b) sample JA 2.

and 150. The standard deviation varies between the two tip types as well. The difference in standard deviation between the two tip falls between 0-50 for the sandstone, 0-35 for the limestone (Lim) and 0-55 for the limestone (Jen) aggregate samples. However, the data does not agree whether the standard deviation increases or decreases changing from the type D to C tip. The standard deviation increases for 12 samples and decreases for 3 samples when the type C is used instead of D for the sandstone sample. The limestone (Lim) shows an increase for 5 samples, a decrease for 7 samples and one sample with similar deviations. Finally, the standard deviation of the limestone (Jen) increases for 11 samples and decreases for 5 samples. Again, the poor consistency is attributed to the different measuring points for the type D and type C tip. In addition, the changes in standard deviation are small. A larger standard deviation would be expected for the type C tip, since this device is designed to be more sensitive to minor defects and thus has a larger spread in rebound data. Nevertheless, both Equotip types are able to detect differences between the aggregate pieces.

The sandstone aggregate pieces in figure 9.9a display a drop in mean rebound for the samples HA 21, 41, 43 and 44. This drop in mean rebound can be explained by the visual appearance of the samples. HA 21 has a higher degree of weathering and clear foliation, while the other mentioned pieces show indications of small clay seams by a clear sequence of intensified weathering in the rock surface. So, all the samples with a reduction in rebound show potential weak planes within the rock fabric. However, sample HA 42 looks very similar to HA 41 but does not drop in rebound with respect to the other tested sandstone samples. The presence of clay seams is less clear in samples HA 42, thus the structure may be stronger than HA 41 resulting in a higher rebound value. The measurements perpendicular to the bedding deviate from the rebounds parallel to the bedding for the samples HA 41, 43 and 44. The measurements parallel are 200 to 300 lower in L-value. These measurements are included in the results, yet it is uncertain if this is the appropriate method.

The variation between the mean rebound values of the limestone (Lim) in figure 9.9b is comparable to the variation in rebound for the sandstone. Although, the aggregate pieces look more similar to one another. The limestone aggregate pieces are less smooth and have an irregular shape, but this has influence on the standard deviation and not the difference spotted between the individual pieces. The obtained difference in mean rebound cannot be explained by the visual examination and is therefore probably related to the measuring grid.

The mean rebound values of the limestone (Jen), displayed in figure 9.9c, are lower for three samples; JA 1, 4 and 6. The samples JA 4 and 6 are weathered and show a beige colour instead of grey. Sample JA 1 has one weathered side with a very rough surface, while the other sides of the sample look rather fresh. The weathering of the samples results in a lower L-value compared to the other pieces. Since sample JA 1 is less weathered its rebound value is higher than JA 4 and JA 6.

Figure 9.10 presents the median and median absolute deviation (MAD) for the same selection of sandstone and limestone aggregate pieces. The MAD is median value of the absolute differences between the measured rebound values and the median value as noted in equation 9.1 where; X_i is the rebound value and X is the median rebound value of the measurements. The pattern of change in median value between the samples is similar to the mean. Moreover, the standard deviation and MAD vary in their magnitude alike. Yet, the distribution of the median values is more narrow compared to the mean values and the MAD is much smaller than the standard deviation. The samples are less

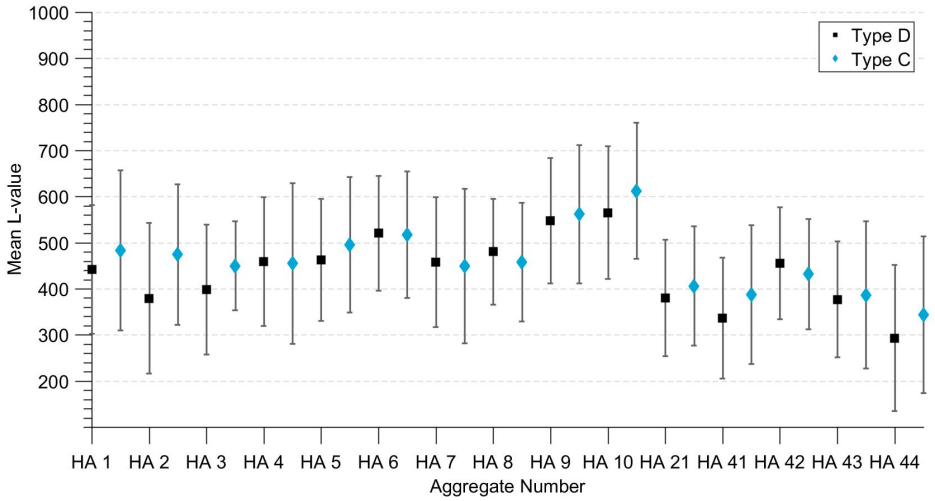

(a)

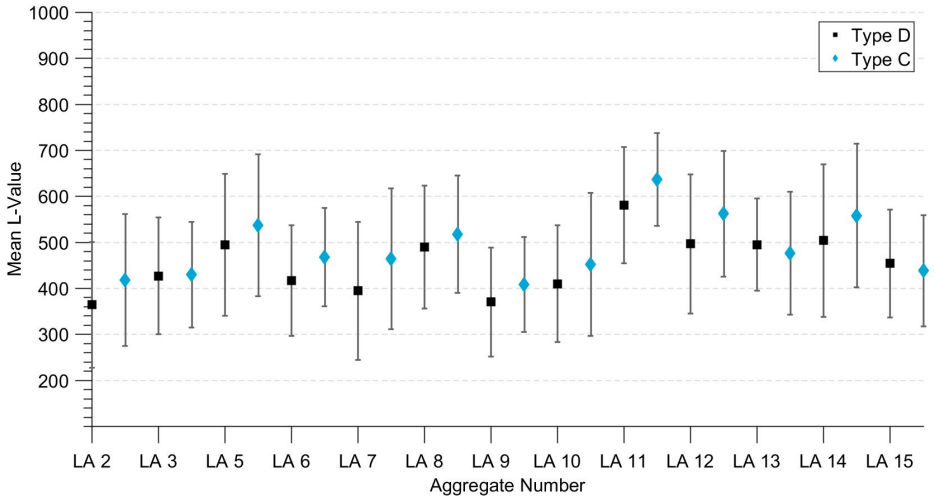

(b)

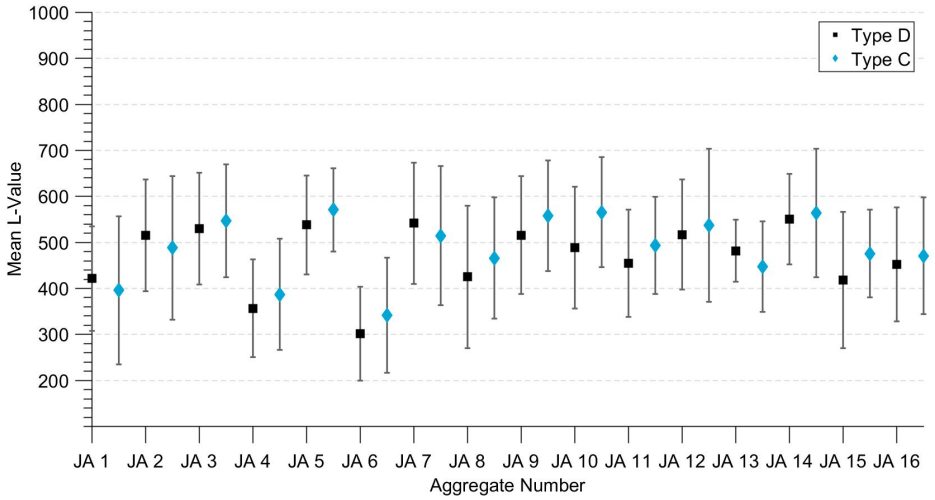

(c)

Figure 9.9: Statistical analysis of the aggregate Equotip measurements on; (a) sandstone, (b) limestone (Lim) and (c) limestone (Jen). The symbols represent the mean value of the measurements on each aggregate piece and the grey bars represent the standard deviation above and below the mean.

unique according to the median value. Consequently, the data may lose valuable information about the aggregate pieces when the median and MAD are used instead of the mean and standard deviation. Especially the influence of low rebound values due to cracks or concentrations of clay minerals is diminished when using the median and mad. Thus, features related to rock durability can be missed.

$$MAD = median(|X_i - X|) \tag{9.1}$$

Sampling Size

The sampling size for the aggregate pieces is rather large with an amount of approximate 45 readings per sample. A smaller sampling size may be used instead, depending on the purpose of the data, since the obtained standard deviations on the samples are large. Therefore, the measuring grid is enlarged. The space between the impact points is increased from 1 to 2 cm and thus the amount of measurements is halved. This results in a change of the mean, median and standard deviation. Table 9.1, 9.2 and 9.3 list the change in mean L-value, median L-value and standard deviation when the sample size is halved for the sandstone, limestone (Lim) and limestone (Jen) respectively. A negative change is a decrease in a certain value when the measurement spacing increases to 2 cm. The shift in mean and median of the aggregate samples is minimal, with a maximum of 40%, relative to the standard deviation of the 1 cm grid, which will be used as a reference value; standard deviation (ref). Consequently, the amount of measurements can probably be reduced. The standard deviation changes as well, next to the change in mean and median. This change is not significant with a maximum change of 36 in rebound value, but may loose valuable information. The standard deviation is greatly influenced by rebound values that deviate strongly from the mean. These rebound values are interesting for the durability estimate of an armourstone, especially the lower rebound values. Cracks and presence of weak minerals, such as active swelling clays, result in low L-values and thus have a strong influence on the standard deviation. These features may have a negative influence on the durability of the armourstone and thus is the standard deviation an important parameter. Both an increase and decrease in standard deviation can be observed for the sandstone, limestone (Lim) and limestone (Jen) samples upon doubling the rebound spacing. It should be kept in mind that the standard deviation for the 2 cm grid spacing is more sensitive to extreme values, because the total amount of measurements is lower. A decrease in standard deviation may indicate that the weak structures in the sample are hit by the Equotip, despite the larger spacing, but have now a bigger impact on the standard deviation. In contrast, an increase in standard deviation presumably means that the low rebound structures are missed in case the spacing between Equotip impact points is enlarged. Table I.16, I.17 and I.18 in Appendix I show the changes upon increasing the spacing of the measurement grid for the type C Equotip. The changes in mean, median and standard deviation are for the type C tip of the same magnitude compared to the type D tip. Nevertheless, in most cases the change is slightly larger for the type D tip especially in ratio to the standard deviation (ref). The different values per sample between the type D and C is possibly a result of the shift in measuring grid. Sometimes the changes in median and mean upon doubling the rebound spacing is far apart, like for sample HA 10 and JA 1, which depends on the shape of the histogram of the rebound values.

Table 9.1: Change in the Equotip type D rebound statistics upon doubling the spacing between measurement points on the sandstone. The doubling results in half of the amount in rebound values compared to the reference case with a spacing of ± 1 cm between the impact points. The standard deviation (ref) is the one for this narrow spacing. A positive difference shows an increase in the specific value for the wider spacing of ± 2 cm, while a negative value shows a decrease.

Sample	HA 1	HA 2	HA 3	HA 4	HA 5	HA 6	HA 7	HA 8	HA 9	HA 10
Standard Deviation (ref)	139	163	141	140	132	124	141	115	136	144
Change in Mean	-34	38	57	32	-15	-15	-19	-10	-1	-14
Change in Median	-32	51	46	42	-30	-11	-37	6	1	-44
Change in Standard Deviation	-11	5	-23	-13	-18	16	11	7	2	-5

Student's T-Test

The Student's t-test of independent samples is performed on the aggregate data next to the determined mean, median, standard deviation and MAD. The t-test is used to see if the mean rebound values of the aggregate pieces are statistically significantly different. In other words, it can be determined if two samples have different means because of chance or because they have different properties by

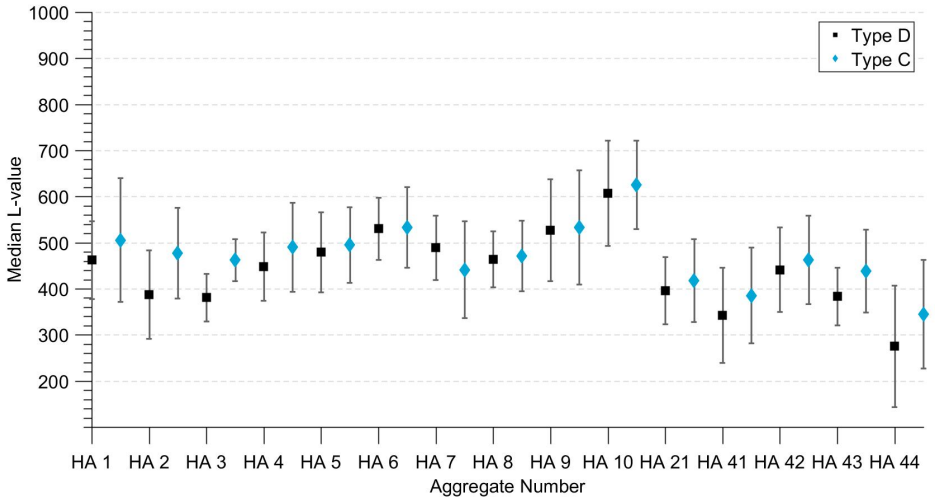

(a)

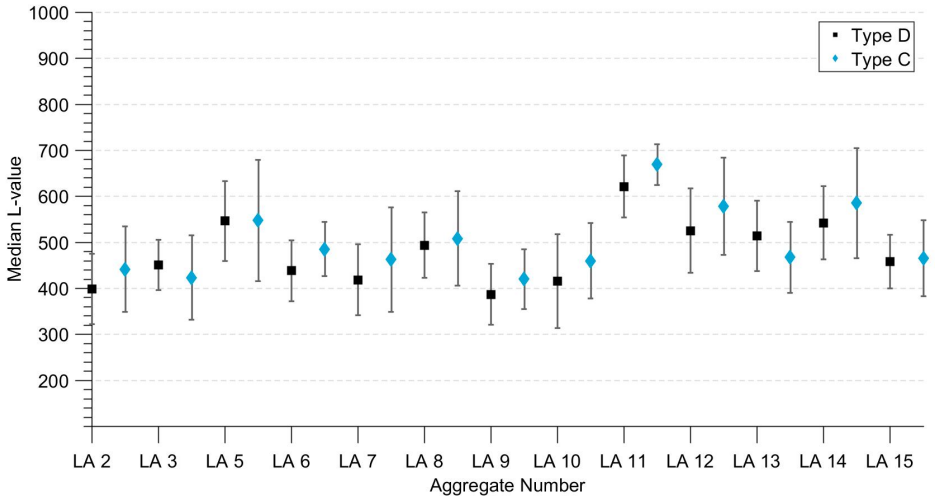

(b)

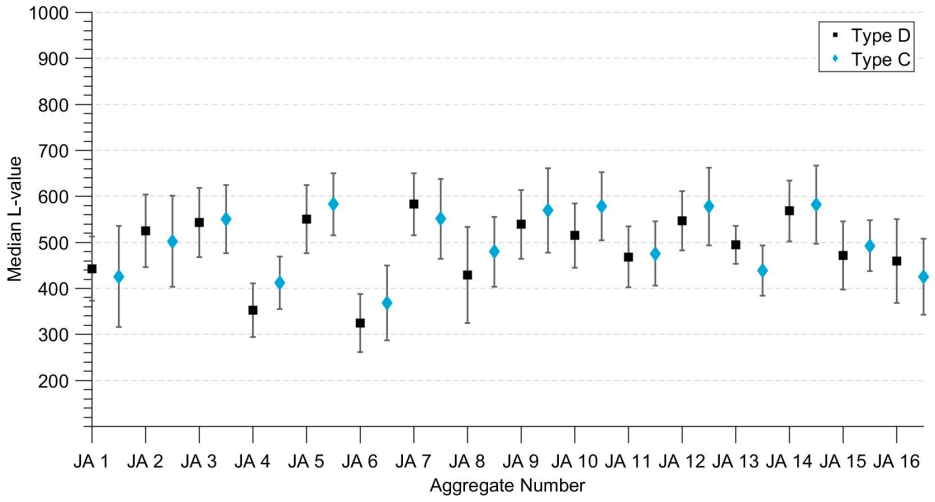

(c)

Figure 9.10: Statistical analysis of the aggregate Equotip measurements on; (a) sandstone, (b) limestone (Lim) and (c) limestone (Jen). The symbols represent the median value of the measurements on each aggregate piece and the grey bars represent the median absolute deviation above and below the median.

Table 9.2: Change in the Equotip type D rebound statistics upon doubling the spacing between measurement points on the limestone (Lim).

Sample	LA 1	LA 2	LA 3	LA 4	LA 5	LA 6	LA 7	LA 8	LA 9	LA 10
Standard Deviation (ref)	120	137	127	89	154	120	150	133	118	127
Change in Mean	5	4	-16	-1	-1	-2	-21	-21	-17	-8
Change in Median	20	17	-24	-8	-3	3	-25	-19	-19	0
Change in Standard Deviation	-7	26	-9	8	0	7	5	21	-2	-22

Table 9.3: Change in the Equotip type D rebound statistics upon doubling the spacing between measurement points on the limestone (Jen).

Sample	JA 1	JA 2	JA 3	JA 4	JA 5	JA 6	JA 7	JA 8	JA 9	JA 10
Standard Deviation (ref)	113	122	121	106	108	102	132	155	128	132
Change in Mean	-12	-17	6	-4	1	-3	-19	-47	2	-30
Change in Median	2	0	21	-8	-5	0	-34	-20	-10	-40
Change in Standard Deviation	21	6	14	-13	-5	9	10	28	-20	0

performing the t-test on the mean rebound values. Thus, it can be established whether one deals with a different rock piece or if the samples can be regarded similar aggregate pieces when purely based on statistics. The t-test takes the mean, standard deviation and number of Equotip measurements into account. The t-test is performed on t-values and the result is presented in p-values. The t-value measures the magnitude of the difference between the mean values relative to variation in sample data. It can be referred to as a signal to noise ratio. The higher the t-value, the greater the evidence against the null hypothesis. The null hypothesis states that the two sets of Equotip measurements are independent random samples with equal means and variances, assuming a normal distribution. Thus, the closer the t-value is to 0, the more likely there is not a significant difference. By taking multiple random samples from the same data set a t-distribution is obtained. The t-value changes slightly due to the random variation within the data set. These t-values can be plotted in a probability density function (PDF) that shows the likelihood of each t-value. The PDF is a normal distribution centred at a t-value of 0. Thus, the likelihood for higher t-values is lower. This is expressed by the p-value. Since the test is two-tailed, the difference can be both higher and lower. The likelihood is the area below the probability density function for a certain t-value on both positive and negative side. In this case a confidence interval of 95% is maintained. This corresponds to a p-value of 0.05, which represents the area of the PDF at both extreme ends. An example is presented in figure 9.11. The null hypothesis is rejected when the p-value is 0.05 or lower. The samples can statistically be related when the p-value is above 0.05. The t-test can be used to indicate if the Equotip is sensitive to changes in the rock pieces, although the results show no perfect normal distributions. The results of the t-test for the sandstone, limestone (Lim) and limestone (Jen) are presented in table I.1, I.5 and I.9 respectively. The tables show the p-values of the null hypothesis.

Table I.1 shows the results of the t-test for the 40 sandstone aggregate samples. All 40 samples are compared to one another. The p-values range from 0.00 to 1.00, thus there are sandstone samples that are statistically related and samples that are probably not related. This makes sense, because the aggregate samples are collected at the same quarry. Consequently, aggregate samples are present that originate from the same source rock. However, the p-values below 0.05 show that the Equotip

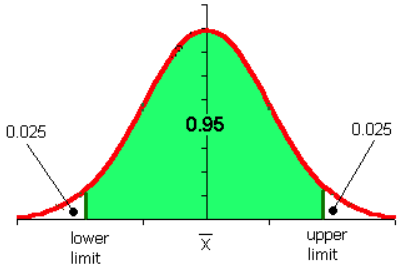

Figure 9.11: Example of a t-distribution with a cutoff confidence interval of 95% after wustl.edu.

recognises variability within the small aggregate samples when measured on their rough, untreatened surface, as the null hypothesis is rejected in these cases. 391 of the in total 780 combinations have a p-value below 0.05 when the 40 sandstone aggregate samples are tested to one another, which is near half of the combinations. Table I.2 shows the p-values for the Equotip measurements with a 2 cm spacing. In this case for 230 of the 780 combinations the null hypothesis is rejected. The p-values increase for 591 of the 780 cases when the spacing between the measurements is doubled. Thus, more aggregate pieces are considered statistically similar when the spacing of Equotip rebound points is doubled. The p-values of the type C measurements are listed in table I.3 and I.4 for the 1 cm and 2 cm measurement grid respectively. The results are compared to the t-test results of the type D measurements. A smaller selection of the samples are tested with the type C tip and these samples are compared to the ones tested with the type D tip. 55 combinations are possible for the t-test for the new sample selection of the sandstone. The null hypothesis is accepted for the type D measurements with a 1 cm spacing in 34 cases, while it is accepted 25 times for the type C for these 55 combinations. This decreases to 18 and 17 when the spacing is extended to 2 cm for the type D and C respectively. In 30 cases the p-value is higher for the type C compared to the the type D with a 1 cm spacing, yet only in 10 cases with a 2 cm spacing. So, there are more statistically, independent random samples according to the type D Equotip. The type D tip recognises more independent sandstone samples than the type C tip, yet they show almost similar results when the rebound spacing in increased to 2cm.

The t-test on the limestone (Lim) aggregate results in similar observations. The null hypothesis is accepted in 23 of the 45 cases for the Equotip type D measurements with a 1 cm spacing, again near half of the combinations. This number decreases to 14 upon doubling the spacing between the impact points. The p-value is larger in 37 of the 45 cases for the larger measuring grid. Again the type C tip measurements are not performed on all aggregate pieces, so the total amount of combinations reduces. The null hypothesis is accepted 11 times in 28 cases and only 5 times in 28 cases for the type C measurements with a 1 cm and 2 cm spacing respectively. The p-value is in 25 of the 28 cases higher when the impact points of the type C tip are 2 cm apart instead of 1 cm. The null hypothesis is accepted for 14 in 28 cases and 7 in 28 cases for the type D tip with a 1 cm and 2 cm spacing respectively, when performed on the same aggregate selection as the type C measurements. Thus, the t-test on the limestone (Lim) concludes that the type D recognises more statistically independent samples. The increase in rebound spacing reduces the uniqueness of the samples and consequently less independent samples are recognised.

The t-test on the limestone (Jen) obtains only minor differences between the two tip types. The null hypothesis is accepted in 30 of 45 cases for the type D measurements with a 1 cm spacing, in 21 of 45 cases for the type D measurements with a 2 cm spacing, in 31 of 45 cases for the type C tip with a 1 cm spacing and finally 21 times of 45 cases for the type C tip with a 2 cm spacing. The p-value increases in 36 of 45 cases when the spacing is doubled for the type D tip and in 39 of 45 cases for the type C tip. The p-value is higher for the type C Equotip than the type D tip in 19 of the 45 cases.

Summarising, the t-test shows a clear decrease in independent samples when the Equotip type D and C rebound spacing is doubled on the sandstone, limestone (lim) and limestone (Jen) aggregate pieces. This decrease suggests that valuable features within the aggregate pieces are lost when the spacing between the rebound points is doubled. The aggregate pieces become less unique when the amount of measurements is reduced and especially important features towards durability, e.g. cracks, concentrations of clay minerals and weak planes, can be missed. The type C tip identifies less independent samples for the sandstone and limestone (lim), but similar amount to the type D tip for the limestone (Jen) aggregate. An increase in identified, independent samples was before hand expected for the type C instead, because the type C tip is more sensitive. Theoretically, small differences between aggregate samples would be better measured with the type C Equotip. The decrease in independent samples for the type C tip indicates that the aggregate pieces are more alike for the type C tip. This possibly originates from the lower impact energy, consequently decreasing the impact volume that is recorded. Small differences below the aggregate surface are better captured by the type D tip, measuring more differences between the aggregate pieces. Finally, it should be noted that the samples with a p-value higher than 0.05 can still be independent samples, however this cannot be confirmed statistically with a confidence interval of 95%.

Sawn Aggregate Samples

A selection of the tested aggregate pieces is sawn in half along their length axis. The sawn pieces are still large enough to obtain a proper rebound according to Wilhelm et al. (2016). The cut aggregate surfaces are smooth and give more insight within the fresh rock matrix. The number of Equotip impact points greatly reduces with respect to the previous on the rough surface, resulting from the decrease in testing surface area. The number of measurements per sample is related to the dimensions of the sample and ranges from 3 to 15 measurements. This is about a quarter or less of the amount of measurements taken on the rough aggregate surface. Table 9.4, 9.5 and 9.6 compare the mean and standard deviation of the Equotip type D measurements on the rough and sawn aggregate surfaces of some sandstone, limestone (Lim) and limestone (Jen) samples respectively. The difference between the results can be large. The difference in mean rebound value for the sandstone ranges from $\pm$120 to over 300. The mean rebound value obtained on the sawn surface is 1.3 to 1.8 times as high as the mean rebound on the rough surface. The limestone (Lim) shows similar increases, where the mean rebound is 1.2 to 1.8 times higher on the sawn surface. The raise for the limestone (Jen) is between 1.3 and 1.9, which corresponds to a rebound on the sawn surface that is $\pm$140 to $\pm$280 higher in L-value. Furthermore, the standard deviation of the measurements on the sawn aggregate samples decreases in an even greater magnitude. The standard deviation is 3 to 5 times as small for the sawn sandstone samples, 2 to 22 times as small for the limestone (Lim) and 2 to 12 times as small for the limestone (Jen). The increase in mean on the sawn surfaces is probably a result of the elimination of the weathered surface and reduction of the surface roughness. The majority of the rock matrix is fresh, which result in a higher rebound compared to weathered material on the outer surface. In addition, a smoother surface is a better rebound surface and results in higher L-values. The reduced standard deviation can partly be explained by the decrease in amount of impact points. Secondly, the reduced surface roughness and removal of the weathered rock exterior possibly decrease the standard deviation as well. The measurements on the cut aggregate samples can be compared to the Equotip rebound on the rock cores, which will be reviewed in the next section.

Table 9.4: Comparison between the mean and standard deviation of the Equotip type D measurements on the rough and sawn surface of a few of the sandstone aggregate samples. The mean L-value is higher and the standard deviation lower for the measurements on the sawn surface compared to the rough surface.

Sample	Mean (sawn surface)	Standard Deviation (sawn surface)	Mean (rough surface)	Standard Deviation (rough surface)
HA 6	761	42	520	124
HA 25	828	54	562	148
HA 30	744	45	410	139
HA 38	815	36	519	149
HA 41	511	25	336	131
HA 42	578	39	455	121
HA 43	580	30	377	126

Table 9.5: Comparison between the mean and standard deviation of the Equotip type D measurements on the rough and sawn surface of a few of the limestone (Lim) aggregate samples.

Sample	Mean (sawn surface)	Standard Deviation (sawn surface)	Mean (rough surface)	Standard Deviation (rough surface)
LA 2	637	19	364	137
LA 3	642	34	426	127
LA 5	664	7	494	154
LA 6	580	41	417	120
LA 7	615	65	394	150
LA 9	602	47	370	118
LA 11	683	17	580	127
LA 13	632	20	494	100

Table 9.6: Comparison between the mean and standard deviation of the Equotip type D measurements on the rough and sawn surface of a few of the limestone (Jen) aggregate samples.

Sample	Mean (sawn surface)	Standard Deviation (sawn surface)	Mean (rough surface)	Standard Deviation (rough surface)
JA 1	659	18	421	113
JA 5	690	9	538	108
JA 6	585	48	301	102
JA 10	627	36	488	132
JA 13	705	22	481	67
JA 15	640	48	417	148

9.2.2. Core Samples

Figure 9.12 presents the statistical analysis of the Equotip SIM measurements on the rock cores. The figure includes the mean and standard deviation of the data from the type D and C Equotip for both dry and saturated conditions. The histograms of the Equotip type D rebounds on the cores are listed in Appendix H. The results on the core samples will first be discussed per rock type.

The sandstone cores can be divided in two classes as clearly visible by the shift in mean rebound value and change in standard deviation. This presumably corresponds to the different sampling locations within the quarry described in chapter 4. One of the sampling locations was at a shear zone, as discussed before, resulting in a higher degree of weathering within the rock blocks. Class 1 contains the cores HA 1 to 7 and class 2 consists of cores HA 8 to 14 as defined by the UCS test. The minimum mean rebound values for the sandstone are 484, 436, 572 and 476 for the type D in dry condition, type D in saturated condition, type C in dry condition and type C in saturated condition respectively. The corresponding maximum mean values are 814, 813, 868 and 867. The mean value from the first core class is about 250 in L-value lower than the second class. Moreover, the second class shows a standard deviation that is approximately twice as small of 30 to 70. Core HA 11 and HA 13 are exceptions. Core HA 11 has a standard deviation of 117 for the type C tip in dry condition and HA 13 has a standard deviation of 93 for the type D tip in dry condition. These higher standard deviations can possibly indicate internal weathering within the cores. The histograms of the type D measurements in figure H.10 give a more detailed insight. The histograms display various patterns, as was the case for the aggregate pieces as well. The two classes are identified by the difference in width of the distribution, corresponding to the standard deviation. The cores of the first class show foliation and a higher degree of weathering. This results in more variation within the L-values, especially towards the lower end. The cores from second class peak within a low range, indication low variability within the hardness of the fresh rock material. The mean L-value is in most cases lower for the cores in a saturated condition compared to an oven-dry condition. Especially the weaker cores from the first class show a great drop of 50-100 in rebound value, which is considerable with respect to the standard deviation. The drop may be caused by wetting of clay minerals present within the rock matrix. Clay minerals can loose up to 70% of their strength upon wetting (Cherblanc et al., 2016). The change in rebound during saturation is negligible for the cores in the second class with a change of 0 to 25 in L-value. Furthermore, the drop in rebound falls greatly within the standard deviation for these cores. Therefore, the change in rebound for the second class may be a result of natural variability within the rocks instead of saturation. The recorded mean rebound for the type C tip is in all cases higher than for the type D tip. The increase in rebound for the type C agrees with the observations on the aggregate samples, but is more obvious for the cores samples as a result of the lower standard deviation.

The limestone (Lim) core samples, displayed in figure 9.12b, show a different pattern compared to the sandstone. All cores display a similar response to the Equotip and have a low spread of ± 30 in mean rebound value. A slight exception are core number 2 and 4, where the standard deviation is ± 60 instead of ± 20 observed for the other samples. The minimum mean values for the limestone (Lim) are 601, 602, 695 and 680 for the type D in dry condition, type D in saturated condition, type C in air-dry condition and type C in saturated condition respectively. The corresponding maximum mean values are 629, 631, 719 and 704. Thus, the difference between the dry and saturated mean is smaller compared to the results obtained on the sandstone. The drop is similar to the stronger cores from sandstone class two. The increase in rebound for the type C Equotip is really clear from the limestone (Lim) data

and all samples show a jump of about 100 in rebound value. The histograms in figure H.11 highlight a new observation. All histograms peak within a close range, except core LIM 9. The histogram of LIM 9 presents a considerable amount of readings with a lower rebound value and has a overall staircase shape. It is presumed by the higher amount of low rebound that the core is internally weathered at several spots. Nevertheless, the crack running through core LIM 9 causes definitely a number of weaker rebounds. The sample is probably not fully weathered, because the peak of the histogram is still comparable to the other limestone (Lim) samples. Additionally, the visual appearance of the core does not suggest a high degree of weathering as can be seen in Appendix E in figure E.4. A small crack and an area with higher degree of weathering around a calcite vein are visible. The histograms of samples LIM 2 and 4 have slightly deviating shapes from the other cores, yet this was already observed within figure 9.12b. Both cores have a larger standard deviation. Sample LIM 4 contains some small cracks and stylolites in the rock matrix, yet sample LIM 2 presents visually no indication for the higher standard deviation.

The minimum mean values for the limestone (Fri) are 539, 482, 599 and 559 for the type D in dry condition, type D in saturated condition, type C in dry condition and type C in saturated condition respectively. The corresponding maximum mean values are 629, 625, 709 and 715. These minimum and maximum values already indicate that there is no large difference between the individual cores and upon saturation. This is confirmed by figure 9.12c, which displays the mean and standard deviation for all limestone (Fri) cores. There is no large difference, maximum a gap of 20 in L-value, between the mean in dry and saturated condition for most limestone (Fri) cores. Only core FRI 2 and 8 have a larger drop in rebound during saturation of 60 and 40 in rebound value respectively. Core number 5 and 8 show a considerable higher standard deviation for the type C tip of 111 and 80 in dry condition. Outstanding to the rest of the cores is core number 2, which has a mean rebound value $\pm$ 100 in L-value lower with respect to the other cores. The histograms draw the main attention to cores FRI 2 and 5. For both the distribution is wider compared to the other cores. Core FRI 5 has only one measurement at a low rebound between 350 and 400. This rebound may corresponds to the concentration of calcite crystals at a particular spot within the sample as can be seen in Appendix E in figure E.6. Core FRI 2 present no visual indication of the larger spread in rebound data, so internal weathering or defects may be the cause of the variation.

The measurements on the cores show, similar to the rebounds on the sawn aggregate surface, a high mean value and relative small standard deviation compared to the measurements on the rough aggregate surface. This is possibly a result of the removal of the weathered surface, which varies more in strength and hardness. Nevertheless, the cores in the first group of sandstone have a high standard deviation ranging from 73 to 162, presumably because of internal weathering. For some samples, like LIM 8 and FRI 5, the standard deviation of one of the tip types is larger in saturated condition that in dry state. This could result from the weakening of clay minerals present within the rock matrix. However, other samples, like LIM 2 and LIM 4, have a higher standard deviation for the dry state. Thus, these shifts are probably a result of variability within the rock cores instead of the weakening of clay minerals. The samples size of the core samples is not big enough to satisfy this hypothesis. The difference between the two tip types is not constant as well and may be an effect of the natural variability within the core samples as well.

9.3. Correctness of Equotip Measurements

The Equotip type C mean rebound values are compared to the type D mean rebound values to investigate the correctness of the equotip measurements on the aggregate and core samples. Especially the measurements on the aggregate are interesting. The statistical analysis provide good results. Yet, many of the previous research with the Equotip stated the test surface should be smooth (Aoki and Matsukura, 2007; Verwaal and Mulder, 1993). Figure 9.13 presents the mean type C value versus the mean type D values for the sandstone, limestone (Lim) and limestone (Jen) aggregate pieces. A straight line would be the result when the measurements would be perfectly similar. The general trend in figure 9.13 is a straight line that does not pass through the origin, because the type C rebound is higher than the type D rebound. The data points scatter around a straight line, probably because the surface of the aggregate varies. The shift in measuring grid for the type C with respect for the type D tip results in slightly different measurements. Overall, the Equotip measurements are

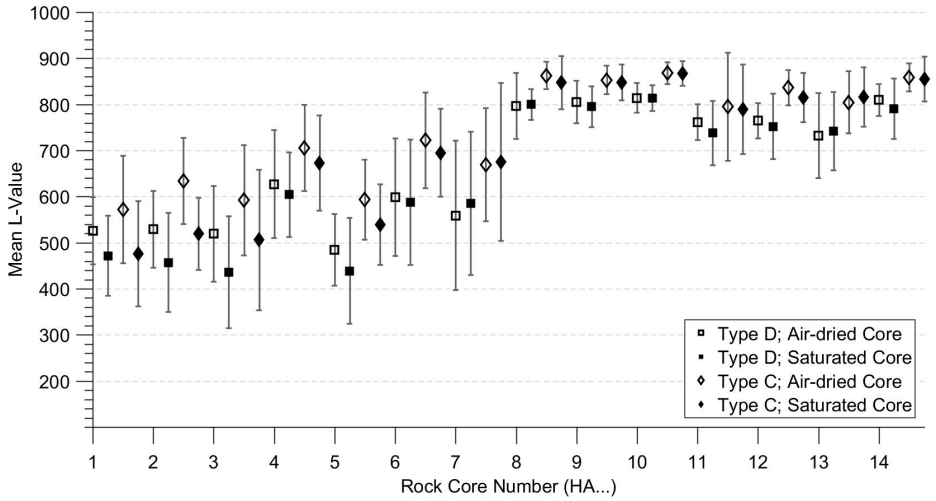

(a)

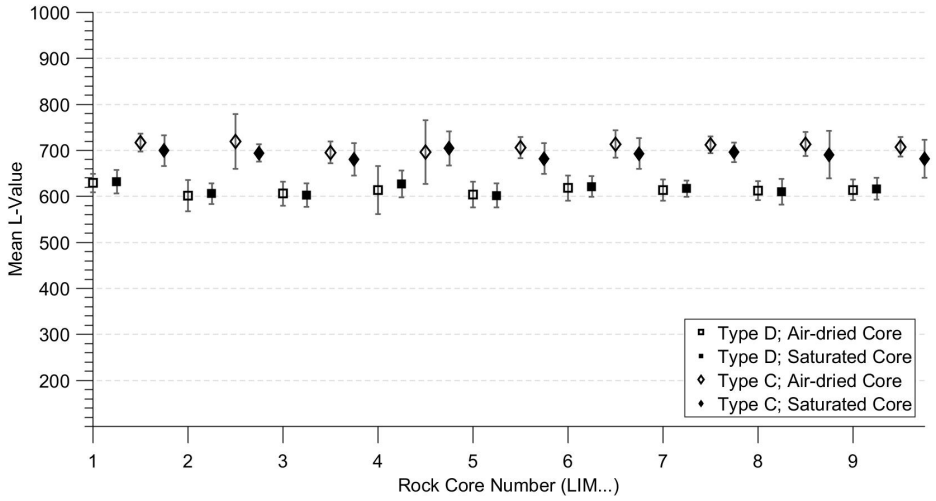

(b)

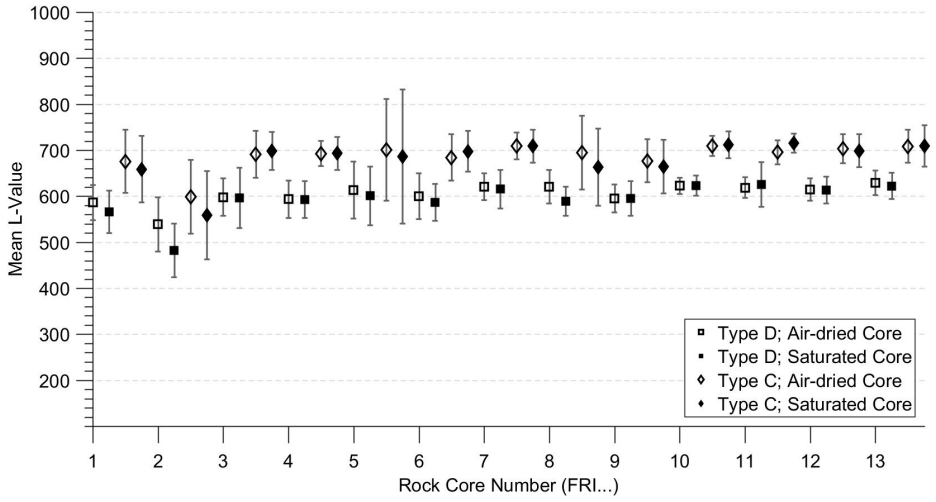

(c)

Figure 9.12: Statistical analysis of the core Equotip measurements on; (a) sandstone from the Hartsteinwerke, (b) limestone from Carrière des Limites and (c) limestone from Carrière de Frimoye. The symbols represent the mean value of the 22 measurements on each core and the grey bars represent the standard deviation above and below the mean.

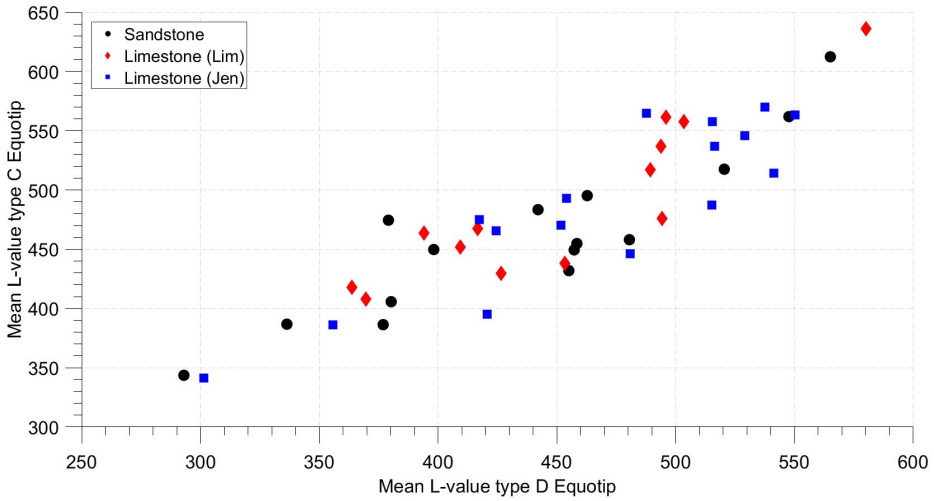

Figure 9.13: The mean type C Equotip value versus the mean type D Equotip value performed on the aggregate samples. The mean values are obtained from ±45 records on the rough aggregate surface.

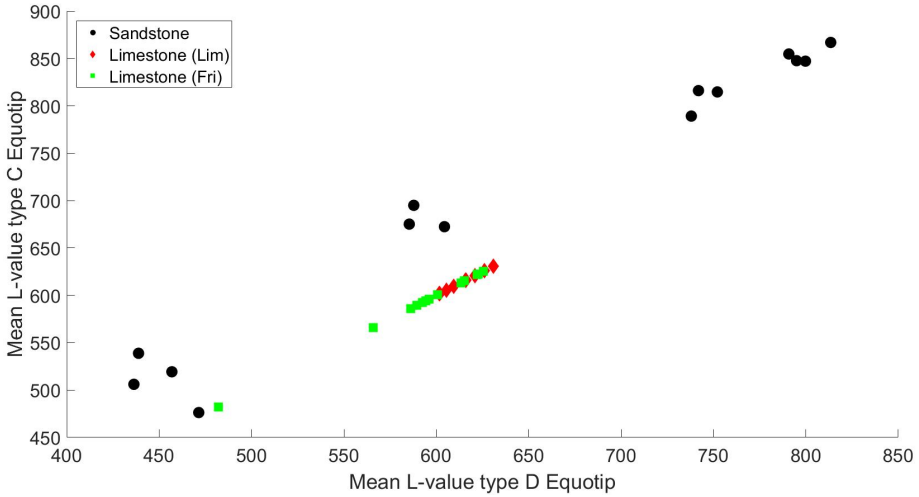

Figure 9.14: The mean type C Equotip value versus the mean type D Equotip value performed on the core samples. The mean values are obtained from 22 records on the smooth core surface.

reasonable consistent on the aggregate pieces.

Figure 9.14 visualises the mean rebounds for the type D and C tip, yet this time performed on the cores samples. The results is a perfect straight line for the limestone and almost perfect for the sandstone, indicating a well performed measurement. The lines are assumed to show less scatter as a result of the smooth prepared surface of the cores. However, the figure provides a new detail. The statistical analysis already noticed a constant difference between the type C and type D L-value. Nevertheless, figure 9.14 indicates a constant drop for the type D versus the type C that varies for the sandstone and limestone. The result suggests that the drop in rebound for the two tip types is dependent on the rock type.

9.4. RIM Measurement

The repeated impact method (RIM) is performed on the aggregate pieces in an attempt to estimate the degree of weathering of the outer surface relative to the fresh inner rock matrix. The RIM was performed on all aggregate pieces tested with the SIM method. However, there was a lot of variation between the samples and no results greatly matched the results from Aoki and Matsukura (2008).

Therefore, the Equotip RIM is tested on 3 aggregate samples for multiple times at several locations to identify if the RIM method actually works on the aggregate pieces. The test includes both the type D and type C Equotip. Each aggregate piece is tested on 3 different faces in order to observe the reproducibility of the method on one aggregate sample. These faces are referred to as location 1, 2 and 3. The aggregate pieces are selected on the condition of the their faces. The tested pieces have three faces that differ in degree of weathering or surface roughness. Moreover, the selected samples are at least 5 cm thick to make sure the three RIM measurements on the different faces do not influence each other. During the RIM the L-value is expected to increase as a result of the compression zone below the tip, which raises the hardness of the impact surface (Aoki and Matsukura, 2008).

Figure 9.15, 9.16 and 9.17 visualise the results of the RIM measurements on the sandstone, limestone (Lim) and limestone (Jen) respectively. The measurements on the sandstone vary between the type D and C tip, and within the results from the type D and C themselves. Figure 9.15 illustrates the RIM patterns on the three surfaces of the sandstone aggregate. The maximum rebound values obtained with the type D are 634, 683 and 783 and differ for more than 100 in L-value. The minimum rebound values show a higher variance with minimum values of 190, 425 and 553 for the three different surfaces. In addition, the rebound does not necessarily increase with the number of impacts. The rebound drops immediately after the first rebound at location 3, and starts to increase from the 5^{th} impact. The logarithmic curves presented by Aoki and Matsukura (2007) are not obtained on the sandstone aggregate. Furthermore, the type D and type C measurements do not develop similar repeated rebound patterns on the 3 locations. The two tip types agree with the order of highest impact after 25 hits for the three different locations on the aggregate. No major change in rebound for the type C is observed at the third location, which may indicate that the impact energy of the type C Equotip is not high enough to create a compression zone within the aggregate surface. L_{max} is the mean value of the three highest L-values from the RIM data and should represent the rebound of the deeper, unweathered rock parts (Aoki and Matsukura, 2007, 2008). Ultimately, the L_{max} should be similar for the three faces since the face should not influence the rebound of the unweathered rock parts. The L_{max} obtained on the sandstone aggregate are 613, 664 and 770 for the type D at the 3 surfaces, and 728, 826 and 904 for the type C at the 3 surfaces. Clearly, the values are not within the same range for both type D and C Equotip.

The results displayed in figure 9.16 from the limestone (Lim) display no clear trend. The maximum rebound values for the type D tip are 689, 612 and 817 at the three locations, and 786, 815 and 784 for the type C tip. The minimum L-values are 515, 509 and 609 for the type D, and 603, 685 and 654 for the type C tip. Although, the scatter is smaller between the three locations than for the sandstone, the behaviour at the three locations is definitely not unique. The expected increase in rebound value with the number of impacts is better obtained with the type C tip than with the type D tip. The logarithmic increase is visible, despite the few sharp drops in rebound value. Consequently, the L_{max} is unique for the type C with 777, 813 and 738 at location 1, 2 and 3 respectively. Since the logarithmic trend is not visible for the type D, the L_{max} values do not agree and are 684, 604 and 804.

Figure 9.17 shows the results from the RIM measurements on the limestone (Jen). Again, there is variability between the curves from the type D and C tip and within the results from one tip type. The maximum rebound values obtained are 803, 738 and 704 for the type D tip, and 795, 704 and 811 for type C tip. The minimum values are 675, 429 and 536 for type D, and 599, 449 and 646 for type C. The L_{max} values are 790, 726 and 700 at the three locations for the type D, and 790, 703 and 805 for the type C tip. The increase in rebound is comparable for the C type between the locations 1 and 3. The increase from the first rebound towards the second rebound is similar as well as the L_{max} value. The data from location 2 and 3 converge eventually to a similar L-value for the type D. Additionally, their L_{max} values are close.

The RIM measurements show a lot of variation on the three surfaces of the identical aggregate pieces. According to Aoki and Matsukura (2008) a similar L_{max} should be obtained, however this is not the case. The type C tip is expected to perform less, due to its lower impact energy. The lower energy creates less of an impact zone and thus the L_{max} should be reached after less impacts compared to the type D tip. However, this is not observed within the test results. In many cases the type C rebound values appear closer to the expected logarithmic curve shape than the type D method. The RIM measurements do not provide satisfactory results and are therefore not continued during this research.

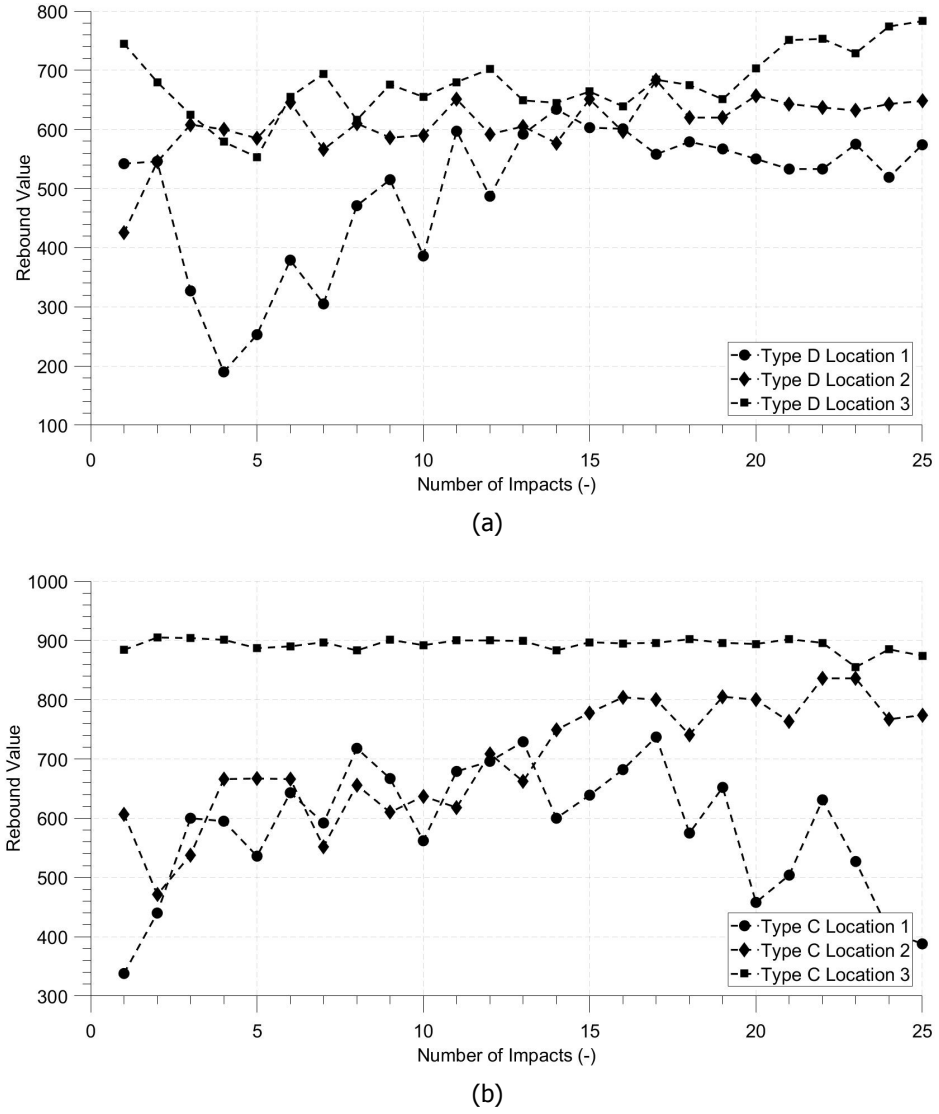

Figure 9.15: RIM measurements on a sandstone aggregate sample; (a) type D at 3 surfaces and (b) type C at three identical surfaces. The measurements include 25 rebounds at 3 locations on the rough, untreated aggregate surface.

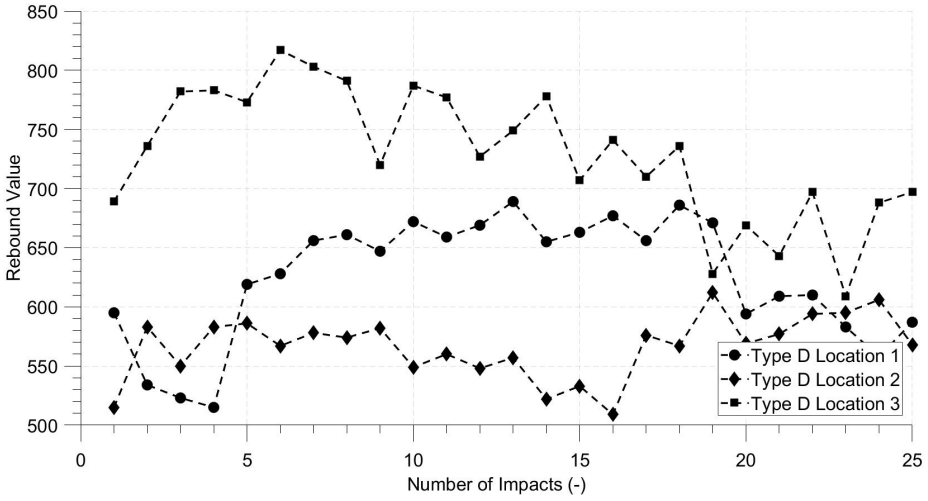

(a)

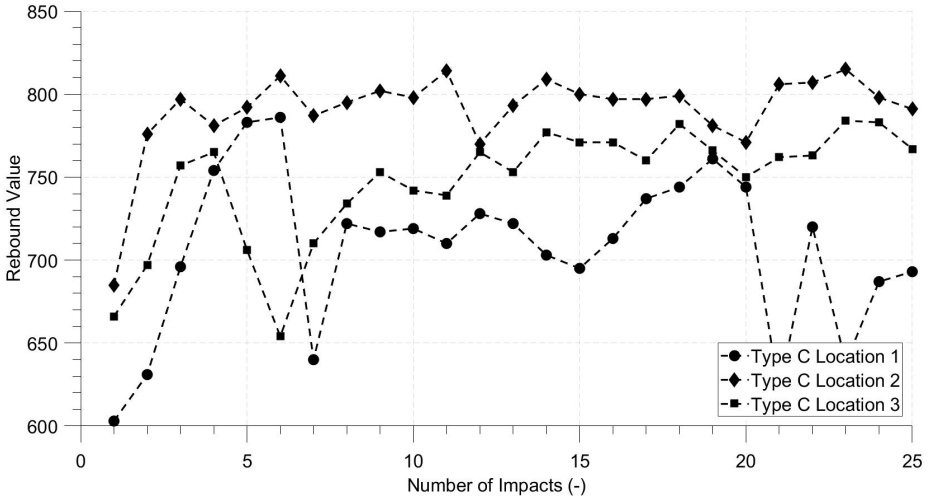

(b)

Figure 9.16: RIM measurements on a limestone (Lim) aggregate sample; (a) type D at 3 surfaces and (b) type C at three identical surfaces. The measurements include 25 rebounds at 3 locations on the rough, untreated aggregate surface.

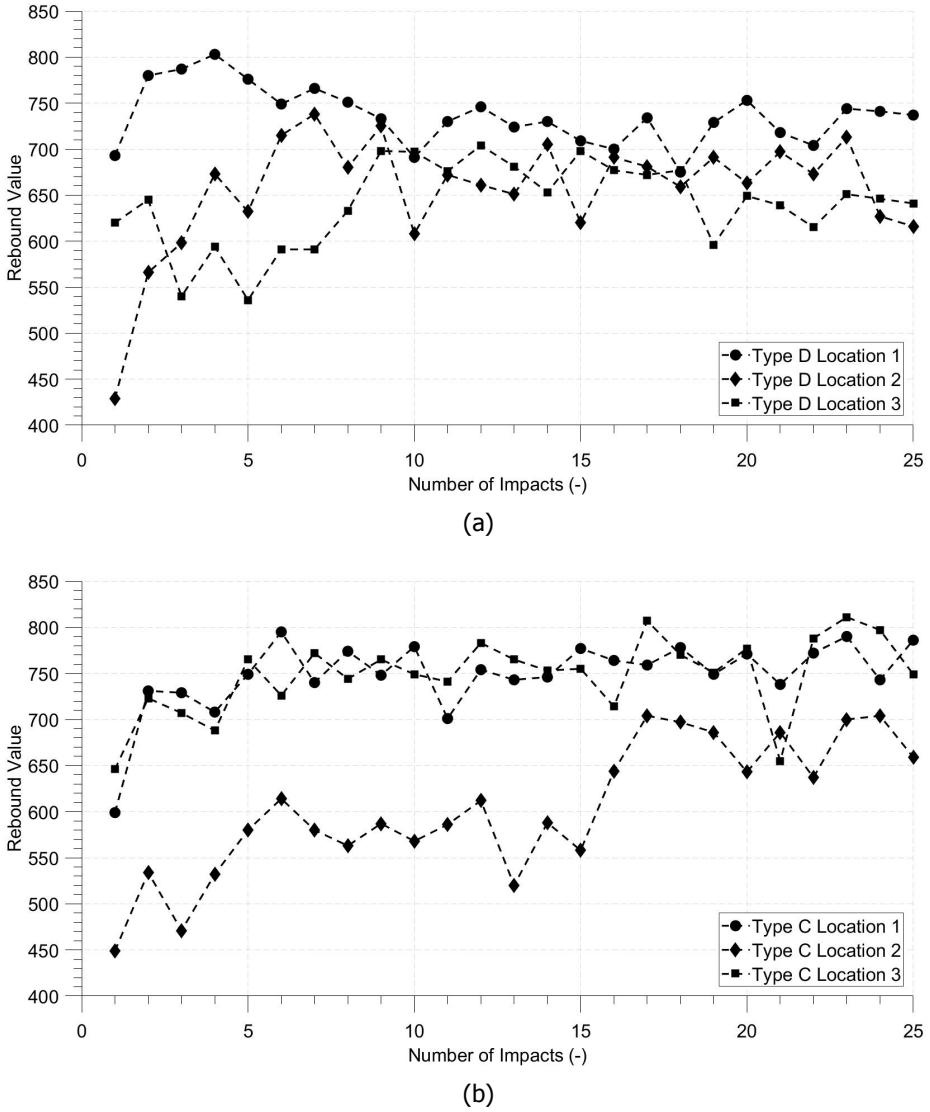

Figure 9.17: RIM measurements on a limestone (Jen) aggregate sample; (a) type D at 3 surfaces and (b) type C at three identical surfaces. The measurements include 25 rebounds at 3 locations on the rough, untreated aggregate surface.

9.5. Relation between L-value and Water Absorption

The rebound values obtained from the aggregate are compared to the WA determined before in chapter 7. The aggregate pieces are evaluated, since these samples may contain a weathered outer surface that absorbs more water. These pieces will be used in the submarine trench backfill and are therefore more representative for the construction. Firstly, the mean of the rebound values is evaluated with the WA. The mean is evaluated first, since surface features like cracks and porosity have a major influence on the water absorption. The lower rebound values on these characteristics will be an outlier compared to the rest of the data set. Using the median instead of the mean would give too little attention to these features. The results are presented in figure 9.18 and 9.19. In the first figure the colour bar displays the density of the aggregate pieces, while it presents the sample weight in the second figure. The Equotip used is the type D.

For all three rock types a decrease in rebound is observed with an increase in water absorption of the aggregate piece. The exponential fit for the sandstone is poor with a coefficient of determination (R^2) of 0.27. The exponential fit for both limestones (Lim and Jen) shows a better result with a R^2 of 0.62 and 0.73 respectively. Yet, these fits are obtained on all the aggregate pieces tested. The colour of the points indicate influence of the sample density and mass. The WA is lower for aggregate pieces with a higher density, as was already noticed in chapter 7. Therefore, the relation between the mean Equotip rebound value and WA is a function of density as well. There seems to be an influence of the sample weight on the Equotip measurements. The heavier the sample pieces, the higher the WA for a similar rebound value. The higher weight is partly caused by the variety in density by mainly by the difference in size of the aggregate pieces. The size of the aggregate piece seems to influence the WA or rebound value. The WA is a change in weight relative to the full sample weight and is assumed not to be the influenced by the sample size. Previous research from Wilhelm et al. (2016) already mentioned that sample size has an influence on the rebound value. Therefore, the aggregate data is separated into weight classes. After evaluating different groups of weight the following classes are considered; 150-250 g, 250-350 g and 300-450 g for the sandstone, 150-180 g, 180-210 g and 210-450 g for the limestone (Lim), and 150-300 g and 300-450 g for the limestone (Jen). These weight groups are chosen in order to have multiple data points within each weight class. From the division no general remark can be made on the data for the three rock types. However, on the individual rock types some trend are observed. The data points start to align more and more as the mass of the sandstone aggregate samples starts to increase. This is clearly shown in by the figures in Appendix J. Thus, the WA relates to the mean Equotip rebound value taking the density of the pieces into account. The aggregate size influences the Equotip measurements. The thickness of the sample is important and needs to be sufficient to remove the influence of the sturdy, underlying support surface on the rebound value.

Besides the type D tip, the type C tip is analysed as well. The change in tip type causes no major difference between the results. The slight changes are probably caused by the natural variability in the aggregate pieces and slight shift in measuring grid for the type D and C type. The plots of the L-value versus WA for the type C tip can be found in Appendix J.

The median rebound for both type D and C tip is correlated to the WA as well. The median rebound correlates less strong to the WA and has more scatter compared to the mean values as can be seen in Appendix H.12m. The lower r^2 value was expected before-hand as the lower rebound values have less impact when the median values are considered instead of the mean value.

The Equotip data can also be evaluated by removing outliers next to the separation into density and weight classes. All the L-values that fall outside the range $\mu - \sigma < L < \mu + \sigma$ are removed from the data set, where; μ is the mean of the rebound values and σ the standard deviation. A new mean is determined from the remaining rebound values and this mean is again evaluated against the WA. Nonetheless, the modified data does not improve the correlation found with the WA. This is presumably due to the same reason the fit with the median value is less strong. The modified data loses the important rebound features that indicate cracks and areas with a higher porosity. Consequently, a worse fit is obtained.

Finally, the rebounds recorded on the sawn aggregate surface are compared to the WA values. The comparison is displayed in figure 9.20, where the clear, coloured data points refer to the sawn aggregate surface and the transparent, coloured points refer to the rough aggregate surface. The

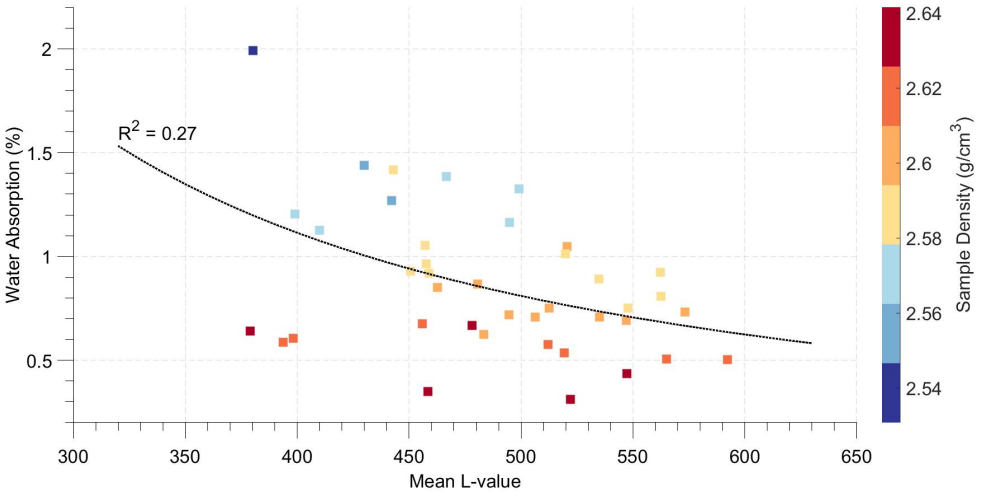

(a)

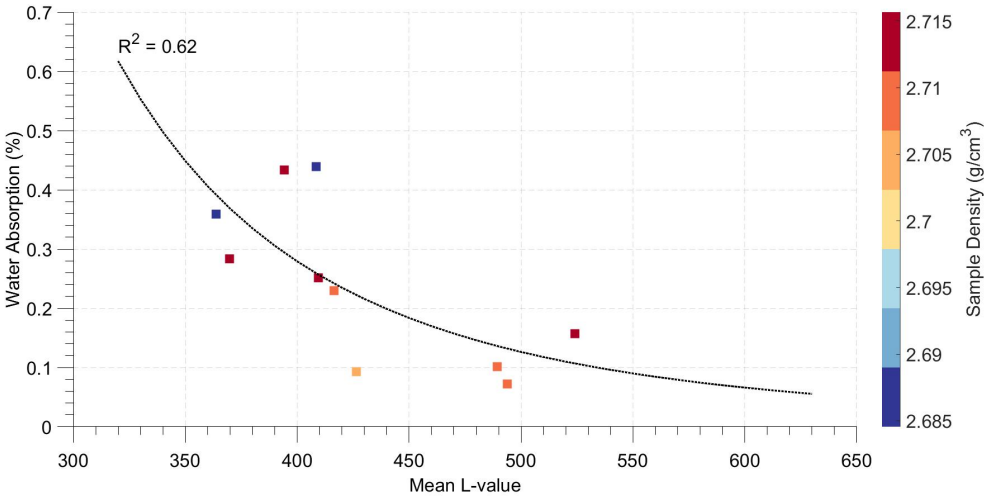

(b)

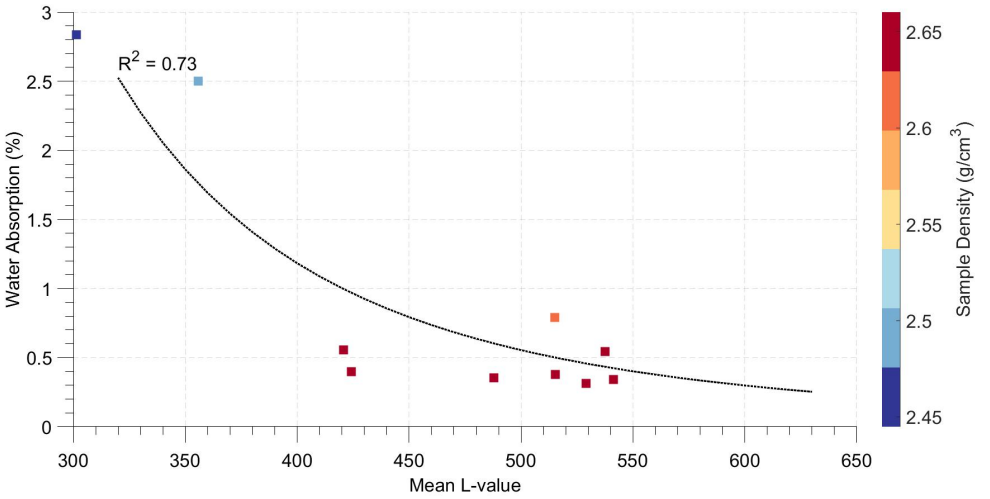

(c)

Figure 9.18: Mean rebound value of the Equotip type D on untreatened aggregate samples; (a) sandstone from the Hartsteinwerke, (b) limestone from Carrière des Limites and (c) limestone from Carrière de Jenneret. The colorbar indicates the density of each individual aggregate piece.

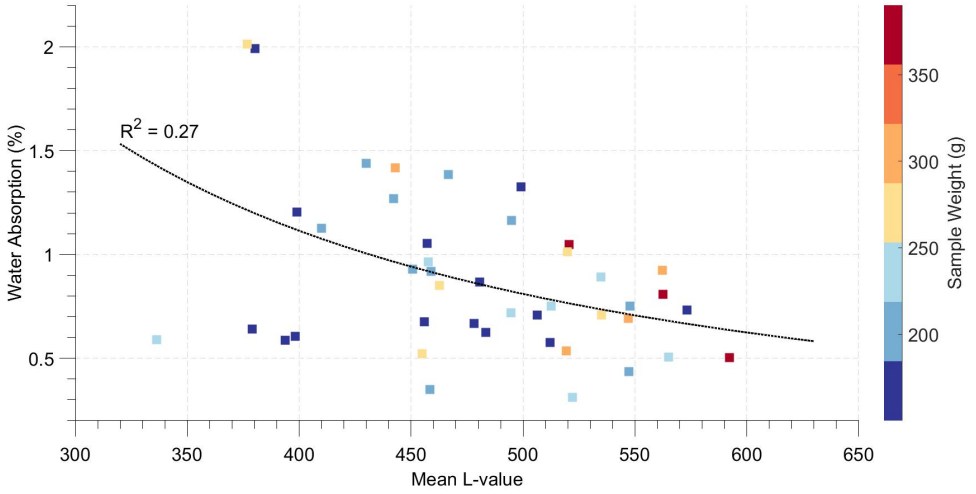

(a)

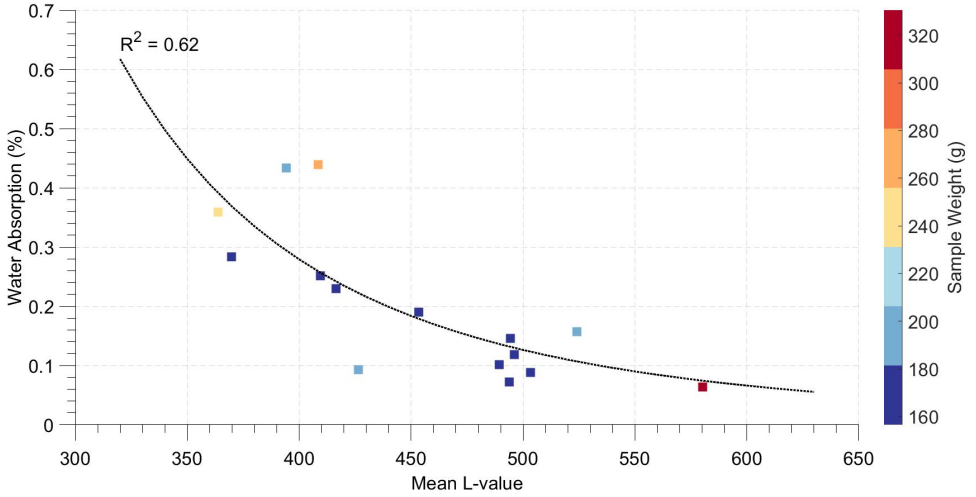

(b)

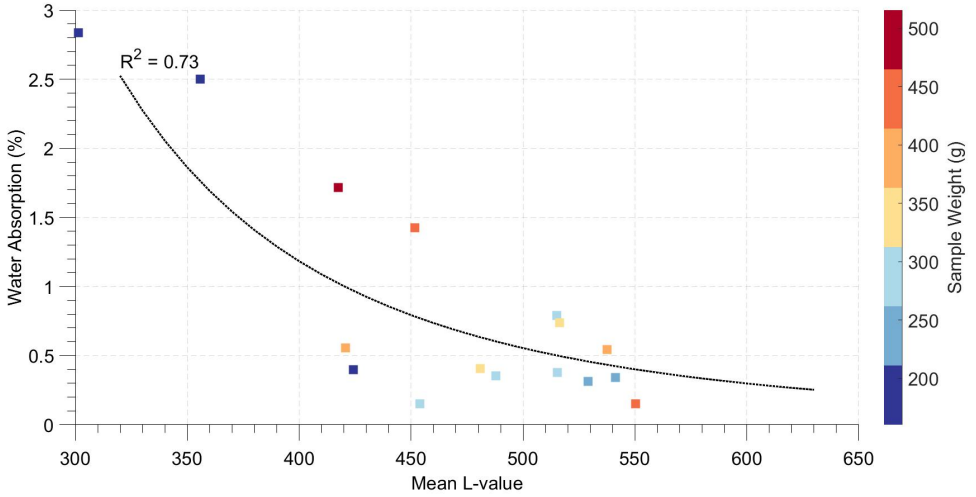

(c)

Figure 9.19: Mean rebound value of the Equotip type D on untreatened aggregate samples; (a) sandstone from the Hartsteinwerke, (b) limestone from Carrière des Limites and (c) limestone from Carrière de Jenneret. The colorbar indicates the weight of each individual aggregate piece.

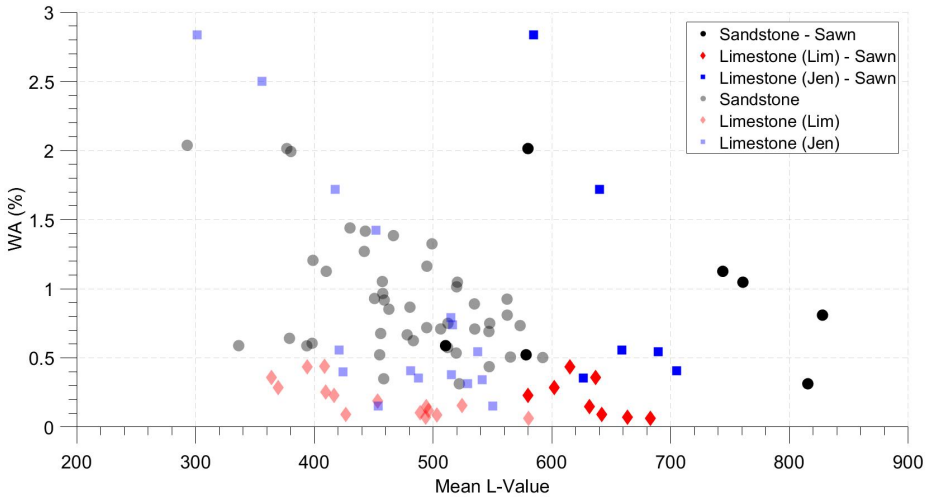

Figure 9.20: The relation between the mean Equotip type D rebound value on sawn aggregate surface and the water absorption. The measurements on the rough aggregate surface are included as the transparent data points.

amount of sawn aggregate samples is considerably less than the rough aggregate pieces. Additionally, the mean rebound values on the sawn surface are higher than on the rough surfaces as mentioned before. The sawn samples still provide a large scatter in rebound data when considering the WA values. The sawn surface does not seem to improve the correlation between the mean rebound value and WA. The difference in rebound values at various WA values even seems to increase for the sandstone samples. Presumably the removal of the outer surface negatively influences the correlation to the WA. The outer surface may greatly influence the WA value, especially when it has a higher degree of weathering. The Equotip rebounds on the fresh, sawn surface miss this information.

9.6. Equotip and UCS

Previous research established that the Equotip L-value correlates well to the UCS of rocks (Aoki and Matsukura, 2007; Lee, 2015; Meulenkamp and Grima, 1999; Verhoef, 2010; Verwaal and Mulder, 1993). These studies used exponential or power functions to fit their data. Yet, most correlations were established with the Equotip type D and on dry cores with a L/D of 2.0. During this research the cores tested with the Equotip have a L/D of 1.0. Moreover, the cores have been tested in both air-dry and saturated condition, and the Equotip type C is used as well to inspect the difference with the type D. It makes sense to evaluate the Equotip L-values in saturated condition, since these cores were compressed in saturated condition.

Figure 9.21 and 9.22 show the UCS of the core samples in saturated condition versus the Equotip type D and type C measurements respectively. The sandstone data follow a trend between the mean L-value in saturated condition and the UCS for both type D and C Equotip. The UCS value increases with increasing mean rebound value. The trend follows strongly the power function noted in equation 9.2 with a r^2 value of 0.93 for the type D Equotip. The trend described by this function is close to the trend established by Verhoef (2010) as can be seen in figure 9.21. The correlation between Equotip and UCS is even stronger for the type C tip as visualised in figure 9.22, with a r^2 value of 0.95. Again, here the correlation is close to the one obtained by Verhoef (2010), yet this time for the type C tip. The data points from the limestone (Lim) are too clustered to provide a clear trend between rebound value and UCS. However, one value differs significantly from the other values and shows a lower compressive strength, core LIM1 as mentioned before. This point is highlighted by removing the fill of the diamond shape. The values from the limestone (Fri) show a larger variation in UCS compared to the limestone (Lim). Consequently, a trend can be observed which seems to be linear according to equation 9.3, which is with a r^2 of 0.69 not as good as the fit for the sandstone. Yet, the observations agree that the UCS value increases upon increase in mean rebound value, like observed with the sandstone cores. The linear trend on the limestone (Lim) cores is only suitable for a certain range of L-values. Negative

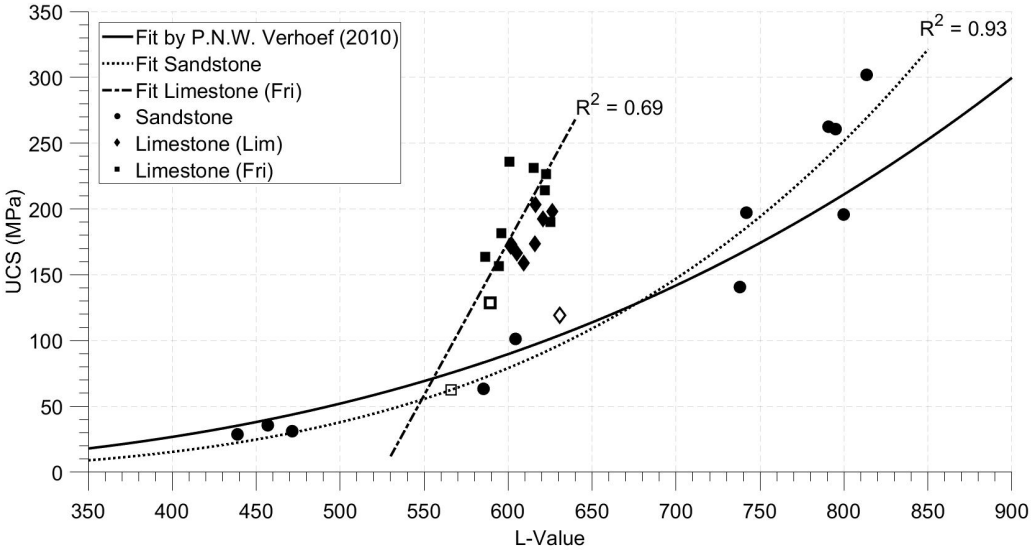

Figure 9.21: The relation between the mean Equotip type D rebound value on saturated cores with a L/D of 1 and their UCS value. The non-filled diamond presents core LIM1. The non-filled square with the thin outline appears for core FRI1 and the non-filled square with the thick outline illustrates core FRI8.

UCS values will be encountered when the rebound value drops below 525 according to the established linear trend. Therefore, it can be assumed that there is a power function that fits the limestone (Fri) better. On the current data set a power function would result in a worse fit, but as soon as samples are included with lower UCS values this may improve. A larger spread in UCS values, especially towards the lower range below 100 MPa, could reveal a possible trend better. This can only be tested by finding similar rocks with a lower uniaxial compressive strength. Fitting a power function to the current data points for the limestone (Fri) results in equation 9.4 with a r^2 of 0.62. The linear trend obtains a better fit especially due to one of the cores, namely core FRI1. This core has a relative low UCS value of 62.5 MPa despite the high mean rebound value. This core fails ductile mode compared to the brittle failure of the other cores as highlighted in chapter 8.

The previous studies also observed an exponential relation between the results. The data agrees with the range in trends proposed by the previous studies as presented in figure 9.23. The standard deviation is indicated by the horizontal bars and are of considerable magnitude compared to the range of literature values. The literature values are good to compare with, although the UCS values are obtained on dry cores with a L/D of 2. The UCS values of the saturated cores with a L/D of 1 are very close to the values of air dried cores with a L/D of 2 as discussed in chapter 8. From the previous studies and this research becomes clear that the correlation between mean L-value and UCS value is not unique for all rock types.

$$UCS = 5.259 \cdot 10^{-10} \cdot L^{4.023} \tag{9.2}$$

$$UCS = 2.327 \cdot L - 1221 \tag{9.3}$$

$$UCS = 1.717 \cdot 10^{-18} \cdot L^{7.1996} \tag{9.4}$$

As discussed before, the rebound on a similar rock piece is higher for the type C Equotip than for the type D. Thus, a higher UCS is expected when the type D tip on one sample gives a similar rebound value as the type C tip on another sample. This is confirmed by the two equations published by Verhoef (2010). The equations reveal that the UCS is higher for the type D tip compared to the type C, until a certain limit. According to these equation the UCS is higher for the Equotip type C as the rebound value exceeds 919.

Until now only the mean L-values on the cores have been related to the UCS values. However, the median value can be suitable as well. The median is less sensitive to outliers and may give a better

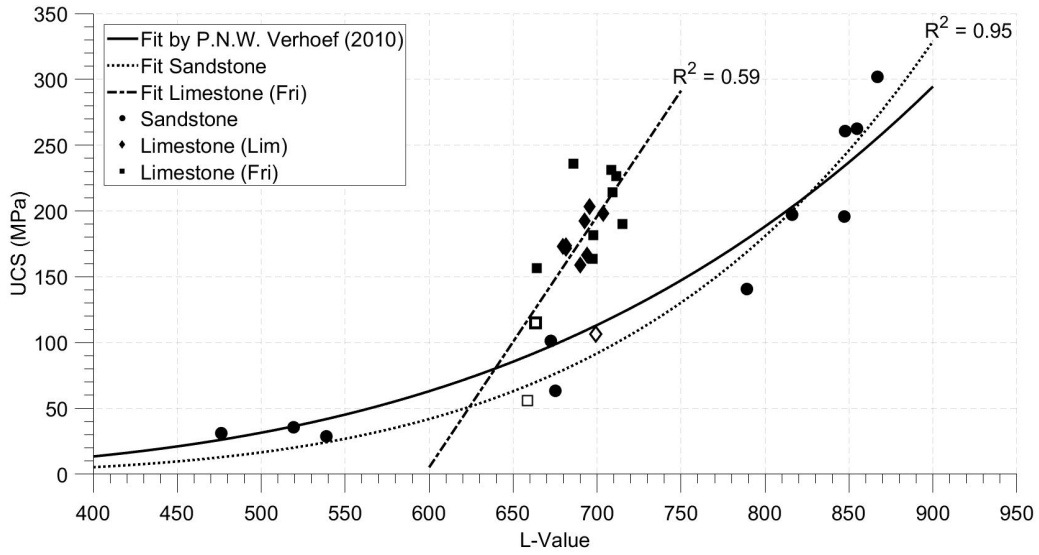

Figure 9.22: The relation between the mean Equotip type C rebound value on saturated cores with a L/D of 1 and their UCS value. The non-filled diamond marks correspond to specific core samples as stated in the caption of figure 9.21.

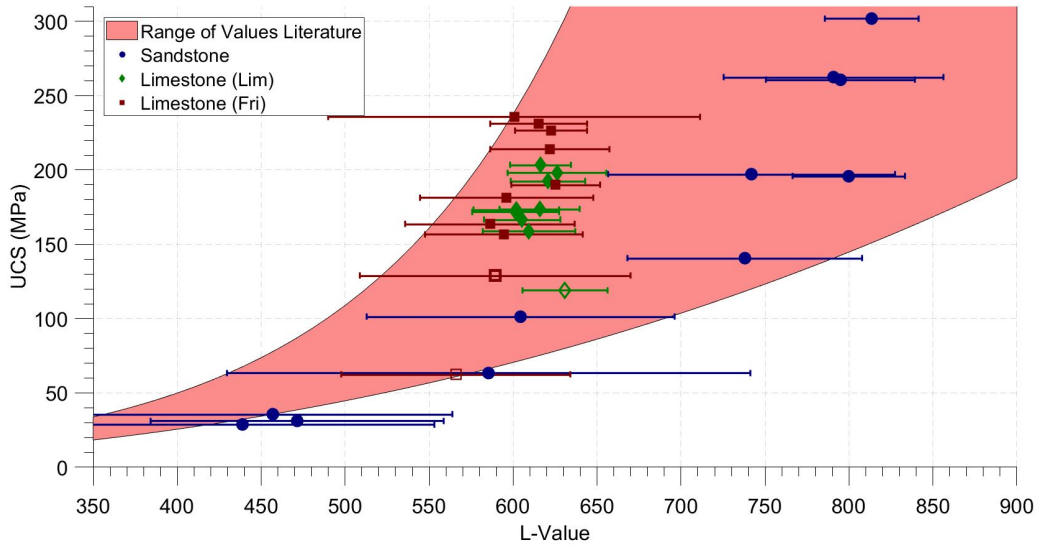

Figure 9.23: The relation between the mean Equotip type D rebound value on saturated cores with a L/D of 1 and their UCS value. The horizontal bars represent the standard deviation of the Equotip measurements on the rock cores. The red shade is the theoretical range of expected UCS values based on the literature study shown in figure 2.6. The upper limit is the trend established by Kee (2010), while the lower limit is conform the trend observed by Aoki and Matsukura (2007); Verwaal and Mulder (1993).

estimate of the UCS. This depends on the influence of the outliers. A lower rebound on the surface can be a very small, local feature that hardly influences the UCS value of a core. In that case the median value would give a better estimate. But, when the outlier turns out to be a rebound value on a crack that runs through the core the mean value may be more appropriate to estimate the UCS. Cracks were observed within some of the cores before crushing and therefore the correlation of UCS with the Equotip is expected to get weaker when the median is used instead of the mean. The same relations as before are this time evaluated with the median rebound values instead of the mean rebound value. Figure K.1 and K.2 in Appendix K display the correlation between the median rebound value for the type D tip on saturated cores and type C tip on saturated cores respectively. Table K.1, K.2 and K.3 within this Appendix provide the median values next to the core data for both tip types in air dried and saturated condition. The r^2 values of the correlations between the Equotip rebounds and UCS values on the cores are compared in table 9.7. The table compares the mean and median value for the type D and C tip in both air dried and saturated condition. Both the mean and median rebound value provide a reasonable to good fit. The L-values obtained on the saturated cores show the strongest correlation, probably because the cores are compressed in the laboratory during UCS testing in saturated condition as well.

Table 9.7: The coefficients of determination for the correlation between the Equotip rebound value and UCS evaluating the variety in tip type and saturation condition of the cores. Both a linear function and power function are considered for the limestone (Fri), because both fits are close in multiple cases.

Equotip Type and Statistical Analysis	Core Condition	r^2 for the Sandstone	r^2 for the Limestone (Fri) Linear Function	r^2 for the Limestone (Fri) Power Function
Type D mean	Saturated	0.93	0.69	0.62
	Air Dried	0.92	0.46	0.43
Type D median	Saturated	0.93	0.72	0.68
	Air Dried	0.92	0.40	0.38
Type C mean	Saturated	0.95	0.59	0.56
	Air Dried	0.93	0.67	0.65
Type C median	Saturated	0.90	0.61	0.64
	Air Dried	0.92	0.56	0.56

9.7. Acoustic Velocity and Equotip

The P-wave, direct wave, velocity (V_p) is measured over the length of the core samples (axial direction) and correlates to the internal structure of the rock cores. The velocity is influenced by several factors, e.g. mineral content, density, porosity, presence of joints, degree of weathering and pore fluids (Kahraman, 2007; Sharma and Singh, 2008). Therefore, V_p is an interesting parameter regarding rock durability. Sharma and Singh (2008) obtained good linear correlations between the p-wave velocity, slake durability index and UCS. Results from this research and previous research already show a good correlation between UCS and Equotip. Therefore, there is expected to be a relation between Equotip and p-wave velocity as well. Figure 9.24 presents the correlation between the type D Equotip rebound on saturated cores and the v_p of these cores. The sandstone and limestone cores obtain a linear relation between the p-wave velocity and Equotip rebound value. The linear fit on the sandstone data is very promising with a r^2 of 0.98. The results of the limestones and sandstone do clearly not align. This is probably a consequence of the difference in mineral content between the limestones and sandstone, since the direct sonic velocity is unique for every mineral. The drop in v_p is stronger for the limestones than for the sandstone for a specific drop in rebound value. This may be linked to the rock structure, where small defects have a stronger impact in the limestone than in the sandstone.

9.8. Equotip and BTS

The Equotip rebound values correlate well the UCS values of the cores as discussed in the previous section. Yet, do the Equotip measurements correlate to the BTS values as well? Figure 9.25 and 9.26 introduce the results for the BTS test on the sandstone and limestone disks versus the mean Equotip

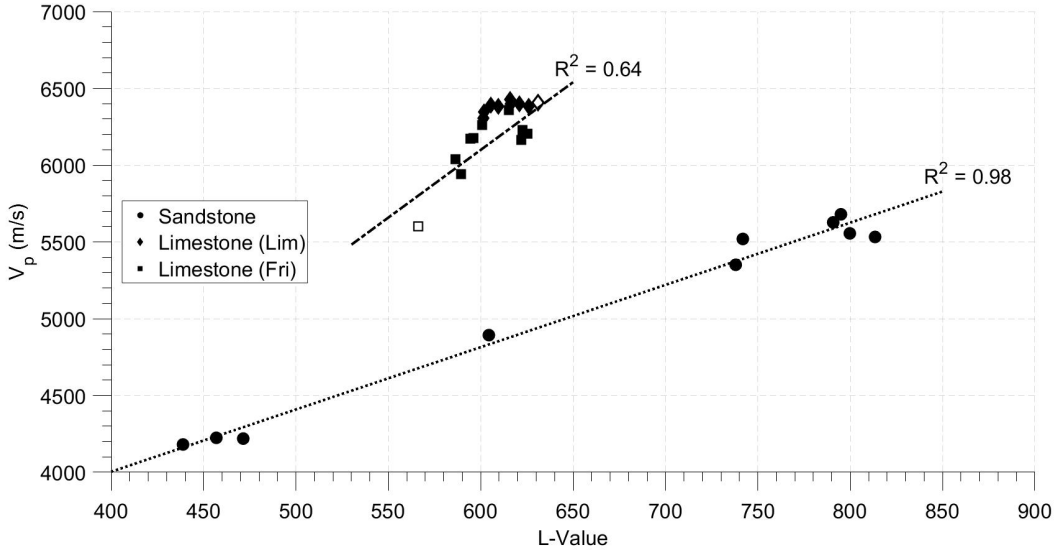

Figure 9.24: The relation between the mean Equotip type D rebound value on saturated cores with a L/D of 1 and their V_p. The non-filled diamond marks correspond to specific core samples as stated in the caption of figure 9.21.

type D and type C rebound respectively. The sandstone disks in figure 9.25a and 9.26a present an increase in BTS with increasing L-value for both the type D and C Equotip. The data points are closer packed for the type C tip, resulting in a slightly better fit. The Equotip measurements are more accurate in predicting the high BTS values of the strong sandstone disks. The fit becomes better when neglecting the red symbols, which include testing at different angles to the bedding and will be discussed later. The r^2 increases to 0.88 for the type D Equotip and to 0.87 for the type C Equotip when these measurements are neglected. Thus, the Equotip gives a good estimate on the BTS value based on the sandstone samples that show no clear bedding. Nevertheless, the fit reduces when the samples with a clear bedding are taken into account. In addition, this fit is on the sandstone only and does not necessarily fit on the limestone data points properly.

The results on the limestone disks in figure 9.25b and 9.26b vary more compared to the sandstone samples. The BTS values of the limestone (Lim) disks are consistent around $\pm$7 MPa and agree with the Equotip trend observed within the sandstone samples with a corresponding L-value of $\pm$540 for the type D tip and $\pm$650 for the type C tip. Yet, the limestone (Fri) disks vary in BTS value of $\pm$8 MPa while the rebound value only differs of $\pm$120. Four of the limestone (Fri) disks have a BTS and L-values as expected by the fit obtained on the sandstone disks. The other four deviate up to $\pm$6 MPa from the trend line. The limestone (Fri) varies already in BTS value between the two disk from the same rock block. For example the samples F12/1 and F12/2. Both disks originate from one core of 40 mm that is halved. Nonetheless, F12/1 has a BTS value of 9.6 MPa and F12/2 7.8 MPa. The intact disks show no clear visible difference and the Equotip measurements are similar with a difference of 7 in mean L-value for the type D tip and 3.5 for the type C tip. But, there is a difference visible between the samples after failure in the BTS test. Both disks after failure are presented in figure 8.10. Sample F12/1 has two large parallel vertical cracks and the final split surface is rough. In contrast, sample F12/2 has a very tight, clean split surface of one single vertical crack. The difference between the two disk has probably a cause that is not visible by the naked eye. It is possible that the grains within the rock matrix have a preferred orientation, since limestones are sedimentary rocks and are deposited in beds. The BTS value can differ as a results of a different orientation of the stress with respect to the bedding. This explanation suits the very straight axial split in sample F12/2. Another explanation can be a slight change in the rock matrix. The disks originate from the same core, nevertheless are changes within the rock matrix possible on a small scale. For example, the amount or size of grains can increase. Yet, the research until now would suggest the mean rebound value would have changed in greater extent. The difference within BTS values of the two disks cannot be explained by the Equotip from this data set. The result from sample F2/1 deviate the most from the trend line obtained on the sandstone disks with a BTS value of 9.2 MPa and a mean type D tip rebound of 420. The disk from

the same core, F2/2, has a BTS of 8.2 and mean type D tip L-value of 490. This two cores indicate the Equotip is not able to prospect the BTS value consistently as well.

Five of the sandstone disks are highlighted in red and refer to one single block sample. This sample is the one used for the directional UCS test and where disks are obtained at different angles to the bedding next to the cores. The BTS test is executed perpendicular, parallel and at an angle of $\pm$30° to the bedding. The test perpendicular to the bedding result in the highest BTS value of $\pm$8 MPa. The BTS parallel to the bedding are 3.9 and 2.2 MPa and are 2 to 4 times lower than the BTS normal to the bedding. The BTS 30° to the bedding is 3.3 MPa and comparable to the values parallel to the bedding. The failed disks for the three angles are depicted in figure 8.8. The disk tested parallel to the bedding split along the bedding during tensile failure. The bedding is a weak plane within the rock matrix along which the sample easily splits. The influence of the orientation of the bedding towards the tensile stress is not captured by the Equotip.

So, the obtained data suggest that the BTS is only predictable by the Equotip for strong rock pieces with a homogeneous rock matrix. Weak planes within the rock matrix, such as the bedding in the sandstone, result in low BTS values when unfavourably orientated to the stress axis. This is not recorded by the type C and D Equotip. The variation in the limestone (Fri), possibly due to the variety in rock structure in the limestone, is not captured either. This suggest a correlation between Equotip and BTS value is only valid for homogeneous, isotropic rocks.

9.9. Discussion and Conclusion

The Equotip rebound on the aggregate pieces is able to obtain valuable information regarding the durability of the aggregate pieces. Firstly, surface roughness, degree of weathering, variety in grain size and presence of cracks appear within the histograms of the Equotip data, especially when samples from similar rock type are compared to one another for reference. Without reference the magnitude and influence of these features on the rebound value is uncertain and cannot be predicted. The amount of approximately 45 readings on the aggregate pieces provide a good basis to identify the various rock pieces. Measurements with the double spacing result in only minor changes in mean and median values. However, the t-test indicates that the amount of unique samples greatly reduces upon doubling the Equotip measuring grid. Therefore, the 45 readings per sample are maintained. The measuring grid is an important factor as well on the rough aggregate surface. The tip is slightly shifted when no proper rebound can be obtained. This occurs at dents within the rock structure, where weaker minerals are present and the degree of weathering is higher. The shift moves the rebound point to the peaks within the rock surface, which are the stronger fresher material. Consequently, the rebound of the aggregate piece may be overestimated. Nevertheless, weathered and weak rock pieces are recognised by a lower mean rebound value and larger standard deviation. This is clearly observed within the measurements on the core samples. The sampling locations in the quarry are recognised within the mean rebound value and standard deviation. Furthermore, the Equotip values correlate well to the UCS value. The BTS value correlates only to the mean Equotip rebound for strong, isotropic samples as a result of the large influence of the orientation of weak planes in the BTS test. Concluding all observations, both the Equotip tip types are able to detect variability within aggregate pieces, relate to WA and strength values and correspond to features like mineral content, grain size, fractures and degree of weathering. The measurements on the rock cores and disks of both Equotip types correlate well to the UCS and BTS. Internally weathered cores are identified by a drop in mean L-value when saturated and a larger standard deviation relative to fresher cores. The type D measurements on the aggregate surface relate better to the WA of the aggregate pieces than the type C tip. A comparison to the measurements on the sawn aggregate surfaces reveals the rebound is higher on the fresh surface and the standard deviation is smaller. Nevertheless, the correlation to the WA and density does not improve by removing the weathered outer surface of the aggregate pieces. Most independent samples are recognised by the type D tip with a rebound spacing of 1 cm. Equotip RIM measurements on the aggregate pieces is not successful to determine the degree of weathering of aggregate pieces. The method is not consistent on the tested aggregate pieces. Weathered aggregate pieces are identified by a lower mean L-value and larger standard deviation of the SIM measurements. The median L-vale and MAD are suitable to predict UCS values, yet valuable information for a durability assessment, like the degree of weathering, is lost as the influence of outliers is reduced for the robust statistics. The Equotip seems to be a simple testing tool able to provide detailed information for an armourstone

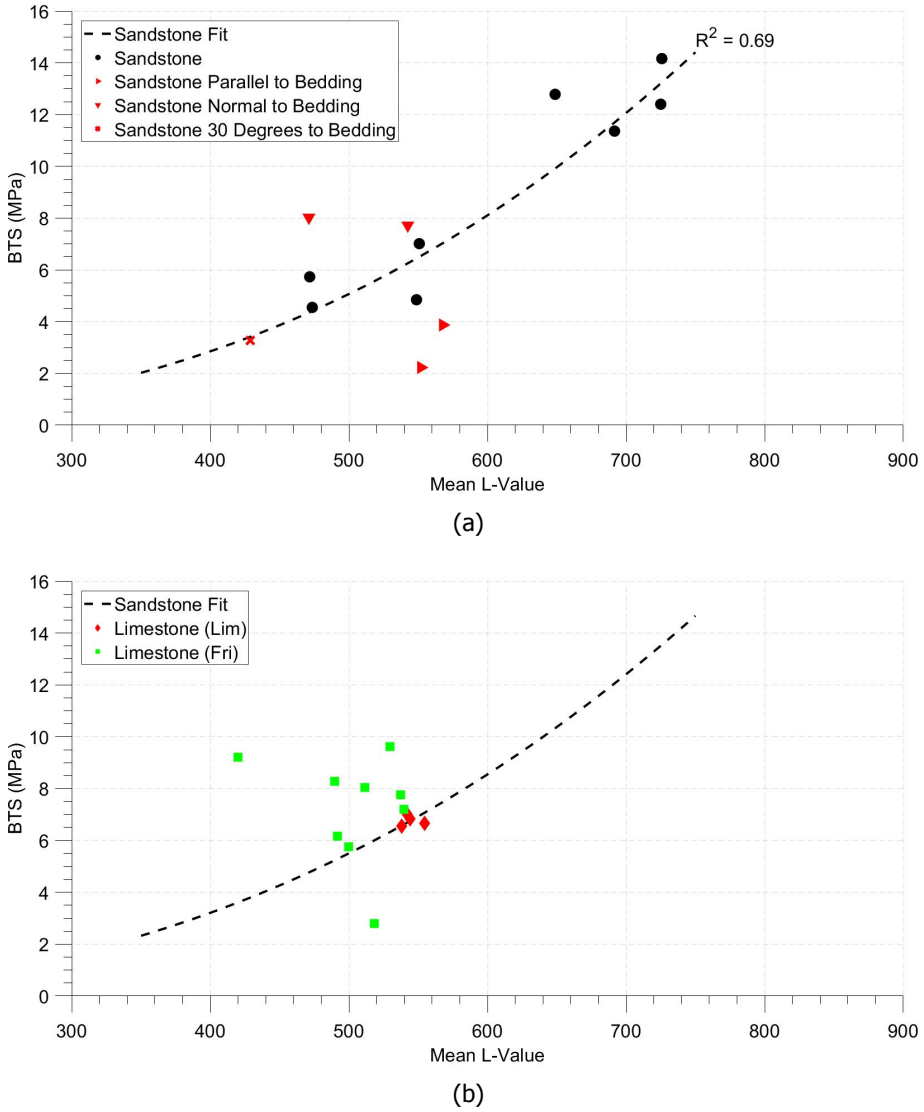

Figure 9.25: Mean type D Equotip rebound value versus the BTS value for; (a) the sandstone disks and (b) the limestone disks. The red symbols in (a) present the disks from one single sandstone block tested at three angles with respect to the bedding.

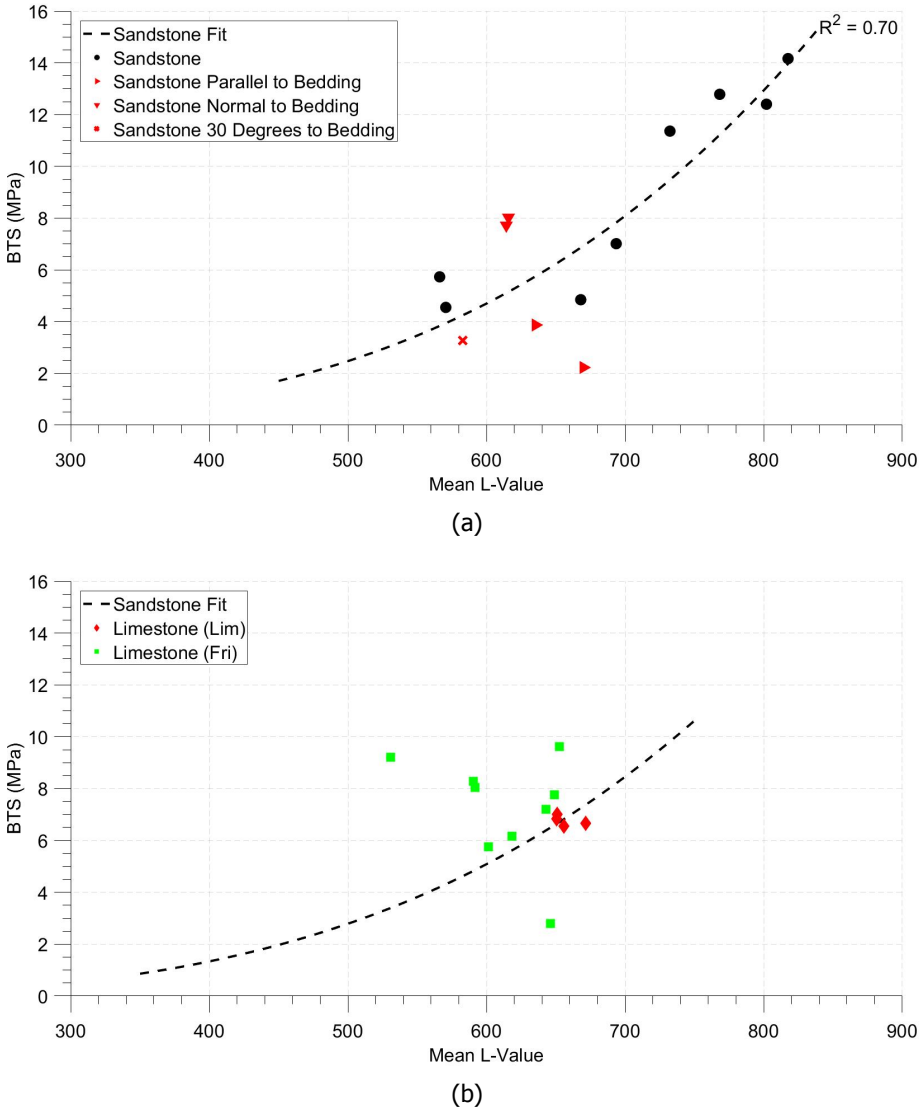

Figure 9.26: Mean type C Equotip rebound value versus the BTS value for; (a) the sandstone disks and (b) the limestone disks. The red symbols in (a) present the disks from one single sandstone block tested at three angles with respect to the bedding.

durability investigation, which is not covered by the standard testing methods alone. Nevertheless, the features within the Equotip data are only properly understood in combination with the other laboratory tests and a detailed visual examination, such as a petrographic analysis. Moreover, compressive and tensile strength anisotropy cannot be quantified using Equotip testing. The conclusions are valid for the tested sandstone and limestone, and can differ for other rock pieces.

10

Methylene Blue

The methylene blue (MB) is used in four different setups. Two runs of MB adsorption tests are performed. The first run is performed on the aggregate mixture sampled from the stockpiles in the quarries. The second run is a test on 4 individual rock pieces that are used for the preparation of 4 thin sections. The MB is applied by staining, next to the adsorption tests. A few aggregate pieces are selected, which show a thin layered structure and indicate the possible presence of a higher clay content in localised zones. The selected samples are cut in half. The sawn surface of one of the halves is stained with methylene blue, in effort to highlight swelling clay structures. A thin section is created from the other half of the sample and dyed with methylene blue as well. The 4 individual rock pieces from the second MB adsorption run, are 4 remaining rock pieces used for the thin sections. By following this procedure the potential presence, structure and type of clay minerals will become clear. Moreover, the effectiveness of the methylene blue staining on the sawn surfaces can be checked.

10.1. Methylene Blue Adsorption

First the MB adsorption tests are executed. The test is performed in two separate runs as mentioned before; (1) on the aggregate mixture of the quarries and (2) on selected rock pieces.

10.1.1. Test Method

The methylene blue adsorption test is executed in order to test the presence of swelling clays within the rock matrix in the armourstones. The absorption tests are executed on the aggregate from the Hartsteinwerke, Carrière des Limites and Carrière de Jenneret. Two separate samples are created from different aggregate bags sampled at the quarries. Rock pieces are collected from the rock blocks for Carrière de Frimoye, resulting in only one representative sample. Furthermore, HA 41, HA 52, LA 1 and LA 3 are the selected rock pieces for the individual adsorption test. The aggregate pieces and rock pieces are first crushed with the jaw crusher on the smallest setting. Next, the broken pieces are dried in the oven at 110°C for 48 hours. The broken aggregate is crushed to powder with a disk mill after drying.

The methylene blue adsorption test is executed seven times during the first run, twice for every quarry except for the limestone from Carrière de Frimoye. The limestone from this quarry is only tested once, as a result of the sample preparation providing only one sample. Four additional tests are executed on the individual crushed rock pieces during the second run. The tests are executed according to the American standard (ASTM, 1984). For the test 20 g of the rock powder is diluted with 300 ml of distilled water and maintained in suspension by means of a stirrer. This is 10 times more than the 2 g as stated in the ASTM standard developed for clayey soils. However, this large sample is required since the test sample contains a low clay content and is heterogeneous. In order to get a reliable measurement a bigger sample size is required. A test was performed with the 2 g according to the standard, yet this did not provide satisfactory results. The solution is mixed for 5 minutes. After the 5 minutes of stirring, the sample in solution is placed below the burette, while continued to be stirred. An amount of methylene blue solution is added to the sample. The amount of solution added varies, depending on the colouring of the different samples and spots on filter paper observed during testing.

After 2 minutes of stirring a spot test is executed. A drop of the sample solution is taken with a pipette and dropped onto a filter paper during a spot test. The spot left on the paper is evaluated by the naked eye. This procedure is repeated until a light blue halo appears around the spot, and saturation of the sample solution is reached. At this point the sample is stirred for 1 more minute and the spot test is repeated to confirm the saturation point found.

The positive methylene blue ion will exchange with the positive ions within the clay mineral structure. First, the methylene blue cations will exchange the cation in the diffuse-ion-layer of the clay mineral structure. Next, the methylene blue cations will replace the cations within the interlayers. The remaining methylene blue ions will stay in the suspension as soon as all the positive ions within the clay mineral are replaced. This phenomena is observed during the spot test in the fluid migrating away from the drop. When a light blue halo appears there is an excess of methylene blue added that stays in solution. The amount of absorbed methylene blue gives an indication on the swelling potential of present clay minerals. None, to very low amounts of swelling clay minerals are present if low amounts of methylene blue are absorbed. Contrarily, high amounts of methylene blue indicate potentially the presence of swelling clay minerals.

10.1.2. Results and Discussion

The spots of the spot test are presented in figure 10.1 for the first run. The halo is hard to see in the scans of the filter paper, so the results are as well summarised in table 10.1. The methylene blue index (MBI), in milliequivalent/100g, is calculated according to equation 10.1 where; E is the milliequivalents (meq) of methylene blue per millilitre (0.01), V is the volume of methylene blue added in the titration process and W is the dry weight of the rock powder. The methylene blue value (V_B), in g/100g, is calculated using equation 10.2. The factor 3.1986 is dependent on the molarity of the methylene blue solution, which is 1.0 in this case.

$$MBI = \frac{E \cdot V \cdot 100}{W} \tag{10.1}$$

$$V_B = \frac{V \cdot 3.1986 \cdot 10^{-3} \cdot 100}{W} \tag{10.2}$$

The results of the two tests of one quarry (rock type) are close, thus the sample preparation was good enough to capture the heterogeneity of the sample. The highest absorption value is observed within the limestone (Lim) with an average MBI of 1.09 meq/100g and V_B of 0.35 g/100g. This still is within the excellent category of <0.4 g/100g according to table 3.12 from CIRIA/CUR/CETMEF (2007), and thus there is no indication of risk on degradation by swelling clay minerals with time over a typical design life. The other rock samples have even lower absorption values. The sandstone has an average MBI of 0.69 meq/100g and V_B of 0.22 g/100g, the limestone (Jen) has an average MBI of 0.47 meq/100g and V_B of 0.15 g/100g, and the limestone (Fri) has a MBI of 0.55 meq/100g and V_B of 0.18 g/100g. No risk on degradation by swelling clay minerals over a typical design lifetime is expected when solely based on these numbers. Nevertheless, the structure of present clay minerals within the rock matrix is not known with the data from the absorption test and is still important to be investigated as indicated by Dunn and Hudec (1966). The MB solution can also be adsorbed by organic matter within the limestone instead of clay minerals. The organic matter can be localised and act as a weak plane. Moreover, Amanullah et al. (1997) showed that an increase in organic content in the rock matrix can increase the swelling behaviour during wetting. Thus, for the organic matter the same interests apply as for the clay minerals; (1) the cation exchange capacity of the material indicated by the MB adsorption test and (2) spread in the rock matrix highlighted by the MB staining. The tested sandstone can be interesting, as some single aggregate pieces show a clear layered structure. Small amounts of swelling clays or localised organic matter in a layered structure can be very destructive.

Therefore, the MB adsorption test is executed on single rock pieces during a second run. The results are displayed in figure 10.2 and table 10.2. All four rock pieces have very low adsorption values, despite the appearance of the rock pieces that suggested a higher clay content. The two sandstone samples, HA 41 and HA 52, have an adsorption value of 0.40 and 0.45 meq/100g clay respectively, which is lower than the adsorption obtained on the sandstone aggregate mixture. The limestone samples, LA

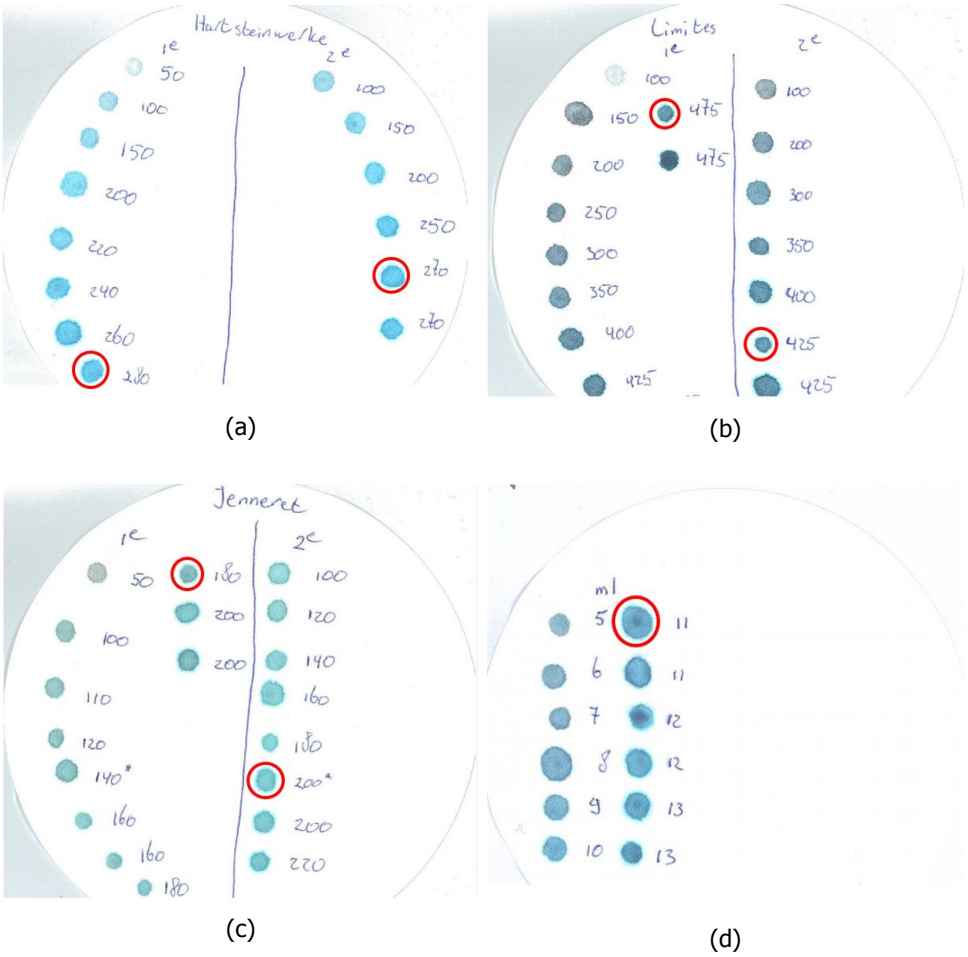

Figure 10.1: Spots from the methylene blue absorption test obtained at the rock powder from; (a) sandstone from the Hartsteinwerke, (b) limestone from Carrière des Limites, (c) limestone from Carrière de Frimoye and (d) limestone from Carrière de Frimoye. The numbers next to the spots are the number of methylene blue drops added to the solution for a,b and c, and the amount of methylene blue added to the solution in ml for d. 1 drop is equal to 0.05 ml. The line separates the first from the second measurement for a, b and c. The red circles mark the spots at which the blue halo is well developed for the first time and those quantities of MB added are used to calculate the methylene blue index.

1 and LA 3, have an adsorption value of 0.30 and 0.55 respectively, which is again lower than the MB adsorption value obtained on the limestone (Lim) aggregate. The adsorption values are lower than expected for both the sandstone and limestone. It can be the case that the samples contain more clay, yet a clay type with a low cation exchange capacity. As a result the adsorption value will be low, despite the higher clay content. This will be checked in the next section, where the staining of the sawn surfaces and thin sections will be discussed.

10.2. Methylene Blue Staining

The sawn surfaces and thin sections are stained with methylene blue in order to investigate the presence of deleterious structures. Concentrations of active clay minerals can decrease the durability of the armourstone, despite the low MB adsorption values found before. The methylene blue is applied directly on the sawn surface in an attempt to highlight the structure of the present clay minerals, without performing a petrographic analysis. Only the samples that show clear stained patterns are discussed in this section. The thin sections of the rock pieces that have been tested individually with the MB adsorption test are compared to the sawn surface staining.

Table 10.1: Results of the methylene blue absorption test on the aggregate mixture. The MBI is the methylene blue index. The test is executed with ±20 g of rock powder instead of 2 g, because of the expected low amount of clay minerals and to capture the heterogeneity between the various aggregate pieces.

Sample	Amount of rock powder (g)	Methylene Blue Solution added (ml)	MBI (meq/100g clay)	V_B (g/100g clay)
Sandstone	20.02 20.04	14.00 13.50	0.70 0.67	0.22 0.21
Limestone (Lim)	20.06 20.07	22.50 21.25	1.12 1.06	0.36 0.34
Limestone (Jen)	20.32 20.25	9.00 10.00	0.44 0.49	0.14 0.16
Limestone (Fri)	20.07	11.00	0.55	0.18

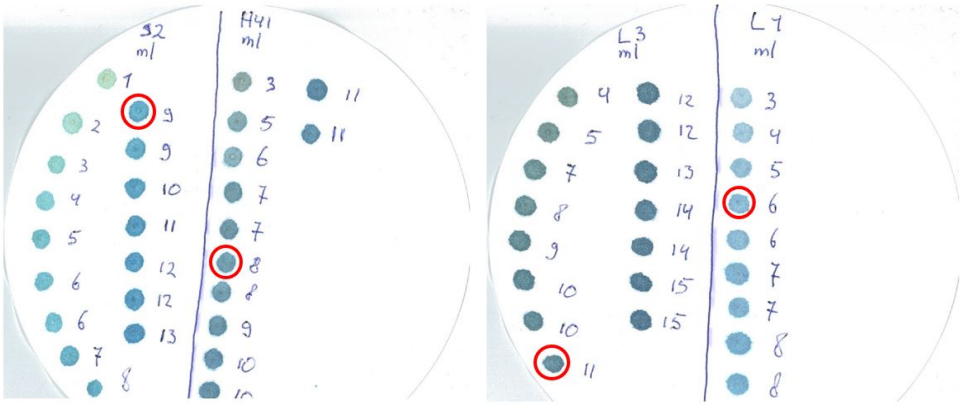

(a) (b)

Figure 10.2: Spots from the methylene blue absorption test obtained at the rock powder from; (a) HA 41 and HA 52, and (b) L1 and L3. The numbers next to the spots is the amount of methylene blue added to the solution in ml for. Again, the first spots that show the blue halo clearly are highlighted with a red circle.

Table 10.2: Results of the methylene blue absorption test on single aggregate pieces from the Hartsteinwerke and Carrière des Limites. These pieces were tested solely, because they displayed possible clay seams and/or concentrations of weak minerals to the naked eye.

Sample	Amount of rock powder (g)	Methylene Blue Solution added (ml)	MBI (meq/100g clay)	V_B (g/100g clay)
HA 41	20.05	8.00	0.40	0.13
HA 52	20.01	9.00	0.45	0.14
L1	20.04	6.00	0.30	0.10
L3	19.99	11.00	0.55	0.18

10.2.1. Test Method

The sawn surfaces are stained with the use of a brush dipped in the methylene blue. The sawn surfaces are thickly covered with methylene blue and then left aside for ten minutes. The samples are rinsed with water after ten minutes. The samples are air dried and then visually examined with the naked eye for deleterious structures highlighted in blue. The thin sections are stained by placing them within the MB for ten minutes. The thin sections are rinsed with water after tens minutes as well. The staining is examined under the microscope during the petrographic analysis.

10.2.2. Results and Discussion

Sawn Aggregate Surface

Figure 10.3, 10.4, 10.5, 10.6, 10.9 and 10.10 are examples of sawn, dyed aggregate surfaces. The sandstone sample in figure 10.3 is coloured entirely blue. Yet, darker blue stained lines are visible that could be concentrated layers of clay minerals. It can be seen that the outer edge of the rock is more weathered at the location of the lines compared to the rest of the surface. So, the rock is at these spots more sensitive to weathering and has a softer characteristic possibly due to the presence of clay minerals.

The staining pattern in figure 10.4 is different from the previous sample and shows less of a layered structure. The colouring has a rather arbitrary form. When the colouring pattern is compared to the non-dyed, sawn surface in figure 10.4a a similar pattern is observed of an alternating light pinkish to beige colour. Therefore, the pattern in the stained surface is probably an effect of the colour difference in the sample. Nevertheless, a clear blue highlighted line runs from the centre of the sample to the right. In addition, the line is coloured darker blue than the other dyed sections. The line is a small crack, but may contain an amount of active swelling clays. A similar dyed crack, yet smaller is observed in bottom right corner of the sample. The left side of the sample is interesting as well, but the features appear not greatly on the photograph. A layered structure of thin, darker stained lines is visible, comparable to the pattern observed on the sample in figure 10.3.

The sandstone sample in figure 10.5 is comparable to sample HA 41. It presents the arbitrary stained sections as well, due to the different colours of the rock material. Furthermore, the sample has some minor cracks that highlight blue. This sample can be distinguished from sample HA 41 by the dark blue stained lines. There are several with a length of about 0.5 cm. They correspond to the dark brown concentration in the non stained half in figure 10.5b. These are expected to be clay seams, based on the adsorption of the methylene blue and brownish colour when not stained.

Sample HA 43 is a sample of the sandstone with a higher water absorption of 2.01 compared to the other samples as mentioned in chapter 7. Its sawn surface in figure 10.6b shows a beige colour and the porous structure. There are no obvious and special features within the rock's matrix. However, there appear multiple highlighted features when the surface is stained with methylene blue, as becomes clear in figure 10.6a. There are roughly three tints of blue visible from light to dark blue. The darkest blue stained concentrations show thicker lines with a thickness of $\pm$ 1 mm. The slightly lighter blue colour is abundant and seems to fill the pore spaces. It is not clear if this colouring is due to the presence of swelling clay minerals or due to the shadow effect caused by the pores, based on the results from the dyed, sawn surface only.

Figure 10.7 visualises the methylene blue stained, sawn surface of sandstone sample HA 52. The full sawn surface of the sample turned blue due to the staining. However, lines of darker blue appear within the sample. Some of these lines end at the rock's surface where weathering has resulted in a 'dent'. Therefore, the dark blue stained layers probably correspond to weaker minerals like a clay seam.

The stained, sawn surface of limestone sample LA 3 is displayed in figure 10.8. The sample indicates a major flaw for the staining method. The blue stain is not clearly visible in all dark parts of the limestone. Sample LA 1 is so dark that no effect of the methylene blue staining can be seen. Yet, sample LA 3 is coloured blue in some regions like the right part of the sample in the figure. The left part of the sample is only slightly turned blue. This is probably due to a change in the rock matrix, as a small change is visible by the naked eye. No highlighted structures are observed in the more obvious stained right part of the sample that could be deleterious. The top left part of LA 3 colours a bit more blue and may contain some active clay minerals in the matrix.

The staining of limestone (Lim) sample LA 13 has turned 2 of the bioclasts clearly blue as visualised in figure 10.9. The other bioclasts have a very light blue tint, which is hard to see in the photographs.

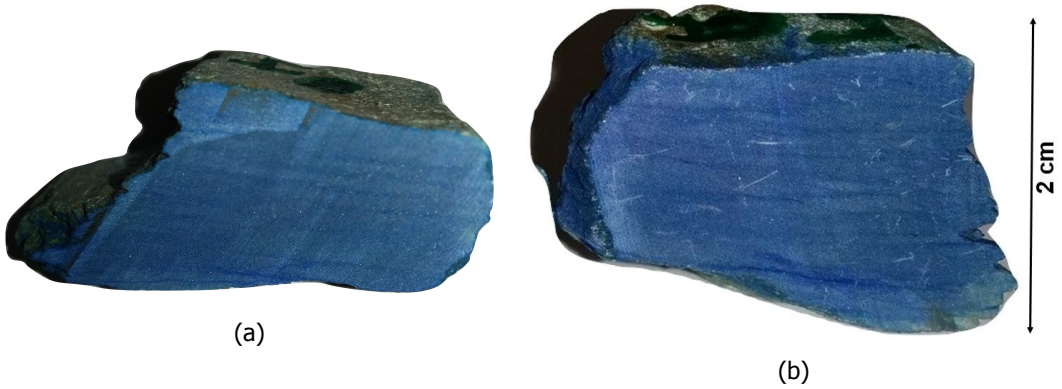

Figure 10.3: Stained, sawn surfaces of sandstone aggregate sample H 4; (a) the stained, sawn surface and (b) the other half stained, sawn surface.

Figure 10.4: Stained, sawn surface of sandstone aggregate sample HA 41; (a) the stained, sawn surface and (b) the sawn surface without staining.

There are no other structures highlighted within the sample next to these fragments.

Limestone (Jen) sample JA 6 has coloured blue around the outer edges of the sample. The outer edge of sample JA 6 is very weathered and has therefore a higher porosity and possibly microporosity. It is assumed that this increase in porosity results in retention of the methylene blue around the outer edges. In the centre some parts are stained as well, yet structures are hard to spot due to the very dark colour of the sample. This is the case for most of the stained limestone samples. Consequently, none deleterious structures are spotted.

Thin Section

The thin sections of the discussed samples are stained as well. A similar staining pattern is expected, since the thin section is almost similar to the sawn surface. However, it turned out that the methylene blue is only clearly visible in thin sections when a 10x magnitude is used. The overview of the thin section is lost with this magnitude and the overall staining pattern is hard to compare. Nevertheless, concentrations that are found can still be compared to the stained, sawn surfaces.

The thin section of sample H 4 does not display the similar staining pattern of lines throughout the thin section, which is seen in the sawn surface. The thin section is stained at some minor spots around the micas, which are distributed over the sample and not aligned in thin lines. A few of these spots are pointed out in figure 10.11.

The staining pattern within the thin section of HA 41 is at some locations similar to the patterns in the sawn surface. A microscopic photograph of a coloured section is presented in figure 10.12. A large part of the matrix between the quartz grains is blue. The staining follows the pattern of iron hydroxide filled cracks (see petrographic analysis in Appendix A). This stained part can coincide with one of the deep blue stained lines in the sawn surface.

Sample HA 52 is coloured pale blue in some parts of the matrix that contain a higher content of chlorite and micas as visualised in figure 10.13. This does not clearly correspond to the stained sawn surface of HA 52. The sawn surface contains darker blue lines, which are not clearly observed within the thin section. The areas of chlorite with a light blue colour due to the MB staining could correspond

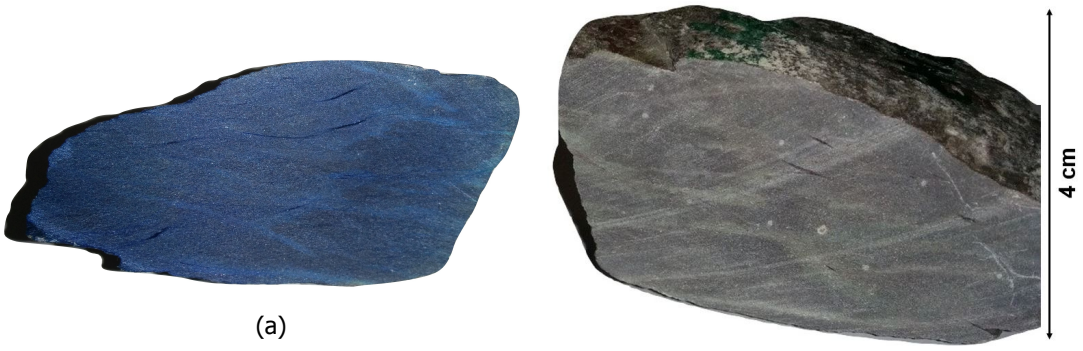

Figure 10.5: Stained, sawn surface of sandstone aggregate sample HA 42; (a) the stained, sawn surface and (b) the sawn surface without staining.

Figure 10.6: Stained, sawn surface of sandstone aggregate sample HA 43; (a) the stained, sawn surface and (b) the sawn surface without staining.

Figure 10.7: Stained, sawn surface of sandstone aggregate sample HA 52.

Figure 10.8: Stained, sawn surface of limestone (Lim) aggregate sample LA 3.

Figure 10.9: Stained, sawn surface of limestone (Lim) aggregate sample LA 13; (a) the stained, sawn surface and (b) the sawn surface without staining.

Figure 10.10: Stained, sawn surface of limestone (Jen) aggregate sample JA 6.

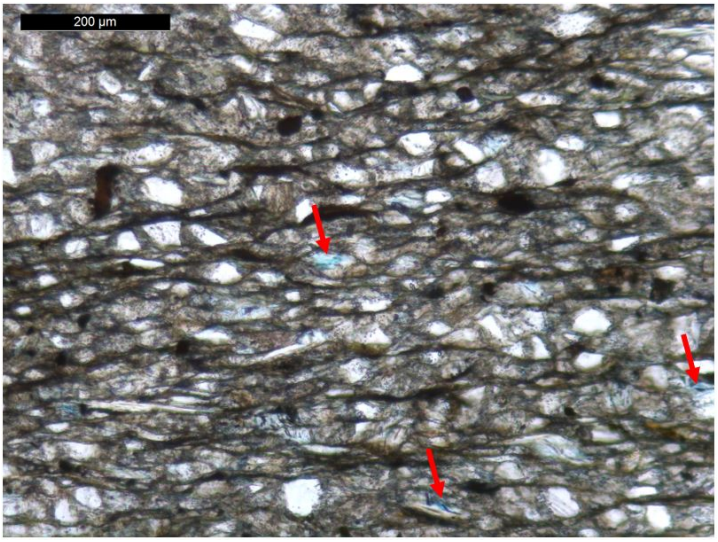

Figure 10.11: Stained, thin section of sandstone aggregate sample H 4. The arrows indicate some examples of localised, stained spots.

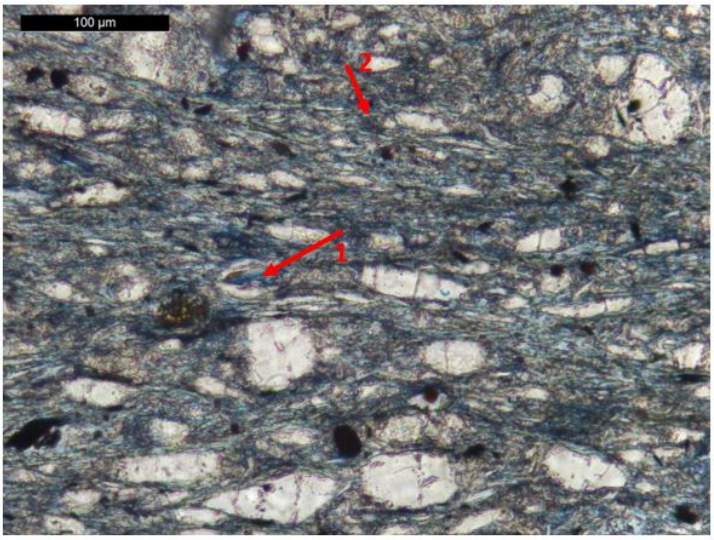

Figure 10.12: Stained, thin section of sandstone aggregate sample HA 41. Both arrow 1 and 2 point to the blue colour as a result of MB staining. The MB staining is mainly located within the iron hydroxide filled crack system as described in Appendix A.

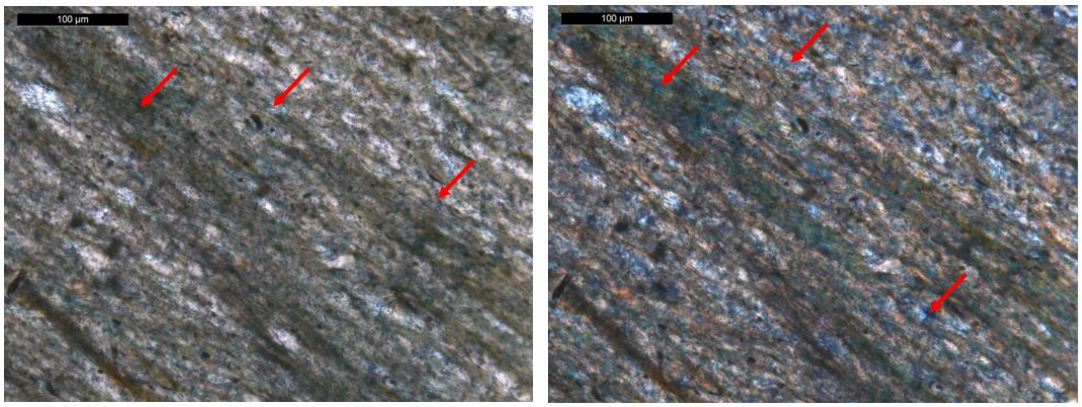

(a) (b)

Figure 10.13: Stained, thin section HA52; (a) in plane polarised light and (b) in crossed polarised light. The arrows in both (a) and (b) point to localised, MB stained spots. The majority of the blue colour in (b) is due to the presence of chlorite, which emits a greenish blue breaking colour in crossed polarised light.

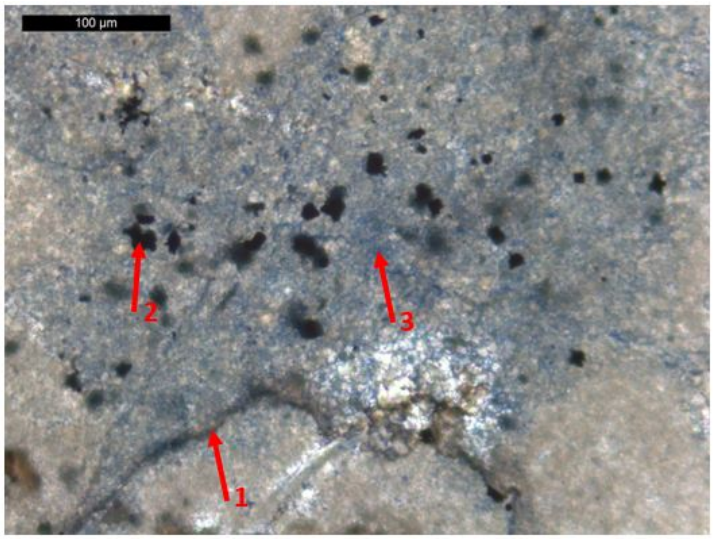

Figure 10.14: Stained, thin section of limestone (Lim) aggregate sample LA 1. Arrow 1 points to a stylolite, which is slightly stained with MB around its edges. Arrow 3 marks a system of MB staining, which is observed throughout sample LA 1 near the stylolite and around opaque minerals, an example indicated by arrow 2.

to these lines, yet a deeper blue colour would be expected in the thin section.

The thin section of limestone (Lim) sample LA 1 has concentrations that are coloured blue in large areas as can be seen in figure 10.14. The staining is in most cases close to a stylolite or opaque minerals. The colouring seems to highlight a network of tiny cemented cracks, which probably contain a higher content of clay. Nevertheless, the staining pattern cannot be compared to the sawn surface, as this presents no clear structures by the methylene blue staining due to its dark colour.

Figure 10.15 provides a microscopic photo of the stained thin section of limestone sample LA 3. The staining by the MB varies between the coarser and finer matrix. The coarser matrix contains a blue pale colour distributed throughout the sample. Yet, the finer matrix is not coloured blue. This division is observed as well within the sawn surface of LA 3. No structures are specifically highlighted by the methylene blue next to this observation in the thin section.

10.3. Determination of Clay Mineral

The combination of the MB adsorption test and staining of the thin sections make it possible to determine the type of clay mineral within the rock samples. The amount of staining within the thin

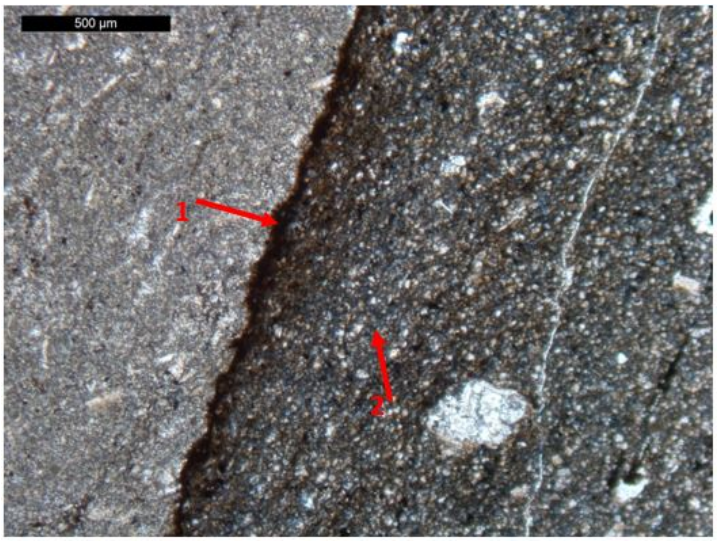

Figure 10.15: Stained, thin section of limestone (Lim) aggregate sample LA 3. Arrow 1 points to a stylolite separating a finer crystallised and coarser crystallised matrix. Arrow 2 highlights some minor MB staining within the coarser crystallised matrix between the grains.

Table 10.3: The cation exchange capacity of the clay mineral present within a selection of the tested aggregate samples.

Sample	Dry sample weight(g)	MB solution added (ml)	Fraction coloured in thin section	Weight of clay (g)	MBI of clay mineral present (meq/100g clay)
HA 41	20.05	8	0.1	2.005	3.99
HA 52	20.01	9	0.1	2.001	4.50
LA 1	20.04	6	0.05	1.002	5.99
LA 3	19.99	11	0.1	1.999	5.50

sections is estimated during the petrographic analysis for the samples HA 41, HA 52, LA 1 and LA 3. The percentage of staining is estimated for various parts within the thin section that show different properties. From these estimates an average amount of staining is determined. The cation exchange capacity of the rock pieces is determined with the MB adsorption test. From both the activity of the coloured material can be approximated. The results are listed in table 10.3. The rock pieces contain only one type of clay mineral by this approach. All samples contain a clay mineral with a MBI in the range of 1-10 meq/100g clay, which is typical for kaolinite (Shainberg and Levy, 2005). However, micas and chlorite are observed in several of the samples during the petrographic analysis. Sample HA 41 has domains with a higher amounts of micas, while sandstone sample HA 52 clearly shows the presence of chlorite (see Appendix A). Small amount of micas are observed in the limestone samples LA 1 and LA 3 as well. Micas have a MBI value that ranges between 20-40 meq/100g clay and chlorite varies between 10-40 meq/100g clay. Small amounts of these minerals increase the MBI value of the rock powder slightly, while most MB adsorption is probably caused by the kaolinite keeping the total adsorption below 10 meq/100g clay. Organic matter is possibly present in the limestones as well, based on the distincitve odour during breaking of the limestone aggregate pieces. The investigation indicates that the chance on the presence of swelling clay minerals like smectite is really low, because these minerals would greatly increase the adsorption value. For example, smectite has a MBI value in the range of 80-120 meq/100g clay. Furthermore, the total content of clay minerals, including the ones with a lower swelling potential, and organic matters is low based on the low MB adsorption values.

10.4. Discussion

The MB adsorption values on the single aggregate pieces are lower than expected, based on the values obtained on the aggregate mixtures. The samples were selected based on visual features, like

weak, weathered planes, that could indicate higher concentrations of clay minerals. Probably, the clay minerals in these areas are the non-swelling kaolinite as concluded by the correlation with MB staining of the thin sections. The higher values within the aggregate mixture must be caused by other samples, which are not tested individually. The staining of the sawn surfaces seems to correlate in some cases to the staining pattern within the thin sections. However, this is doubtful as the overview of the sawn surface is lost during the analysis on the thin section. Staining patterns observed on the sawn surfaces are not necessarily seen within the thin sections and are presumably influenced by retention of MB in cracks and micropores. The staining on the sawn surface is doubtful due to sandstone samples that coloured entirely blue and dark limestone samples that show no clear colouring at all. A change in staining method could result in better MB staining of the sandstone samples, however the dark limestone samples are probably not suitable for an analysis by surface staining. The improved staining should involve less methylene blue during staining and rinsing with water after a shorter period of time.

10.5. Conclusion

The methylene blue adsorption tests indicate a low concentration of clay minerals and organic matter within the tested armourstone aggregate mixtures and individual samples. A combination of the adsorption test and staining of the thin sections suggest that the majority of the present clay is kaolinite. The staining patterns on the sawn surface correlate in some cases to the staining patterns within the thin sections, yet seem to be influenced by a shadowing effect and retention of MB solution in pores and cracks. The dark background of several limestone pieces prevents a successful colouring by methylene blue on the sawn surface. Therefore, the stained surfaces provide no clear insight in deleterious clay structures using the tested method. However the similarities in staining pattern suggest an improved surface staining method is possible. The low MB adsorption values and low amount of localised MB spots in the thin sections indicate that no additional testing by means of a slaking test and/or wet-dry cyclic tests are required, to investigate the degradation by swelling constituents in the aggregate pieces.

11

Discussion

This research was performed because several waterway protection structures within the Netherlands dealt with rapid degradation of armourstones shortly after construction. The goal of the research was to provide a contribution in the quality control and quality assessment of armourstone and rock fill to ensure proper handling and installation in coastal and waterway protection structures.

In preceding studies the applicability of simple testing tools (like the Equotip) to investigate the deterioration of armourstones was already shown to be successful (Coombes et al., 2013). Furthermore, correlations between the Equotip and rock parameters, such as the UCS, were previously obtained by other studies (Meulenkamp and Grima, 1999; Verwaal and Mulder, 1993). The Equotip measurements of these studies were performed on sawn and sanded surfaces to provide a smooth rebound surface, while during this research also untreated, rough aggregate surfaces were tested. The surface roughness is the result of surface weathering as described by Wilhelm et al. (2016) and was therefore incorporated into the measurements. Viles et al. (2011) described that the surface roughness will decrease the rebound value, since the irregularities are crushed before the rebound. The single impact method Equotip (SIM) measurements from this research on the rough aggregate surfaces could be linked to features like the presence of cracks and concentrations of weak minerals in the weathered outer parts of the armourstone before placement, which are not recorded by Equotip measurements on a freshly cut surface. The Equotip rebounds can be performed using the SIM and repeated impact method (RIM) (Aoki and Matsukura, 2008). Both methods were executed during this research. SIM measurements on smooth surfaces were successful. Unfortunately, the RIM was not successful during this research. The RIM is used to identify the degree of weathering of the outer rock surfaces with respect to the inner fresh rock matrix. A logarithmic increase in rebound was expected, based on the study of Aoki and Matsukura (2008), but not obtained during testing on hand specimens. The results were inconsistent and did not indicate the degree of weathering properly. Possibly, the RIM method is not applicable to hand specimens due to their smaller size and mass. The aggregate surfaces of the tested pieces in this research varied in roughness and degree of weathering. As a result the rebounds did not converge to a similar L_{max} value and no proper indication of degree of weathering was obtained. Nevertheless, the degree of weathering of the hand specimens was noticed by the mean and standard deviation of the SIM measurements, as was expected by the study of Wilhelm et al. (2016) which studied the influence of surface roughness on the Equotip measurements.

Multiple studies established correlations between the mean Equotip rebound value and UCS value for dry cores, depending on the rock type (Kee, 2010; Lee, 2015; Meulenkamp and Grima, 1999; Verhoef, 2010; Verwaal and Mulder, 1993). Relations between UCS value and mean Equotip rebound value are observed as well for saturated sandstone and limestone cores during this research. The correlations are not similar to previously obtained results, due to variety in degree of saturation and a change in dimensions of the rock cores. The degree of saturation and the dimension of rock cores influence the recorded UCS value (Brown and Hoek, 1980; Colback and Wiid, 1965; Halleux et al., 2015; Hawkins, 1998; John, 1972; Palmstrom, 1995). However, the magnitude in change of rebound value was not recorded. This research has established that even though the trends are not similar for dry

and saturated cores, and are influenced by the dimension, they still fall within the recorded rebound range obtained during previous studies. This applies only on the tested sandstone and limestone in this research. The saturation of a core could have a larger influence in decrease in UCS or mean rebound value for other rock types and consequently not agree with correlations obtained during previous studies.

The used Equotip tip type effects the rebound values and correlations between rock parameters and mean rebound value (Verhoef, 2010). The type D and C Equotip were used during this research. Both tip types resulted in different correlations. Moreover, the coefficient of determination varied for the tip types as well. The accuracy of the tips were similar for the SIM measurement on the smooth and fresh surfaces, which was already recognised by Verhoef (2010). However, the type D measurements on the rough, untreated aggregate surface related better to the water absorption (WA) and density of the aggregate pieces. The impact force is smaller for the type C tip, consequently reducing the recorded thickness of the rock surface. The fresh, smooth surfaces do not vary in great amount moving into the rock mass, while a larger change occurs moving from the weathered outer parts to the fresh inner parts. This explains the similarity in accuracy on the fresh, smooth rock surface and difference on the rough, weathered aggregate surfaces between the two tip types.

The BTS test clearly indicated the layer activation described by Tavallali and Vervoort (2010) when the disks were tested with an orientation of the bedding parallel to the major stress direction. Central failure through the rock matrix was seen for the disks orientated perpendicular to the major stress direction. The BTS test emphasised the magnitude of the influence of bedding orientation towards the major stress direction. The BTS values recorded parallel to the bedding are low, around 3 MPa, which indicates that tensile failure along the bedding by swelling minerals or crystal growth could lead to rapid degradation of armourstones.

The methylene blue staining of thin sections is a common method to highlight deleterious minerals within a thin section (Pieters, 1992). However, the MB staining of a sawn rock surface is new. The success in highlighting deleterious minerals and structures by MB staining of the sawn surfaces is not consistent and does not fully corresponds to the MB stained thin sections, which are capable of showing the deleterious minerals and structures. The dark colour of the dark grey limestones prevented clear blue colouring to the naked eye. Some of the sandstone sections seemed to retain MB solution in cracks and pore spaces, presenting a blue colour while the presence of deleterious structures is questionable. However, some of the highlighted structures in the sawn surfaces corresponded to the deleterious structures visible within the thin sections. Nevertheless, some of the structures coloured in the sawn surface correspond to the coloured structures within the thin sections. The method of sawn surface staining is quicker and needs less equipment than the MB staining and analysis of the thin sections. Yet, the method is possibly not applicable to all rock types as the dark grey limestones did not reveal any blue colouring due to their dark colour. Decreasing the MB adsorption time could reduce the colouring of cracks and pore spaces within the sandstone.

This research has tested several testing tools next to the standard durability investigation according to EN 13383-1&2:2002, to make a contribution to a successful durability assessment and quality control system. In the introduction, the observation was raised that the current selection procedure of armourstone selection is not flawless to all degradation mechanisms, especially in dynamic environments. This research highlights the limitation of only performing the standard durability test according EN 13383-1&2:2002. The aggressive degradation by salt in the capillary zone reviewed by Benavente et al. (2001) is not included in the magnesium sulfate soundness test, where the aggregate is fully submerged. The tensile strength is not obtained within the standard, yet this is an important parameter considering degradation by e.g. salt crystallisation and swelling lay minerals (Benavente et al., 2001; Gonzalez and Scherer, 2004; Sebastián et al., 2008). The unconfined compressive strength is determined parallel to the bedding within the standard, yet minimum strength values are not necessarily obtained at this angle as indicated by the model of Tien and Kuo (2001). Therefore this research provided tools to deal with durability issues in the dynamic environments that are not captured within the standard EN 13382-1&2:2002. One should start a durability investigation by considering the construction, climate, and function of the armourstone, in order to obtained understanding of the exposed stress on the armourstones. A quarry visit should be performed to recognise variability in the armourstone product and to select a representative testing sample. The Equotip SIM test on aggregate pieces and rock cores, the BTS test, MB adsorption test, and MB staining provide detailed information in armourstone variability, degree of weathering, and

presence of deleterious constituents and structures. In combination with a petrographic analysis, the degradation of the armourstones can be better predicted. The tested rock pieces in this research turned out to contain only low amounts of deleterious minerals and structures. However, if the executed laboratory tests like the petrographic analysis and MB adsorption test indicate a higher amount of deleterious minerals and structures, additional specially designed mechanical tests are required such as the slaking durability test or wet-dry cyclic testing. These test prospect the mass loss of armourstone by the swelling and shrinking of the deleterious constituents (van de Wall and Verhoef, 1996).

12

Conclusion

After the armourstone samples were collected at the quarries, the research started with a standard durability investigation according to EN 13383-1&2:2002. Based on these tests the armourstone revealed no indication for concern of rapid degradation after placement. Nevertheless, variation was spotted in water adsorption (WA), density and unconfined compressive strength (UCS) value of various aggregate and core samples, which indicated a variety in durability between the rock pieces. Some of the pieces obtained poor parameter values and thereby approached or exceeded the lower margins of the durability requirement. Additional index tests were executed to assess the rock durability in greater detail.

The Brazilian tensile strength (BTS) test was the first simple index test described in this research. The literature review highlighted that the tensile strength is an important rock parameter for a durability investigation, since many degradation mechanisms, like salt crystallisation or slaking, are tensile failure of the armourstone. One of the sub-questions raised in the introduction was; what is the influence of the stress orientation with respect to the bedding within an anisotropic rock sample on its strength values? The BTS tests as described in this work concluded that the tensile strength strongly depends on the orientation of the stress axis towards the discontinuity plane. The BTS values for sandstone were twice as high when compressed perpendicular to the bedding instead of parallel to the bedding. The limestone BTS values varied as well, yet in a smaller magnitude than the sandstone. So the stress orientation with respect to the bedding has a great influence on the recorded BTS value. The BTS values are lower when the stress orientation is parallel to the bedding, since the rock disks split more easily along the weaker bedding plane. The disks fail through the rock matrix when tested perpendicular to the bedding, providing more resistance. When compared to the UCS values the BTS values are low, emphasising the tensile strength should not be neglected during a durability investigation.

One of the other sub-questions asked in the indtroduction was; can reliable Equotip measurements be taken on irregular, untreated, small aggregate samples? Tens of sandstone and limestone aggregate pieces were tested with the Equotip to answer this sub-question. The rebound values on the untreated surface correlated to the petrographic analysis and visual appearance of the aggregate pieces, like mineral content, presence of cracks and degree of weathering. A good correlation was obtained between the WA and mean rebound value as soon as the aggregate pieces were divided into proper density and mass classes. The difference in rebounds of the type C and D Equotip were consistent over the various samples. Thus, the Equotip takes good measurements on the irregular, untreated, small aggregate samples considering the previous observations. The type D Equotip distinguished more independent aggregate pieces than the type C tip.

The next sub-question is; is the Equotip capable in showing the degree of weathering of single rock pieces and what statistical analysis suits the Equotip data best for a weatherability study? The Equotip measurements were performed on untreated aggregate pieces, sawn aggregate pieces and rock cores. The untreated aggregate pieces have a weathered outer surface, which is removed for the sawn aggregate pieces and rock cores. The single impact method (SIM) Equotip measurements on the untreated aggregate pieces have a lower mean value and higher standard deviation compared to the sawn surfaces and rock cores. In addition, the sandstone rock cores have a clear deviation between weathered cores from the shear zone, and fresh, isotropic, homogeneous cores. The

weathered sandstone cores are identified by their lower mean rebound value and higher standard deviation as well. Weathering within the limestone cores was detected as well by an increase in standard deviation and/or decrease in mean rebound value. Moreover, the mean L-value drops in greater amount for the weathered cores when these are saturated. Thus, the weathering is detected by the Equotip when compared to fresh or less weathered samples of the same rock type. As mentioned, the mean and standard deviation do indicate the degree of weathering of the sample. The median and median absolute deviation (MAD) are too robust and the influence of extreme rebound values is too low, which are considered to be equally important in a durability investigation. The mean and median rebound value do not differ in predicting the UCS value of a rock core. The repeated impact method (RIM) was not successful during this research to determine the degree of weathering of aggregate pieces.

Can the water absorption of rock pieces be derived from Equotip measurements? The water absorption values of the aggregate pieces are compared to the mean rebound values. This provides an exponential trend between the WA and mean rebound, yet the scatter is large for the sandstone aggregate pieces. Separating the aggregate pieces into density classes provides a better result by reducing the scatter of the data points. Additionally, the performance of the fit depends on the mass of the tested aggregate pieces. The mean rebound increases with increasing density and increasing mass of the tested sample. Besides, the trend observed for the sandstone and limestone are not similar. All together, the water absorption is a valuable parameter in a durability investigation and the correlation to the Equotip highlights the applicability of the Equotip in a durability investigation.

Are previous correlations between Equotip and UCS valid for saturated samples? The Equotip measurements on the saturated cores with a L/D of 1 show a good correlation with the UCS that falls within the prediction range of previous research. The saturation of the cores with a L/D of 1 seems to compensate for the decrease in sample length with respect to the cores tested by previous studies, which mainly used dry cores with a L/D of 2. Nonetheless, the established correlations in this research do not perfectly match the trends from previous research and display different trends for the sandstone and limestones.

Does the Equotip correlate to the Brazilian tensile strength? As indicated, the BTS varies when the orientation of the anisotropic disks is changed. This is not captured within the Equotip measurements. The Equotip is only able to predict the BTS value for isotropic rock disks. Moreover, the correlation depends on the rock type just like the correlations with UCS vary with rock type.

Is the Equotip suitable in estimating rock durability? The Equotip is solely not suitable to predict the rock durability. The scatter in rebound values and variation in response on the sandstone and limestone indicate that the durability cannot be estimated only based on these rebound values. However, the rebound values increase the understanding of variation in the aggregate pieces when compared to one another. Therefore, the Equotip is definitely suitable to be used for a durability assessment.

Does the type C or type D Equotip provide better results for a durability investigation? Both the type C and type D Equotip provide good results. The rebound values for the type C are higher than for the type D tip. The correlation between the Equotip measurements on sawn and sanded cores and their strength values are accurate for both tip types. However, the correlation between the WA, density and mean L-value on untreated, rough aggregate surface is better for the type D tip. Both tip types are able to execute consistent measurements on both rock cores and aggregate pieces.

Is methylene blue surface staining capable of showing deleterious clay structures? The MB staining of the sawn surface is a very quick method to highlight deleterious structures in aggregate pieces. The MB stained sawn aggregate surfaces were compared to the MB stained thin sections, which are used to highlight the deleterious minerals and structures in a petrographic analysis under the microscope. The MB staining of the sawn surfaces resulted in some similarities with the thin sections. However, some of the sandstone pieces turned completely blue due to the MB staining, and some limestone pieces could not reveal any deleterious structures due to their dark grey colour. Thus, the MB staining of a sawn surface is able to reveal deleterious structures in some cases, yet the method is not consistent. Possible better results on the sandstone could be obtained by reducing the amount of MB and decreasing the adsorption time.

Finally answering the research question; can simple index test successfully contribute to the design of a quality assessment and quality control system for armourstone rock that ensures a workable and sound procedure for the acquisition and proper handling and placement in coastal and waterway protection structures? According to the performed tests simple index tests like the Equotip, BTS test,

methylene blue adsorption test, and methylene blue staining are capable os assisting during a quality assessment and quality control system for armourstone rock. These tests provide detailed information next to the standard durability tests in order to give an indication of variability in the armourstone behaviour. The combinations of the simple testing tools give more insight in the possible presence of deleterious constituents and structures like clay mineral, anisotropy and degree of weathering. The simple test should always be accompanied by the standard laboratory test according to EN 13383-1&2:2002, since the correlations with simple testing tools depend on rock type and need a proper reference. Additional testing by means of slaking or wet-dry cyclic tests is required, if deleterious minerals and structures are abundant.

13

Recommendations

Some recommendations with respect to selection of durable armourstones are suggested in this chapter based on the observations and test results obtained during this research.

A change in the methylene blue staining method of the sawn aggregate pieces could possibly reveal deleterious structures more consistent than recorded during this research. The tested pieces in this research coloured in some cases fully blue and the methylene blue seemed to be retained in cracks and pores close to the surface. Therefore, it is recommended to reduce the amount of methylene blue applied on the sawn surface and to reduce the adsorption time by rinsing the stained, sawn surface within 10 minutes. The method is not applicable to all rock types, since the dark grey limestones in this research revealed no colouring when stained with methylene blue.

The results of this research are based on tests on Devonian sandstone, Devonian limestone and Carboniferous limestone. The results vary between the three rock types. Consequently, correlations found during this research cannot be linked to other rock pieces. The tests should be performed on multiple rock types in order to develop a good understanding of the use of simple testing tools and set limitations for various rock types.

The methylene blue adsorption test is suitable to be used as a regular quality control for armourstone. The test is recommended to be included in a durability investigation as it is cheap, quick to perform and gives a first indication on the presence of deleterious constituents.

A petrographic analysis gives next to the presence of deleterious structures a view on the deleterious structures. Moreover, the analysis gives insight into the details of the rock matrix, which can explain rock behaviour during the other durability test, like the micro-Deval and UCS test. Therefore, a petrographic analysis is recommended to be performed during a durability assessment.

The tensile strength is a key parameter to assess degradation of armourstones, as many of the degradation mechanisms are tensile failure of the rock matrix. Therefore, the Brazilian tensile strength test is recommended for a durability investigation. This test is quick and simple to perform, because it reaches indirect tensile failure by compression of a rock disk. Care should be taken in the platens to prevent compressive failure at the contact points before tensile failure in the tensioned centre of the rock disks.

Equotip measurements can be performed on hand specimens as shown in this research. A quality controller can select various hand specimens from a stockpile, which can be distinguished by visual features, like colour, anisotropy or degree of weathering. Equotip measurements are recommended to be performed to investigate variability between the selected pieces.

The strength tests should be performed at angles to the weakness planes rather than parallel or perpendicular. The unconfined compressive strength and Brazilian tensile strength may be lowest at an angle to the weakness plane.

Slaking or wet-dry cyclic tests are recommended when the petrographic analysis on methylene blue stained thin sections concludes the presence of a considerable amount of deleterious minerals and/or concentrated, deleterious structures, and when the methylene blue adsorption test exceeds 0.7 g/100g clay.

Bibliography

Acir, Ö. and Kiliç, R. (2012). Determining abrasion rate of armourstones using physical modeling techniques. *Coastal Engineering Journal*, 54(4):1250021–1.

Adams, A. E. and MacKenzie, W. S. (1999). *A Colour Atlas of Carbonate Sediments and Rocks Under the-Microscope*. Manson Publishing.

Adams, A. E., MacKenzie, W. S., and Guilford, C. (1984). *Atlas of sedimentary rocks under the microscope*. Longman Group UK Ltd.

Amanullah, M., Marsden, J., Shaw, H., et al. (1997). An experimental study of the swelling behaviour of mudrocks in the presence of water-based mud systems. *Journal of Canadian Petroleum Technology*, 36(03).

Aoki, H. and Matsukura, Y. (2007). A new technique for non-destructive field measurement of rock-surface strength: an application of the equotip hardness tester to weathering studies. *Earth Surface Processes and Landforms: The Journal of the British Geomorphological Research Group*, 32(12):1759–1769.

Aoki, H. and Matsukura, Y. (2008). Estimating the unconfined compressive strength of intact rocks from equotip hardness. *Bulletin of Engineering Geology and the Environment*, 67(1):23–29.

ASTM (1984). Standard test method for methylene blue index of clay (C 837-99). *In 1984 Annual Book of ASTM Standards*, 15(2).

ASTM (2001). Standard practices for preparing rock core specimens and determining dimensional and shape tolerances. *ASTM International, West Conshohocken, PA D4543–01*.

Ballivy, G. and Dayre, M. (1984). The mechanical behaviour of aggregates related to physicomechanical properties of rocks. *Int Assoc Eng Geol Bull*, 29:339–342.

Benavente, D., Cueto, N., Martínez-Martínez, J., Del Cura, M. G., and Cañaveras, J. (2007). The influence of petrophysical properties on the salt weathering of porous building rocks. *Environmental Geology*, 52(2):215–224.

Benavente, D., del Cura, M. A. G., Bernabéu, A., and Ordóñez, S. (2001). Quantification of salt weathering in porous stones using an experimental continuous partial immersion method. *Engineering Geology*, 59(3-4):313–325.

Benavente, D., del Cura, M. A. G., Fort, R., and Ordóñez, S. (2004). Durability estimation of porous building stones from pore structure and strength. *Engineering geology*, 74(1-2):113–127.

Boulvain, F. and Vandenberghe, N. (2018). An introduction to the geology of belgium and luxembourg. In *Landscapes and Landforms of Belgium and Luxembourg*, pages 9–33. Springer.

Briševac, Z., Hrženjak, P., and Buljan, R. (2016). Models for estimating uniaxial compressive strength and elastic modulus. *Građevinar*, 68(1):19–28.

Broch, E. (1979). Changes in rock strength caused by water. In *4th ISRM Congress*. International Society for Rock Mechanics and Rock Engineering.

Brown, E. T. and Hoek, E. (1980). *Underground excavations in rock*. CRC Press.

Burshtein, L. S. (1969). Effect of moisture on the strength and deformability of sandstone. *Journal of Mining Science*, 5(5):573–576.

Cargill, J. S. and Shakoor, A. (1990). Evaluation of empirical methods for measuring the uniaxial compressive strength of rock. In *International Journal of Rock Mechanics and Mining Sciences & Geomechanics Abstracts*, volume 27, pages 495–503. Elsevier.

Cherblanc, F., Berthonneau, J., Bromblet, P., and Huon, V. (2016). Influence of water content on the mechanical behaviour of limestone: Role of the clay minerals content. *Rock Mechanics and Rock Engineering*, 49(6):2033–2042.

Chiappone, A., Marello, S., Scavia, C., and Setti, M. (2004). Clay mineral characterization through the methylene blue test: comparison with other experimental techniques and applications of the method. *Canadian Geotechnical Journal*, 41(6):1168–1178.

CIRIA/CUR/CETMEF (2007). The rock manual; the use of rock in hydraulic engineering. *C683, CIRIA, London*, page 1268.

Colback, P. S. B. and Wiid, B. L. (1965). The influence of moisture content on the compressive strength of rocks. *Geophysics*.

Coombes, M. A., Feal-Pérez, A., Naylor, L. A., and Wilhelm, K. (2013). A non-destructive tool for detecting changes in the hardness of engineering materials: Application of the Equotip durometer in the coastal zone. *Engineering Geology*, 167:14–19.

Deere, D. U. and Miller, R. (1966). Engineering classification and index properties for intact rock. Technical report, Illinois Univ At Urbana Dept Of Civil Engineering.

Douw, W. (2009). *Nutzung von massenschwere-bewegungen im tagebau*, volume 1. Conchbooks.

Dunn, J. R. and Hudec, P. P. (1966). Water, clay and rock soundness. *Ohio Journal of Science*, 66(2):153–168.

EN 1097-1 (1996). Tests for Mechanical and Physical Properties of Aggregates. Part 1: Determination of the Resistance to Wear (micro-Deval).

EN 13383-1 (2002). Armourstone Part 1: Specification.

EN 13383-2 (2002). Armourstone Part 2: Test methods.

EN 1367-2 (2009). Tests for Termal and Weathering Properties of Aggregates. Magnesium Sulfate Test.

EN 1926 (1999). Natural Stone Test Methods. Determination of Compressive Strength.

Erguler, Z. A. and Ulusay, R. (2009). Assessment of physical disintegration characteristics of clay-bearing rocks: Disintegration index test and a new durability classification chart. *Engineering Geology*, 105(1-2):11–19.

Feal-Pérez, A. and Blanco-Chao, R. (2013). Characterization of abrasion surfaces in rock shore environments of NW Spain. *Geo-Marine Letters*, 33(2-3):173–181.

Franke, W. R. and Anderle, H. J. (2001). *CC 6310 Frankfurt/Main West*. Bundesanstalt für Geowissenschaften und Rohstoffe (BGR).

Franklin, J., ZONGQI, S., Atkinson, B., Meredith, P., Rummel, F., Mueller, W., Nishimatsu, Y., Takahahsi, H., Costin, L., Ingraffea, A., et al. (1988). Suggested methods for determining the fracture toughness of rock. *International Journal of Rock Mechanics and Mining & Geomechanics Abstracts*, 25(2).

Gonzalez, I. J. and Scherer, G. W. (2004). Effect of swelling inhibitors on the swelling and stress relaxation of clay bearing stones. *Environmental Geology*, 46(3-4):364–377.

Goudie, A. S. (1999). Experimental salt weathering of limestones in relation to rock properties. *Earth Surface Processes and Landforms: The Journal of the British Geomorphological Research Group*, 24(8):715–724.

Halleux, L., Heeling, A., La Casta, M., Lee, M., Roukema, D., Sraders, G. A., van Damme, L., Van den Broeck, M., Verhoef, P. N., and Majid, Y. (2015). Classification of soils and rocks for the maritime dredging process. Technical report, PIANC, The World Association for Waterborne Transport Infrastructure.

Hawkins, A. B. (1998). Aspects of rock strength. *Bulletin of Engineering Geology and the Environment*, 57(1):17–30.

Huang, C., Subhash, G., and Vitton, S. J. (2002). A dynamic damage growth model for uniaxial compressive response of rock aggregates. *Mechanics of Materials*, 34(5):267–277.

Hujer, W. H., Finkbeiner, T., and Persaud, M. (2014). Estimating rock strength from non-destructive strength testing (equotip) and related benefits. In *EAGE Workshop on Geomechanics in the Oil and Gas Industry*.

ISRM (1978). Suggested method for determining tensile strength of rock materials. *International Journal of Rock Mechanics and Mining Sciences & Geomechanical Abstracts*, 15:99–103.

ISRM (1985). Suggested method for determining point load strength. *International Journal of Rock Mechanics and Mining Sciences & Geomechanical Abstracts*, 22:51–60.

Jefferson, D. P. (1993). Building stone: the geological dimension. *Quarterly Journal of Engineering Geology and Hydrogeology*, 26(4):305–319.

Jenny, H. (1941). Factors of soil formation. *A system of quantitative pedology*.

John, M. (1972). The influence of length to diameter ratio on rock properties in uniaxial compression: a contribution to standardisation in rock mechanics testing. *Rep S Afr CSIR No ME1083/5*.

Kahraman, S. (2007). The correlations between the saturated and dry p-wave velocity of rocks. *Ultrasonics*, 46(4):341–348.

Kahraman, S. and Gunaydin, O. (2007). Empirical methods to predict the abrasion resistance of rock aggregates. *Bulletin of Engineering Geology and the Environment*, 66(4):449–455.

Kee, L. J. F. (2010). Assessment of armourstone degradation in boskalis-built coastal constructions in the kingdom of bahrein, middle-east. Technical report, Boskalis.

Latham, J. P. (1991). Degradation model for rock armour in coastal engineering. *Quarterly Journal of Engineering Geology and Hydrogeology*, 24(1):101–118.

Latham, J.-P. (1993). A mill abrasion test for wear resistance of armour stone. In *Rock for Erosion Control*. ASTM International.

Latham, J. P., Lienhart, D., and Dupray, S. (2006). Rock quality, durability and service life prediction of armourstone. *Engineering Geology*, 87(1-2):122–140.

Lee, J. S. (2015). Calibration of rebound hardness numbers to unconfined compressive strength in shale formations. *Journal of Petroleum Technology*, 67(01):41–45.

Lienhart, D. A. (1998). Rock engineering rating system for assessing the suitability of armourstone sources. *Geological Society, London, Engineering Geology Special Publications*, 13(1):91–106.

Lienhart, D. A. (2003). A systems approach to evaluation of riprap and armor stone sources. *Environmental and Engineering Geoscience*, 9(2):131–149.

MacKenzie, W. S., Adams, A. E., and Brodie, K. H. (2017). *Rocks and Minerals in Thin Section*. CRC Press.

Meulenkamp, F. and Grima, M. A. (1999). Application of neural networks for the prediction of the unconfined compressive strength (ucs) from equotip hardness. *International Journal of rock mechanics and mining sciences*, 36(1):29–39.

Nicholson, D. T. (2001). Pore properties as indicators of breakdown mechanisms in experimentally weathered limestones. *Earth Surface Processes and Landforms: The Journal of the British Geomorphological Research Group*, 26(8):819–838.

Okawa, S., Ohoka, M., and Funato, A. (1999). Application of hardness tester to rock specimens. In *Proceedings of the 29th symposium of rock mechanics*, pages 256–260.

Palmstrom, A. (1995). *RMI - a rock mass characterisation system for rock engineering purposes*.

Pieters, W. E. (1992). Petrographic examination. Technical report, TU Delft.

Pieters, W. E., van Tooren, M., and Verhoef, P. N. W. (1992). Geomaterials characterisation and testing. Technical report, TU Delft.

Price, D. G. (2008). *Engineering geology: principles and practice*. Springer Science & Business Media.

Ramamurthy, T. (1993). Strength and modulus responses of anisotropic rocks. *Comprehensive rock engineering*, 1(13):313–329.

Roelen, M. (2017). Test report 7608. Technical report, Geos Laboratories.

Sebastián, E., Cultrone, G., Benavente, D., Fernandez, L. L., Elert, K., and Rodriguez-Navarro, C. (2008). Swelling damage in clay-rich sandstones used in the church of San Mateo in Tarifa (spain). *Journal of cultural heritage*, 9(1):66–76.

Shainberg, I. and Levy, G. (2005). Flocculation and dispersion.

Sharma, P. and Singh, T. (2008). A correlation between p-wave velocity, impact strength index, slake durability index and uniaxial compressive strength. *Bulletin of Engineering Geology and the Environment*, 67(1):17–22.

Singh, T. N., Verma, A. K., Singh, V., and Sahu, A. (2005). Slake durability study of shaly rock and its predictions. *Environmental Geology*, 47(2):246–253.

Tavallali, A. and Vervoort, A. (2010). Effect of layer orientation on the failure of layered sandstone under brazilian test conditions. *International journal of rock mechanics and mining sciences*, 47(2):313–322.

Tien, Y. M. and Kuo, M. C. (2001). A failure criterion for transversely isotropic rocks. *International Journal of Rock Mechanics and Mining Sciences*, 38(3):399–412.

Turk, N. and Dearman, W. (1986). A correction equation on the influence of length-to diameter ratio on the uniaxial compressive strength of rocks. *Engineering geology*, 22(3):293–300.

Valdeon, L., De Freitas, M. H., and King, M. S. (1996). Assessment of the quality of building stones using signal processing procedures. *Quarterly Journal of Engineering Geology and Hydrogeology*, 29(4):299–308.

van Beusekom, X. M. (1999). Design of an ore-pass in hartsteinwerke sooneck. Technical report, TU Delft.

van de Wall, A. R. G. and Verhoef, P. N. W. (1996). Geological construction materials. Technical report, TU Delft.

Van der Meer, J. W. (1987). Stability of breakwater armour layers—design formulae. *Coastal engineering*, 11(3):219–239.

Van Eeckhout, E. M. (1976). The mechanisms of strength reduction due to moisture in coal mine shales. In *International Journal of Rock Mechanics and Mining Sciences & Geomechanics Abstracts*, volume 13, pages 61–67. Elsevier.

Verhoef, P. N. W. (2010). Equotip Hardness Tester. Technical report, Ingeokring.

Verhoef, P. N. W. and Wezenberg, U. (2018). Duurzaamheidsevaluatie van schalie uit een belgische steengroeve, met betrekking tot de beoordeling van duurzaamheid van steen en de aankoop van steen bij boskalis nederland. Technical report, Boskalis.

Verwaal, W. and Mulder, A. (1993). Estimating rock strength with the equotip hardness tester. In *International Journal of Rock Mechanics and Mining Sciences and Geomechanics Abstracts*, volume 30, pages 659–662. Elsevier Science.

Viles, H., Goudie, A., Grab, S., and Lalley, J. (2011). The use of the Schmidt Hammer and Equotip for rock hardness assessment in geomorphology and heritage science: a comparative analysis. *Earth Surface Processes and Landforms*, 36(3):320–333.

Voskuilen, J. L. M. and Verhoef, P. N. W. (2003). Causes of premature ravelling failure in porous asphalts. *Performance Testing and Evaluation of Bituminous Materials*, pages 191–297.

Waltham, T. (2002). *Foundations of engineering geology*. CRC Press.

Wilhelm, K., Viles, H., and Burke, Ó. (2016). Low impact surface hardness testing (equotip) on porous surfaces–advances in methodology with implications for rock weathering and stone deterioration research. *Earth Surface Processes and Landforms*, 41(8):1027–1038.

Xu, S., De Freitas, M., Clarke, B., et al. (1988). The measurement of tensile strength of rock. In *ISRM International Symposium*. International Society for Rock Mechanics and Rock Engineering.

Zezza, U. (1990). Physical-mechanical properties of quarry and building stones. In *Advanced Workshop: Analytical Methodologies for the Investigation of Damaged Stone, F. Veniale, U. Zezza (Eds.), Pavia University, Pavia, Italy*.

A

Petrographic Analysis

A.1. Sandstone

A few aggregate samples from the sandstone are selected for the petrographic analysis. Most of them show already potentially weak features, like an anisotropic structure that could have an influence on its durability. Sample HA 51 is a strong sample that is representative for approximately 95% of the aggregate content. The thin sections are described piece by piece.

Sample HA 4 and HA 53

The first thin section is sawn from aggregate sample HA 4. The rock structure of the sample is displayed in figure A.1. The figure clearly shows two distinct structures within the rock fabric; (1) the left part shows a higher concentration of quartz grains, (2) while a system of iron hydroxide filled cracks in between micas (mainly muscovite) and quartz grains runs diagonal from the top middle to bottom right corner over the image. Both structures are displayed in detail in figure A.2. The two structures alternate in bands of various thickness ranging from 300 to 2000 µm. The alternation is likely to be a result of the sedimentation history of the rock. A change in the coarseness of the sediment has resulted in layers with different properties. The quartz grains within structure 1 are subrounded grains with a diameter of $\pm$20 to $\pm$100 µm and make up a moderately sorted structure. The grains are slightly larger in the aggregate sample itself, since the thin section is not cut perfectly through the centre of the grains. The majority of the quartz grain is monocrystalline denoted by B in figure A.1b, but some polycrystalline grains are present as well which is indicated by A. One of the subgrains shows undulose extinction, the different grey tints within one grain in crossed polarised light, within the figure. This phenomena is observed in the monocrystalline quartz grains as well and indicates plastic deformation within the quartz grains. The grains float within a fine iron rich, quartz cement and show a preferred orientation. This direction is emphasised by tiny, iron hydroxide filled cracks between the quartz grains. The quartz grains show point contacts, straight contacts or are not in contact at all. The minor amount of micas agrees to the preferential direction as well, shown by D in figure A.1b. Some of the micas show a birds eye appearance, indicated by A in figure A.2a. This texture is created by kinking of the mica, resulting in a bumpy internal structure. This bumpy structure appears blurry, bright coloured and dotty within the thin section in crossed polarised light. Micas that show this structure have been exposed to diagenesis and are not secondary minerals formed during this process. The quartz grains take up approximately 95% of the mineral content, 4-5% consists of opaque minerals and remaining $\pm$1% is occupied by micas. A small amount, less than 0.5% of chlorite is present as well. There is no clear adsorption of MB in this structure within the rock fabric, which indicates a very low active clay content. The second structure shows an increase in the amount of micas to $\pm$5%. The micas have a strong preferential orientation, highlighted by D in figure A.1b and A in figure A.2b. Parallel to this orientation is a structure of cracks filled with iron hydroxide, denoted by E in figure A.1b and B in figure A.2b, which are abundant within structure 2. The quartz grains within the second structure are smaller and all have a length below 50 µm. In addition, the grains have more of an elongated shape with their length axis parallel to the micas. The quartz grains are smaller, more elongated and take gradually more of a preferential orientation,

moving through the sample from structure 1 towards structure 2. Additionally, the amount of quartz grains is less. The quantity of chlorite slightly increases to about 1-2%. Within the second structure about 5% of the matrix around the micas is coloured blue due to the MB staining. The clay minerals probably originate from decay of the muscovite. The overall rock fabric has a low porosity, as a result of the iron hydroxide infill within the cracks and the cementation between the grains after deposition. Only a few small pore spaces with a diameter below 80 µm are observed within the sample and overall the porosity is below 1%. The structure of iron hydroxide filled cracks is a feature that suspects a fluid flow through the sample in the past. This may have occurred during a shear motion, which is clearly visible within the Hartsteinwerke. The quartz grains and micas are reorientated and plastically deformed as indicated by the undolose extinction within the quartz grains and birds eye structure within the micas during the low grade metamorphic process. In addition, small amounts of chlorite were formed by the break down of small rock fragments. The metamorphic processes are low grade indicated by the presence of muscovite and chlorite. The sample is a quartzitic meta-sandstone.

Sample HA 53 shows very similar features to HA 4. A microscopic image from the thin section can be seen in figure A.3. The alternation of the two domains described before is present within this sample as well. The majority of the quartz grains in HA 53 are larger than the ones in HA 4 and the amount of cement is reduced, especially within the first structure. In addition, the muscovite shows longer crystals, up to 200 µm in length, especially in the second structure. The quartz grains within HA 53 show straight and a few sutured contacts next to the point contacts and are more closely packed. Mineral content, porosity and MB adsorption are all similar to HA 4. The increase in grain contact and increase in size of micas suggest that sample HA 53 was exposed to higher grade of metamorphism than sample HA4 and was potentially closer to one of the present shear zones within the quarry.

Sample HA 41

Sample HA 41 shows a constant structure throughout the thin section and not the alternation of sedimentary layers as seen within the two previous thin sections. The structure can be observed in figure A.4 and is considered to be a mica quartzite. The quartz grains are smaller than within the samples HA 4 and HA 53, yet present in a higher quantity. Most of the grains are monocrystalline, yet a few polycrystalline grains are present. Sign A in figure A.4b shows clearly the undulose extinction within one of the quartz grains, showing the grain has been plastically deformed. Throughout the full thin section the elongated quartz grains show a preferential orientation. On a 10 to 20 µm scale the quartz grains are roughly reshaped in order to follow this preferential orientation. The size of the quartz grains varies from $\pm$10 to $\pm$80 µm and show a moderately sorted composition. The grains are subangular and their contacts are limited to point and straight contacts. The grains float within a fine quartz, iron rich matrix indicated by its light brown/reddish colour in figure A.4a. The sample consists of $\pm$94% of quartz, $\pm$5% of opaque minerals and $\pm$1% of mica and chlorite. The micas have the same preferential orientation as the quartz grains. Yet, bends within the mica and the birds eye texture suggest that this orientation is the result of a shear deformation. Iron hydroxide filled cracks, with a thickness of 1 to 10 µm, run parallel to the preferential direction between the micas and quartz grains. The MB adsorption is high at several of these concentrations and can stain up to 20% of the sample volume. However, the colouring is only pale blue as visualised in figure A.5. This indicates that the amount of clays present is still low, despite the blue colouring. These clays are probably a decay product of the micas. At selective spots the MB adsorption can result in a very deep blue colour, which may indicate clays with a higher swelling potential. Nevertheless, the MB adsorption is below 1% when averaged over the thin section and is distributed over the sample. The porosity within the sample is low. Only a few small pores are observed and a crack of approximately 50 µm in length. This sample has been influenced by metamorphism as well, based on the made observations. The preferential orientation of the grains, presence of muscovite and chlorite and the iron hydroxide filled cracks within the same direction all indicate a low grade metamorphism. The system of filled cracks also suspects a fluid flow through the sample in the past, similar to the samples before.

Sample HA 42

Sample HA 42 consists of a similar mineral composition as HA 4, HA 41 and HA 53 and is a mica quartzite. About 94% is quartz, 5% are opaque minerals and the remaining 1% consists of micas and

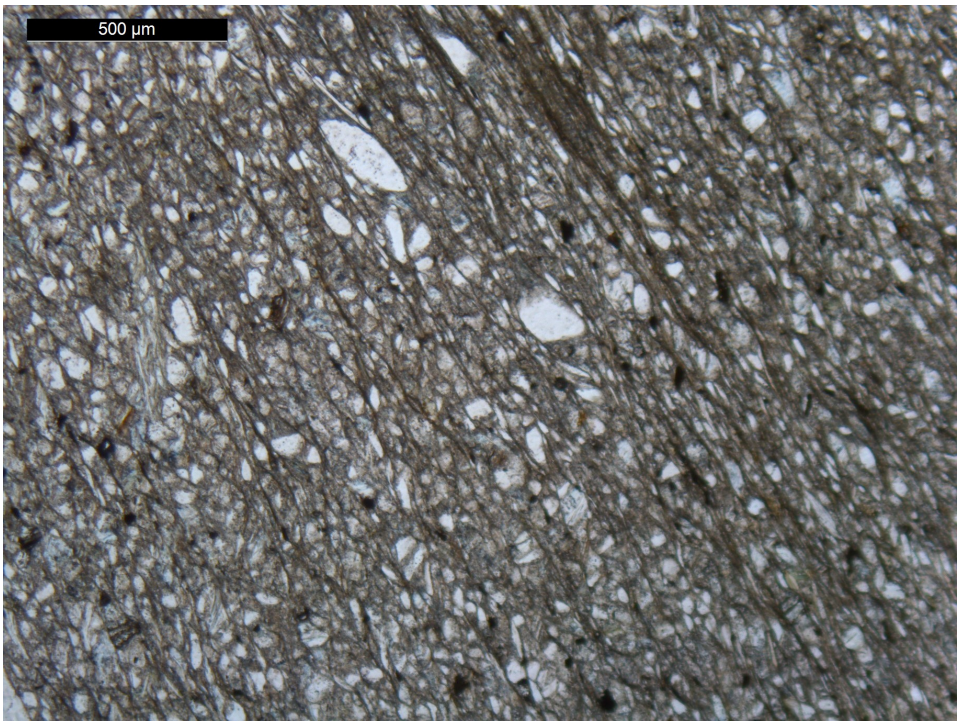

(a)

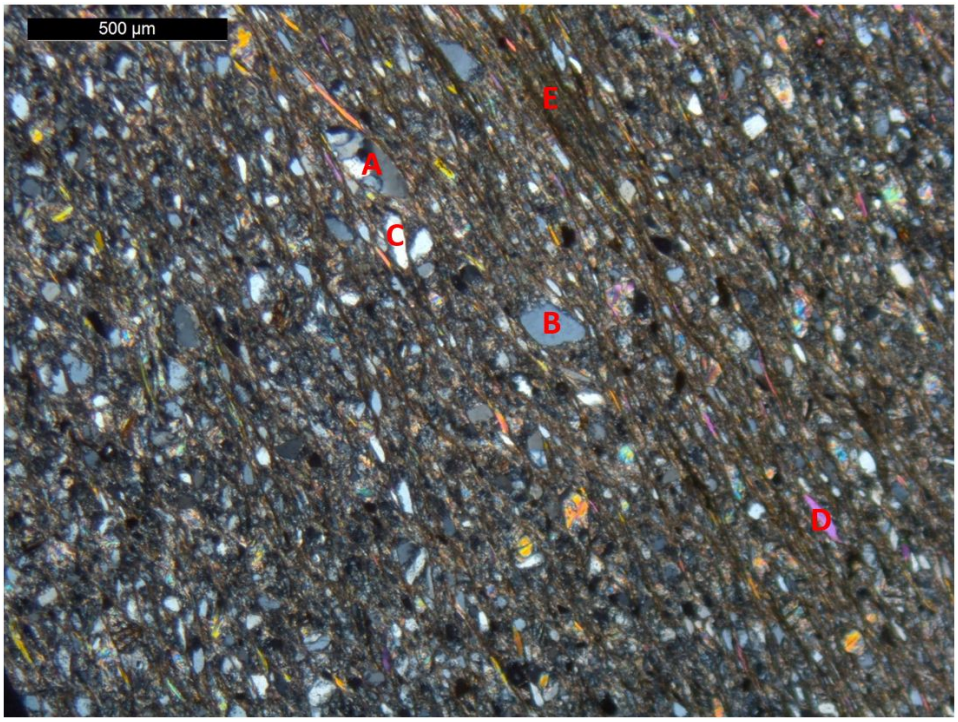

(b)

Figure A.1: Microscopic photograph of sandstone aggregate sample HA 4; (a) taken with plane polarised light and (b) taken with crossed polarised light. A indicates an example of a polycrystalline quartz grain and B a monocrystalline quartz grain, which are abundant in this sample. C highlights an elongated quartz grain that has a preferential orientation, which is maintained by the micas, an example indicated by D, as well. Finally, E shows the system of iron hydroxide filled cracks, which follow the same preferential orientation as the elongated quartz grains and micas.

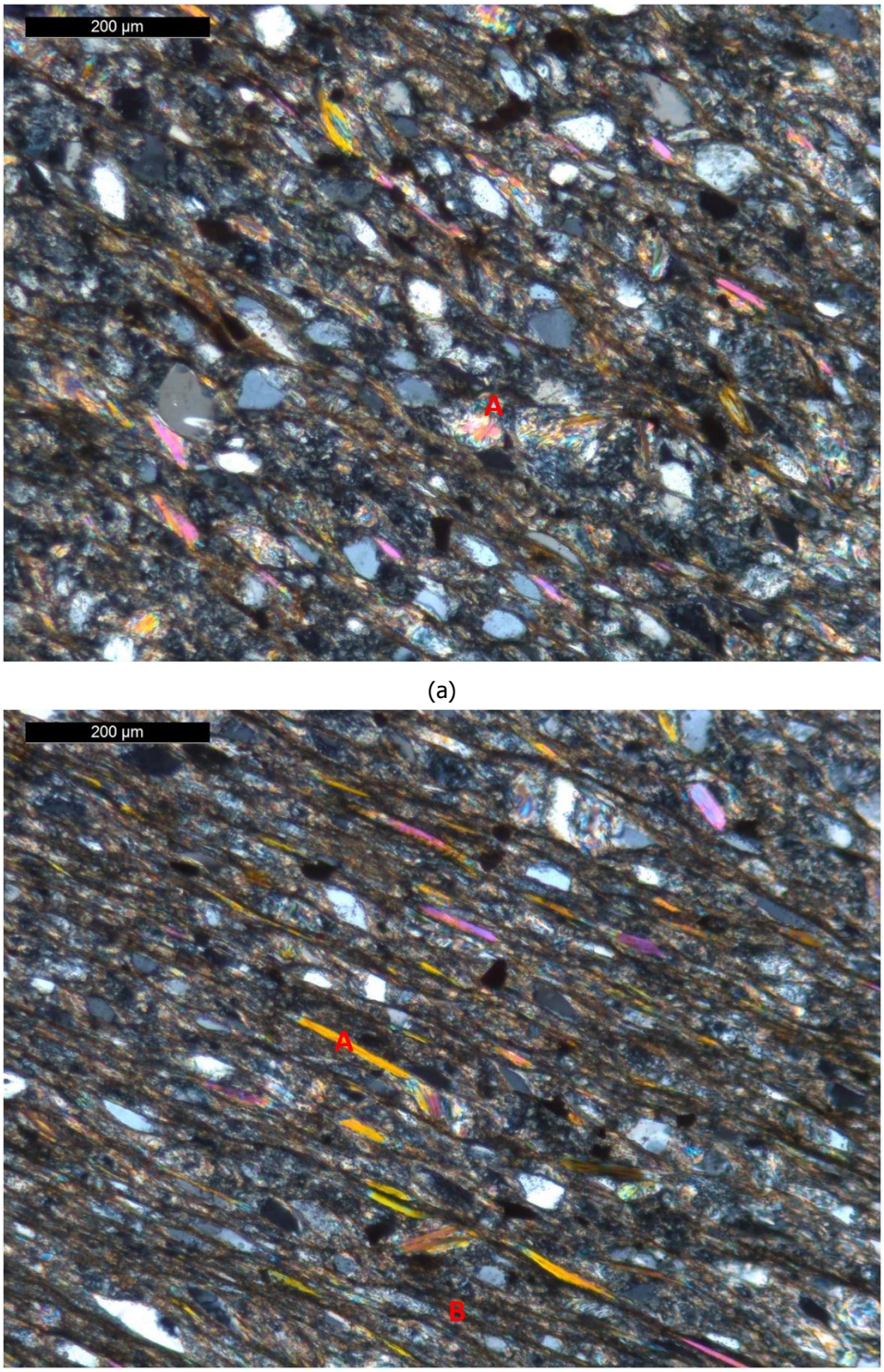

Figure A.2: Microscopic photograph highlighting the two types of structures within the sandstone aggregate sample HA 4; (a) the quartz crystals in crossed polarised light and (b) the iron hydroxide bands with micas in crossed polarised light. A in (a) points to a mica with a birds eye structure, indicating the grain was exposed to a low grade of metamorphism by deformation. A in (b) indicates the clear preferential orientation of the elongated mica grains, which is maintained by the iron hydroxide filled cracks at B.

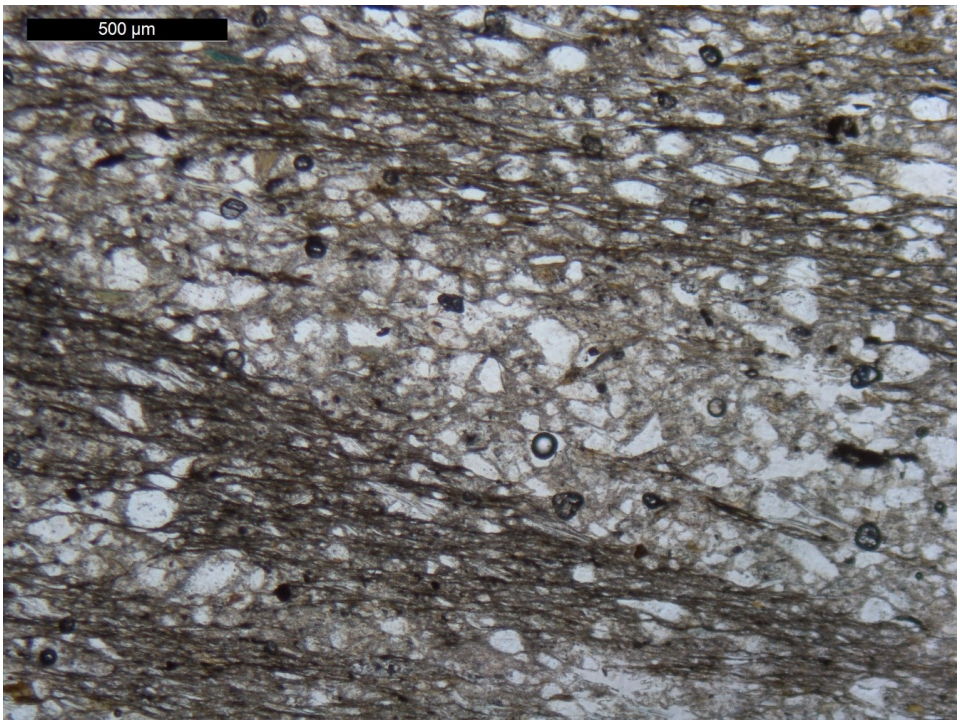

(a)

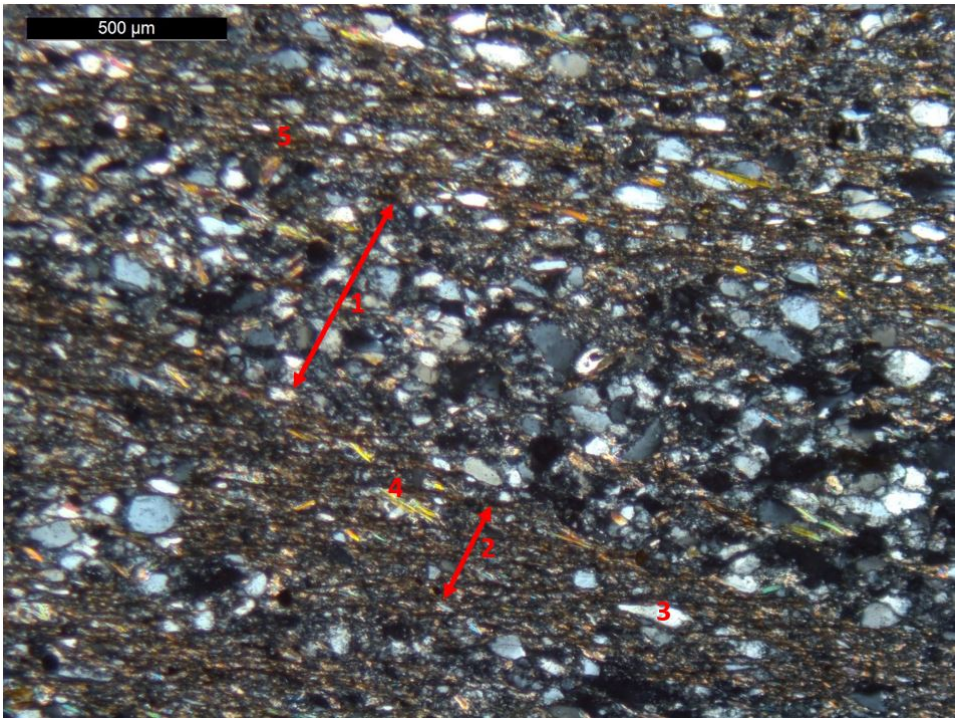

(b)

Figure A.3: Microscopic photograph of sandstone aggregate sample HA 53; (a) taken with plane polarised light and (b) taken with crossed polarised light. The two arrows 1 and 2 present the thickness of the two distinguishable domains within the rock matrix. Number 3 presents an example of an elongated quartz grain following the preferential orientation within the sample. Number 4 points to a mica with the birds eye structure. Finally, 5 represent the system of iron hydroxide filled cracks.

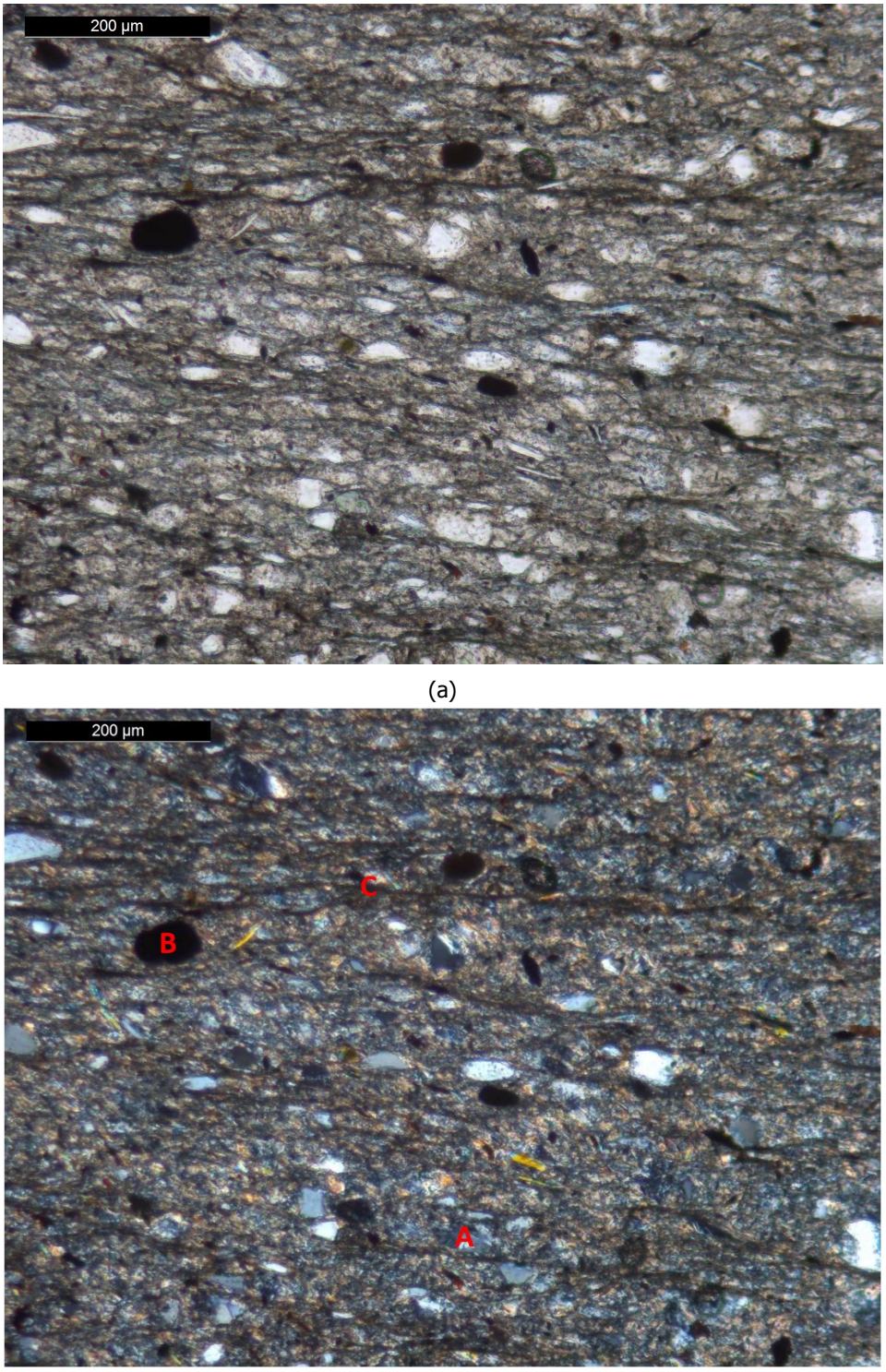

Figure A.4: Microscopic photograph of sandstone aggregate sample HA 41; (a) taken with plane polarised light and (b) taken with crossed polarised light. A in (b) displays the undolose extinction present in most quartz grains in the sample. This indicate the presence of dents in the grain as a result of deformation. B is one of the opaque minerals within the sample with a black colour in both plane and crossed polarised light. C points to a iron hydroxide filled crack inside the rock matrix.

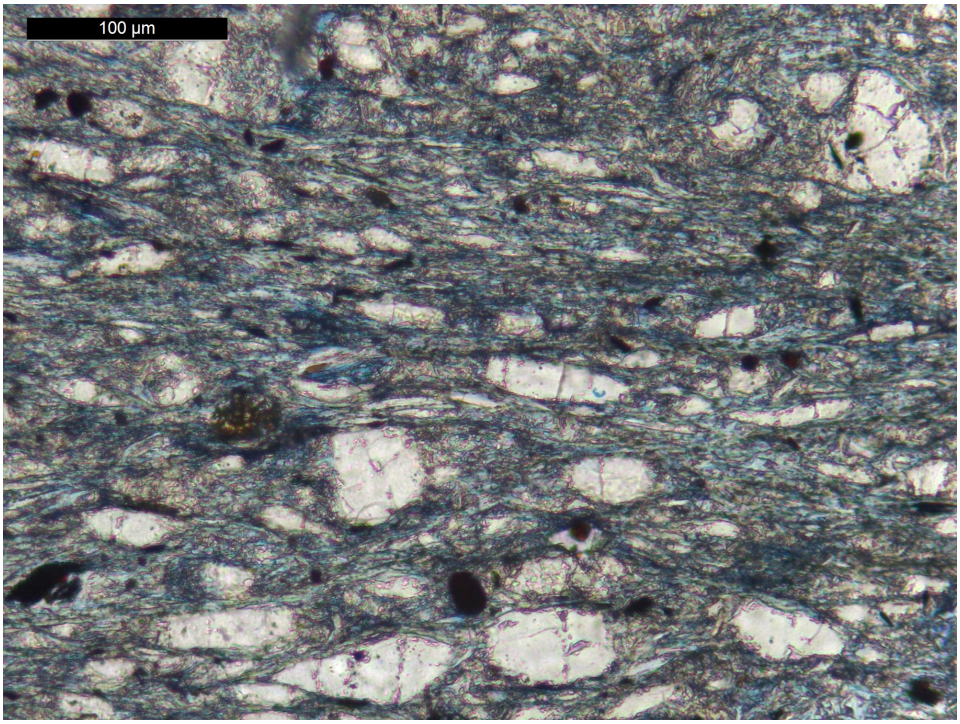

Figure A.5: A concentrated area of MB colouring within sample HA 41.

chlorite. The rock structure of sample HA 42 is shown in the microscopic image in figure A.6. The number of quartz grains in the range of 10-100 µm is considerable larger than within the previous mentioned samples. This has an influence on the contacts between the grains, which are still limited to point and straight contacts. The grains are more closely packed and the number of straight contacts has increased with respect to the previous samples. Most grains are mono-crystalline and several of the grains show undolose extinction. The quartz grains are aligned into a preferential orientation that is parallel to the orientation of the micas and bands of iron hydroxide. The orientation of the grains has changed due to deformation as clearly highlighted by the mica mineral in figure A.7. The mica is not perfectly aligned but shows some bends along the length axis of the grain, denoted by A in figure A.7, which suggest the orientation of the grain has changed over time as a result of deformation at low grade of metamorphism. Furthermore, the birds eye structure is visible, indicated by B in figure A.7, and agrees with the previous observation. Several spots within the sample show a higher mica content of $\pm$5%. Thin lines of iron hydroxide are abundant in these areas and minor amounts chlorite is observed around these lines. The size of the quartz grains in these areas is reduced as well as their number. Consequently the amount of cement between the grains increases. This change is a result of change in composition of the sedimentary layers. The porosity within the sample is below 1%. Only a few small pores with a length of approximately 20 µm and smaller are observed. The MB colouring is mainly located around the bands of iron hydroxide. At these locations the MB can stain about 10% of the surface as depicted in figure A.8. The staining in these areas is concentrated to thin lines between the quartz grains. Overall the colouring by MB is below 1% throughout the sample. Thus, locally some higher concentration of active clay minerals are present.

Sample HA 43

Sample HA 43 contains about 97% quartz, 2-3% opaque minerals and less than 1% mica. An overview of the rock structure is displayed in figure A.9. The sample is like HA 41 and HA 42 a mica quartzite. Low amounts of cement are present and the quartz grains show straight, concave-convex and slightly sutured contacts. The concave-convex contact is present around the grain marked with A in figure A.9b and an example of the sutured contact is around the grain highlighted with B in the same figure. The concave-convex and sutured contacts indicate a higher temperature and pressure during the metamorphism compared to the other samples, in order to possibly reach pressure dissolution at the edges of the quartz grains. Therefore, this sample is exposed to a higher degree of

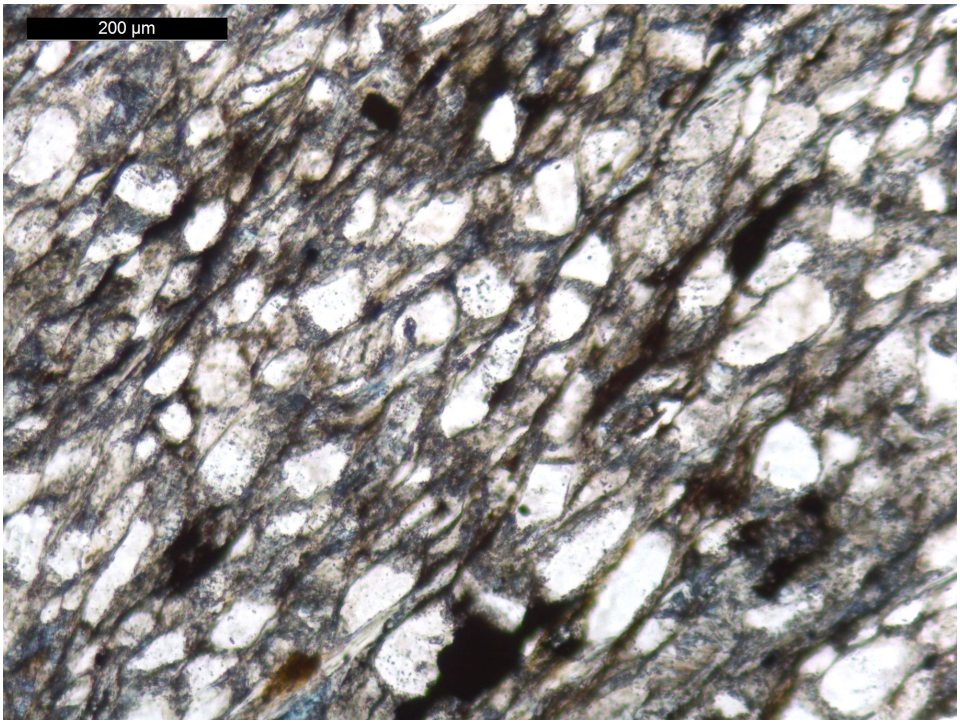

(a)

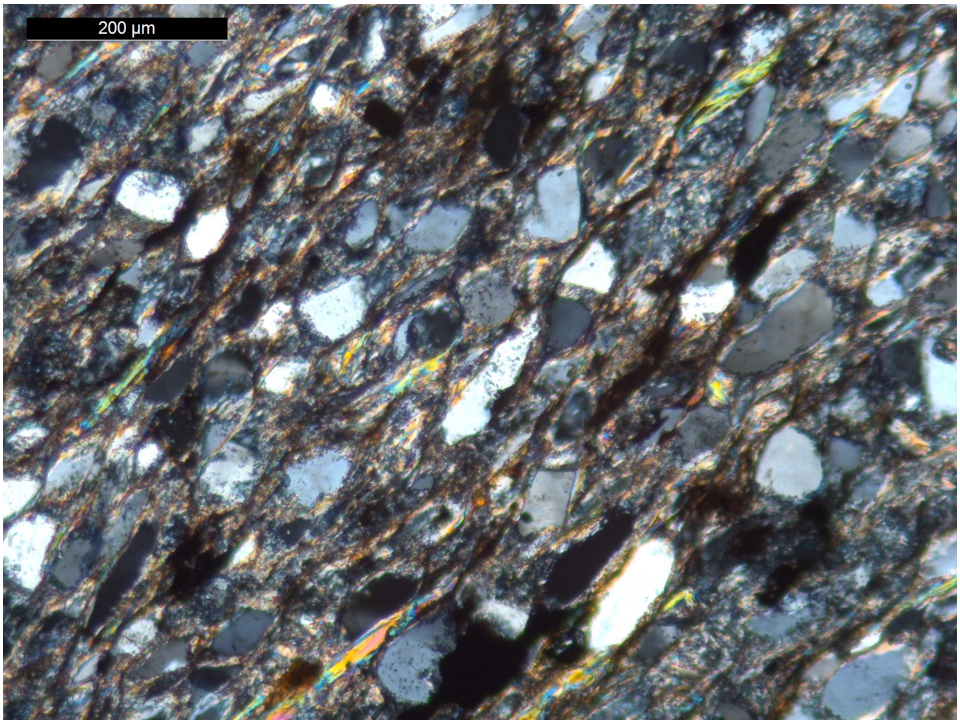

(b)

Figure A.6: Microscopic photograph of sandstone aggregate sample HA 42; (a) taken with plane polarised light and (b) taken with crossed polarised light.

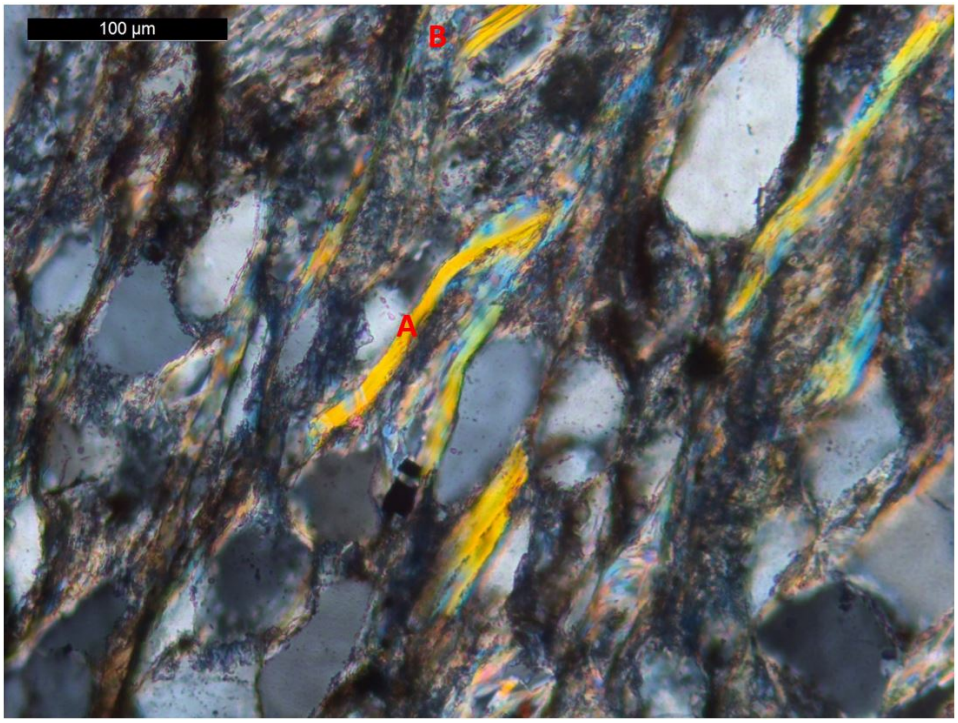

Figure A.7: Micas within sample HA 42 that show bends in their orientation and internal structure, indicating a change in orientation with respect to previous orientation as a result of diagenesis. At a is a mica grain which shows some bends along its length axis, which suggests the orientation of the grain has changed over time as result of deformation at a low grade of metamorphism. Other micas have the birds eye structure as can be seen at B, again a sign for deformation at low grade of metamorphism.

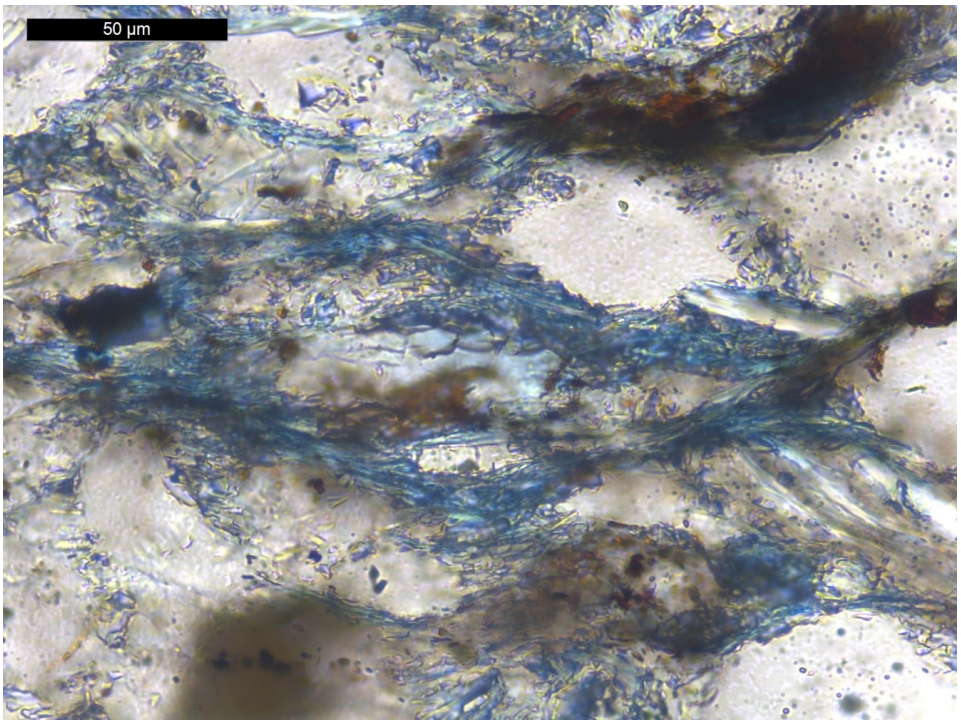

Figure A.8: Concentration of MB staining within sample HA 42.

metamorphism. Nevertheless, the presence of muscovite and absence of biotite show the metamorphism is still of a low grade because biotite crystallises at higher temperatures. The quartz grains' size ranges from 20 to 200 µm. Additionally, the grains have an angular shape and combine to a poorly sorted structure. Most of the grains are again monocrystalline, yet some polycrystalline grains are present of which one is indicated by C in figure A.9b. Undulose extinction is plainly visible in larger quartz grains within the thin section as presented by D in the same figure. The grains still show a slight preferential orientation, despite many quartz do not have an elongated shape. The preferential orientation is accentuated by cracks filled with iron rich cement. A remarkable pattern is present within the quartz grains at the boundary of the thin section. A blocky structure is present within the grains that seem to be little fractures within the grain, filled with cement. The pattern is orientated differently for every grain suggesting the fractures are related to the internal crystallographic structure of the quartz grains. The same phenomena is observed in sample HA 51 as well. A microscopic image of the structure within that sample is included. The preferential orientation within the thin section is emphasised by the micas, which all align in the same direction. Some of the micas show again the features inherent to deformation, like bends and birds eye structure displayed in E and F in figure A.9b respectively. The porosity within the sample is below 1%, since only a few pores are observed of approximately 50 µm in diameter. There is almost no MB adsorption within the sample and only two minor blue coloured spots are found within the thin section. Therefore, the active clay content within the rock is very low.

Sample HA 51

Sample HA 51 is a quartzite, whose structure can be seen in figure A.10. Cement between the quartz grains is only present at a few minor locations. The grains show concave-convex and sutured contacts, which are better developed than within sample HA43. 98 to 99% of the sample is quartz, $\pm$1% opaque minerals and the remaining 0-1% mica. The quartz grains range from 10 to 250 µm and have an angular shape. The quartz grains in sample HA 51 are the largest from the previously discussed samples, but still the overall structure is poorly sorted. Also most quartz grains are monocrystalline within this sample and undulose extinction is seen within the larger grains. A fine quartz, iron rich cement shows at places where the quartz grains are not in full contact. The same blocky, fractured structure within the quartz grains is present as observed within sample HA 43. This structure can be seen in figure A.11. The birds eye texture present within micas exposed to metamorphism is very well seen at C within figure A.10b. There are some larger pore spaces within the matrix, despite the close packing of quartz grains. A pore space of 1000 µm by 300 µm is present, depicted in figure A.12 and nearby are smaller pores of about 50 µm diameter. This specific spot shows a porosity of about 5%. Yet, the porosity is below 1% averaged over the full thin section. MB adsorption is extremely low (<0.1%) and shows only at a few single spots distributed over the thin section. So, the amount of active clay minerals is negligible.

Sample HA 52

Sample HA 52 distinguishes from the other sandstone samples. The sample is a meta-siltstone, as the grains within the rock matrix are all below 2 µm. Within the thin section of HA 52 several sedimentary layers can be observed. The layers include a more sandy layer, with quartz grains larger than 2 µm, a silt layer with a high chlorite content and a silt layer with higher clay content. The sandy layers are only thin seems within the sample of $\pm$100-400 µm thick. The sand layers are the minority within the thin section. Figure A.13 presents the interface of two sedimentary layers. The blue layer in the crossed polar light, marked with A in figure A.13b, is the silt layer with a high chlorite content, while the brown layer, indicated with B in the same figure, has the high clay content. A few thin bands of the clay rich silt, with a maximum thickness of approximately 50 µm, are present within the chlorite rich layer, highlighted with C in figure A.13b. Additionally, the clay rich silt layer contains also chlorite, which appears as the pale blue, greyish spots within the matrix. The two layers are separated by a thin band of iron hydroxide. The amount of micas slightly increases, moving closer towards this band. However, the amount of micas within the sample is below 1%. Furthermore, the micas are small with a maximum length of $\pm$25 µm. The micas are all orientated parallel to the direction of the band, which is the orientation of the bedding during sedimentation. The rock is exposed to low grade metamorphic processes. The quartz grains and micas have a preferential orientation. In addition, schistosity is visible in the interface of two sedimentary layers, highlighted in figure A.14. The boundaries of the two layers show a folded structure. The schistosity and folds indicate a deviatoric stress perpendicular to these

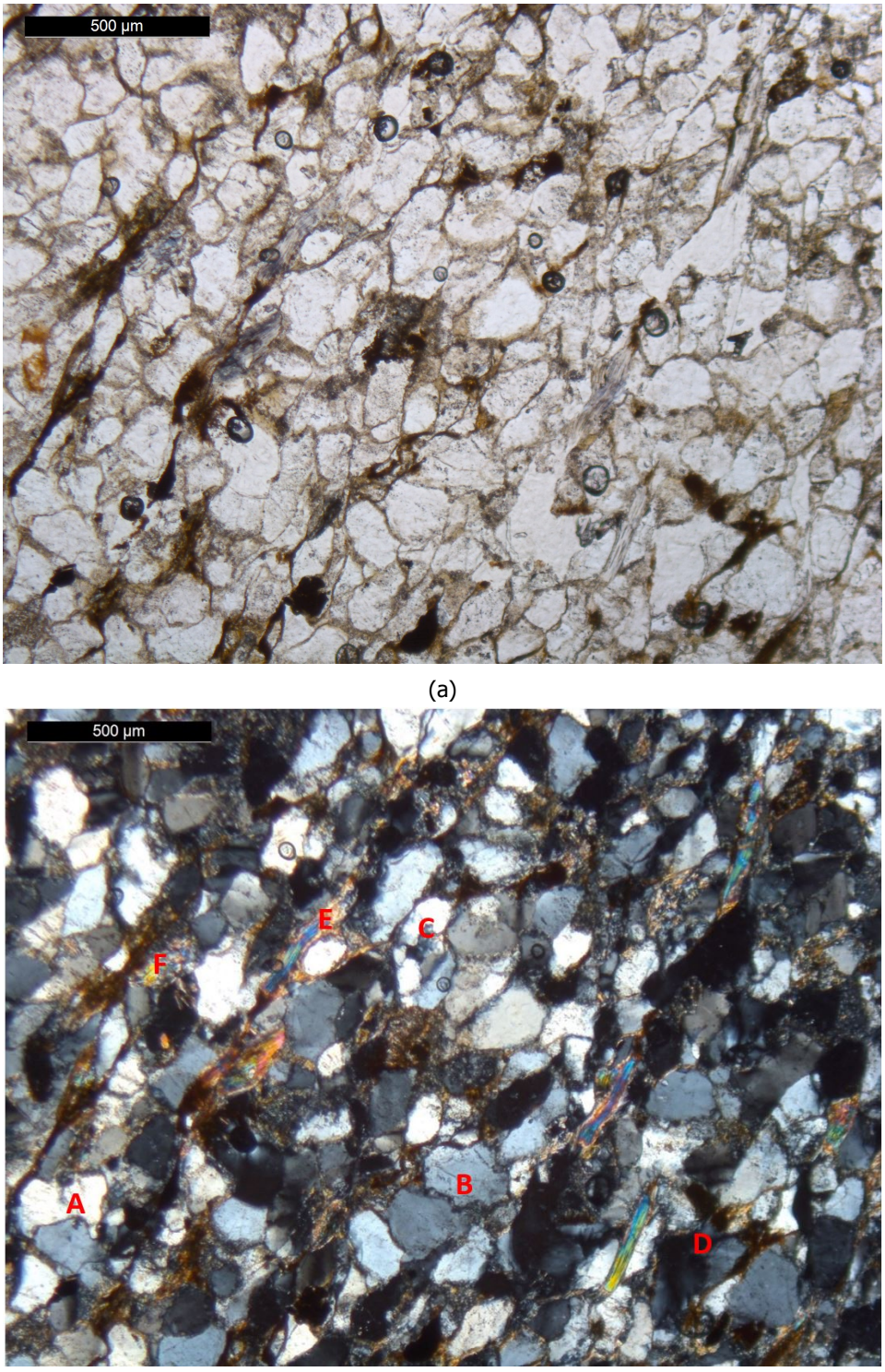

Figure A.9: Microscopic photograph of sandstone aggregate sample HA 43; (a) taken with plane polarised light and (b) taken with crossed polarised light. A marks a concave-convex contact between two of the quartz grains. A sutured contact between two quartz grains is denoted by B. These contacts indicate a higher degree of metamorphism compared to the previous samples. A polycrystalline quartz grain is located at C and D highlights a grain showing undolose extinction. Both E and F point to deformed micas that have a birds eye structure.

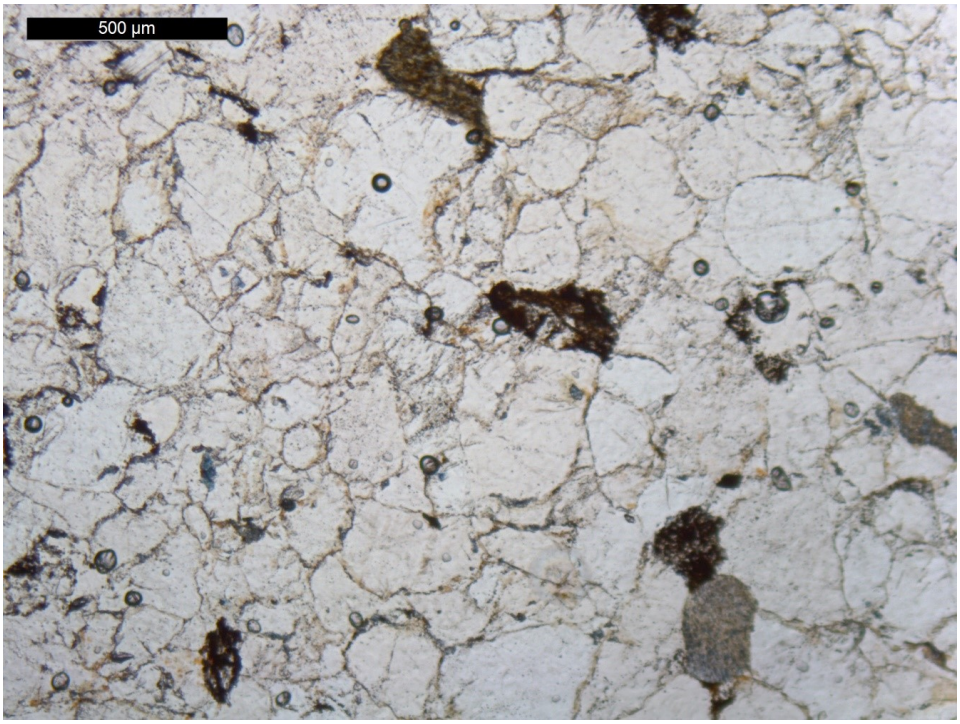

(a)

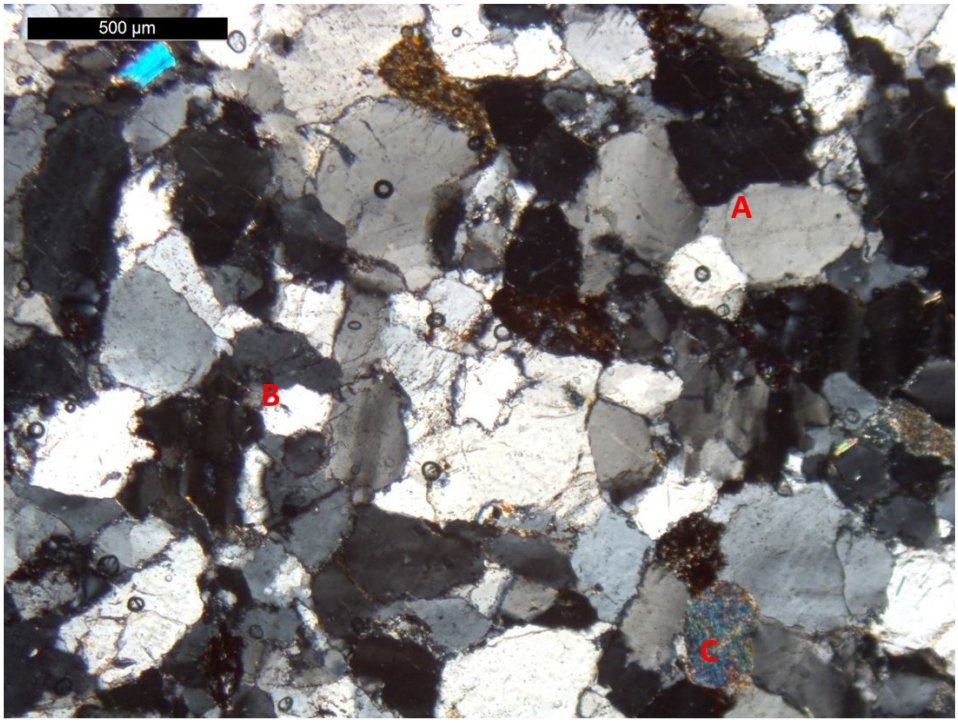

(b)

Figure A.10: Microscopic photograph of sandstone aggregate sample HA 51; (a) taken with plane polarised light and (b) taken with crossed polarised light. Two examples of sutured contacts between the quartz grains are marked by A and B. C points to a mica with a developed birds eye structure due to deformation at a low grade of metamorphism.

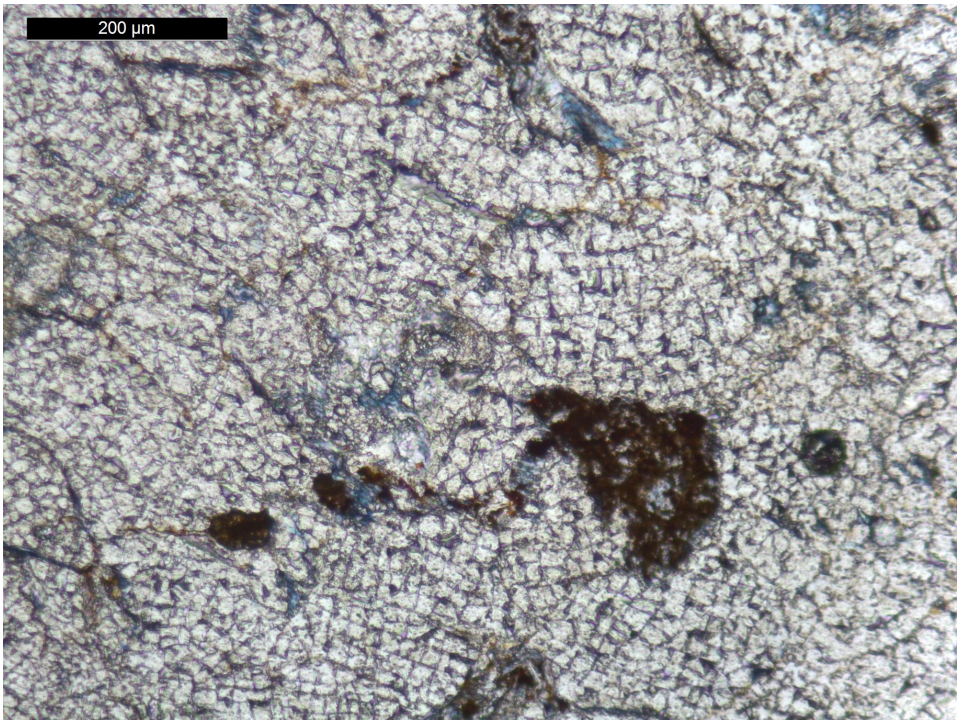

(a)

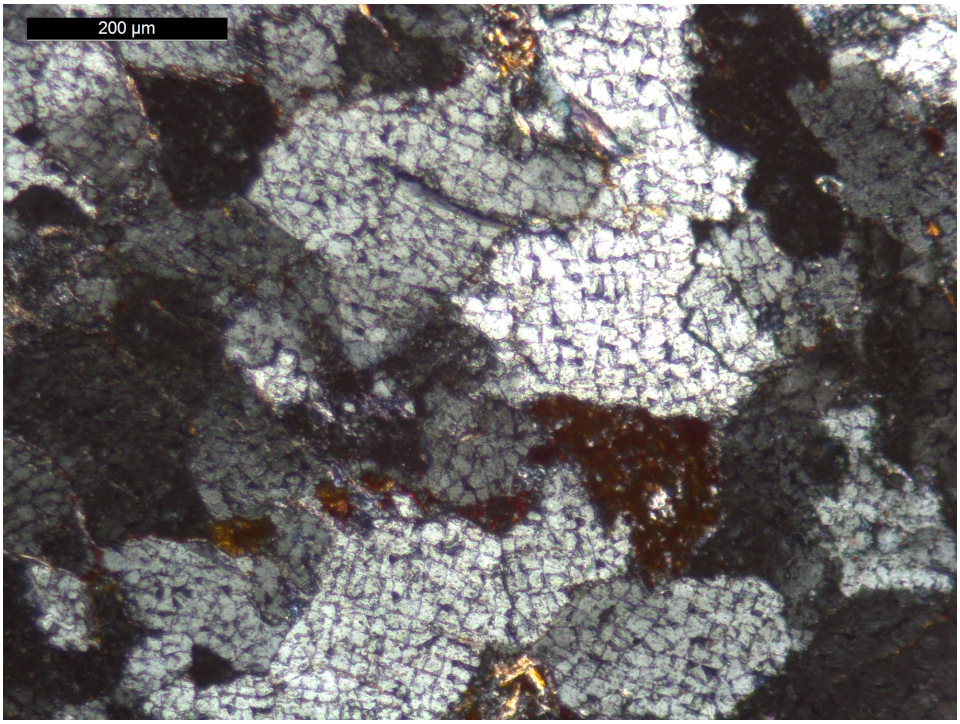

(b)

Figure A.11: Blocky, fractured structure within quartz grains present in aggregate sample HA 51; (a) taken with plane polarised light and (b) taken with crossed polarised light.

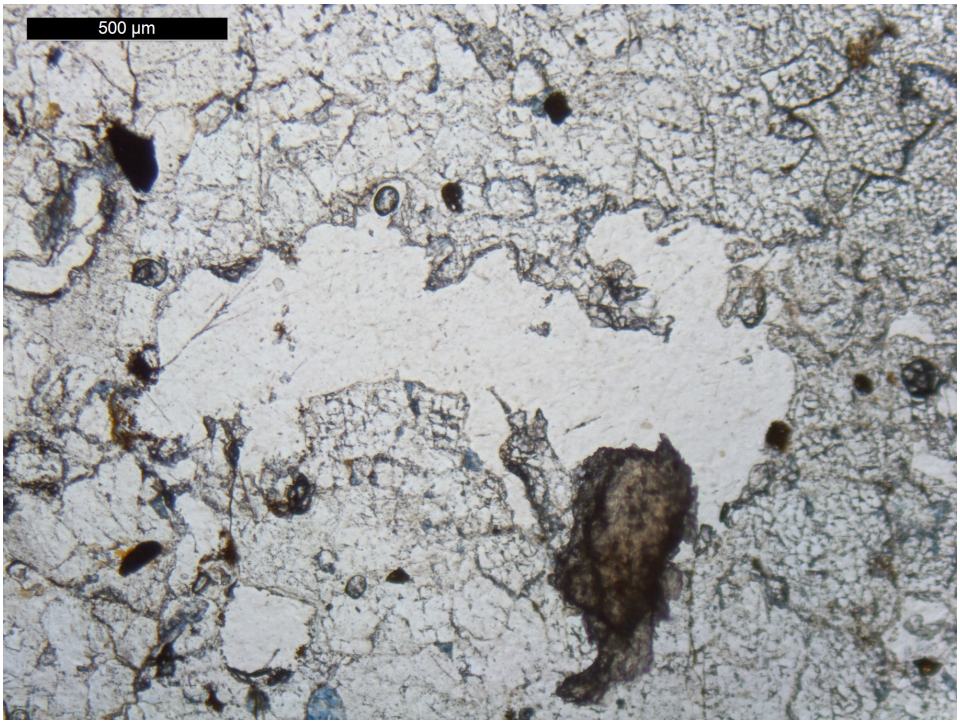

Figure A.12: Large pore space within sample HA 51.

structures during a low grade metamorphic process. The deviatoric stress direction was orientated from the bottom left to top right in the case of figure A.14a as shown by the arrow. The clay rich layer shows some pale blue colour in plane polarised light as a result of the MB staining, indicating the presence of active clay minerals. The other layers show no colouring as a result of the staining. The porosity within the sample is very low (<1%) and no visible pores spaces are detected.

A.2. Limestone

The limestone aggregate samples analysed with the microscope originate from Carrière des Limites and Carrière de Jenneret. The thin sections are described piece by piece.

Sample LA 1

Sample LA 1 is a limestone (Lim) that shows a variety of structures within its thin section. The first main texture present within LA 1 is shown in figure A.15. The photograph shows intraclasts of micrite within a sparite cement. Two bivalves can be seen just top right of the centre. Small concentrations of quartz and opaque minerals are present. Both do not make up 1% of the total mineral content. The quartz concentrations are small, silica rich nodules within the limestone. Some iron hydroxide stylolites are present within the sample, of which one is highlighted in figure A.16. The stylolite of iron hydroxide marks the barrier of the micrite cement in the upper part and sparite cement in the lower part. Both contain micrite intraclasts. The amount of bioclasts in the sample is low. Only a few small bivalve fragments of 100 to 200 µm in length and 10 to 20 µm thick are present and a few pieces of coral with a diameter of $\pm$50 µm. The high amount of carbonate mud and low amount of grains classify the rock as a wackestone according to Dunham's classification. The MB adsorption is localised to a network within the micrite. The concentrations can stain locally up to 20%, however is distributed within the matrix. The colouring does not exceed 1% averaged over the entire sample. The concentrated network of MB is presented in figure A.17.

Sample LA 2

Sample LA 2 is a grainstone, according to Dunham's classification, with a high amount of bioclasts such as bivalves, brachiopods, corals, bryozoans and foraminifera. The bioclasts are considerably larger than the ones in LA 1. Several fossils can be recognised with the naked eye in the thin section, e.g. a

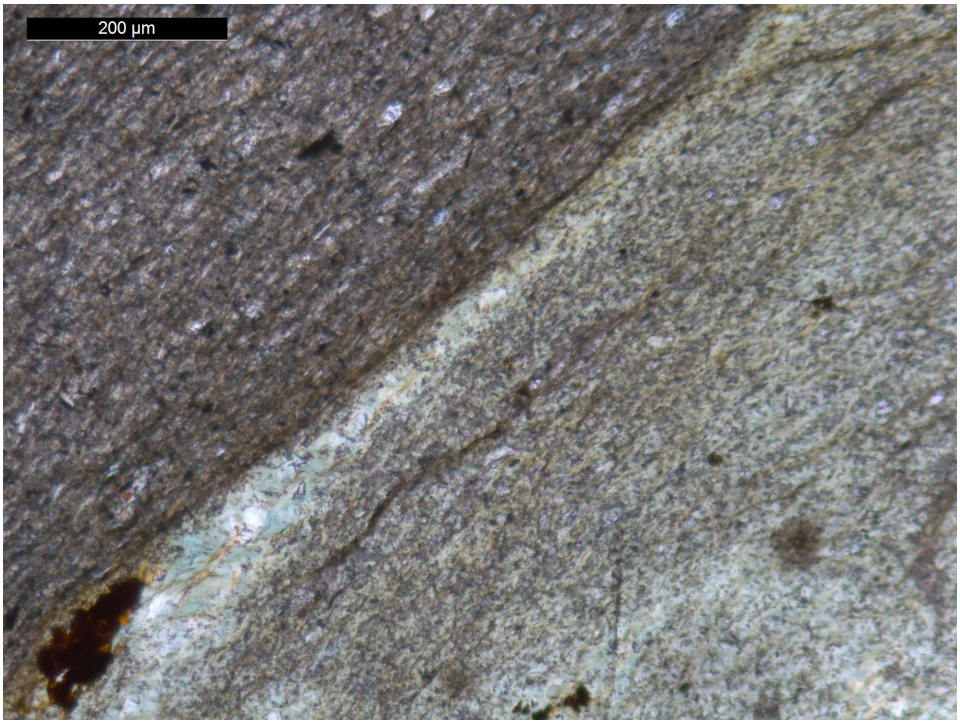

(a)

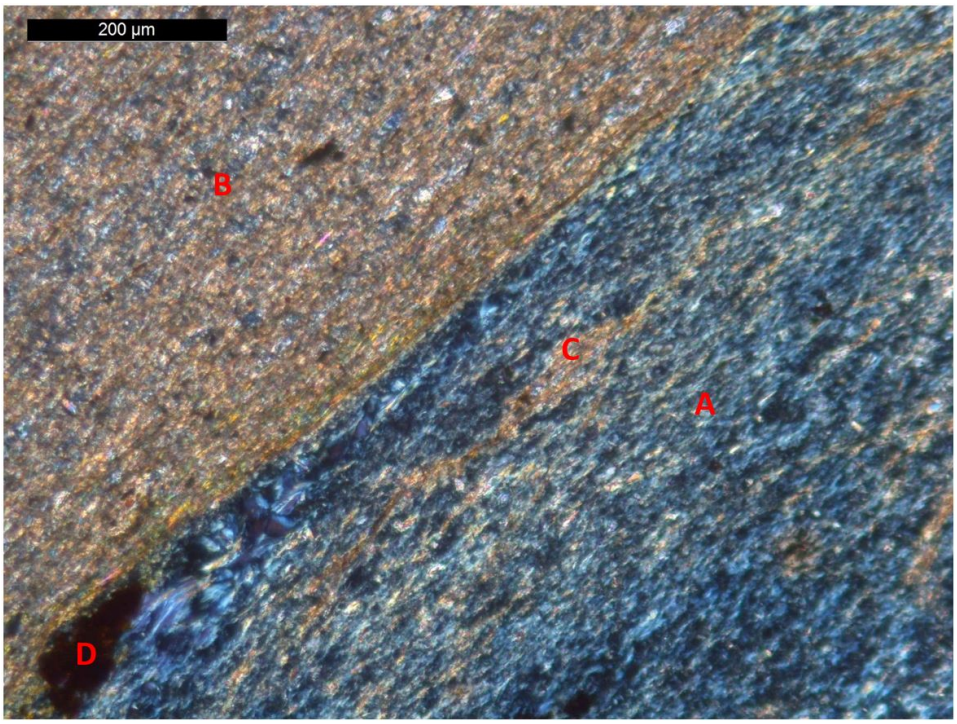

(b)

Figure A.13: Microscopic photograph of sandstone aggregate sample HA 52, showing the boundary between two sedimentary layers; (a) taken with plane polarised light and (b) taken with crossed polarised light. A and B mark two sedimentary domains. The domain A contains a higher chlorite content while the domain B contains a higher clay content. C highlights a few clay rich bands within the chlorite rich domain. A concentration of iron hydroxide is present at D.

(a)

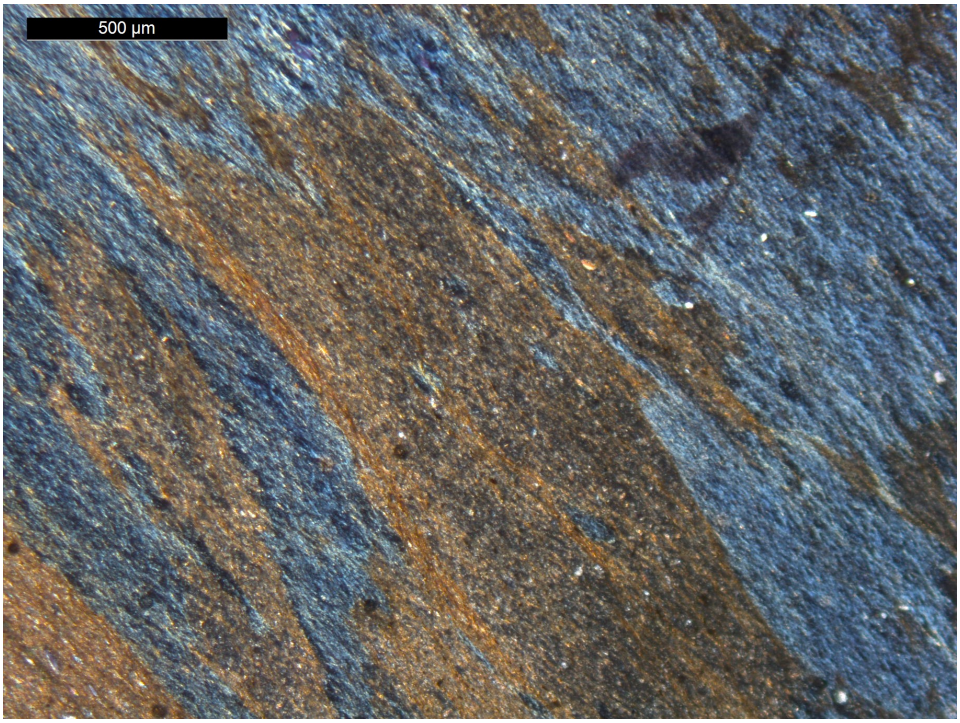

(b)

Figure A.14: Microscopic photograph of sandstone aggregate sample HA 52, showing schistosity between two sedimentary layers; (a) taken with plane polarised light and (b) taken with crossed polarised light. The dark brown silt has a higher clay content. The blue colour in the crossed polar view highlights the presence of chlorite.

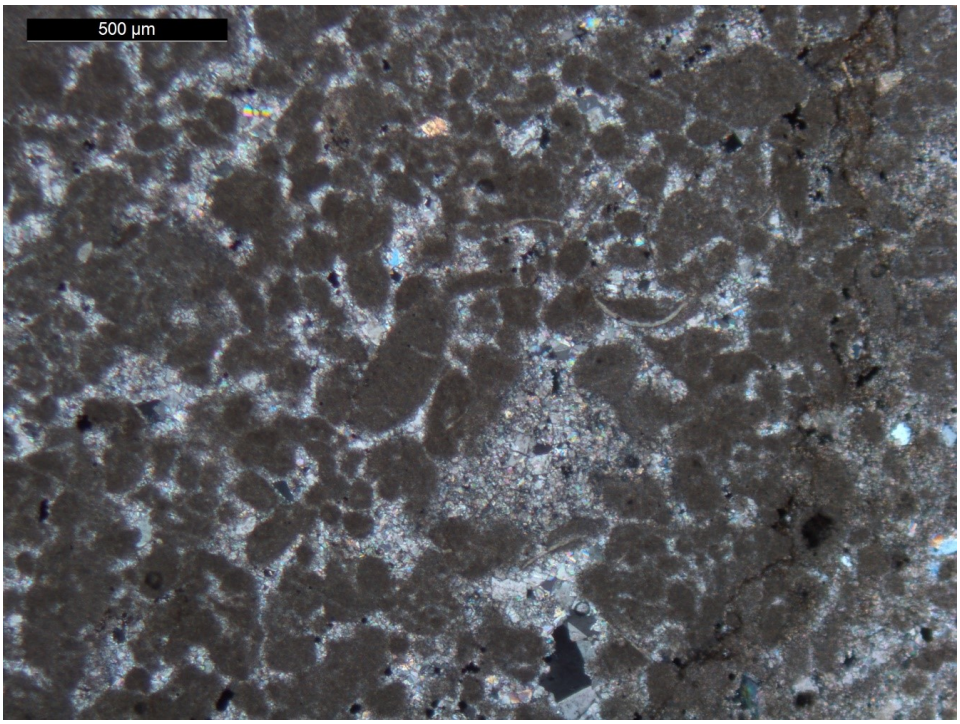

Figure A.15: Intraclasts of micrite within a sparite cement in sample LA 1.

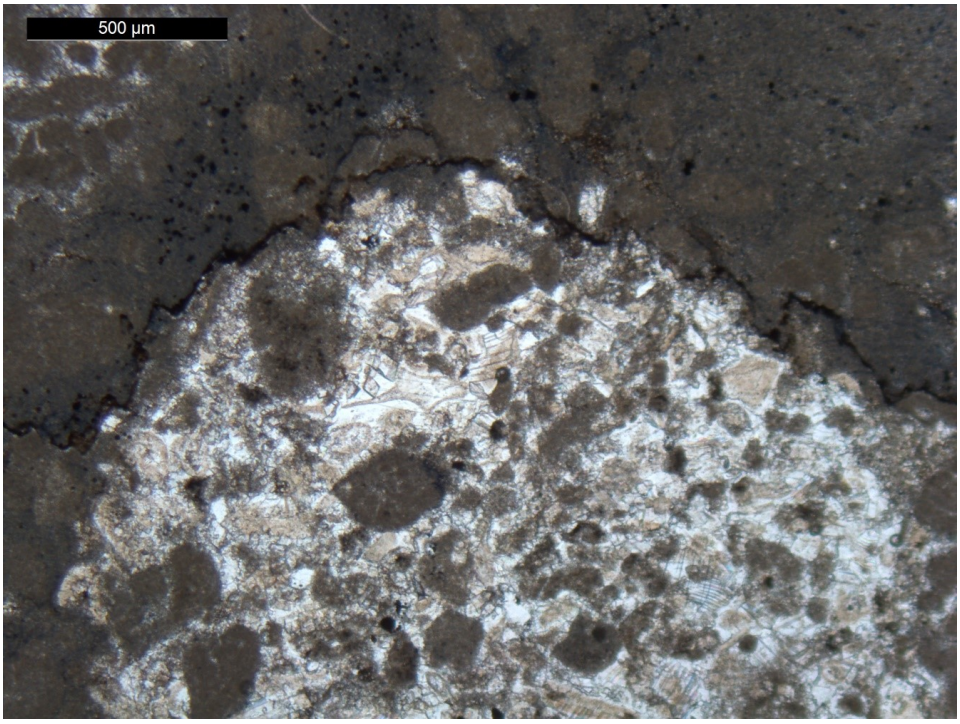

Figure A.16: Stylolite within sample LA 1.

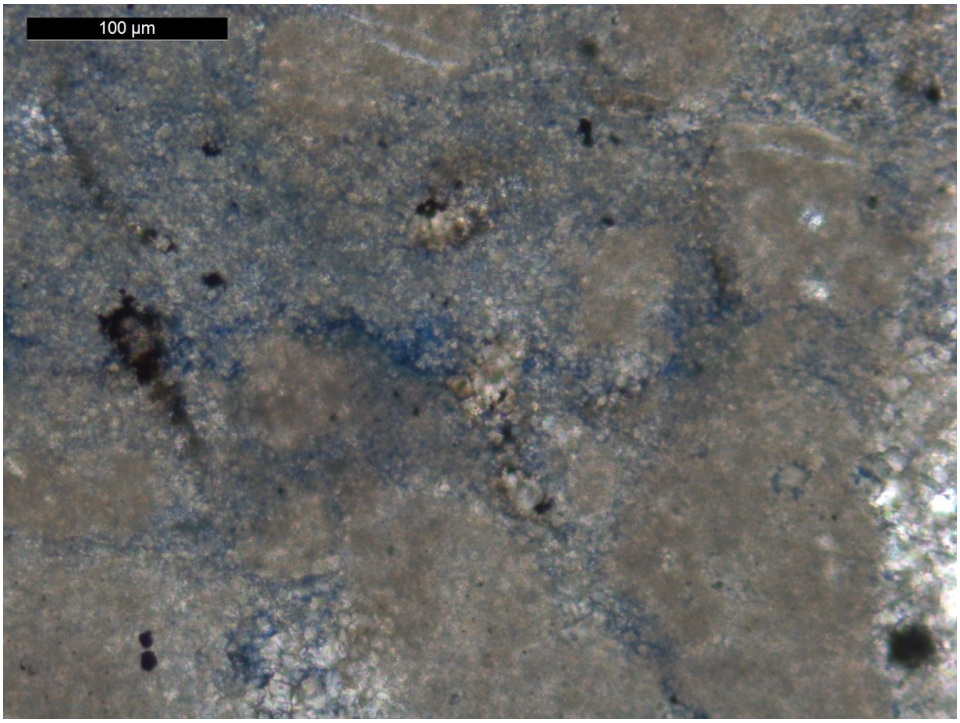

Figure A.17: MB colouring within sample LA 1.

piece of coral with a diameter of ±50 mm. The rock structure is presented in figure A.18. A very dark brown micrite cement is present between the bioclast fragments. The bioclasts show a preferential orientation from the left to right, especially the elongated bivalve fragments. This direction represents the bedding during time of deposition. A system of tiny cracks is visible perpendicular to the bedding. The cracks are filled with a fine recrystallised, calcite cement. The system of parallel cracks is a result of a deviatioric stress that occurred within the rock during diagenesis. The infill of the cracks shows that the temperature within the rock was high enough to ensure recrystallisation within the formed cracks. Some of the bivalves are recrystallised and show well developed calcite grains. Additionally, some edges of the fragments are partly dissolved by pressure dissolution, visualised in figure A.19. All dissolved bioclasts are fully recrystallised. The result is a rock with a very low porosity, due combination with the fine carbonate mud between the fragments. No colouring as a result of the MB staining is observed, indicating no presence of active swelling clay minerals.

Sample LA 3

The thin section shows a boundary between two sedimentary layers within sample LA 3, of which the microscopic image can be seen in figure A.20. The layers are separated by a stylolite of iron hydroxide, marked by the A in figure A.20, recognisable by the irregular border of the iron hydroxide band. Both layers consist of micrite with a mix of various calcite grain sizes. The micrite is not fully recrystallised, resulting into the matrix of fine calcite grains throughout the micrite. The two layers can be distinguished on the coarseness of the matrix. The coarser grained matrix is shown in figure A.21a (B in figure A.20) and contains grains up to 20 µm in diameter. The fine grained matrix is displayed in figure A.21b (C in figure A.20) and contains grains all below 10 µm. The coarser matrix is partly dolomitized, shown by the rhombohedral shaped grains indicated by the arrows in figure A.21a. Some recrystallised calcite nodules are present within the coarser matrix. An example is displayed in figure A.22. The black opaque minerals are clearly visible in this figure as well, which contribute to 1-2% of the rock's mineral content. The fine grained sedimentary layer shows a higher content of bioclasts, mainly bivalves, which are small and all below 200 µm in length. The bioclasts hinder the growth of calcite grains, resulting in the finer calcite grains compared to the other layer. A crack runs parallel to the stylolite through the coarser matrix, as can be seen at D in figure A.20. The crack is filled with a fine, recrystallised calcite cement. Red, brownish coloured concentrations of iron hydroxide are present within both layers and two examples are pointed out by the arrows in the same figure. The rock can

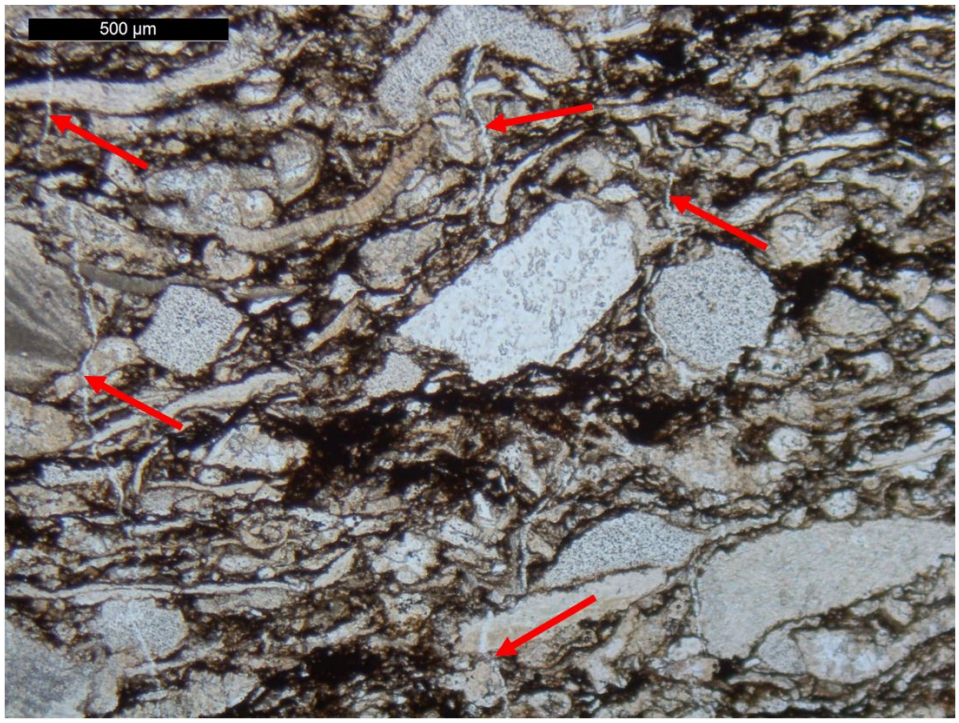

(a)

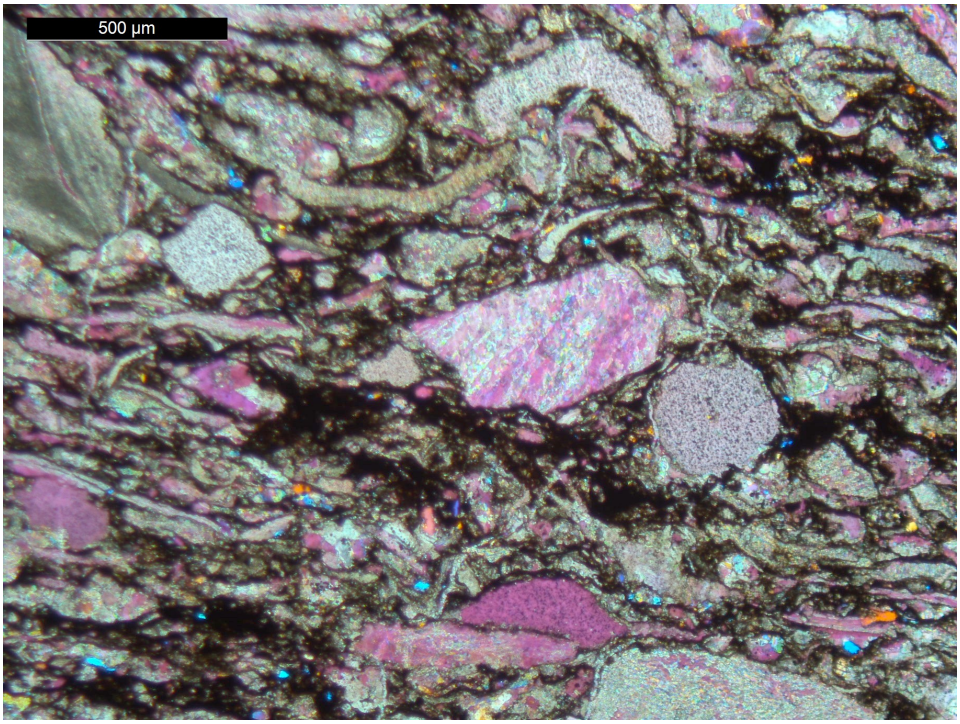

(b)

Figure A.18: Microscopic photograph of limestone (Lim) aggregate sample LA 2; (a) taken with plane polarised light and (b) taken with crossed polarised light. The arrows in (a) point to tiny recrystallised cracks which are all orientated normal to the bedding orientation, suggesting the sample has been exposed to stress in the past.

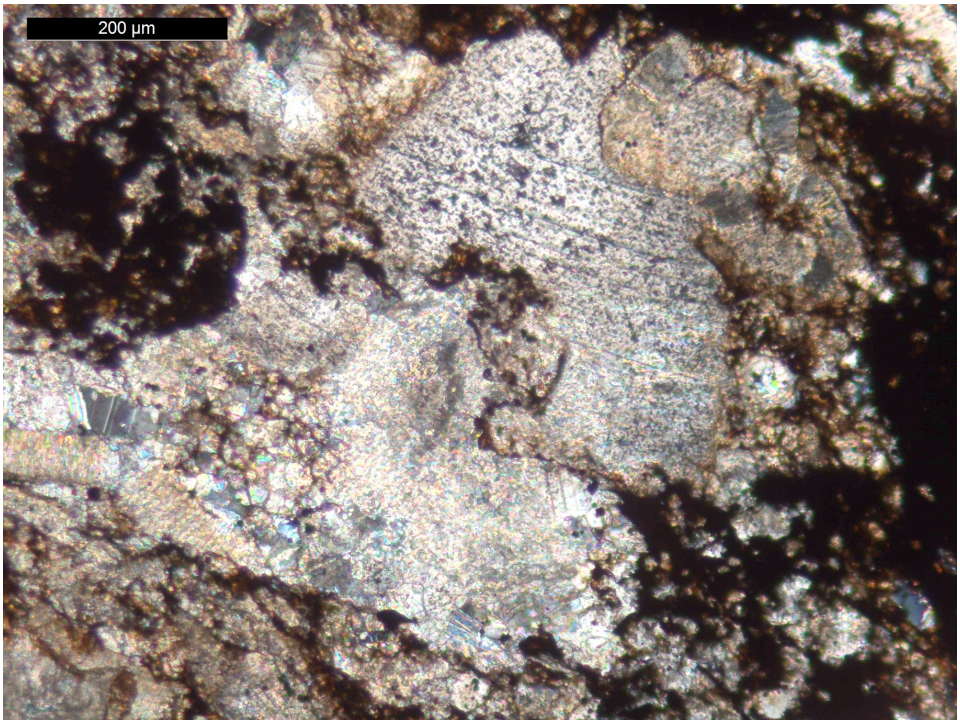

Figure A.19: Pressure dissolution at the contact of fragments within LA 2.

be described as a wackestone according to Dunham's classification, due to the low amount of fossils and fragments in the rock matrix. The porosity within the sample is low. The coarser grained matrix shows some pale blue colouring as a result of the MB staining. The blue colour is distributed between the grains within the matrix and does not show clear concentrations. The fine micrite between the calcite grains contains probably some clay minerals.

Sample LA 13

Sample LA 13 is a packstone that shows large bioclast fragments of $\pm$1 cm in diameter. The section contains bryozoans, corals, bivales and brachiopods. The smaller bioclast are mainly bivalves. The fossils are recrystallised or influenced by neomorphism from aragonite to calcite and float within a dark brown micrite cement. During neomorphism a mineralogical change takes and not only recrystallisation. The structure of bioclasts within the micrite is presented in figure A.23. Some parts of the sample are dolomitized, showing dolomite crystals of approximately 40 µm in diameter throughout the carbonate mud. The dolomite is recognisable by the euhedral rhombohedra shape of the grains. This is visible in figure A.24. Several stylolites run through the sample resulting from pressure dissolution at grain contacts, leaving insoluble residue along the grain surface. They result from a high stress within the rock during diagenesis. All stylolites within LA 13 are of iron hydroxide. An example is the stylolite in figure A.25. The sample has a very low porosity (<1%), because no pore spaces are found within the thin section. Furthermore, the thin section shows only minor signs of MB adsorption located at minor distributed spots, which indicates a very low active clay content.

Sample JA 6

The last thin section is from limestone (Jen) aggregate sample JA 6. A microscopic image of the thin section can be seen in figure A.26. The sample shows bioclasts that were exposed to neomorphism within a fine matrix of recrystallised carbonate mud with calcite grains of $\pm$5 to $\pm$10 µm. In this case the aragonite shells are replaced by calcite grains, which crystallised within the created space by dissolution of the shells. The thin section shows a fine matrix, yet the very fine carbonate mud observed within the thin limestone (Lim) sections is not observed within this sample. The carbonate mud is recrystallised into a fine crystalline matrix. Yet, a finer matrix is observed in some parts, which can be seen in figure A.27. This could be microspar cement, where the aragonite rich mud start to transform into small calcite grains between 5 and 30 µm. Nevertheless, it is not clear to see weather

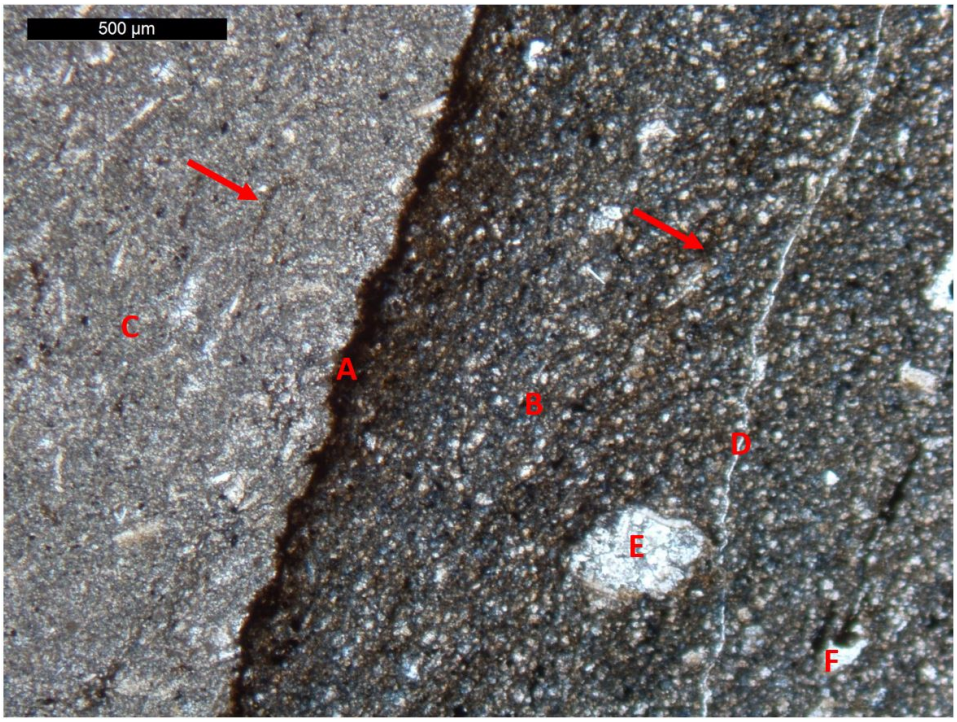

Figure A.20: Boundary between two sedimentary layers separated by a iron hydroxide stylolite within LA 3. A marks the stylolite of iron hydroxide separating two sedimentary layers. B represents the sedimentary layer with a coarser matrix (larger grains). The fine grained matrix is highlighted by C. D denotes a crack that runs parallel to the stylolite through the coarser matrix, which is filled with a recrystallised calcite cement. E and F are both recrystallised calcite fragments.

it is a fine recrystallised carbonate mud or indeed the microspar. The change in matrix could also be a result of a change within the depositional environment. Some silica rich nodules are present within the sample as well, but make up less than 1% of the rock's content. Some concentration of iron hydroxide are visible in the thin section by their red/brown colour. An example can be seen within figure A.27, where a concentration of iron hydroxide runs between the two pore spaces. The thin section indicates the presence of bioclasts in the past, however they are completely dissolved now. The result is a pore space within the rock structure, as visualised in figure A.27. The figure shows two pore spaces, which result of dissolution of aragonite gastropod shells. More of these pore spaces are existing throughout the section. In addition, a few small cracks runs through the rock matrix. The combination results in a higher porosity compared to all previous sample. Nevertheless, the total porosity does not exceed 1-2%. Finally, no blue staining by the MB is perceived within the sample, showing the active clay content within the sample is negligible.

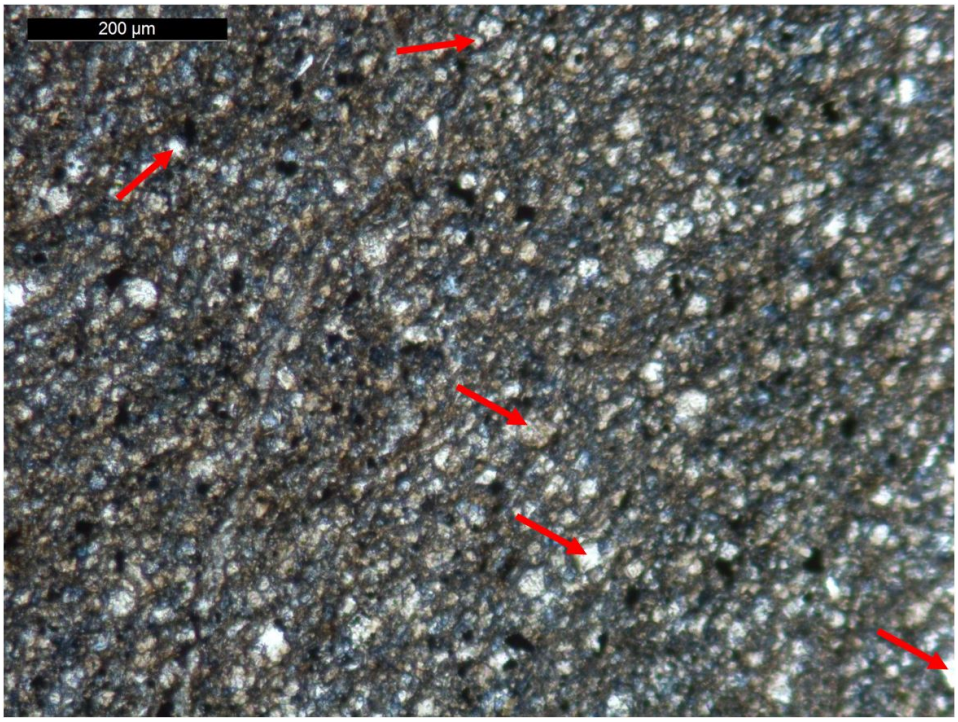

(a)

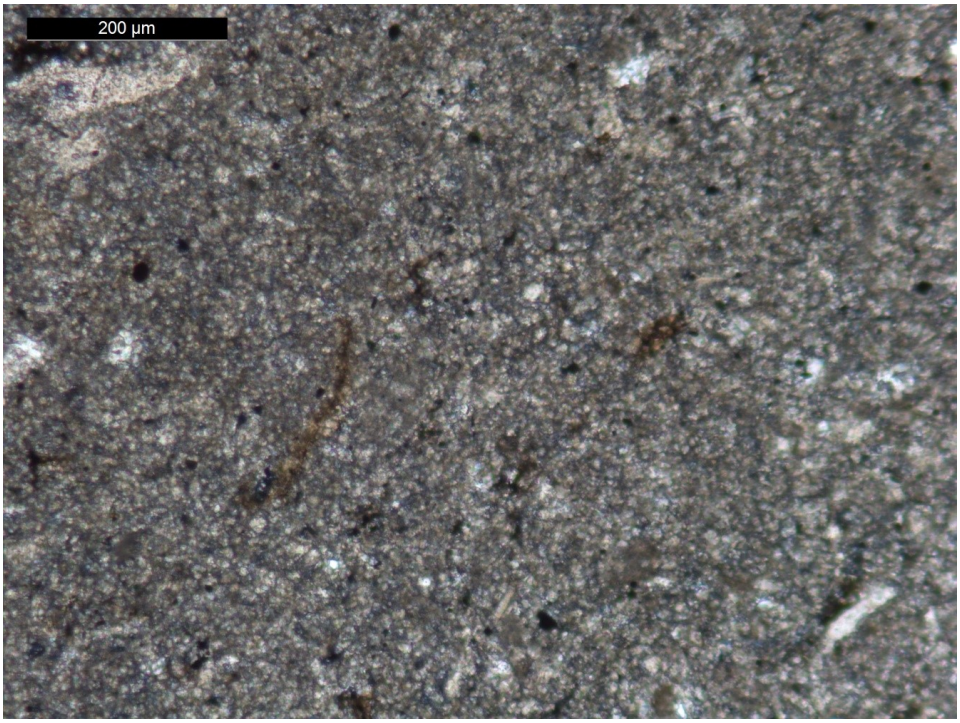

(b)

Figure A.21: Microscopic photograph of limestone (Lim) aggregate sample LA 3; (a) the coarse matrix in plane polarised light and (b) the fine matrix in plane polarised light. The arrows in (a) point to dolomite grains, which can be recognised by their rhombohedral shape.

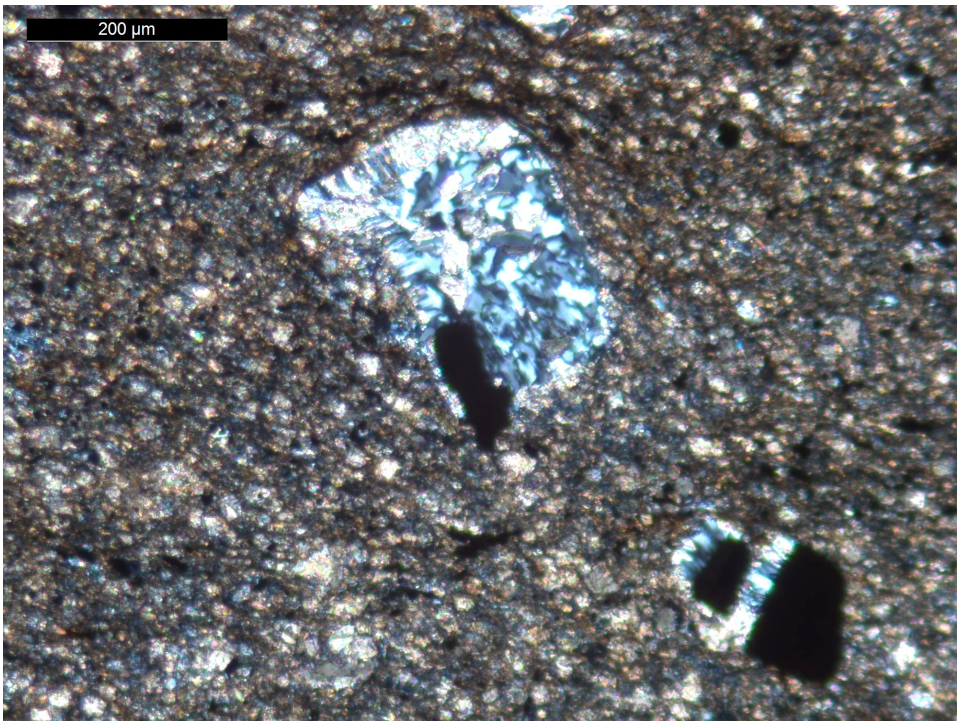

Figure A.22: Recrystallised nodule within LA 3.

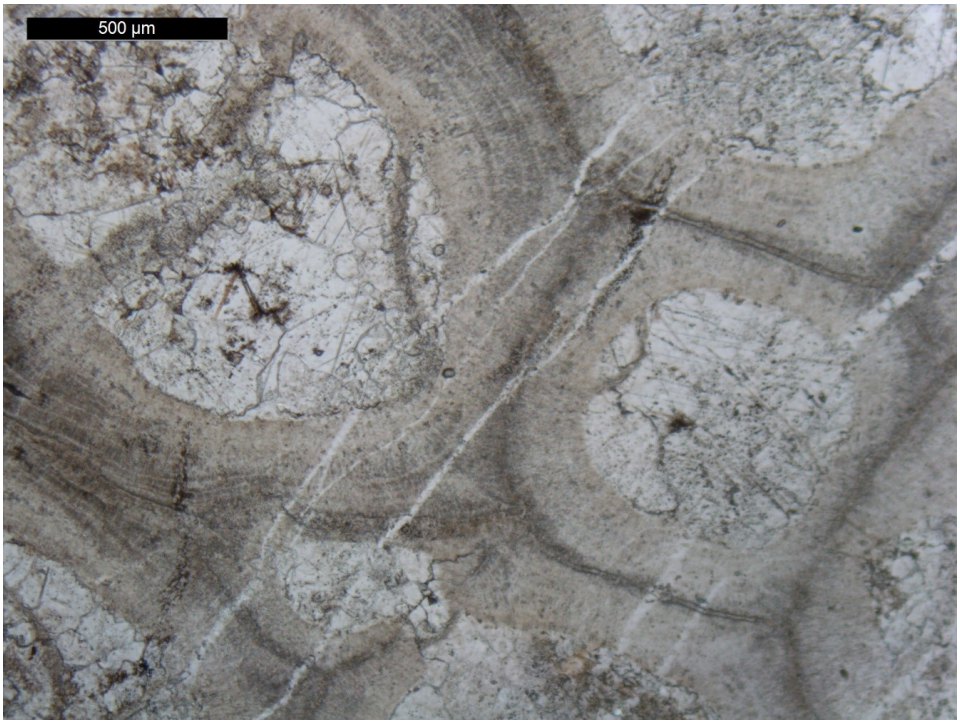

(a)

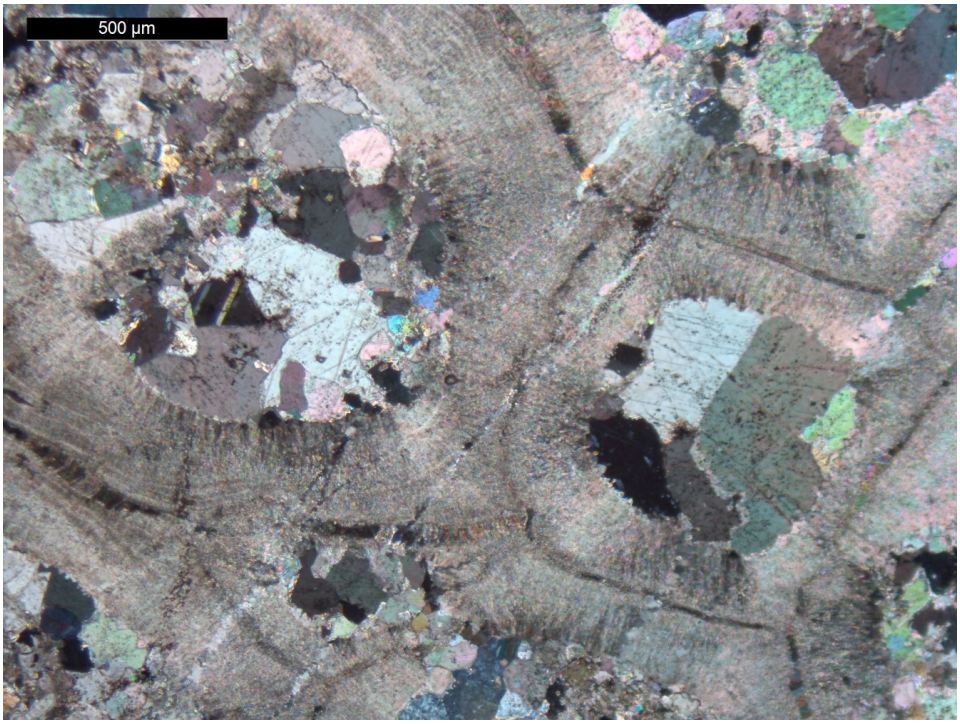

(b)

Figure A.23: Microscopic photograph of limestone (Lim) aggregate sample LA 13; (a) taken with plane polarised light and (b) taken with crossed polarised light.

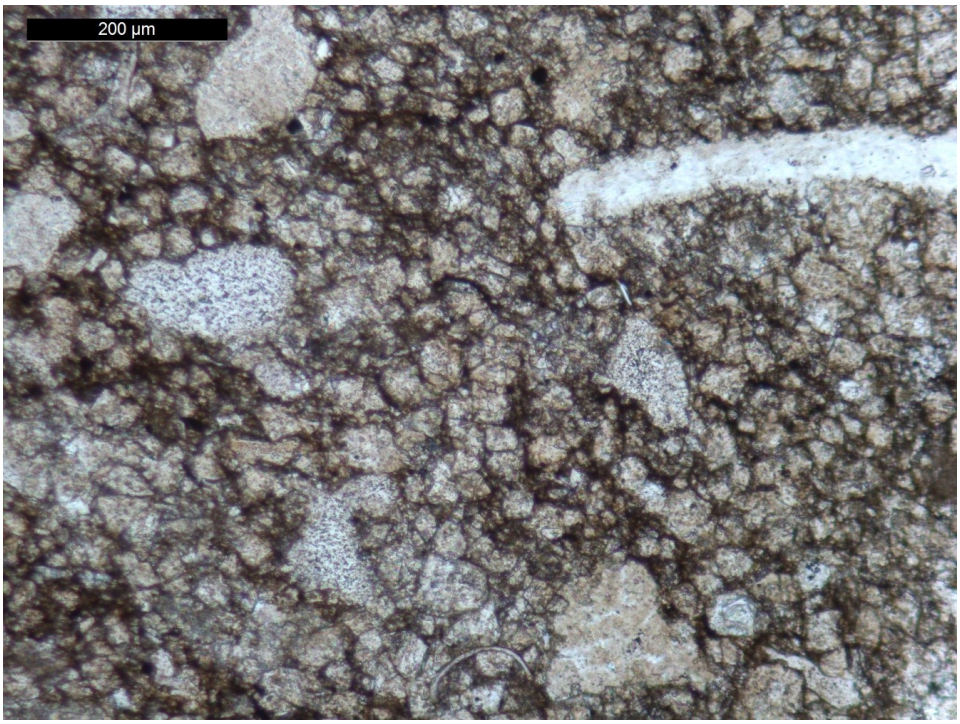

Figure A.24: Dolomite grains in micrite cement between bioclasts within LA 13.

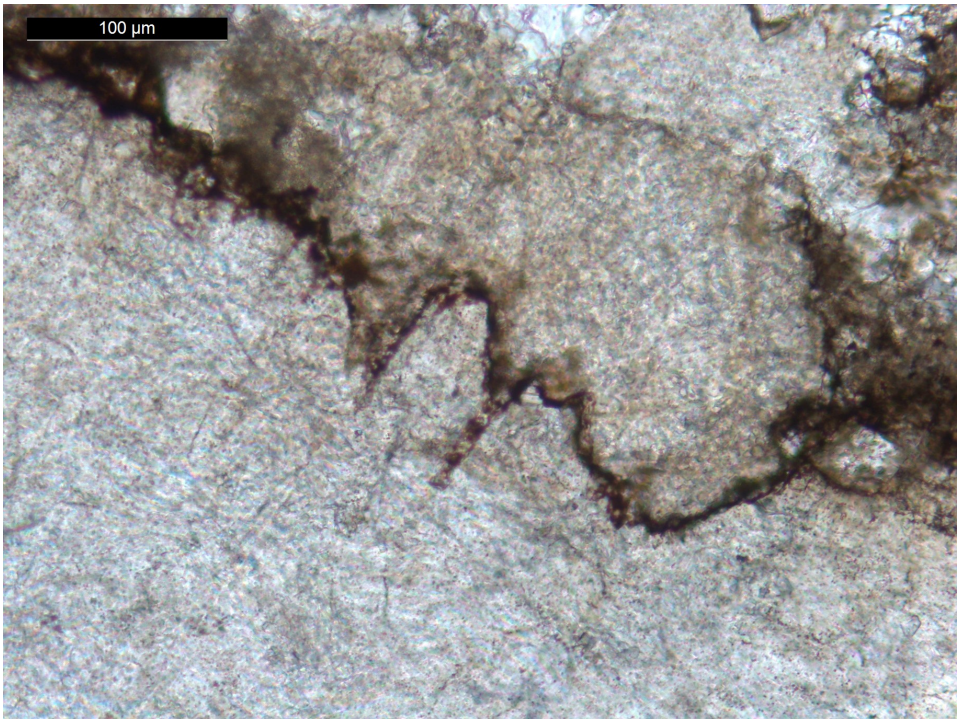

Figure A.25: Stylolite of iron hydroxide within LA 13.

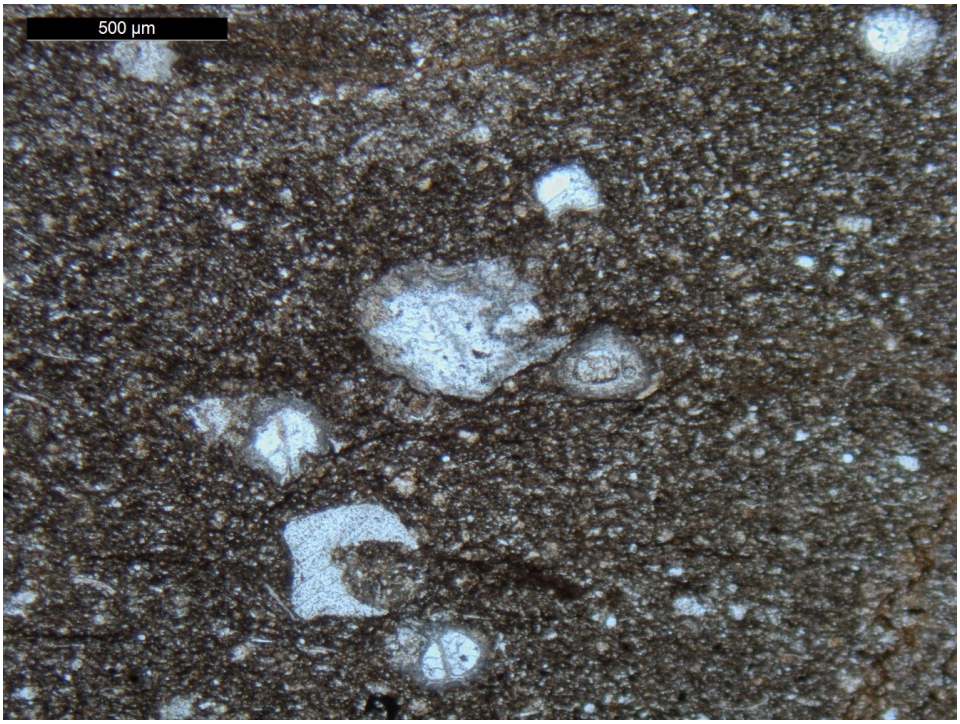

(a)

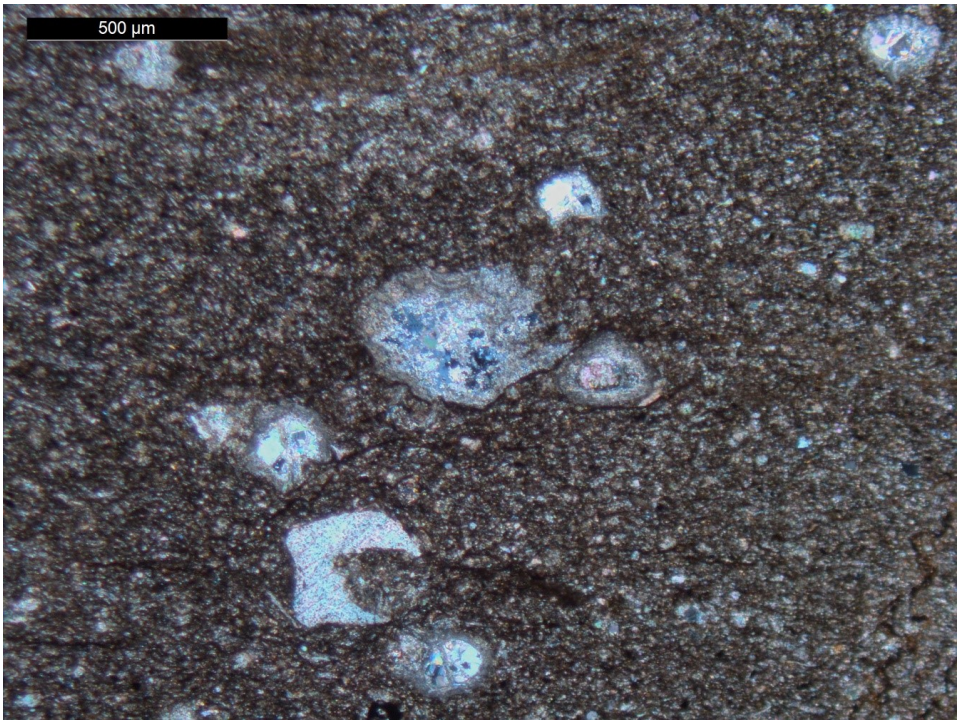

(b)

Figure A.26: Microscopic photograph of limestone (Lim) aggregate sample JA 6; (a) taken with plane polarised light and (b) taken with crossed polarised light.

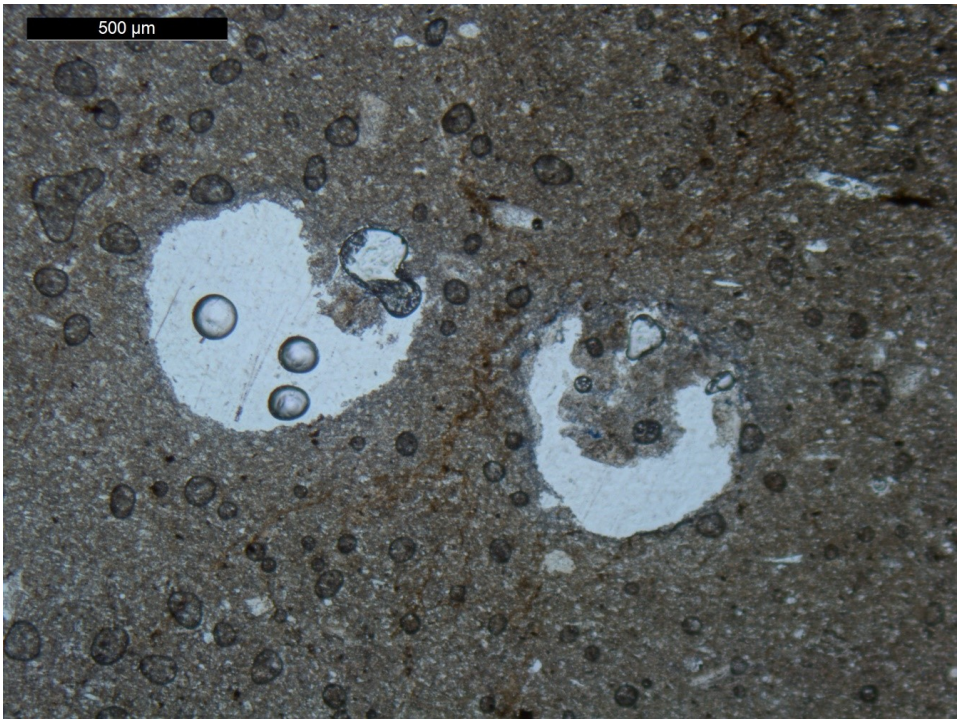

Figure A.27: Dissolved bioclast leaving a pore space within sample JA 6.

B

MCWI and Parameters for MDE Method

Table B.1: Factors a to h and MCWI value for the MDE method.

Factor	Amount	Unit
a	6	[degrees]
b	12	[degrees]
c	361	[nr of days]
d	4	[nr of days]
e	43	[degrees]
f	136	[nr of days]
g	62	[cm]
h	2602	[degrees]
MCWI	0.74	$\left[\frac{degrees^2 \cdot cm}{numberofdays^2}\right]$

Table B.2: Ratings estimates for parameters in armourstone degradation model after Latham et al. (2006).

Parameter	Rating estimates							Parameter influence X_{max}/X_{min}	Calibration reliability*
k_s	Rock fabric strength Use MDE test and relation: $k_s = 4.12 \times 10^{-5}\ M_{DE}^{1.485}$ or AQD value and relation: $k_s = 0.032\ AQD^{-2.0}$							~500	Excellent
X_1	Size								
	Effect given by $0.5(M_{50})^{1/3}$ (M_{50} in tonnes)							~10	Good
	M_{50}	15.0	8.0	1	0.1	0.01			
	Rating	1.23	1.00	0.50	0.23	0.11			
X_2	Grading							~2.5	Fair
	$(M_{85}/M_{15})^{1/3}$	1.1–1.4	1.5–2.4	2.5–2.4					
	Rating	1.2	1.0	0.5					
X_3	Initial shape							~2	Fair
		Angular/ irregular	Blocky/equant	Semi-rounded	Rounded				
	Rating	1.0	1.1	1.5	2.0				
X_4	Incident wave or current energy (treat as independent of size of stone)							~10	Fair
		Significant wave height, H_s (m)		>8.0	4.0–8.0	<4.0			
	Rating	If I_{M50}>15%		0.3	1.0	2.0			
		If I_{M50}=5.0–15.0%		0.5	1.3	2.3			
		If I_{M50}=2.0–5.0%		0.7	1.6	2.6			
		If I_{M50}<2%		1.0	2.0	3.0			
	Rating	If using AQD method		0.7	1.6	2.6			
X_5	Zone of structure							~10	Good
		Inter-tidal			Supra-tidal/ hot	Supra-tidal/ temperate	Always submerged		
	Rating	1.0			2.5	8	10		
X_6	Meteorological climate weathering intensity (Use MCWI Index of Lienhart, 2003—see Table 4)							~7	Good
		MCWI index		<100	100–300	300–600	>600		
	Rating	If WA>2.0%		0.8	0.6	0.4	0.2		
		If WA=0.5–2.0%		1.0	0.8	0.6	0.4		
		If WA<0.5%		1.4	1.2	1.0	0.8		
	Rating	If using AQD method		1.0	0.8	0.6	0.4		
X_7	Water-borne attrition agents							~7.5	Poor
	Sediment type		Shingle	Gravel	Sand	Silt	None		
	Rating		0.2	0.5	1.0	1.2	1.50		
X_8	Concentration of wave attack							~2	Fair
	Tidal range (m):			<2.0	2.0–6.0	>6.0			
	Rating for slope angle of 1:2.5 or steeper			1.0	1.2	1.5			
	Rating for slope angle of 1:3.0 or gentler			1.5	1.8	2.0			
X_9	Mobility of armour in design concept							~20	Fair
		$H_s/\Delta D_{n50}$:		1–2.4	2.5–3.9	4–6.9	7–20		
	Rating	If I_{M50}>15%		1.5	0.6	0.3	0.1		
		If I_{M50}=5.0–15.0%		2.0	1.0	0.5	0.2		
		If I_{M50}=2.0–5.0%		2.0	1.5	1.0	0.5		
		If I_{M50}<2%		2.0	1.8	1.6	1.4		
	Rating	If using AQD method		1.5	1.3	1.1	0.7		

*Calibration reliability used to set the ratings estimates is variable, ranging from a simple reasoning using qualitative field observations of factor influence; (Poor), to extensive confirmatory data; (Excellent).

C

Density and WA

Table C.1: Results of additional density and WA test for the Hartsteinwerke aggregate.

Sample	Number	M_1 (g)	M_2 (g)	M_3 (g)	ρ (g/cm^3)	WA (%)
Hartsteinwerke	11	197.70	112.30	178.51	2.64	0.67
	12	210.65	130.25	208.71	2.59	0.93
	13	187.95	115.99	186.24	2.58	0.92
	14	279.87	173.36	277.90	2.60	0.71
	15	177.20	109.74	175.91	2.60	0.73
	16	162.24	100.76	161.15	2.61	0.68
	17	180.33	111.56	179.06	2.60	0.71
	18	183.90	113.63	181.71	2.58	1.21
	19	313.19	193.92	310.32	2.59	0.92
	20	194.85	120.15	192.61	2.57	1.16
	21	184.80	113.42	181.19	2.53	1.99
	22	325.10	201.33	320.56	2.58	1.42
	23	258.07	159.49	255.48	2.58	1.01
	24	392.09	243.77	390.13	2.62	0.50
	25	360.07	222.37	357.18	2.59	0.81
	26	166.15	103.14	165.18	2.61	0.59
	27	180.21	111.95	179.18	2.62	0.57
	28	190.25	117.20	187.55	2.56	1.44
	29	200.70	123.96	197.96	2.57	1.38
	30	205.68	126.76	203.39	2.57	1.13
	31	184.31	113.68	181.90	2.57	1.32
	32	162.75	100.77	161.74	2.60	0.62
	33	319.25	197.82	317.06	2.60	0.69
	34	202.51	126.08	201.63	2.63	0.44
	35	226.97	140.46	225.28	2.60	0.75
	36	222.82	137.85	221.23	2.60	0.72
	37	247.08	152.60	244.90	2.58	0.89
	38	289.33	179.74	287.79	2.62	0.54
	39	227.69	142.02	226.98	2.64	0.31
	40	222.79	137.77	220.66	2.59	0.97
	Mean	-	-	-	2.60	0.87
	Standard Deviation	-	-	-	0.02	0.34

D

Magnesium Sulfate Soundness

The magnesium sulphate soundness test is executed to prospect the resistance against salt crystallisation within the rock pores. The test is executed according to EN 1367-2 (2009).

The aggregates collected at the quarry are firstly broken by the jaw crusher and sieved to the 10-14 mm range. For the Hartsteinwerke bag 3 of 4 is taken, for Carrière des Limites bag 2 of 3, and for Carrière de Jenneret bag 1 of 2. After sieving the selection is cleaned and dried in the oven at 105°C. The dried selection is then sieved again on the 10 and 14 mm sieve in order to be sure all aggregate falls within this range. Finally, between 420 and 430 g of the material is weighted.

The magnesium sulphate soundness test is executed according to EN 1367-2. The soundness value is determined according to equation D.1 where; M_1 is the mass of the test specimen and M_2 is the final mass of aggregate retained on the 10 mm sieve. The results of the magnesium sulphate soundness test are shown in table D.1.

$$MS = 100 \cdot \frac{M_1 - M2}{M_1} \tag{D.1}$$

Table D.1: Results of the magnesium sulphate soundness test.

Sample	M_1	M_2	MS
Sandstone	425.91 g	417.44 g	1.99
Limestone (Jen)	425.88 g	419.56 g	1.48

E

Photos of Intact and Crushed Rock Cores

Figure E.1: Photos of the sandstone cores number H 1 to H 14.

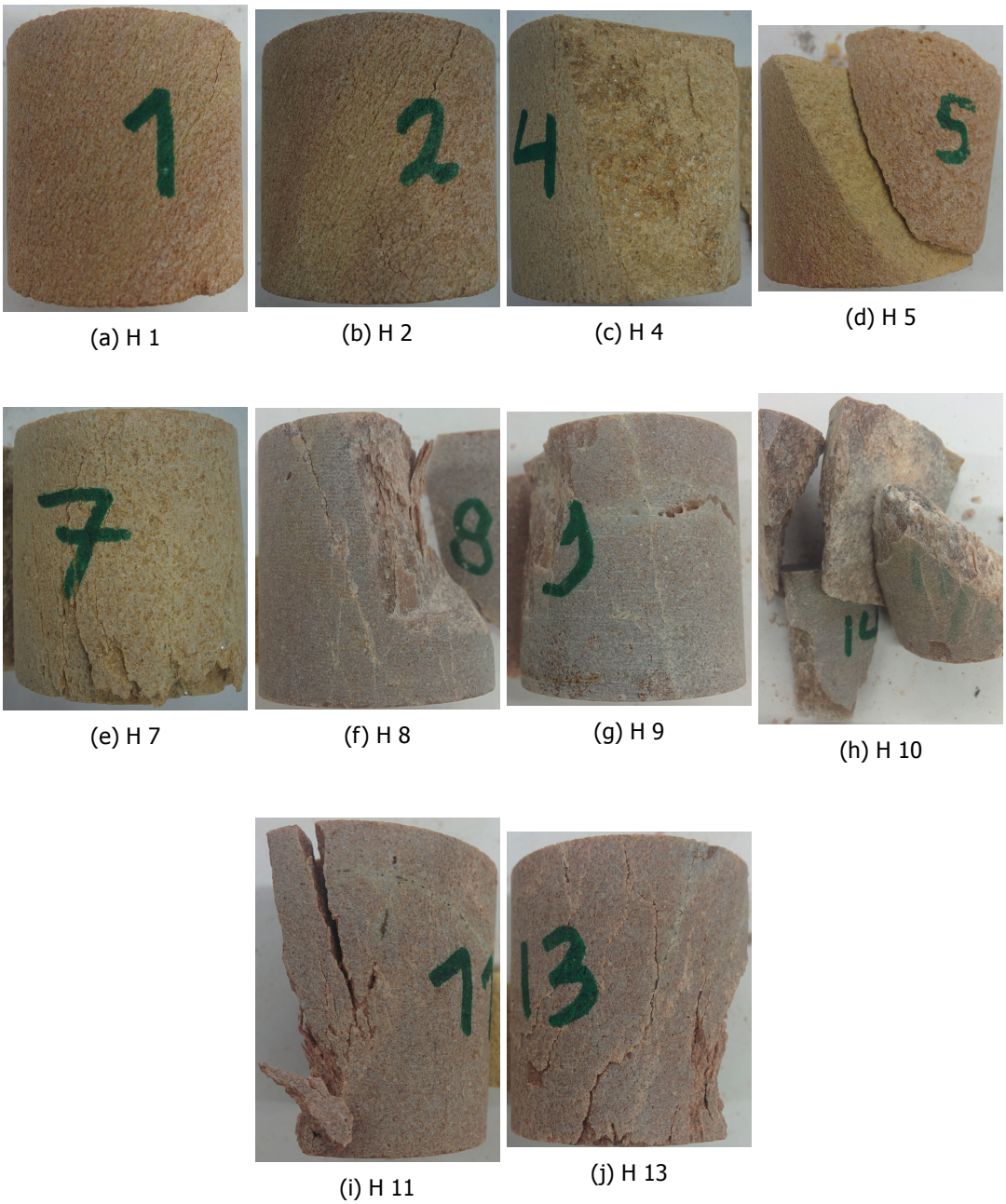

(a) H 1 (b) H 2 (c) H 4 (d) H 5

(e) H 7 (f) H 8 (g) H 9 (h) H 10

(i) H 11 (j) H 13

Figure E.2: Photos of the sandstone cores number H 1 to H 14 after failure.

(a) S1 (b) S2 (c) S4

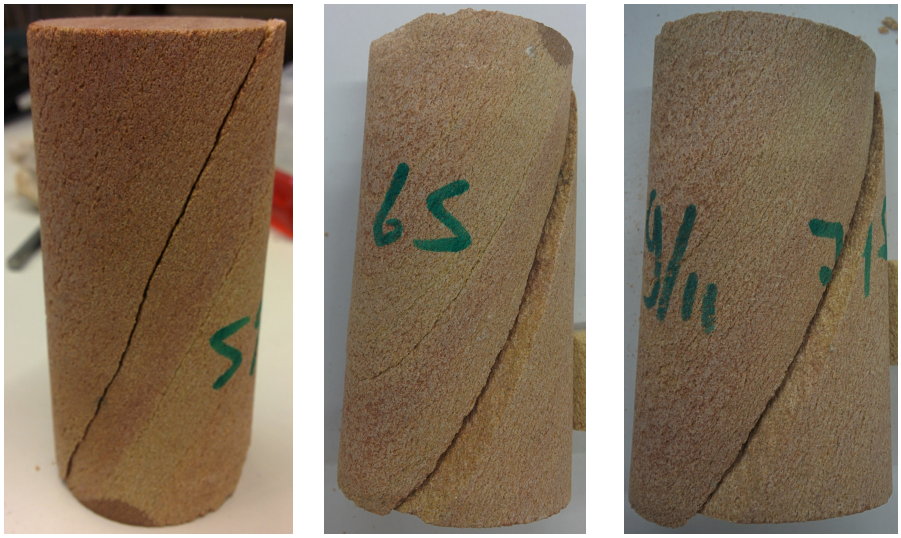

(d) S5 (e) S6 (f) S7

(g) S⊥ (h) S∥ (i) $S_{30°}$

Figure E.3: Photos of the sandstone cores number S1 to S7 and sandstone cores with various angles to the bedding after failure.

Figure E.4: Photos of the limestone (Lim) cores number LIM 1 to LIM 10.

(a) LIM 1

(b) LIM 2

(c) LIM 3

(d) LIM 4

(e) LIM 5

(f) LIM 6

(g) LIM 7

(h) LIM 8

(i) LIM 9

(j) LIM 10

Figure E.5: Photos of the limestone (Lim) cores number LIM 1 to LIM 10 after failure.

Figure E.6: Photos of the limestone (Fri) cores number FRI 1 to FRI 13.

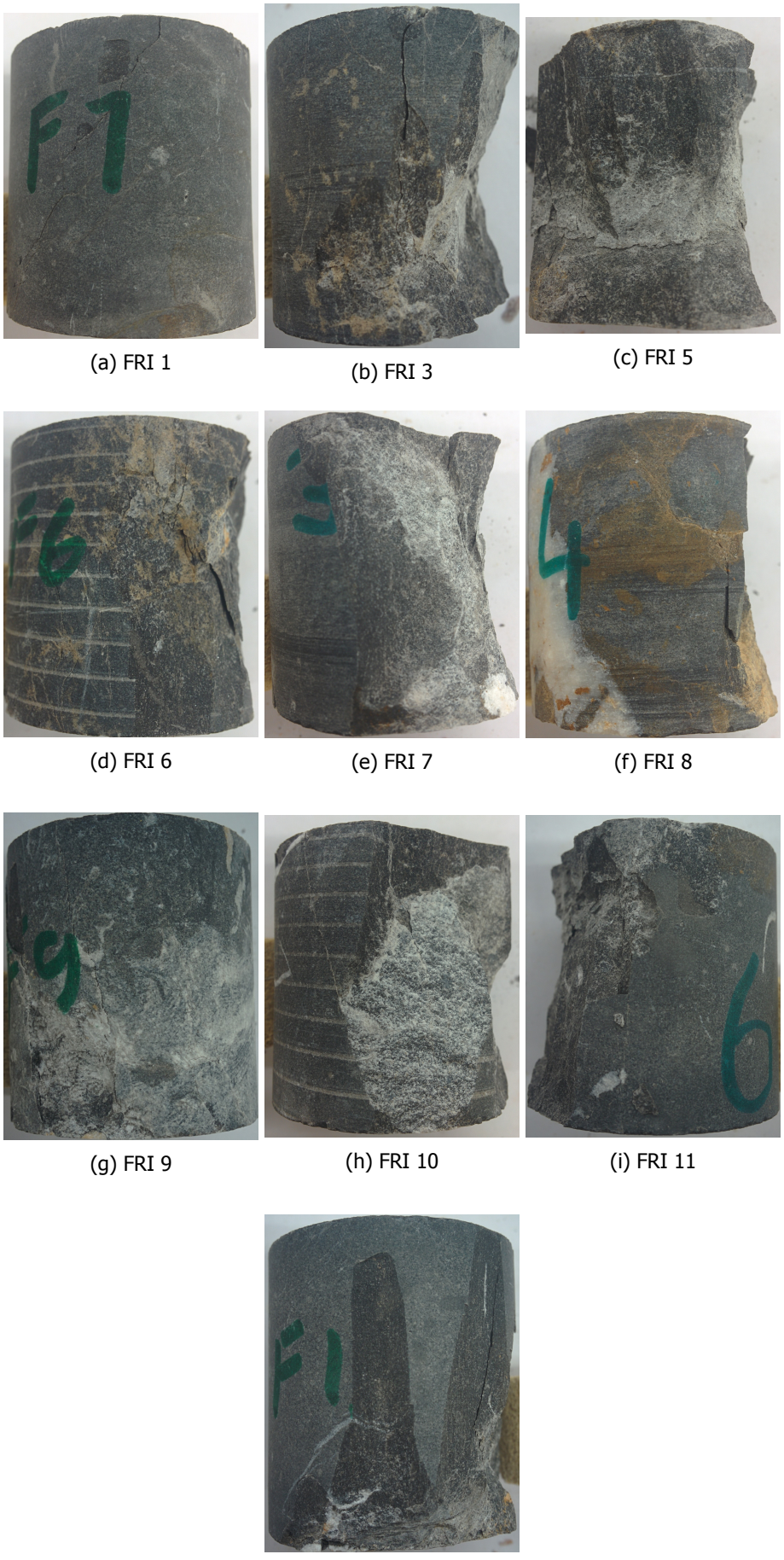

(a) FRI 1 (b) FRI 3 (c) FRI 5

(d) FRI 6 (e) FRI 7 (f) FRI 8

(g) FRI 9 (h) FRI 10 (i) FRI 11

(j) FRI 13

Figure E.7: Photos of the limestone (Fri) cores number FRI 1 to FRI 13 after failure.

F

Strength Test Results

Table F.1: Sonic velocity, UCS value, Young's modulus, and mean Equotip L-values; for dry, saturated condition, the type D and type C tip, of sandstone cores.

L/D	Sample	V_p (m/s)	V_s (m/s)	V_p/V_s	UCS (MPa)	E (GPa)	MEAN D-TYPE DRY	MEAN D-TYPE WET	MEAN C-TYPE DRY	MEAN C-TYPE WET
1	HA1	4219	2720	1.55	31.2	7.2	526	471	572	476
	HA2	4224	2566	1.65	35.7	6.5	529	457	633	519
	HA4	4893	2713	1.80	101.3	23.9	627	604	706	672
	HA5	4181	2534	1.65	28.8	7.6	484	439	594	539
	HA7	5010	2852	1.76	63.4	13.3	559	548	669	635
	HA8	5556	3688	1.51	195.8	37.8	797	800	863	847
	HA9	5680	-	-	260.7	42.6	805	795	853	848
	HA10	5532	3507	1.58	301.9	44.6	814	813	868	867
	HA11	5351	3845	1.39	140.7	32.1	762	738	795	789
	HA13	5519	3539	1.56	197.2	38.2	732	742	804	816
	HA14	5627	3555	1.58	262.5	45.1	809	791	859	855
2	S1	5263	3601	1.46	208	51.6				
	S2	5232	3433	1.52	182	49.3	-	-	-	-
	S3	5215	3492	1.49	206	52.1	-	-	-	-
	S4	4797	3174	1.51	94	31.9	-	-	-	-
	S5	4823	3221	1.50	59	18.3	-	-	-	-
	S6	3879	2709	1.43	28	13.3	-	-	-	-
	S7	4053	2681	1.51	33	13.9	-	-	-	-

Table F.2: Sonic velocity, UCS value, Young's modulus, and mean Equotip L-values; for dry, saturated condition, the type D and type C tip, of limestone (Lim) cores.

L/D	Sample	V_p (m/s)	V_s (m/s)	V_p/V_s	UCS (MPa)	E (GPa)	MEAN D-TYPE DRY	MEAN D-TYPE WET	MEAN C-TYPE DRY	MEAN C-TYPE WET
1	LIM1	6409	3110	2.06	119.1	40.0	629	631	716	699
	LIM2	6391	3162	2.02	166.7	44.3	601	605	719	694
	LIM3	6347	-	-	173.2	44.8	606	602	695	680
	LIM4	6385	-	-	198.1	46.2	613	626	696	704
	LIM5	6305	3092	2.04	171.8	45.4	603	602	705	682
	LIM6	6400	3089	2.07	192.6	45.2	618	621	713	693
	LIM7	6400	3115	2.05	203.4	47.3	613	616	712	695
	LIM8	6384	3048	2.09	158.8	44.0	612	609	713	690
	LIM9	6256	2948	2.12	184.3	43.6	517	548	629	655
	LIM10	6428	3075	2.09	173.7	42.5	614	616	707	682
2	L1	6104	3423	1.78	180	65.7	-	-	-	-
	L2	6359	3310	1.92	182	69.5	-	-	-	-
	L3	6472	3414	1.90	182	63.0	-	-	-	-
	L4	5483	3319	1.65	187	60.5	-	-	-	-
	L5	6231	3375	1.85	138	64.0	-	-	-	-
	L6	6361	3434	1.85	172	66.7	-	-	-	-
	L7	6360	3349	1.90	166	65.3	-	-	-	-

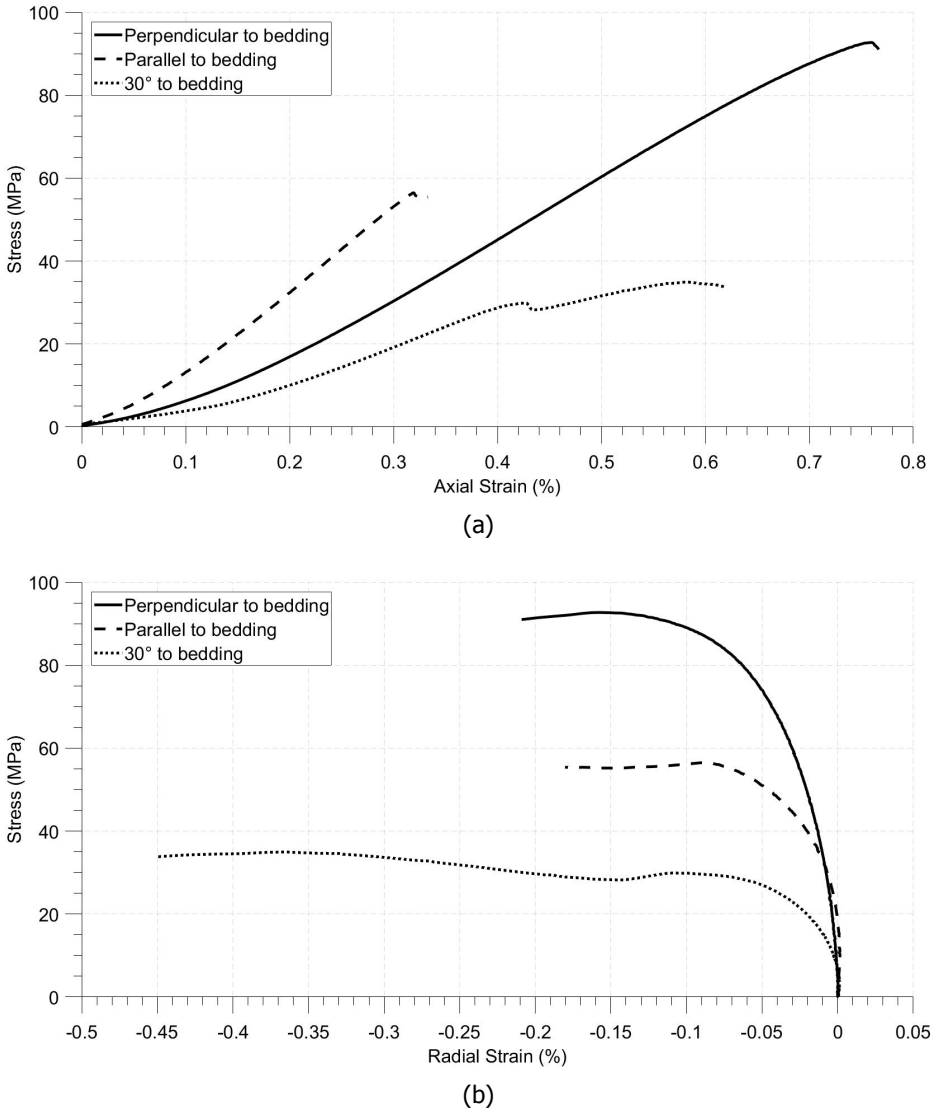

Figure F.1: Stress-strain curves obtained during the unconfined compressive strength testing at different angles towards the bedding in sandstone cores with a L/D of 2; (a) shows the axial strain versus the stress and (b) shows the radial strain versus the stress applied on the cores.

Table F.3: Sonic velocity, UCS value, Young's modulus, and mean Equotip L-values; for dry, saturated condition, the type D and type C tip, of limestone (Fri) cores.

L/D	Sample	V_p (m/s)	V_s (m/s)	V_p/V_s	UCS (MPa)	E (GPa)	MEAN D-TYPE DRY	MEAN D-TYPE WET	MEAN C-TYPE DRY	MEAN C-TYPE WET
1	FRI1	5603	3104	1.81	62.5	20	586	566	676	659
	FRI3	6176	3653	1.69	181.4	42.3	598	596	691	698
	FRI5	6260	3775	1.66	235.9	47.7	613	601	701	686
	FRI6	6037	3291	1.83	163.7	44.4	599	586	684	698
	FRI7	6358	3644	1.75	231.3	47.9	621	615	709	709
	FRI8	5943	3540	1.68	128.9	34.3	620	589	695	663
	FRI9	6173	3715	1.66	156.8	44.2	594	594	677	664
	FRI10	6228	3419	1.82	226.6	42.4	623	623	709	711
	FRI11	6205	3653	1.70	190.0	44.9	619	625	695	715
	FRI13	6165	3598	1.71	214.1	43.6	629	622	708	709

G

Relation UCS and L-value

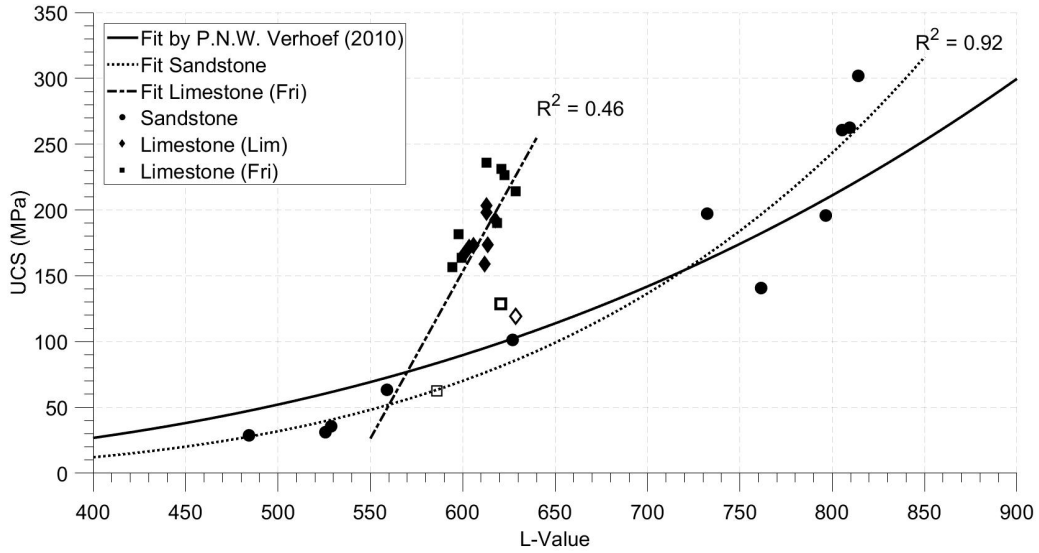

Figure G.1: The relation between the mean Equotip type D rebound value on air-dried cores with a L/D of 1.0 and their UCS value. The non-filled marks correspond to specific core samples as stated in the caption of figure 9.21.

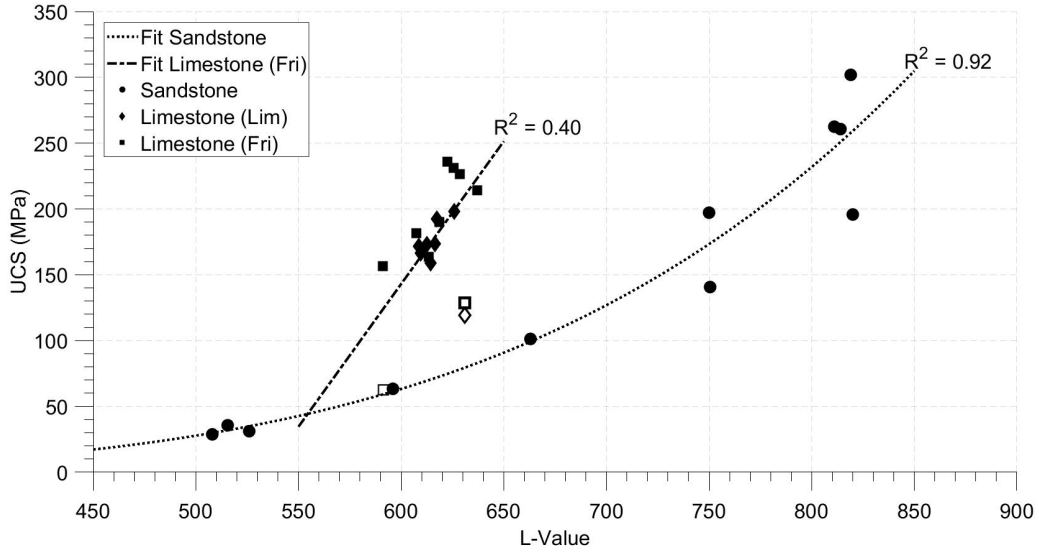

Figure G.2: The relation between the median Equotip type D rebound value on air-dried cores with a L/D of 1.0 and their UCS value. The non-filled marks correspond to specific core samples as stated in the caption of figure 9.21.

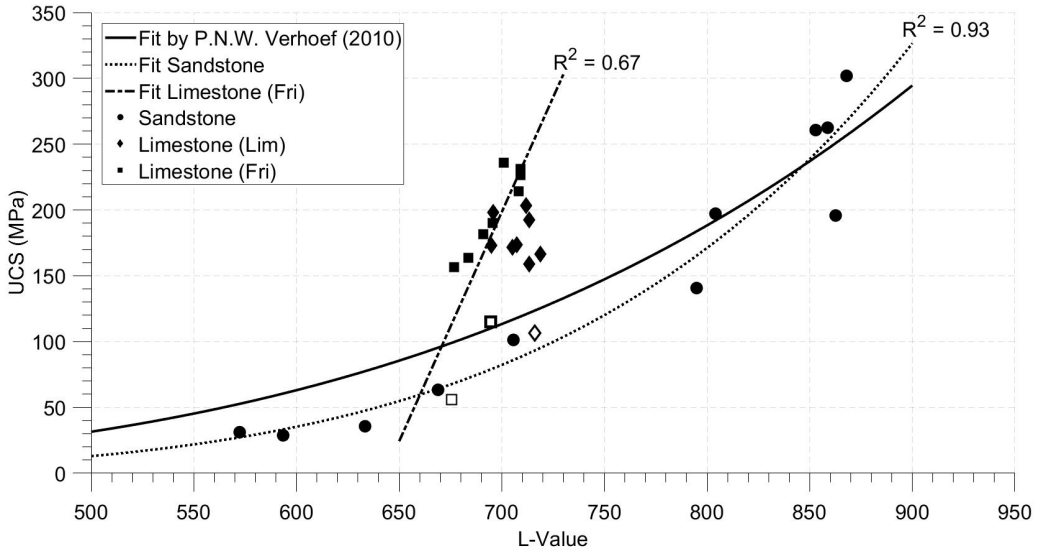

Figure G.3: The relation between the mean Equotip type C rebound value on air-dried cores with a L/D of 1.0 and their UCS value. The non-filled marks correspond to specific core samples as stated in the caption of figure 9.21.

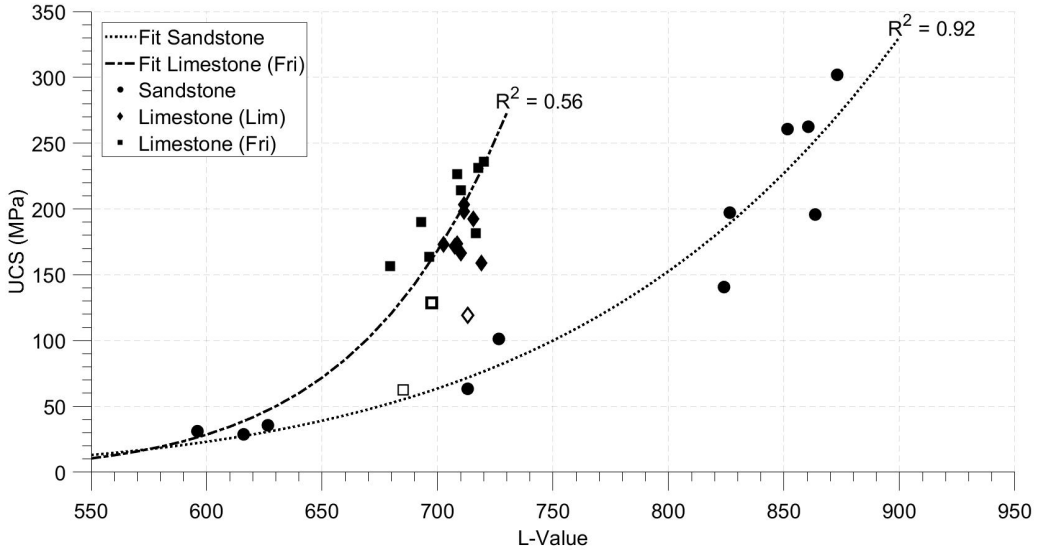

Figure G.4: The relation between the median Equotip type C rebound value on air-dried cores with a L/D of 1.0 and their UCS value. The non-filled marks correspond to specific core samples as stated in the caption of figure 9.21.

H

Equotip Data Histograms

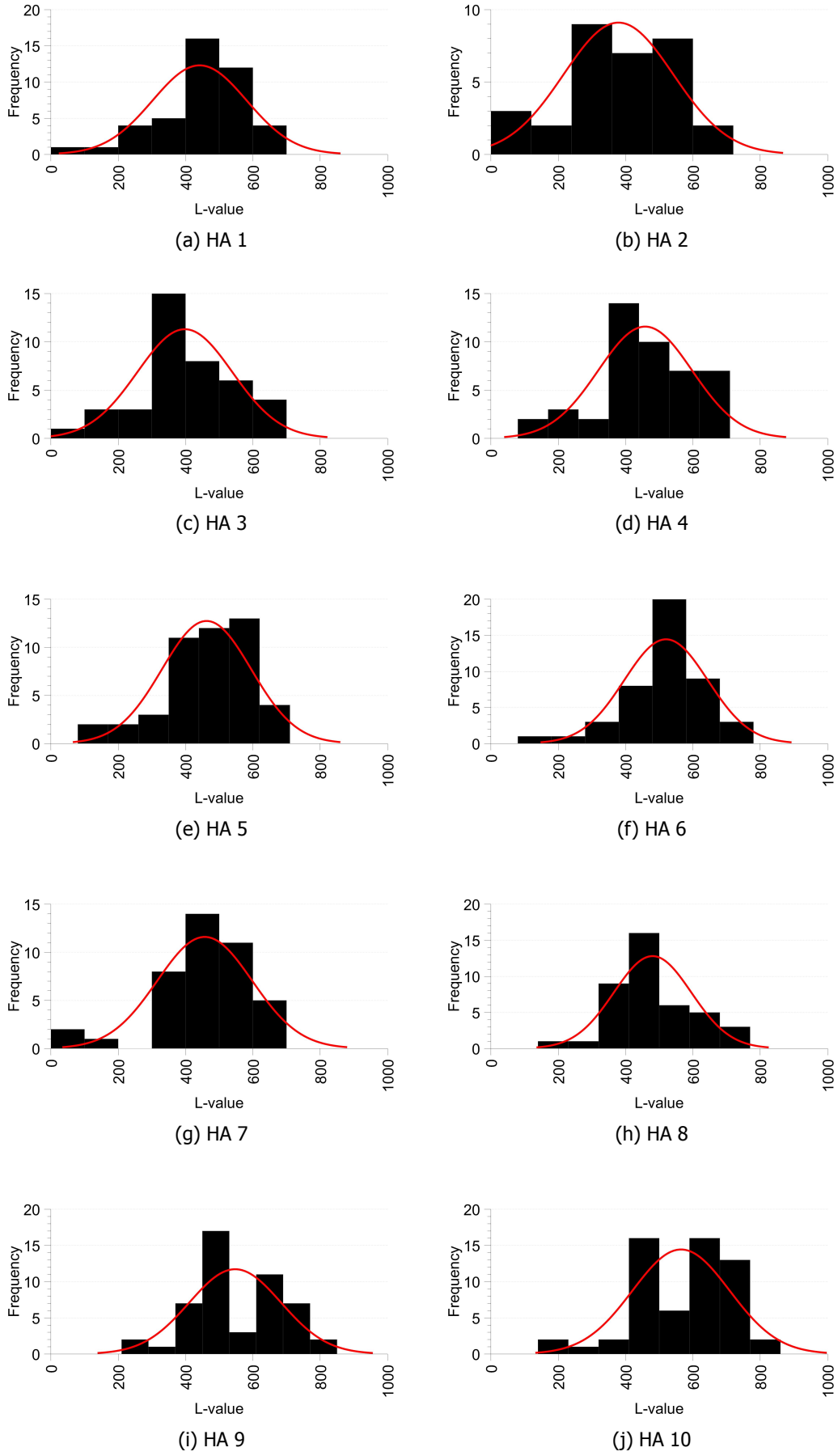

Figure H.1: Histograms for the Equotip type D measurements on the sandstone aggregate pieces HA 1 to HA 10.

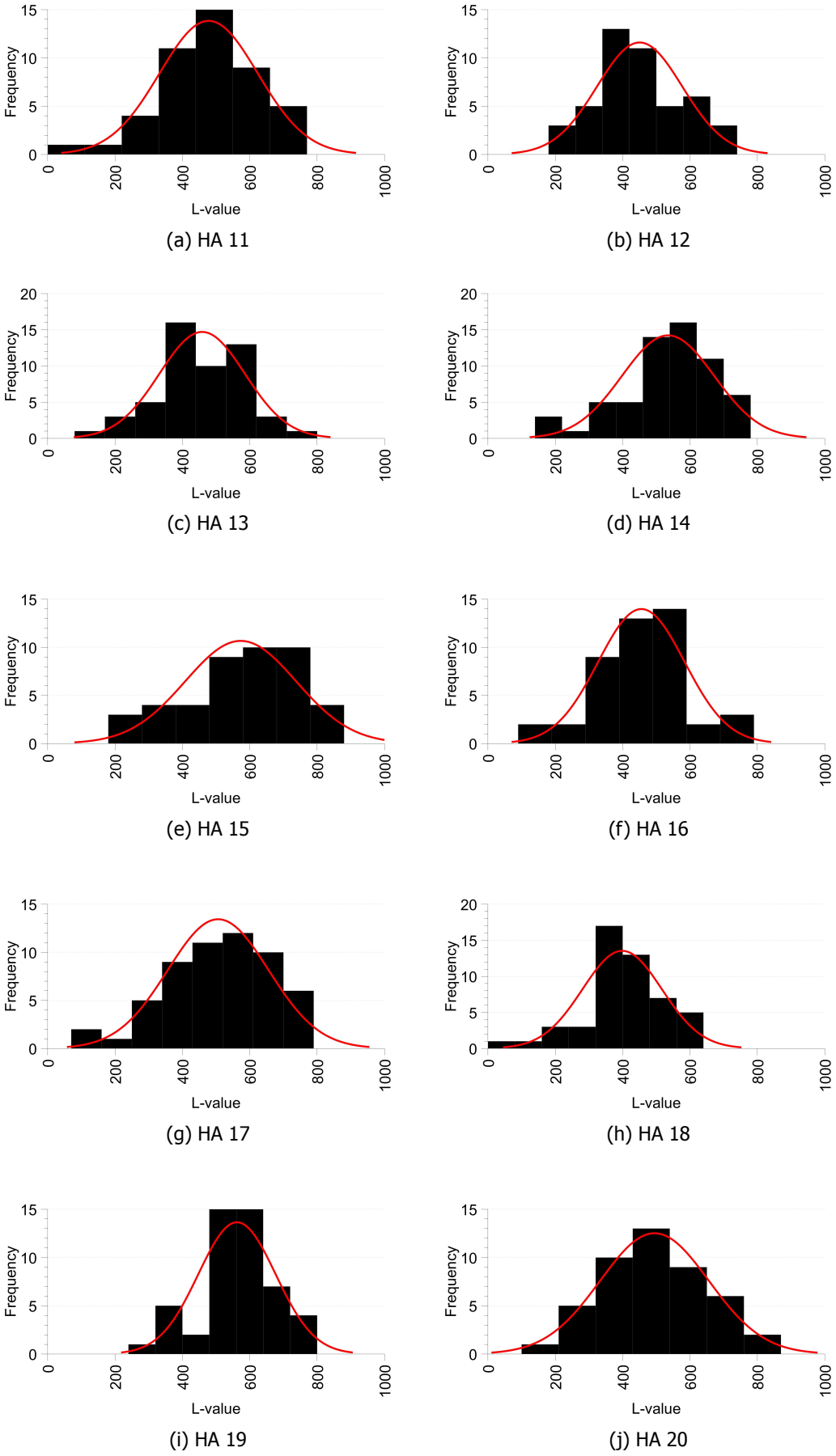

Figure H.2: Histograms for the Equotip type D measurements on the sandstone aggregate pieces HA 11 to HA 20.

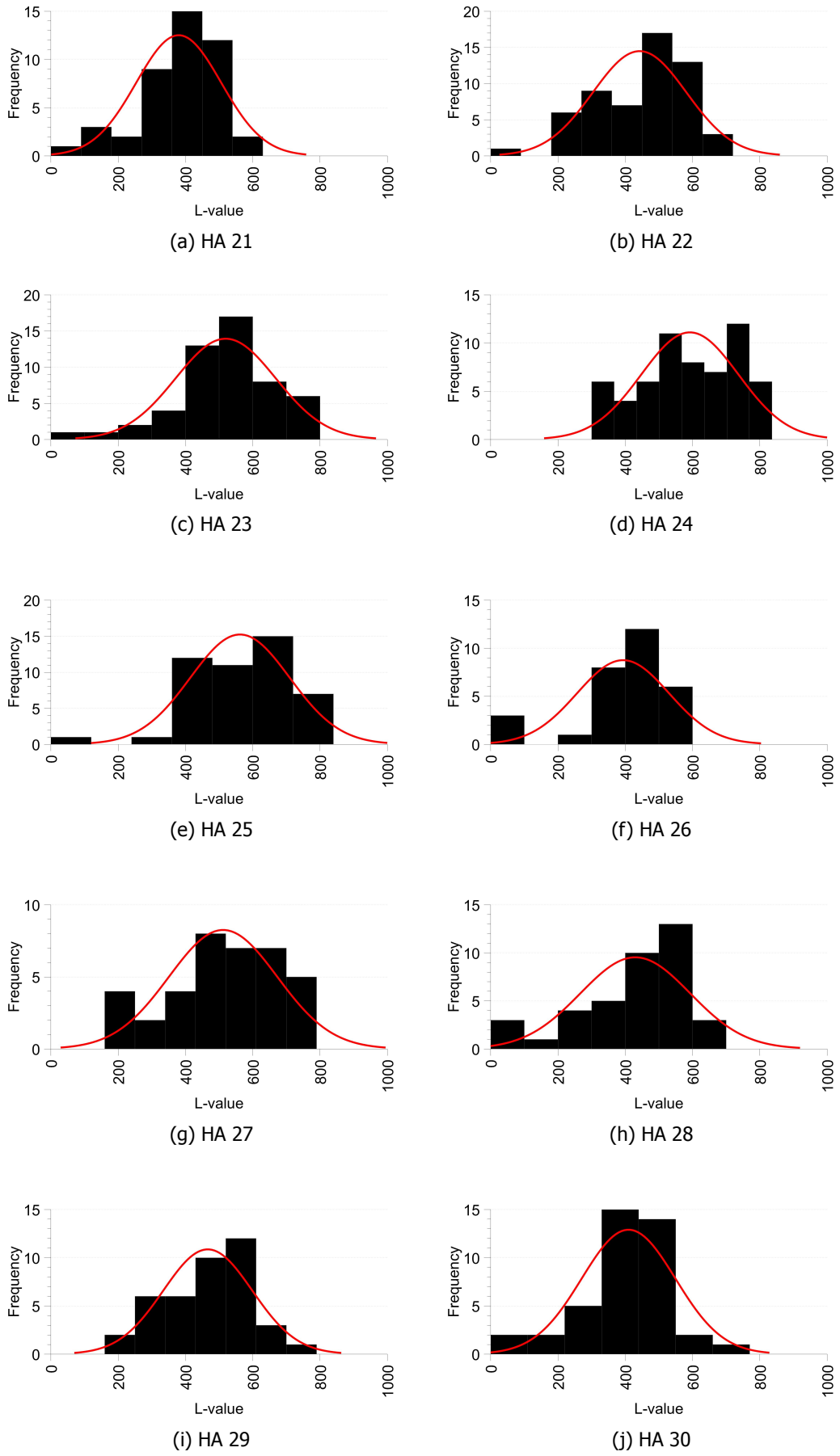

Figure H.3: Histograms for the Equotip type D measurements on the sandstone aggregate pieces HA 21 to HA 30.

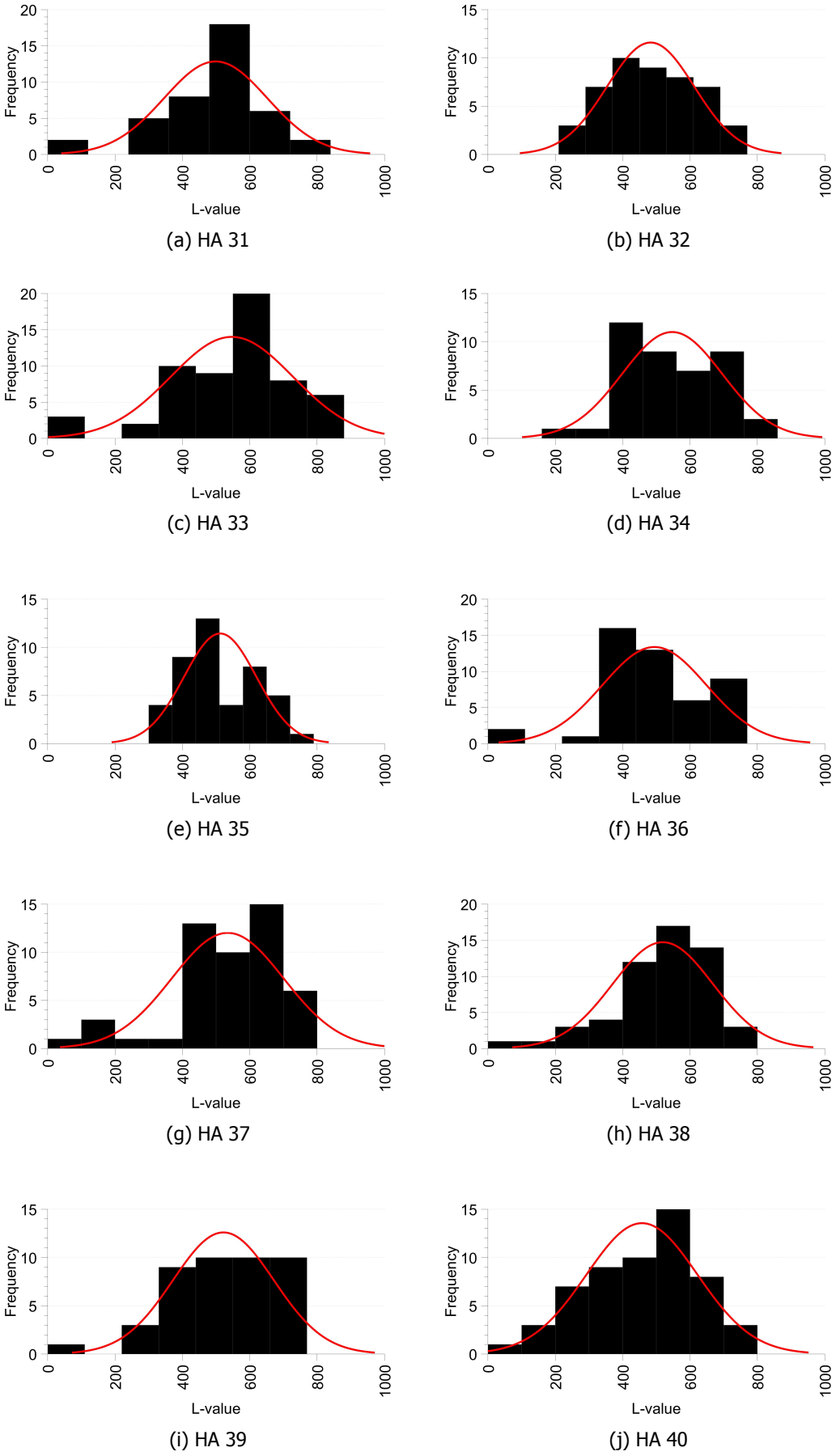

Figure H.4: Histograms for the Equotip type D measurements on the sandstone aggregate pieces HA 31 to HA 40.

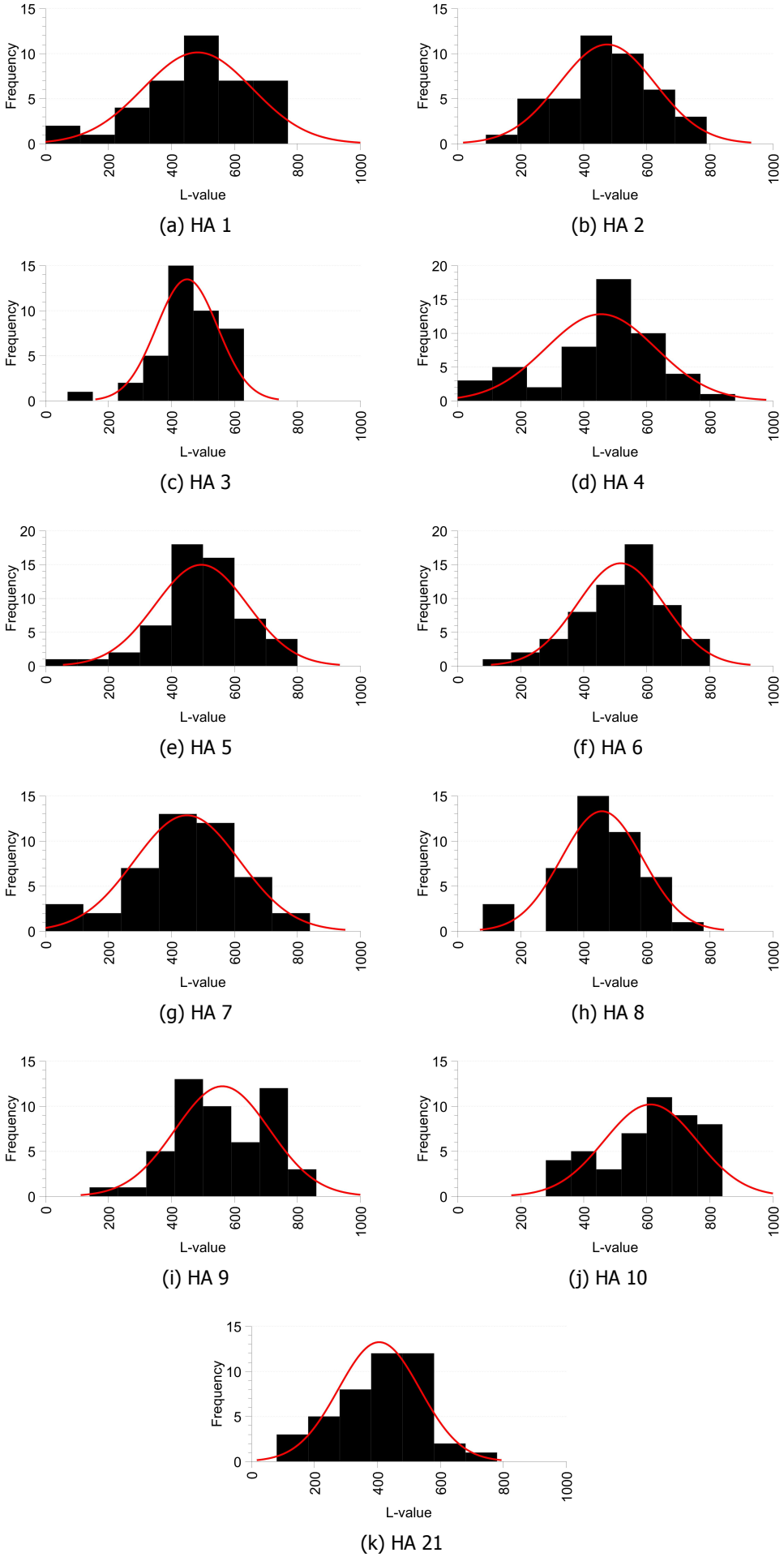

(a) HA 1 (b) HA 2

(c) HA 3 (d) HA 4

(e) HA 5 (f) HA 6

(g) HA 7 (h) HA 8

(i) HA 9 (j) HA 10

(k) HA 21

Figure H.5: Histograms for the Equotip type C measurements on the sandstone aggregate pieces HA 1 to HA 10 and HA 21.

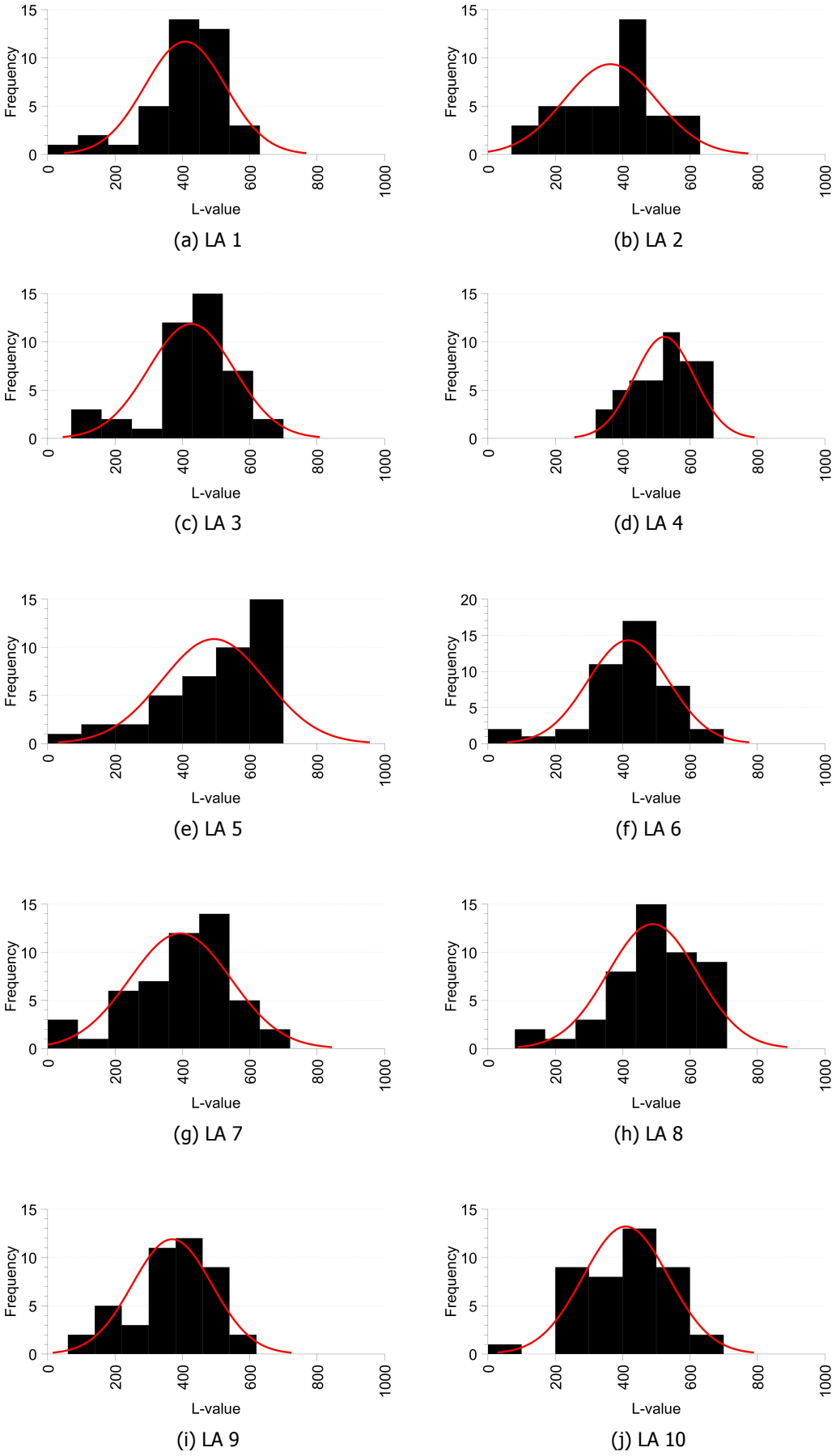

Figure H.6: Histograms for the Equotip type D measurements on the limestone (Lim) aggregate pieces LA 1 to LA 10.

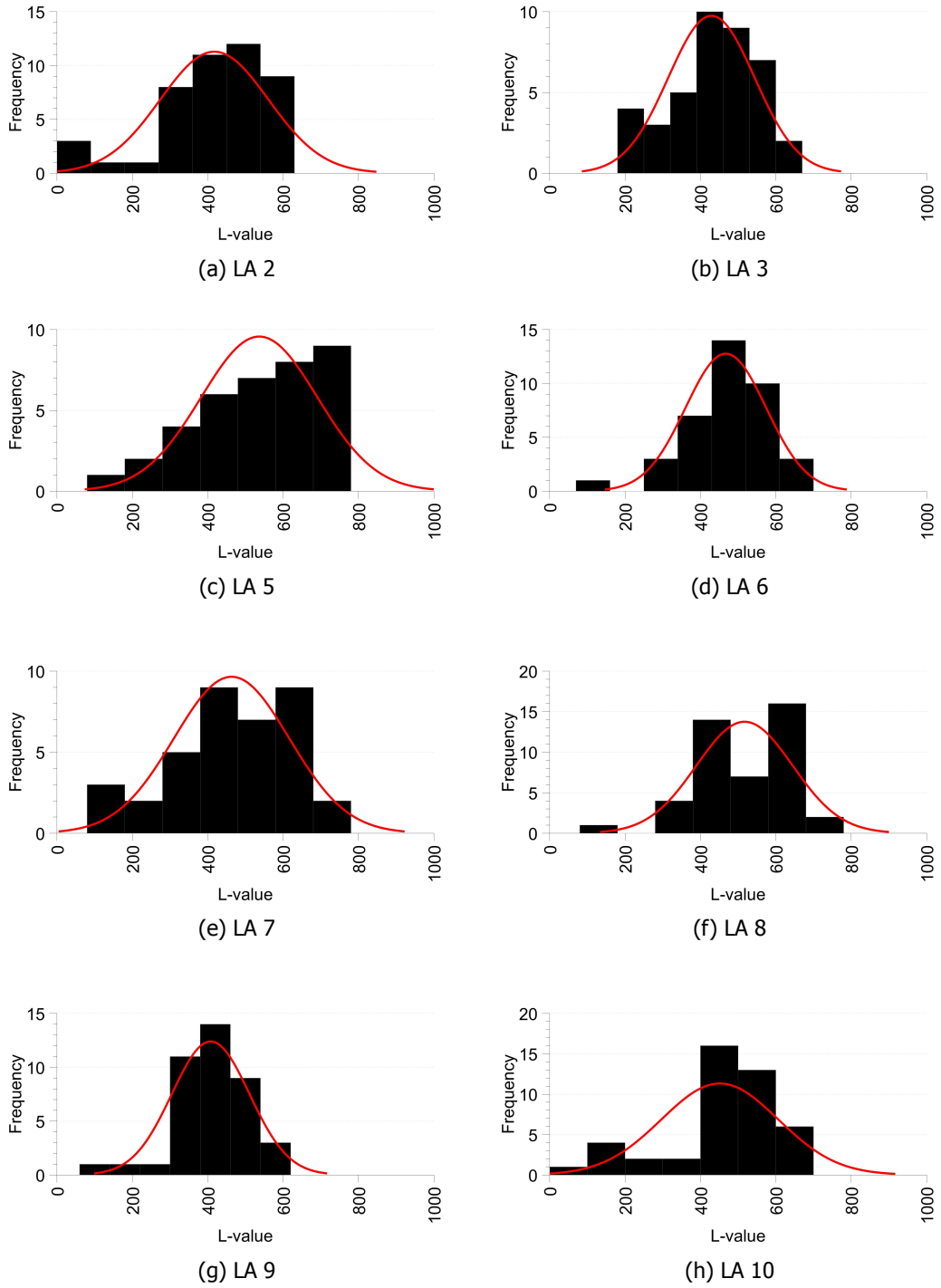

Figure H.7: Histograms for the Equotip type C measurements on the limestone (Lim) aggregate pieces LA 2 to LA 10, except LA 4..

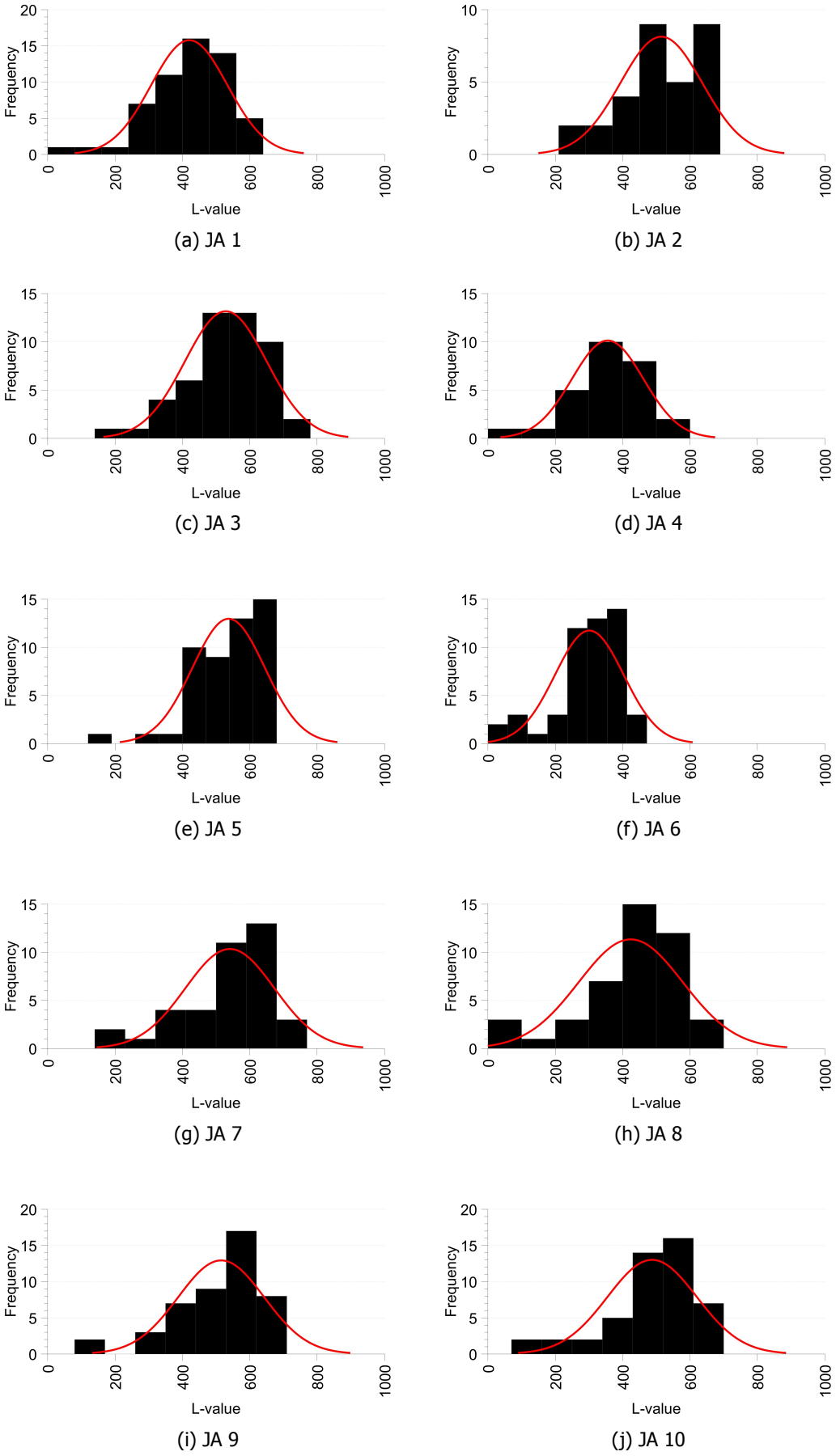

Figure H.8: Histograms for the Equotip type D measurements on the limestone (Jen) aggregate pieces JA 1 to JA 10.

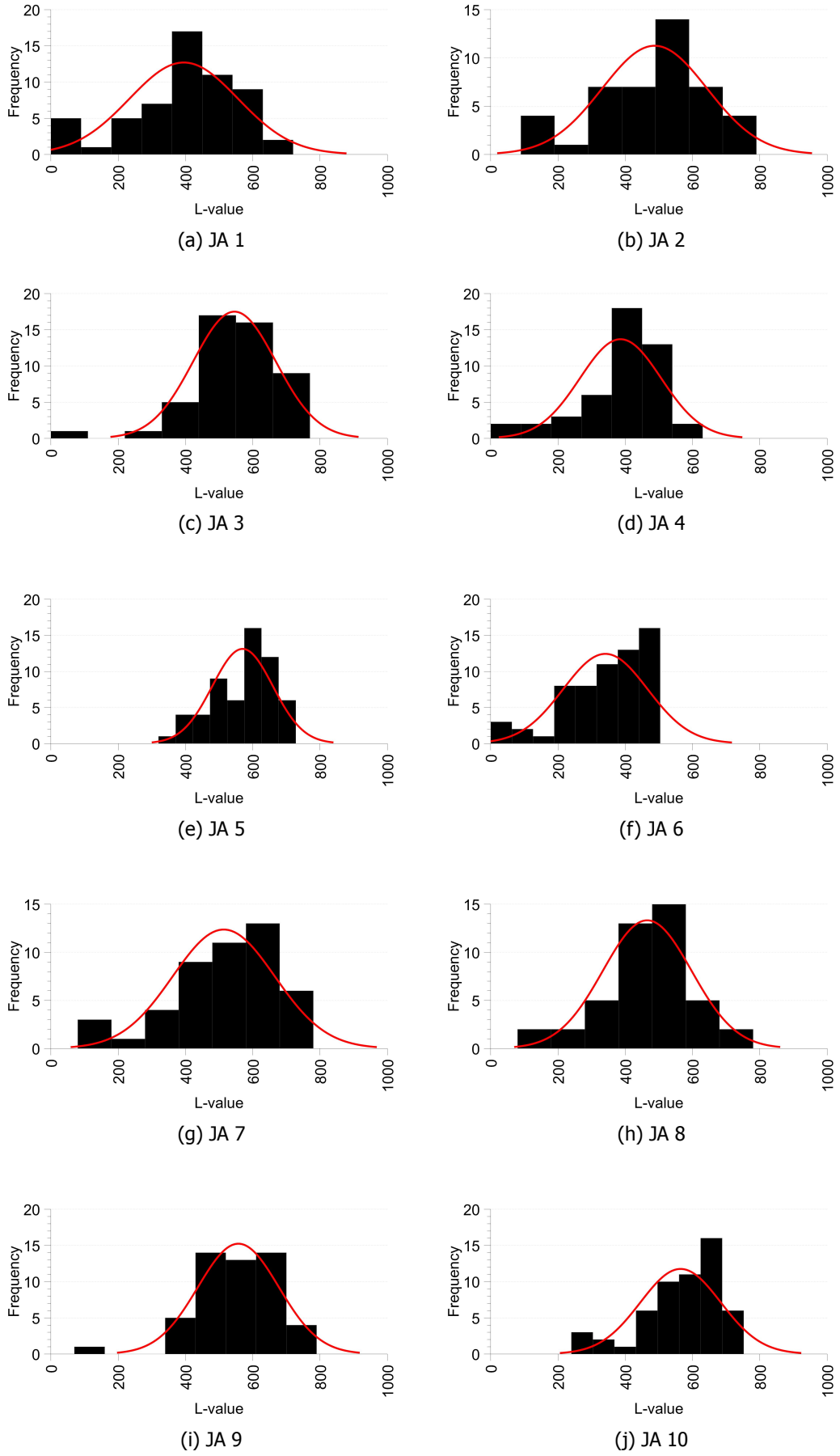

Figure H.9: Histograms for the Equotip type C measurements on the limestone (Jen) aggregate pieces JA 1 to JA 10.

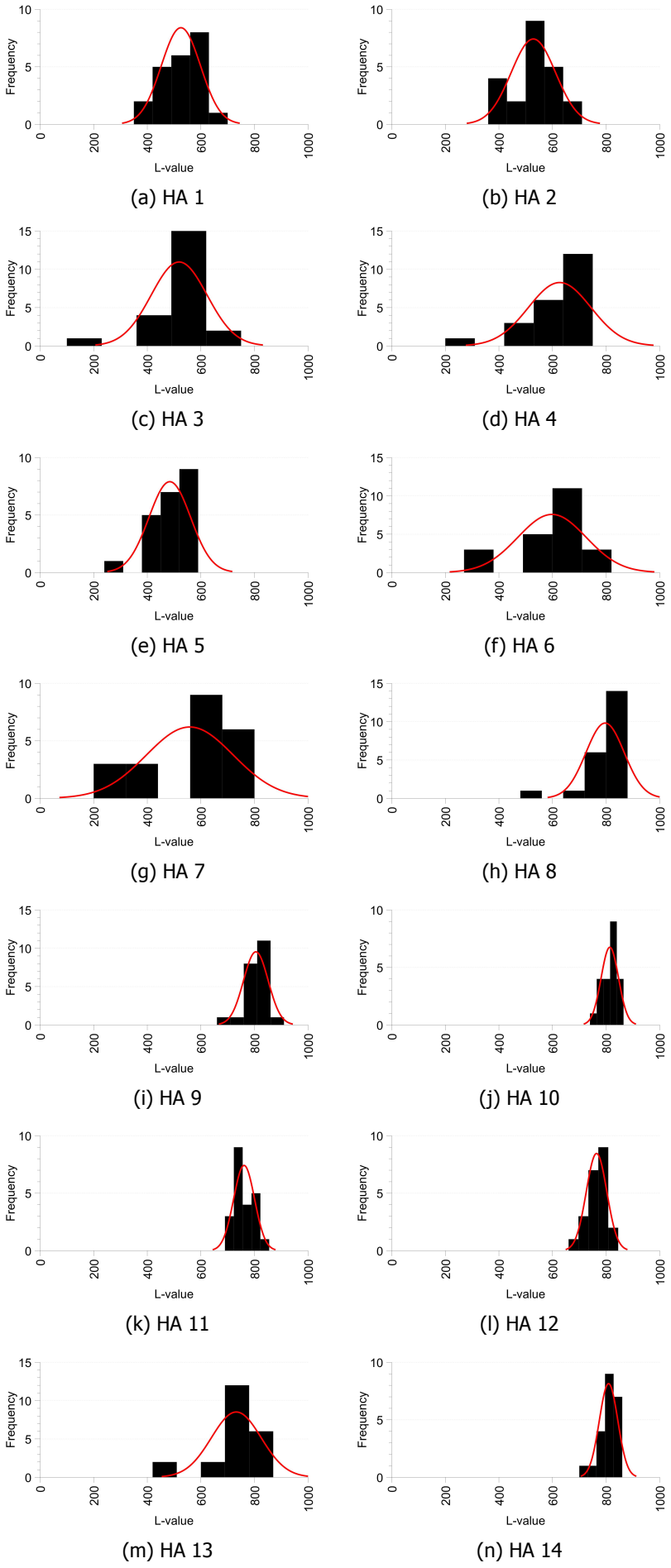

Figure H.10: Histograms for the Equotip type D measurements on the sandstone cores HA 1 to HA 14.

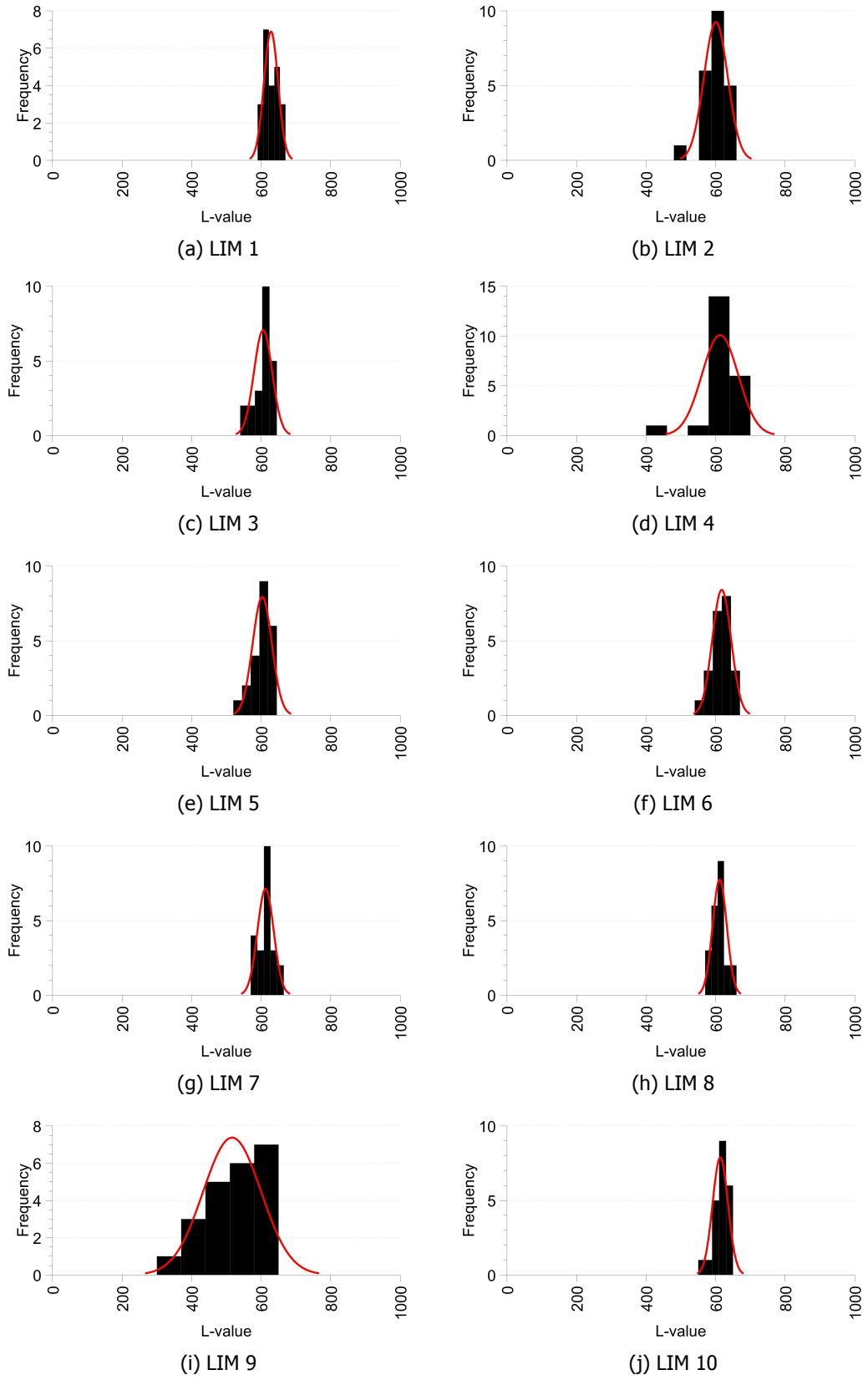

Figure H.11: Histograms for the Equotip type D measurements on the sandstone cores LIM 1 to LIM 10.

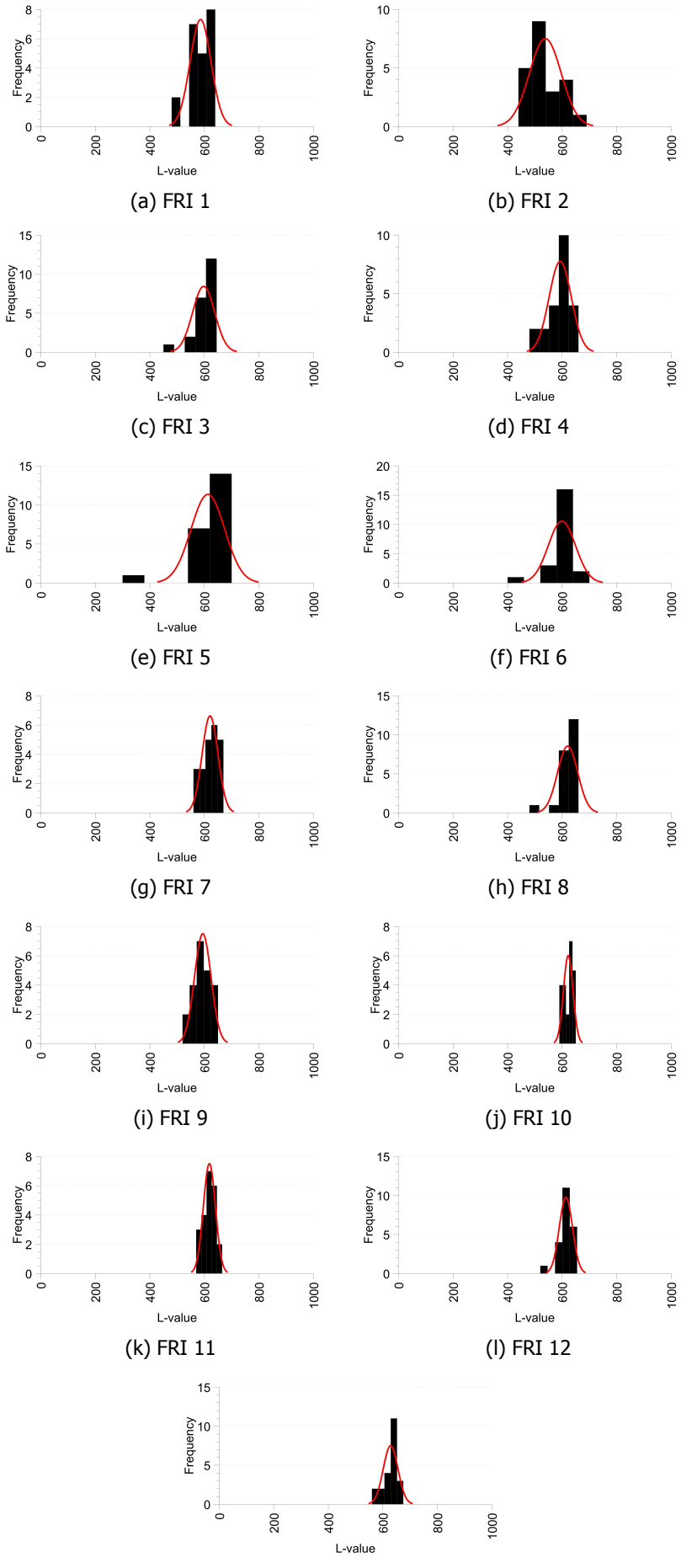

Figure H.12: Histograms for the Equotip type D measurements on the sandstone cores FRI 1 to FRI 13.

I

Equotip T-test Results

Table I.1: Student's T-test p-values for the Equotip type D measurements with a 1 cm grid spacing on the sandstone aggregate.

Sample	HA 1	HA 2	HA 3	HA 4	HA 5	HA 6	HA 7	HA 8	HA 9	HA 10	HA 11	HA 12	HA 13	HA 14	HA 15	HA 16	HA 17	HA 18	HA 19	HA 20
HA 1	-	0.08	0.16	0.58	0.47	0.01	0.62	0.17	0.00	0.00	0.24	0.76	0.54	0.00	0.00	0.63	0.03	0.11	0.00	0.10
HA 2	0.08	-	0.60	0.03	0.01	0.00	0.03	0.00	0.00	0.00	0.01	0.03	0.01	0.00	0.00	0.02	0.00	0.53	0.00	0.00
HA 3	0.16	0.60	-	0.05	0.03	0.00	0.06	0.01	0.00	0.00	0.01	0.07	0.03	0.00	0.00	0.05	0.00	0.98	0.00	0.00
HA 4	0.58	0.03	0.05	-	0.88	0.03	0.97	0.43	0.00	0.00	0.51	0.78	0.99	0.01	0.00	0.93	0.10	0.03	0.00	0.25
HA 5	0.47	0.01	0.03	0.88	-	0.03	0.85	0.51	0.00	0.00	0.60	0.65	0.88	0.01	0.00	0.80	0.12	0.01	0.00	0.30
HA 6	0.01	0.00	0.00	0.03	0.03	-	0.03	0.13	0.31	0.10	0.14	0.01	0.02	0.57	0.09	0.02	0.61	0.00	0.09	0.40
HA 7	0.62	0.03	0.06	0.97	0.85	0.03	-	0.42	0.00	0.00	0.50	0.82	0.95	0.01	0.00	0.96	0.11	0.03	0.00	0.25
HA 8	0.17	0.00	0.01	0.43	0.51	0.13	0.42	-	0.01	0.00	0.93	0.26	0.40	0.04	0.00	0.35	0.36	0.00	0.00	0.64
HA 9	0.00	0.00	0.00	0.00	0.00	0.31	0.00	0.01	-	0.52	0.02	0.00	0.00	0.63	0.41	0.00	0.14	0.00	0.57	0.09
HA 10	0.00	0.00	0.00	0.00	0.00	0.10	0.00	0.00	0.52	-	0.00	0.00	0.00	0.25	0.79	0.00	0.04	0.00	0.91	0.02
HA 11	0.24	0.01	0.01	0.51	0.60	0.14	0.50	0.93	0.02	0.00	-	0.34	0.49	0.04	0.00	0.44	0.34	0.00	0.00	0.61
HA 12	0.76	0.03	0.07	0.78	0.65	0.01	0.82	0.26	0.00	0.00	0.34	-	0.75	0.00	0.00	0.85	0.05	0.04	0.00	0.15
HA 13	0.54	0.01	0.03	0.99	0.88	0.02	0.95	0.40	0.00	0.00	0.49	0.75	-	0.00	0.00	0.91	0.08	0.02	0.00	0.22
HA 14	0.00	0.00	0.00	0.01	0.01	0.57	0.01	0.04	0.63	0.25	0.04	0.00	0.00	-	0.20	0.00	0.28	0.00	0.27	0.17
HA 15	0.00	0.00	0.00	0.00	0.00	0.09	0.00	0.00	0.41	0.79	0.00	0.00	0.00	0.20	-	0.00	0.04	0.00	0.71	0.02
HA 16	0.63	0.02	0.05	0.93	0.80	0.02	0.96	0.35	0.00	0.00	0.44	0.85	0.91	0.00	0.00	-	0.08	0.03	0.00	0.21
HA 17	0.03	0.00	0.00	0.10	0.12	0.61	0.11	0.36	0.14	0.04	0.34	0.05	0.08	0.28	0.04	0.08	-	0.00	0.04	0.71
HA 18	0.11	0.53	0.98	0.03	0.01	0.00	0.03	0.00	0.00	0.00	0.00	0.04	0.02	0.00	0.00	0.03	0.00	-	0.00	0.00
HA 19	0.00	0.00	0.00	0.00	0.00	0.09	0.00	0.00	0.57	0.91	0.00	0.00	0.00	0.27	0.71	0.00	0.04	0.00	-	0.02
HA 20	0.10	0.00	0.00	0.25	0.30	0.40	0.25	0.64	0.09	0.02	0.61	0.15	0.22	0.17	0.02	0.21	0.71	0.00	0.02	-
HA 21	0.03	0.97	0.54	0.01	0.00	0.00	0.01	0.00	0.00	0.00	0.00	0.01	0.00	0.00	0.00	0.01	0.00	0.46	0.00	0.00
HA 22	0.97	0.06	0.13	0.58	0.46	0.00	0.62	0.16	0.00	0.00	0.22	0.77	0.54	0.00	0.00	0.63	0.02	0.08	0.00	0.08
HA 23	0.01	0.00	0.00	0.04	0.05	0.98	0.04	0.17	0.33	0.11	0.17	0.02	0.03	0.57	0.10	0.03	0.64	0.00	0.11	0.43
HA 24	0.00	0.00	0.00	0.00	0.00	0.01	0.00	0.00	0.10	0.31	0.00	0.00	0.00	0.03	0.53	0.00	0.00	0.00	0.24	0.00
HA 25	0.00	0.00	0.00	0.00	0.00	0.14	0.00	0.01	0.61	0.92	0.01	0.00	0.00	0.32	0.74	0.00	0.06	0.00	1.00	0.04
HA 26	0.15	0.71	0.89	0.05	0.03	0.00	0.06	0.00	0.00	0.00	0.01	0.07	0.03	0.00	0.00	0.05	0.00	0.86	0.00	0.01
HA 27	0.04	0.00	0.00	0.11	0.13	0.79	0.11	0.32	0.27	0.10	0.32	0.05	0.08	0.46	0.10	0.08	0.86	0.00	0.10	0.63
HA 28	0.72	0.20	0.36	0.39	0.31	0.01	0.43	0.11	0.00	0.00	0.16	0.51	0.35	0.00	0.00	0.42	0.02	0.30	0.00	0.07
HA 29	0.41	0.01	0.03	0.78	0.89	0.06	0.76	0.61	0.01	0.00	0.70	0.57	0.78	0.01	0.00	0.71	0.18	0.01	0.00	0.38
HA 30	0.30	0.39	0.70	0.11	0.07	0.00	0.13	0.01	0.00	0.00	0.03	0.16	0.08	0.00	0.00	0.12	0.00	0.68	0.00	0.01
HA 31	0.08	0.00	0.00	0.20	0.24	0.48	0.20	0.54	0.11	0.03	0.52	0.11	0.17	0.22	0.03	0.16	0.81	0.00	0.03	0.90
HA 32	0.15	0.00	0.00	0.38	0.45	0.16	0.37	0.91	0.02	0.00	0.86	0.22	0.35	0.05	0.00	0.31	0.41	0.00	0.00	0.71
HA 33	0.00	0.00	0.00	0.01	0.01	0.40	0.01	0.04	0.98	0.55	0.04	0.00	0.00	0.69	0.45	0.01	0.20	0.00	0.61	0.13
HA 34	0.00	0.00	0.00	0.01	0.01	0.37	0.01	0.03	0.99	0.55	0.03	0.00	0.00	0.67	0.45	0.00	0.19	0.00	0.59	0.12
HA 35	0.01	0.00	0.00	0.04	0.05	0.75	0.04	0.19	0.17	0.05	0.21	0.01	0.03	0.37	0.04	0.03	0.82	0.00	0.03	0.54
HA 36	0.09	0.00	0.00	0.24	0.29	0.38	0.24	0.63	0.08	0.02	0.60	0.14	0.21	0.15	0.02	0.19	0.70	0.00	0.02	1.00
HA 37	0.00	0.00	0.00	0.02	0.02	0.64	0.02	0.08	0.67	0.31	0.08	0.01	0.01	0.99	0.26	0.01	0.36	0.00	0.34	0.24
HA 38	0.01	0.00	0.00	0.04	0.05	0.97	0.04	0.17	0.32	0.10	0.16	0.02	0.03	0.56	0.09	0.03	0.65	0.00	0.11	0.43
HA 39	0.01	0.00	0.00	0.04	0.05	0.96	0.04	0.16	0.39	0.15	0.17	0.02	0.03	0.65	0.13	0.03	0.61	0.00	0.15	0.41
HA 40	0.62	0.04	0.07	0.98	0.86	0.04	0.99	0.45	0.00	0.00	0.51	0.82	0.96	0.01	0.00	0.95	0.10	0.04	0.00	0.26

Sample	HA 21	HA 22	HA 23	HA 24	HA 25	HA 26	HA 27	HA 28	HA 29	HA 30	HA 31	HA 32	HA 33	HA 34	HA 35	HA 36	HA 37	HA 38	HA 39	HA 40
HA 1	0.03	0.97	0.01	0.00	0.00	0.15	0.04	0.72	0.41	0.30	0.08	0.15	0.00	0.00	0.01	0.09	0.00	0.01	0.01	0.62
HA 2	0.97	0.06	0.00	0.00	0.00	0.71	0.00	0.20	0.01	0.39	0.00	0.00	0.00	0.00	0.00	0.00	0.00	0.00	0.00	0.04
HA 3	0.54	0.13	0.00	0.00	0.00	0.89	0.00	0.36	0.03	0.70	0.00	0.00	0.00	0.00	0.00	0.00	0.00	0.00	0.00	0.07
HA 4	0.01	0.58	0.04	0.00	0.00	0.05	0.11	0.39	0.78	0.11	0.20	0.38	0.01	0.01	0.04	0.24	0.02	0.04	0.04	0.98
HA 5	0.00	0.46	0.05	0.00	0.00	0.03	0.13	0.31	0.89	0.07	0.24	0.45	0.01	0.01	0.05	0.29	0.02	0.05	0.05	0.86
HA 6	0.00	0.00	0.98	0.01	0.14	0.00	0.79	0.01	0.06	0.00	0.48	0.16	0.40	0.37	0.75	0.38	0.64	0.97	0.96	0.04
HA 7	0.01	0.62	0.04	0.00	0.00	0.06	0.11	0.43	0.76	0.13	0.20	0.37	0.01	0.01	0.04	0.24	0.02	0.04	0.04	0.99
HA 8	0.00	0.16	0.17	0.00	0.01	0.00	0.32	0.11	0.61	0.01	0.54	0.91	0.04	0.03	0.19	0.63	0.08	0.17	0.16	0.45
HA 9	0.00	0.00	0.33	0.10	0.61	0.00	0.27	0.00	0.01	0.00	0.11	0.02	0.98	0.99	0.17	0.08	0.67	0.32	0.39	0.00
HA 10	0.00	0.00	0.11	0.31	0.92	0.00	0.10	0.00	0.00	0.00	0.03	0.00	0.55	0.55	0.05	0.02	0.31	0.10	0.15	0.00
HA 11	0.00	0.22	0.17	0.00	0.01	0.01	0.32	0.16	0.70	0.03	0.52	0.86	0.04	0.03	0.21	0.60	0.08	0.16	0.17	0.51
HA 12	0.01	0.77	0.02	0.00	0.00	0.07	0.05	0.51	0.57	0.16	0.11	0.22	0.00	0.00	0.01	0.14	0.01	0.02	0.02	0.82
HA 13	0.00	0.54	0.03	0.00	0.00	0.03	0.08	0.35	0.78	0.08	0.17	0.35	0.00	0.00	0.03	0.21	0.01	0.03	0.03	0.96
HA 14	0.00	0.00	0.57	0.03	0.32	0.00	0.46	0.00	0.01	0.00	0.22	0.05	0.69	0.67	0.37	0.15	0.99	0.56	0.65	0.01
HA 15	0.00	0.00	0.10	0.53	0.74	0.00	0.10	0.00	0.00	0.00	0.03	0.00	0.45	0.45	0.04	0.02	0.26	0.09	0.13	0.00
HA 16	0.01	0.63	0.03	0.00	0.00	0.05	0.08	0.42	0.71	0.12	0.16	0.31	0.01	0.00	0.03	0.19	0.01	0.03	0.03	0.95
HA 17	0.00	0.02	0.64	0.00	0.06	0.00	0.86	0.02	0.18	0.00	0.81	0.41	0.20	0.19	0.82	0.70	0.36	0.65	0.61	0.10
HA 18	0.46	0.08	0.00	0.00	0.00	0.86	0.00	0.30	0.01	0.68	0.00	0.00	0.00	0.00	0.00	0.00	0.00	0.00	0.00	0.04
HA 19	0.00	0.00	0.11	0.24	1.00	0.00	0.10	0.00	0.00	0.00	0.03	0.00	0.61	0.59	0.03	0.02	0.34	0.11	0.15	0.00
HA 20	0.00	0.08	0.43	0.00	0.04	0.01	0.63	0.07	0.38	0.01	0.90	0.71	0.13	0.12	0.54	1.00	0.24	0.43	0.41	0.26
HA 21	-	0.02	0.00	0.00	0.00	0.67	0.00	0.12	0.00	0.30	0.00	0.00	0.00	0.00	0.00	0.00	0.00	0.00	0.00	0.01
HA 22	0.02	-	0.01	0.00	0.00	0.12	0.03	0.68	0.40	0.25	0.06	0.13	0.00	0.00	0.01	0.08	0.00	0.01	0.01	0.61
HA 23	0.00	0.01	-	0.01	0.16	0.00	0.82	0.01	0.08	0.00	0.51	0.20	0.40	0.38	0.79	0.41	0.63	0.99	0.94	0.04
HA 24	0.00	0.00	0.01	-	0.29	0.00	0.01	0.00	0.00	0.00	0.00	0.00	0.14	0.13	0.00	0.00	0.05	0.01	0.02	0.00
HA 25	0.00	0.00	0.16	0.29	-	0.00	0.14	0.00	0.00	0.00	0.05	0.01	0.64	0.63	0.07	0.03	0.39	0.15	0.20	0.00
HA 26	0.67	0.12	0.00	0.00	0.00	-	0.00	0.33	0.03	0.62	0.00	0.00	0.00	0.00	0.00	0.00	0.00	0.00	0.00	0.07
HA 27	0.00	0.03	0.82	0.01	0.14	0.00	-	0.03	0.18	0.00	0.71	0.37	0.34	0.32	0.99	0.61	0.53	0.83	0.78	0.12
HA 28	0.12	0.68	0.01	0.00	0.00	0.33	0.03	-	0.28	0.56	0.05	0.09	0.00	0.00	0.01	0.06	0.00	0.01	0.01	0.42
HA 29	0.00	0.40	0.08	0.00	0.00	0.03	0.18	0.28	-	0.06	0.31	0.55	0.02	0.01	0.08	0.37	0.04	0.08	0.08	0.78
HA 30	0.30	0.25	0.00	0.00	0.00	0.62	0.00	0.56	0.06	-	0.01	0.01	0.00	0.00	0.00	0.01	0.00	0.00	0.00	0.14
HA 31	0.00	0.06	0.51	0.00	0.05	0.00	0.71	0.05	0.31	0.01	-	0.60	0.17	0.15	0.64	0.89	0.29	0.51	0.49	0.21
HA 32	0.00	0.13	0.20	0.00	0.01	0.00	0.37	0.09	0.55	0.01	0.60	-	0.05	0.03	0.25	0.70	0.09	0.20	0.19	0.39
HA 33	0.00	0.00	0.40	0.14	0.64	0.00	0.34	0.00	0.02	0.00	0.17	0.05	-	0.99	0.27	0.12	0.72	0.38	0.46	0.01
HA 34	0.00	0.00	0.38	0.13	0.63	0.00	0.32	0.00	0.01	0.00	0.15	0.03	0.99	-	0.22	0.11	0.71	0.37	0.44	0.01
HA 35	0.00	0.01	0.79	0.00	0.07	0.00	0.99	0.01	0.08	0.00	0.64	0.25	0.27	0.22	-	0.53	0.45	0.80	0.73	0.06
HA 36	0.00	0.08	0.41	0.00	0.03	0.00	0.61	0.06	0.37	0.01	0.89	0.70	0.12	0.11	0.53	-	0.22	0.41	0.40	0.24
HA 37	0.00	0.00	0.63	0.05	0.39	0.00	0.53	0.00	0.04	0.00	0.29	0.09	0.72	0.71	0.45	0.22	-	0.62	0.70	0.02
HA 38	0.00	0.01	0.99	0.01	0.15	0.00	0.83	0.01	0.08	0.00	0.51	0.20	0.38	0.37	0.80	0.41	0.62	-	0.93	0.04
HA 39	0.00	0.01	0.94	0.02	0.20	0.00	0.78	0.01	0.08	0.00	0.49	0.19	0.46	0.44	0.73	0.40	0.70	0.93	-	0.05
HA 40	0.01	0.61	0.04	0.00	0.00	0.07	0.12	0.42	0.78	0.14	0.21	0.39	0.01	0.01	0.06	0.24	0.02	0.04	0.05	-

Table I.2: Student's T-test p-values for the Equotip type D measurements with a 2 cm grid spacing on the sandstone aggregate.

Sample	HA 1	HA 2	HA 3	HA 4	HA 5	HA 6	HA 7	HA 8	HA 9	HA 10	HA 11	HA 12	HA 13	HA 14	HA 15	HA 16	HA 17	HA 18	HA 19	HA 20
HA 1	-	0.86	0.24	0.05	0.29	0.03	0.51	0.13	0.00	0.00	0.03	0.11	0.30	0.01	0.00	0.27	0.05	0.90	0.00	0.26
HA 2	0.86	-	0.45	0.15	0.52	0.10	0.71	0.30	0.01	0.01	0.11	0.28	0.50	0.06	0.01	0.48	0.14	0.92	0.00	0.44
HA 3	0.24	0.45	-	0.37	0.84	0.23	0.70	0.70	0.03	0.02	0.25	0.72	0.94	0.15	0.02	0.98	0.33	0.24	0.00	0.89
HA 4	0.05	0.15	0.37	-	0.26	0.72	0.24	0.62	0.16	0.12	0.74	0.56	0.35	0.54	0.09	0.38	0.83	0.04	0.02	0.54
HA 5	0.29	0.52	0.84	0.26	-	0.15	0.81	0.55	0.01	0.01	0.17	0.55	0.92	0.09	0.01	0.87	0.23	0.31	0.00	0.75
HA 6	0.03	0.10	0.23	0.72	0.15	-	0.15	0.41	0.33	0.26	0.98	0.35	0.22	0.81	0.18	0.23	0.90	0.02	0.07	0.36
HA 7	0.51	0.71	0.70	0.24	0.81	0.15	-	0.47	0.02	0.01	0.16	0.47	0.76	0.09	0.01	0.72	0.21	0.54	0.00	0.64
HA 8	0.13	0.30	0.70	0.62	0.55	0.41	0.47	-	0.06	0.04	0.43	0.96	0.66	0.28	0.04	0.69	0.52	0.12	0.01	0.85
HA 9	0.00	0.01	0.03	0.16	0.01	0.33	0.02	0.06	-	0.90	0.32	0.04	0.02	0.44	0.59	0.03	0.28	0.00	0.43	0.07
HA 10	0.00	0.01	0.02	0.12	0.01	0.26	0.01	0.04	0.90	-	0.25	0.03	0.01	0.35	0.65	0.02	0.22	0.00	0.49	0.05
HA 11	0.03	0.11	0.25	0.74	0.17	0.98	0.16	0.43	0.32	0.25	-	0.37	0.23	0.79	0.17	0.25	0.92	0.02	0.07	0.38
HA 12	0.11	0.28	0.72	0.56	0.55	0.35	0.47	0.96	0.04	0.03	0.37	-	0.67	0.23	0.02	0.71	0.46	0.11	0.00	0.88
HA 13	0.30	0.50	0.94	0.35	0.92	0.22	0.76	0.66	0.02	0.01	0.23	0.67	-	0.12	0.01	0.96	0.28	0.31	0.00	0.83
HA 14	0.01	0.06	0.15	0.54	0.09	0.81	0.09	0.28	0.44	0.35	0.79	0.23	0.12	-	0.22	0.14	0.71	0.01	0.11	0.24
HA 15	0.00	0.01	0.02	0.09	0.01	0.18	0.01	0.04	0.59	0.65	0.17	0.02	0.01	0.22	-	0.02	0.15	0.00	0.91	0.04
HA 16	0.27	0.48	0.98	0.38	0.87	0.23	0.72	0.69	0.03	0.02	0.25	0.71	0.96	0.14	0.02	-	0.32	0.28	0.00	0.87
HA 17	0.05	0.14	0.33	0.83	0.23	0.90	0.21	0.52	0.28	0.22	0.92	0.46	0.28	0.71	0.15	0.32	-	0.04	0.07	0.44
HA 18	0.90	0.92	0.24	0.04	0.31	0.02	0.54	0.12	0.00	0.00	0.02	0.11	0.31	0.01	0.00	0.28	0.04	-	0.00	0.25
HA 19	0.00	0.00	0.00	0.02	0.00	0.07	0.00	0.01	0.43	0.49	0.07	0.00	0.00	0.11	0.91	0.00	0.07	0.00	-	0.01
HA 20	0.26	0.44	0.89	0.54	0.75	0.36	0.64	0.85	0.07	0.05	0.38	0.88	0.83	0.24	0.04	0.87	0.44	0.25	0.01	-
HA 21	0.74	0.65	0.11	0.01	0.14	0.01	0.32	0.05	0.00	0.00	0.01	0.04	0.15	0.00	0.00	0.13	0.02	0.62	0.00	0.14
HA 22	0.18	0.37	0.89	0.44	0.73	0.26	0.59	0.80	0.03	0.02	0.28	0.83	0.83	0.16	0.01	0.87	0.35	0.18	0.00	0.98
HA 23	0.01	0.06	0.13	0.49	0.08	0.75	0.08	0.25	0.51	0.42	0.73	0.20	0.12	0.93	0.28	0.13	0.66	0.01	0.15	0.23
HA 24	0.00	0.00	0.00	0.01	0.00	0.03	0.00	0.00	0.17	0.19	0.02	0.00	0.00	0.03	0.51	0.00	0.02	0.00	0.50	0.00
HA 25	0.00	0.02	0.03	0.15	0.02	0.28	0.02	0.07	0.83	0.91	0.28	0.05	0.03	0.36	0.77	0.03	0.24	0.00	0.64	0.07
HA 26	0.77	0.69	0.15	0.03	0.19	0.02	0.38	0.08	0.00	0.00	0.02	0.07	0.22	0.01	0.00	0.19	0.04	0.66	0.00	0.20
HA 27	0.02	0.08	0.16	0.49	0.10	0.73	0.11	0.28	0.61	0.52	0.71	0.23	0.15	0.88	0.37	0.16	0.65	0.01	0.22	0.26
HA 28	0.55	0.75	0.68	0.25	0.79	0.16	0.97	0.47	0.02	0.01	0.17	0.46	0.74	0.09	0.01	0.71	0.21	0.58	0.00	0.63
HA 29	0.15	0.33	0.75	0.58	0.60	0.38	0.52	0.95	0.06	0.04	0.41	0.99	0.71	0.26	0.04	0.74	0.49	0.15	0.01	0.90
HA 30	0.92	0.80	0.21	0.04	0.26	0.02	0.46	0.11	0.00	0.00	0.03	0.10	0.26	0.01	0.00	0.24	0.04	0.82	0.00	0.23
HA 31	0.07	0.19	0.40	0.95	0.29	0.79	0.27	0.62	0.24	0.18	0.81	0.56	0.37	0.62	0.14	0.40	0.89	0.06	0.05	0.54
HA 32	0.03	0.11	0.26	0.82	0.17	0.89	0.17	0.47	0.24	0.18	0.91	0.41	0.25	0.69	0.13	0.27	1.00	0.02	0.04	0.41
HA 33	0.04	0.12	0.24	0.60	0.16	0.82	0.15	0.37	0.55	0.46	0.80	0.32	0.19	0.97	0.32	0.22	0.73	0.03	0.22	0.31
HA 34	0.05	0.17	0.37	0.94	0.26	0.79	0.25	0.59	0.22	0.17	0.81	0.54	0.35	0.61	0.12	0.37	0.90	0.05	0.04	0.52
HA 35	0.01	0.06	0.15	0.65	0.08	0.98	0.10	0.31	0.28	0.22	0.95	0.26	0.16	0.81	0.14	0.16	0.87	0.01	0.04	0.30
HA 36	0.17	0.35	0.81	0.53	0.65	0.34	0.55	0.89	0.05	0.03	0.36	0.92	0.76	0.22	0.03	0.80	0.44	0.16	0.00	0.95
HA 37	0.00	0.00	0.00	0.04	0.00	0.10	0.00	0.01	0.53	0.61	0.10	0.01	0.00	0.16	0.97	0.00	0.09	0.00	0.85	0.02
HA 38	0.00	0.00	0.01	0.06	0.00	0.15	0.00	0.02	0.70	0.79	0.15	0.01	0.01	0.23	0.81	0.01	0.14	0.00	0.66	0.02
HA 39	0.00	0.03	0.04	0.19	0.02	0.34	0.03	0.09	0.91	1.00	0.33	0.06	0.04	0.43	0.71	0.05	0.30	0.00	0.57	0.09
HA 40	0.18	0.36	0.82	0.54	0.67	0.34	0.56	0.89	0.05	0.03	0.36	0.93	0.76	0.21	0.03	0.80	0.43	0.18	0.01	0.95

Sample	HA 21	HA 22	HA 23	HA 24	HA 25	HA 26	HA 27	HA 28	HA 29	HA 30	HA 31	HA 32	HA 33	HA 34	HA 35	HA 36	HA 37	HA 38	HA 39	HA 40
HA 1	0.74	0.18	0.01	0.00	0.00	0.77	0.02	0.55	0.15	0.92	0.07	0.03	0.04	0.05	0.01	0.17	0.00	0.00	0.00	0.18
HA 2	0.65	0.37	0.06	0.00	0.02	0.69	0.08	0.75	0.33	0.80	0.19	0.11	0.12	0.17	0.06	0.35	0.00	0.00	0.03	0.36
HA 3	0.11	0.89	0.13	0.00	0.03	0.15	0.16	0.68	0.75	0.21	0.40	0.26	0.24	0.37	0.15	0.81	0.00	0.01	0.04	0.82
HA 4	0.01	0.44	0.49	0.01	0.15	0.03	0.49	0.25	0.58	0.04	0.95	0.82	0.60	0.94	0.65	0.53	0.04	0.06	0.19	0.54
HA 5	0.14	0.73	0.08	0.00	0.02	0.19	0.10	0.79	0.60	0.26	0.29	0.17	0.16	0.26	0.08	0.65	0.00	0.00	0.02	0.67
HA 6	0.01	0.26	0.75	0.03	0.28	0.02	0.73	0.16	0.38	0.02	0.79	0.89	0.82	0.79	0.98	0.34	0.10	0.15	0.34	0.34
HA 7	0.32	0.59	0.08	0.00	0.02	0.38	0.11	0.97	0.52	0.46	0.27	0.17	0.15	0.25	0.10	0.55	0.00	0.00	0.03	0.56
HA 8	0.05	0.80	0.25	0.00	0.07	0.08	0.28	0.47	0.95	0.11	0.62	0.47	0.37	0.59	0.31	0.89	0.01	0.02	0.09	0.89
HA 9	0.00	0.03	0.51	0.17	0.83	0.00	0.61	0.02	0.06	0.00	0.24	0.24	0.55	0.22	0.28	0.05	0.53	0.70	0.91	0.05
HA 10	0.00	0.02	0.42	0.19	0.91	0.00	0.52	0.01	0.04	0.00	0.18	0.18	0.46	0.17	0.22	0.03	0.61	0.79	1.00	0.03
HA 11	0.01	0.28	0.73	0.02	0.28	0.02	0.71	0.17	0.41	0.03	0.81	0.91	0.80	0.81	0.95	0.36	0.10	0.15	0.33	0.36
HA 12	0.04	0.83	0.20	0.00	0.05	0.07	0.23	0.46	0.99	0.10	0.56	0.41	0.32	0.54	0.26	0.92	0.01	0.01	0.06	0.93
HA 13	0.15	0.83	0.12	0.00	0.03	0.22	0.15	0.74	0.71	0.26	0.37	0.25	0.19	0.35	0.16	0.76	0.00	0.01	0.04	0.76
HA 14	0.00	0.16	0.93	0.03	0.36	0.01	0.88	0.09	0.26	0.01	0.62	0.69	0.97	0.61	0.81	0.22	0.16	0.23	0.43	0.21
HA 15	0.00	0.01	0.28	0.51	0.77	0.00	0.37	0.01	0.04	0.00	0.14	0.13	0.32	0.12	0.14	0.03	0.97	0.81	0.71	0.03
HA 16	0.13	0.87	0.13	0.00	0.03	0.19	0.16	0.71	0.74	0.24	0.40	0.27	0.22	0.37	0.16	0.80	0.00	0.01	0.05	0.80
HA 17	0.02	0.35	0.66	0.02	0.24	0.04	0.65	0.21	0.49	0.04	0.89	1.00	0.73	0.90	0.87	0.44	0.09	0.14	0.30	0.43
HA 18	0.62	0.18	0.01	0.00	0.00	0.66	0.01	0.58	0.15	0.82	0.06	0.02	0.03	0.05	0.01	0.16	0.00	0.00	0.00	0.18
HA 19	0.00	0.00	0.15	0.50	0.64	0.00	0.22	0.00	0.01	0.00	0.05	0.04	0.22	0.04	0.04	0.00	0.85	0.66	0.57	0.01
HA 20	0.14	0.98	0.23	0.00	0.07	0.20	0.26	0.63	0.90	0.23	0.54	0.41	0.31	0.52	0.30	0.95	0.02	0.02	0.09	0.95
HA 21	-	0.08	0.00	0.00	0.00	1.00	0.01	0.36	0.06	0.83	0.03	0.01	0.02	0.02	0.00	0.07	0.00	0.00	0.00	0.08
HA 22	0.08	-	0.14	0.00	0.03	0.12	0.17	0.58	0.85	0.16	0.45	0.31	0.23	0.43	0.20	0.91	0.00	0.01	0.04	0.91
HA 23	0.00	0.14	-	0.05	0.43	0.01	0.95	0.09	0.24	0.01	0.58	0.64	0.96	0.56	0.74	0.20	0.20	0.29	0.50	0.20
HA 24	0.00	0.00	0.05	-	0.31	0.00	0.10	0.00	0.00	0.00	0.02	0.01	0.08	0.02	0.01	0.00	0.40	0.28	0.28	0.00
HA 25	0.00	0.03	0.43	0.31	-	0.00	0.53	0.03	0.07	0.00	0.22	0.21	0.47	0.20	0.25	0.05	0.75	0.91	0.93	0.05
HA 26	1.00	0.12	0.01	0.00	0.00	-	0.02	0.43	0.10	0.86	0.05	0.02	0.04	0.04	0.00	0.12	0.00	0.00	0.00	0.14
HA 27	0.01	0.17	0.95	0.10	0.53	0.02	-	0.12	0.26	0.02	0.58	0.62	0.93	0.56	0.71	0.23	0.28	0.38	0.59	0.23
HA 28	0.36	0.58	0.09	0.00	0.03	0.43	0.12	-	0.51	0.50	0.28	0.18	0.16	0.25	0.11	0.54	0.00	0.01	0.04	0.55
HA 29	0.06	0.85	0.24	0.00	0.07	0.10	0.26	0.51	-	0.14	0.59	0.44	0.35	0.56	0.30	0.94	0.01	0.02	0.09	0.94
HA 30	0.83	0.16	0.01	0.00	0.00	0.86	0.02	0.50	0.14	-	0.06	0.02	0.04	0.05	0.01	0.15	0.00	0.00	0.00	0.16
HA 31	0.03	0.45	0.58	0.02	0.22	0.05	0.58	0.28	0.59	0.06	-	0.89	0.66	1.00	0.75	0.53	0.07	0.11	0.26	0.54
HA 32	0.01	0.31	0.64	0.01	0.21	0.02	0.62	0.18	0.44	0.02	0.89	-	0.73	0.88	0.85	0.39	0.06	0.10	0.26	0.40
HA 33	0.02	0.23	0.96	0.08	0.47	0.04	0.93	0.16	0.35	0.04	0.66	0.73	-	0.66	0.83	0.30	0.27	0.34	0.53	0.28
HA 34	0.02	0.43	0.56	0.02	0.20	0.04	0.56	0.25	0.56	0.05	1.00	0.88	0.66	-	0.73	0.51	0.06	0.09	0.24	0.52
HA 35	0.00	0.20	0.74	0.01	0.25	0.00	0.71	0.11	0.30	0.01	0.75	0.85	0.83	0.73	-	0.26	0.06	0.11	0.30	0.28
HA 36	0.07	0.91	0.20	0.00	0.05	0.12	0.23	0.54	0.94	0.15	0.53	0.39	0.30	0.51	0.26	-	0.01	0.01	0.07	1.00
HA 37	0.00	0.00	0.20	0.40	0.75	0.00	0.28	0.00	0.01	0.00	0.07	0.06	0.27	0.06	0.06	0.01	-	0.80	0.68	0.01
HA 38	0.00	0.01	0.29	0.28	0.91	0.00	0.38	0.01	0.02	0.00	0.11	0.10	0.34	0.09	0.11	0.01	0.80	-	0.83	0.01
HA 39	0.00	0.04	0.50	0.28	0.93	0.00	0.59	0.04	0.09	0.00	0.26	0.26	0.53	0.24	0.30	0.07	0.68	0.83	-	0.07
HA 40	0.08	0.91	0.20	0.00	0.05	0.14	0.23	0.55	0.94	0.16	0.54	0.40	0.28	0.52	0.28	1.00	0.01	0.01	0.07	-

Table I.3: Student's T-test p-values for the Equotip type C measurements with a 1 cm grid spacing on sandstone aggregate.

Sample	HA 1	HA 2	HA 3	HA 4	HA 5	HA 6	HA 7	HA 8	HA 9	HA 10	HA 21
HA 1	-	0.81	0.28	0.44	0.72	0.28	0.36	0.45	0.02	0.00	0.02
HA 2	0.81	-	0.38	0.57	0.50	0.14	0.47	0.59	0.01	0.00	0.03
HA 3	0.28	0.38	-	0.87	0.09	0.01	0.99	0.74	0.00	0.00	0.08
HA 4	0.44	0.57	0.87	-	0.20	0.04	0.88	0.92	0.00	0.00	0.13
HA 5	0.72	0.50	0.09	0.20	-	0.41	0.15	0.19	0.02	0.00	0.00
HA 6	0.28	0.14	0.01	0.04	0.41	-	0.03	0.03	0.11	0.00	0.00
HA 7	0.36	0.47	0.99	0.88	0.15	0.03	-	0.79	0.00	0.00	0.18
HA 8	0.45	0.59	0.74	0.92	0.19	0.03	0.79	-	0.00	0.00	0.06
HA 9	0.02	0.01	0.00	0.00	0.02	0.11	0.00	0.00	-	0.10	0.00
HA 10	0.00	0.00	0.00	0.00	0.00	0.00	0.00	0.00	0.10	-	0.00
HA 21	0.02	0.03	0.08	0.13	0.00	0.00	0.18	0.06	0.00	0.00	-

Table I.4: Student's T-test p-values for the Equotip type C measurements with a 2 cm grid spacing on sandstone aggregate.

Sample	HA 1	HA 2	HA 3	HA 4	HA 5	HA 6	HA 7	HA 8	HA 9	HA 10	HA 21
HA 1	-	0.86	0.24	0.05	0.29	0.03	0.51	0.13	0.00	0.00	0.93
HA 2	0.86	-	0.45	0.15	0.52	0.10	0.71	0.30	0.01	0.01	0.90
HA 3	0.24	0.45	-	0.37	0.84	0.23	0.70	0.70	0.03	0.02	0.24
HA 4	0.05	0.15	0.37	-	0.26	0.72	0.24	0.62	0.16	0.12	0.04
HA 5	0.29	0.52	0.84	0.26	-	0.15	0.81	0.55	0.01	0.01	0.30
HA 6	0.03	0.10	0.23	0.72	0.15	-	0.15	0.41	0.33	0.26	0.02
HA 7	0.51	0.71	0.70	0.24	0.81	0.15	-	0.47	0.02	0.01	0.53
HA 8	0.13	0.30	0.70	0.62	0.55	0.41	0.47	-	0.06	0.04	0.12
HA 9	0.00	0.01	0.03	0.16	0.01	0.33	0.02	0.06	-	0.90	0.00
HA 10	0.00	0.01	0.02	0.12	0.01	0.26	0.01	0.04	0.90	-	0.00
HA 21	0.93	0.90	0.24	0.04	0.30	0.02	0.53	0.12	0.00	0.00	-

Table I.5: Student's T-test p-values for the Equotip type D measurements with a 1 cm grid spacing on limestone (Lim) aggregate.

Sample	LA 1	LA 2	LA 3	LA 4	LA 5	LA 6	LA 7	LA 8	LA 9	LA 10
LA 1	-	0.13	0.52	0.00	0.01	0.76	0.63	0.00	0.14	0.97
LA 2	0.13	-	0.03	0.00	0.00	0.06	0.32	0.00	0.83	0.12
LA 3	0.52	0.03	-	0.00	0.03	0.71	0.27	0.02	0.03	0.54
LA 4	0.00	0.00	0.00	-	0.25	0.00	0.00	0.14	0.00	0.00
LA 5	0.01	0.00	0.03	0.25	-	0.01	0.00	0.88	0.00	0.01
LA 6	0.76	0.06	0.71	0.00	0.01	-	0.43	0.01	0.07	0.79
LA 7	0.63	0.32	0.27	0.00	0.00	0.43	-	0.00	0.39	0.60
LA 8	0.00	0.00	0.02	0.14	0.88	0.01	0.00	-	0.00	0.00
LA 9	0.14	0.83	0.03	0.00	0.00	0.07	0.39	0.00	-	0.14
LA 10	0.97	0.12	0.54	0.00	0.01	0.79	0.60	0.00	0.14	-

Table I.6: Student's T-test p-values for the Equotip type D measurements with a 2 cm grid spacing on the limestone (Lim) aggregate.

Sample	LA 1	LA 2	LA 3	LA 4	LA 5	LA 6	LA 7	LA 8	LA 9	LA 10
LA 1	-	0.34	0.95	0.00	0.08	0.97	0.37	0.21	0.11	0.74
LA 2	0.34	-	0.36	0.00	0.02	0.32	0.91	0.05	0.73	0.45
LA 3	0.95	0.36	-	0.00	0.07	0.92	0.39	0.18	0.12	0.80
LA 4	0.00	0.00	0.00	-	0.46	0.00	0.00	0.17	0.00	0.00
LA 5	0.08	0.02	0.07	0.46	-	0.09	0.01	0.60	0.00	0.03
LA 6	0.97	0.32	0.92	0.00	0.09	-	0.35	0.23	0.11	0.72
LA 7	0.37	0.91	0.39	0.00	0.01	0.35	-	0.04	0.62	0.50
LA 8	0.21	0.05	0.18	0.17	0.60	0.23	0.04	-	0.01	0.11
LA 9	0.11	0.73	0.12	0.00	0.00	0.11	0.62	0.01	-	0.17
LA 10	0.74	0.45	0.80	0.00	0.03	0.72	0.50	0.11	0.17	-

Table I.7: Student's T-test p-values for the Equotip type C measurements with a 1 cm grid spacing on limestone (Lim) aggregate.

Sample	LA 2	LA 3	LA 5	LA 6	LA 7	LA 8	LA 9	LA 10
LA 2	-	0.68	0.00	0.08	0.17	0.00	0.72	0.29
LA 3	0.68	-	0.00	0.13	0.27	0.00	0.38	0.46
LA 5	0.00	0.00	-	0.03	0.04	0.53	0.00	0.02
LA 6	0.08	0.13	0.03	-	0.89	0.06	0.01	0.60
LA 7	0.17	0.27	0.04	0.89	-	0.09	0.06	0.73
LA 8	0.00	0.00	0.53	0.06	0.09	-	0.00	0.03
LA 9	0.72	0.38	0.00	0.01	0.06	0.00	-	0.14
LA 10	0.29	0.46	0.02	0.60	0.73	0.03	0.14	-

Table I.8: Student's T-test p-values for the Equotip type C measurements with a 2 cm grid spacing on limestone (Lim) aggregate.

Sample	LA 2	LA 3	LA 5	LA 6	LA 7	LA 8	LA 9	LA 10
LA 2	-	0.95	0.02	0.35	0.60	0.07	0.57	0.55
LA 3	0.95	-	0.01	0.27	0.53	0.05	0.58	0.50
LA 5	0.02	0.01	-	0.08	0.07	0.44	0.00	0.10
LA 6	0.35	0.27	0.08	-	0.75	0.29	0.10	0.85
LA 7	0.60	0.53	0.07	0.75	-	0.22	0.27	0.93
LA 8	0.07	0.05	0.44	0.29	0.22	-	0.01	0.29
LA 9	0.57	0.58	0.00	0.10	0.27	0.01	-	0.27
LA 10	0.55	0.50	0.10	0.85	0.93	0.29	0.27	-

Table I.9: Student's T-test p-values for the Equotip type D measurements with a 1 cm grid spacing on limestone (Jen) aggregate.

Sample	JA 1	JA 2	JA 3	JA 4	JA 5	JA 6	JA 7	JA 8	JA 9	JA 10
JA 1	-	0.00	0.00	0.01	0.00	0.00	0.00	0.89	0.00	0.01
JA 2	0.00	-	0.62	0.00	0.39	0.00	0.40	0.01	0.99	0.36
JA 3	0.00	0.62	-	0.00	0.71	0.00	0.65	0.00	0.59	0.11
JA 4	0.01	0.00	0.00	-	0.00	0.03	0.00	0.05	0.00	0.00
JA 5	0.00	0.39	0.71	0.00	-	0.00	0.88	0.00	0.36	0.04
JA 6	0.00	0.00	0.00	0.03	0.00	-	0.00	0.00	0.00	0.00
JA 7	0.00	0.40	0.65	0.00	0.88	0.00	-	0.00	0.37	0.07
JA 8	0.89	0.01	0.00	0.05	0.00	0.00	0.00	-	0.00	0.04
JA 9	0.00	0.99	0.59	0.00	0.36	0.00	0.37	0.00	-	0.31
JA 10	0.01	0.36	0.11	0.00	0.04	0.00	0.07	0.04	0.31	-

Table I.10: Student's T-test p-values for the Equotip type D measurements with a 2 cm grid spacing on the limestone (Jen) aggregate.

Sample	JA 1	JA 2	JA 3	JA 4	JA 5	JA 6	JA 7	JA 8	JA 9	JA 10
JA 1	-	0.03	0.00	0.40	0.00	0.40	0.00	0.05	0.00	0.00
JA 2	0.03	-	0.36	0.06	0.02	0.00	0.25	0.71	0.20	0.18
JA 3	0.00	0.36	-	0.00	0.23	0.00	0.81	0.18	0.75	0.72
JA 4	0.40	0.06	0.00	-	0.00	0.05	0.00	0.12	0.00	0.00
JA 5	0.00	0.02	0.23	0.00	-	0.00	0.36	0.00	0.39	0.41
JA 6	0.40	0.00	0.00	0.05	0.00	-	0.00	0.00	0.00	0.00
JA 7	0.00	0.25	0.81	0.00	0.36	0.00	-	0.11	0.94	0.91
JA 8	0.05	0.71	0.18	0.12	0.00	0.00	0.11	-	0.08	0.07
JA 9	0.00	0.20	0.75	0.00	0.39	0.00	0.94	0.08	-	0.97
JA 10	0.00	0.18	0.72	0.00	0.41	0.00	0.91	0.07	0.97	-

Table I.11: Student's T-test p-values for the Equotip type C measurements with a 1 cm grid spacing on limestone (Jen) aggregate.

Sample	JA 1	JA 2	JA 3	JA 4	JA 5	JA 6	JA 7	JA 8	JA 9	JA 10
JA 1	-	0.00	0.00	0.76	0.00	0.04	0.00	0.02	0.00	0.00
JA 2	0.00	-	0.05	0.00	0.00	0.00	0.41	0.48	0.02	0.01
JA 3	0.00	0.05	-	0.00	0.25	0.00	0.26	0.00	0.63	0.43
JA 4	0.76	0.00	0.00	-	0.00	0.06	0.00	0.00	0.00	0.00
JA 5	0.00	0.00	0.25	0.00	-	0.00	0.02	0.00	0.54	0.79
JA 6	0.04	0.00	0.00	0.06	0.00	-	0.00	0.00	0.00	0.00
JA 7	0.00	0.41	0.26	0.00	0.02	0.00	-	0.11	0.12	0.06
JA 8	0.02	0.48	0.00	0.00	0.00	0.00	0.11	-	0.00	0.00
JA 9	0.00	0.02	0.63	0.00	0.54	0.00	0.12	0.00	-	0.76
JA 10	0.00	0.01	0.43	0.00	0.79	0.00	0.06	0.00	0.76	-

Table I.12: Student's T-test p-values for the Equotip type C measurements with a 2 cm grid spacing on limestone (Jen) aggregate.

Sample	JA 1	JA 2	JA 3	JA 4	JA 5	JA 6	JA 7	JA 8	JA 9	JA 10
JA 1	-	0.03	0.00	0.40	0.00	0.40	0.00	0.05	0.00	0.00
JA 2	0.03	-	0.36	0.06	0.02	0.00	0.25	0.71	0.20	0.18
JA 3	0.00	0.36	-	0.00	0.23	0.00	0.81	0.18	0.75	0.72
JA 4	0.40	0.06	0.00	-	0.00	0.05	0.00	0.12	0.00	0.00
JA 5	0.00	0.02	0.23	0.00	-	0.00	0.36	0.00	0.39	0.41
JA 6	0.40	0.00	0.00	0.05	0.00	-	0.00	0.00	0.00	0.00
JA 7	0.00	0.25	0.81	0.00	0.36	0.00	-	0.11	0.94	0.91
JA 8	0.05	0.71	0.18	0.12	0.00	0.00	0.11	-	0.08	0.07
JA 9	0.00	0.20	0.75	0.00	0.39	0.00	0.94	0.08	-	0.97
JA 10	0.00	0.18	0.72	0.00	0.41	0.00	0.91	0.07	0.97	-

Table I.13: Student's T-test p-values for the Equotip type D measurements on the saturated sandstone cores.

Sample	HA C 1	HA C 2	HA C 3	HA C 4	HA C 5	HA C 6	HA C 7	HA C 8	HA C 9	HA C 10	HA C 11	HA C 12	HA C 13	HA C 14
HA C 1	-	0.08	0.16	0.58	0.47	0.01	0.62	0.17	0.00	0.00	0.24	0.76	0.54	0.00
HA C 2	0.08	-	0.60	0.03	0.01	0.00	0.03	0.00	0.00	0.00	0.01	0.03	0.01	0.00
HA C 3	0.16	0.60	-	0.05	0.03	0.00	0.06	0.01	0.00	0.00	0.01	0.07	0.03	0.00
HA C 4	0.58	0.03	0.05	-	0.88	0.03	0.97	0.43	0.00	0.00	0.51	0.78	0.99	0.01
HA C 5	0.47	0.01	0.03	0.88	-	0.03	0.85	0.51	0.00	0.00	0.60	0.65	0.88	0.01
HA C 6	0.01	0.00	0.00	0.03	0.03	-	0.03	0.13	0.31	0.10	0.14	0.01	0.02	0.57
HA C 7	0.62	0.03	0.06	0.97	0.85	0.03	-	0.42	0.00	0.00	0.50	0.82	0.95	0.01
HA C 8	0.17	0.00	0.01	0.43	0.51	0.13	0.42	-	0.01	0.00	0.93	0.26	0.40	0.04
HA C 9	0.00	0.00	0.00	0.00	0.00	0.31	0.00	0.01	-	0.52	0.02	0.00	0.00	0.63
HA C 10	0.00	0.00	0.00	0.00	0.00	0.10	0.00	0.00	0.52	-	0.00	0.00	0.00	0.25
HA C 11	0.24	0.01	0.01	0.51	0.60	0.14	0.50	0.93	0.02	0.00	-	0.34	0.49	0.04
HA C 12	0.76	0.03	0.07	0.78	0.65	0.01	0.82	0.26	0.00	0.00	0.34	-	0.75	0.00
HA C 13	0.54	0.01	0.03	0.99	0.88	0.02	0.95	0.40	0.00	0.00	0.49	0.75	-	0.00
HA C 14	0.00	0.00	0.00	0.01	0.01	0.57	0.01	0.04	0.63	0.25	0.04	0.00	0.00	-

Table I.14: Student's T-test p-values for the Equotip type D measurements on the saturated limestone (Lim) cores.

Sample	LIM C 1	LIM C 2	LIM C 3	LIM C 4	LIM C 5	LIM C 6	LIM C 7	LIM C 8	LIM C 9	LIM C 10
LIM C 1	-	0.00	0.00	0.57	0.00	0.17	0.03	0.01	0.00	0.05
LIM C 2	0.00	-	0.63	0.01	0.61	0.03	0.09	0.59	0.00	0.14
LIM C 3	0.00	0.63	-	0.01	0.97	0.01	0.04	0.35	0.00	0.07
LIM C 4	0.57	0.01	0.01	-	0.01	0.50	0.19	0.06	0.00	0.21
LIM C 5	0.00	0.61	0.97	0.01	-	0.01	0.04	0.33	0.00	0.06
LIM C 6	0.17	0.03	0.01	0.50	0.01	-	0.45	0.14	0.00	0.48
LIM C 7	0.03	0.09	0.04	0.19	0.04	0.45	-	0.34	0.00	0.95
LIM C 8	0.01	0.59	0.35	0.06	0.33	0.14	0.34	-	0.00	0.41
LIM C 9	0.00	0.00	0.00	0.00	0.00	0.00	0.00	0.00	-	0.00
LIM C 10	0.05	0.14	0.07	0.21	0.06	0.48	0.95	0.41	0.00	-

Table I.15: Student's T-test p-values for the Equotip type D measurements on the saturated limestone (Fri) cores.

Sample	FRI C 1	FRI C 2	FRI C 3	FRI C 4	FRI C 5	FRI C 6	FRI C 7	FRI C 8	FRI C 9	FRI C 10	FRI C 11	FRI C 12	FRI C 13
FRI C 1	-	0.00	0.11	0.10	0.22	0.27	0.00	0.31	0.12	0.00	0.00	0.01	0.00
FRI C 2	0.00	-	0.00	0.00	0.00	0.00	0.00	0.00	0.00	0.00	0.00	0.00	0.00
FRI C 3	0.11	0.00	-	0.78	0.86	0.53	0.14	0.74	0.92	0.03	0.02	0.19	0.06
FRI C 4	0.10	0.00	0.78	-	0.74	0.61	0.01	0.86	0.87	0.00	0.00	0.03	0.00
FRI C 5	0.22	0.00	0.86	0.74	-	0.58	0.56	0.70	0.81	0.37	0.32	0.61	0.39
FRI C 6	0.27	0.00	0.53	0.61	0.58	-	0.02	0.88	0.58	0.00	0.00	0.04	0.01
FRI C 7	0.00	0.00	0.14	0.01	0.56	0.02	-	0.16	0.09	0.33	0.23	0.84	0.49
FRI C 8	0.31	0.00	0.74	0.86	0.70	0.88	0.16	-	0.80	0.07	0.05	0.20	0.09
FRI C 9	0.12	0.00	0.92	0.87	0.81	0.58	0.09	0.80	-	0.01	0.01	0.13	0.03
FRI C 10	0.00	0.00	0.03	0.00	0.37	0.00	0.33	0.07	0.01	-	0.71	0.26	0.94
FRI C 11	0.00	0.00	0.02	0.00	0.32	0.00	0.23	0.05	0.01	0.71	-	0.18	0.73
FRI C 12	0.01	0.00	0.19	0.03	0.61	0.04	0.84	0.20	0.13	0.26	0.18	-	0.39
FRI C 13	0.00	0.00	0.06	0.00	0.39	0.01	0.49	0.09	0.03	0.94	0.73	0.39	-

Table I.16: Change in the Equotip type C rebound statistics upon doubling the spacing between measurement points on the sandstone. The doubling results in half of the amount in rebound values compared to the reference case with a spacing of ± 1 cm between the impact points. The standard deviation (ref) is the one for this narrow spacing. A positive difference shows an increase in the specific value for the wider spacing of ± 2 cm, while a negative value shows a decrease.

Sample	HA 1	HA 2	HA 3	HA 4	HA 5	HA 6	HA 7	HA 8	HA 9	HA 10
Standard Deviation (ref)	173	152	97	175	147	137	168	129	150	147
Change in Mean	-26	-3	12	-33	19	12	-35	-11	-3	24
Change in Median	-8	-8	12	-4	0	20	-12	7	30	33
Change in Standard Deviation	18	-26	14	-4	-19	0	-5	10	-12	-16

Table I.17: Change in the Equotip type C rebound statistics upon doubling the spacing between measurement points on the limestone (Lim). The doubling results in half of the amount in rebound values compared to the reference case with a spacing of ± 1 cm between the impact points. The standard deviation (ref) is the one for this narrow spacing. A positive difference shows an increase in the specific value for the wider spacing of ± 2 cm, while a negative value shows a decrease.

Sample	LA 2	LA 3	LA 5	LA 6	LA 7	LA 8	LA 9	LA 10
Standard Deviation (ref)	143	115	154	107	153	128	103	155
Change in Mean	6	-8	4	-6	-16	-14	-6	1
Change in Median	13	13	31	5	-9	30	2	-3
Change in Standard Deviation	-5	-2	6	-1	-11	14	10	17

Table I.18: Change in the Equotip type C rebound statistics upon doubling the spacing between measurement points on the limestone (Jen). The doubling results in half of the amount in rebound values compared to the reference case with a spacing of ± 1 cm between the impact points. The standard deviation (ref) is the one for this narrow spacing. A positive difference shows an increase in the specific value for the wider spacing of ± 2 cm, while a negative value shows a decrease.

Sample	JA 1	JA 2	JA 3	JA 4	JA 5	JA 6	JA 7	JA 8	JA 9	JA 10
Standard Deviation (ref)	161	156	123	121	90	125	152	132	120	120
Change in Mean	-3	4	-14	36	2	20	28	10	-12	-18
Change in Median	-33	-10	-9	17	9	12	29	-4	-1	1
Change in Standard Deviation	-11	-12	24	-36	-10	0	-9	-4	16	17

J

Relation L-value and WA

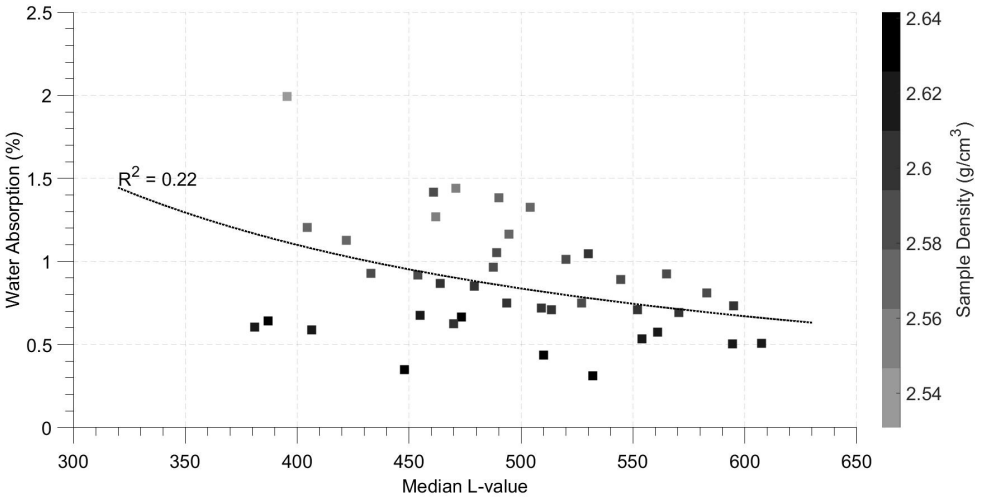

Figure J.1: Median Equotip type D L-value versus the WA of the untreatened sandstone aggregate pieces.

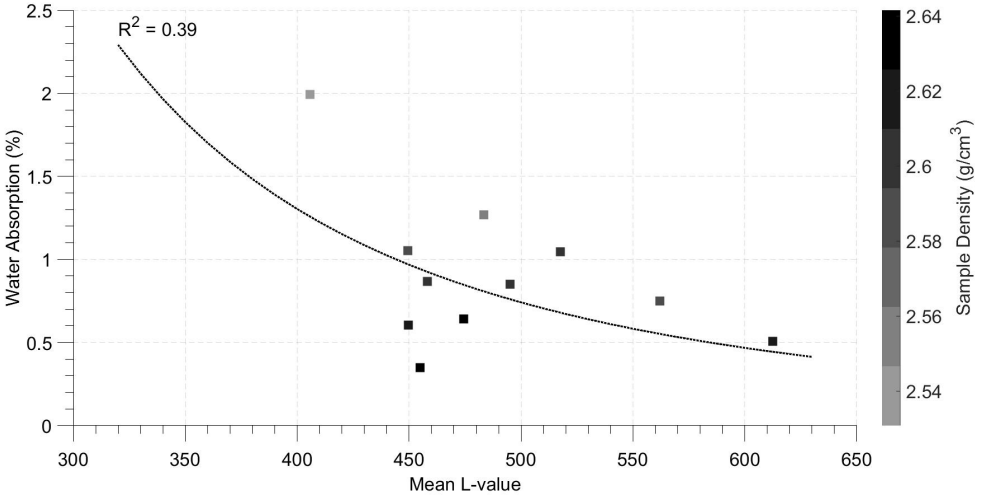

Figure J.2: Mean Equotip type C L-value versus the WA of the untreatened sandstone aggregate pieces.

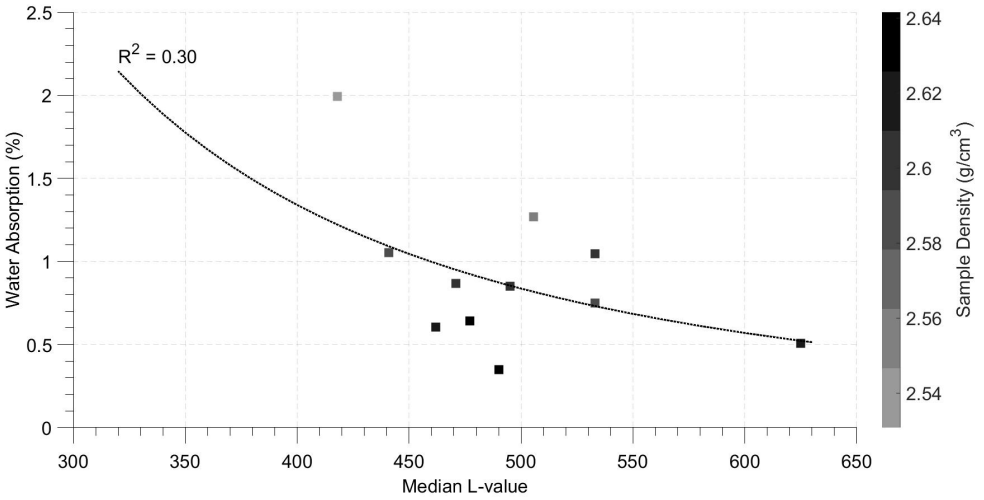

Figure J.3: Median Equotip type C L-value versus the WA of the untreatened sandstone aggregate pieces.

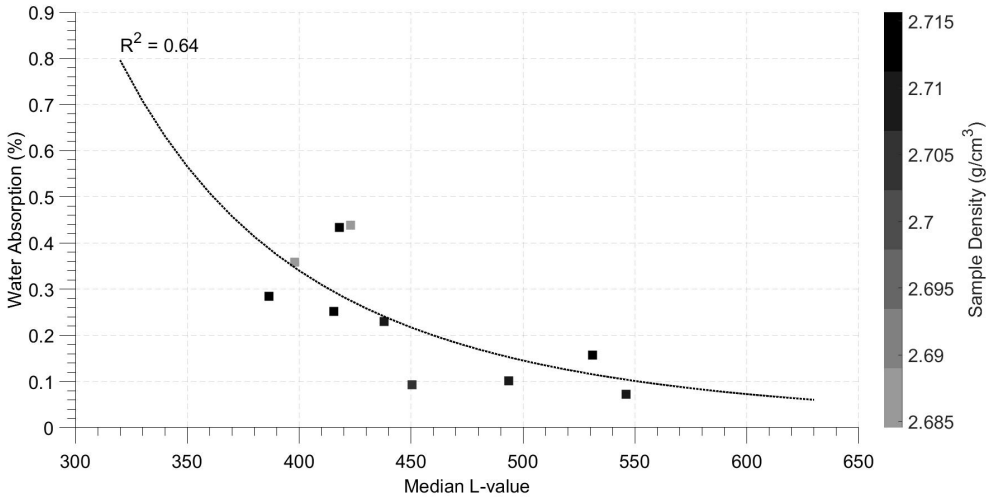

Figure J.4: Median Equotip type D L-value versus the WA of the untreatened limestone (Lim) aggregate pieces.

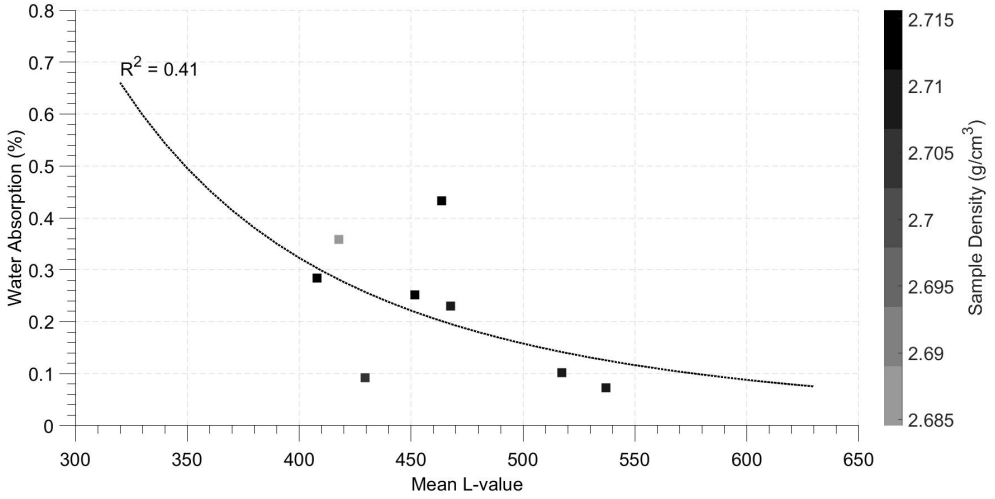

Figure J.5: Mean Equotip type C L-value versus the WA of the untreatened limestone (Lim) aggregate pieces.

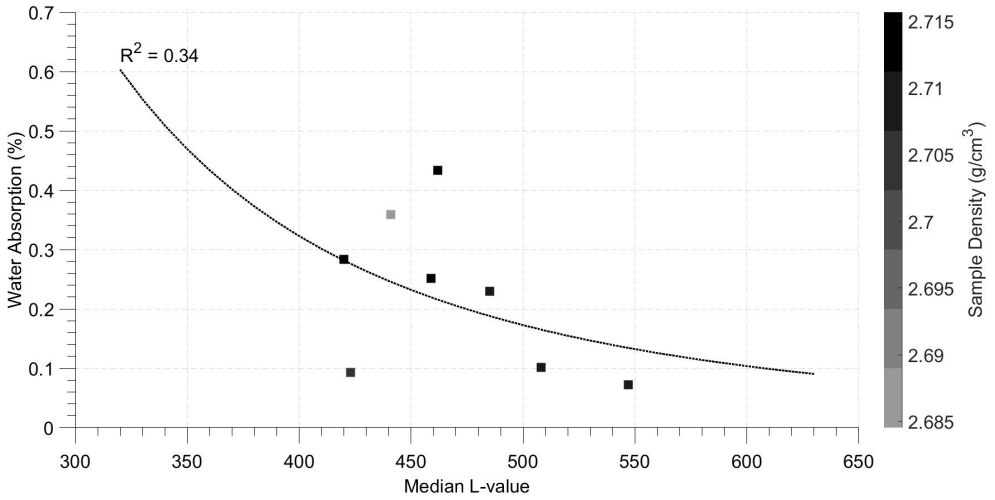

Figure J.6: Median Equotip type C L-value versus the WA of the untreatened limestone (Lim) aggregate pieces.

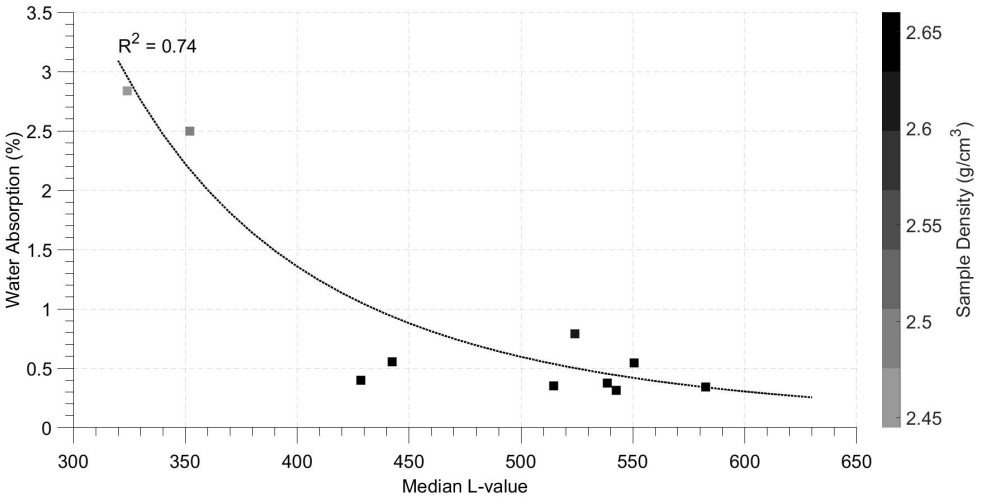

Figure J.7: Median Equotip type D L-value versus the WA of the untreatened limestone (Jen) aggregate pieces.

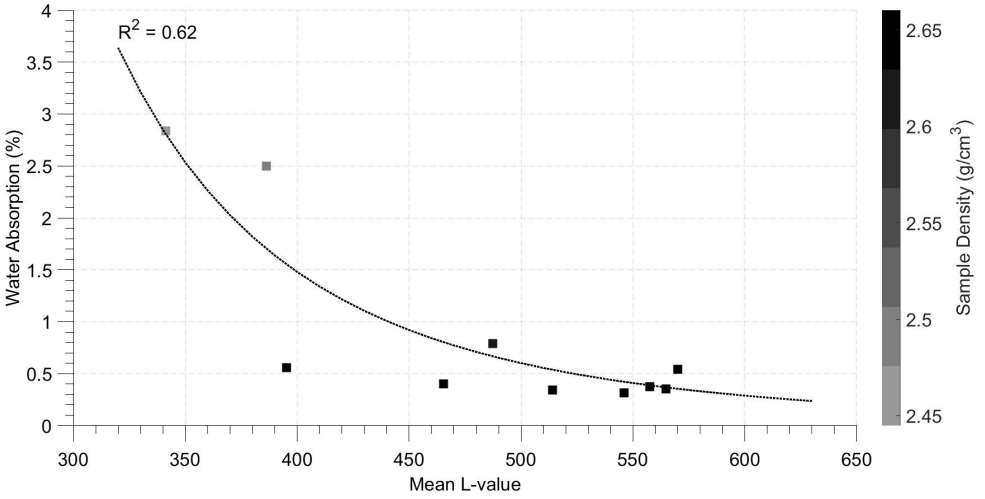

Figure J.8: Mean Equotip type C L-value versus the WA of the untreatened limestone (Jen) aggregate pieces.

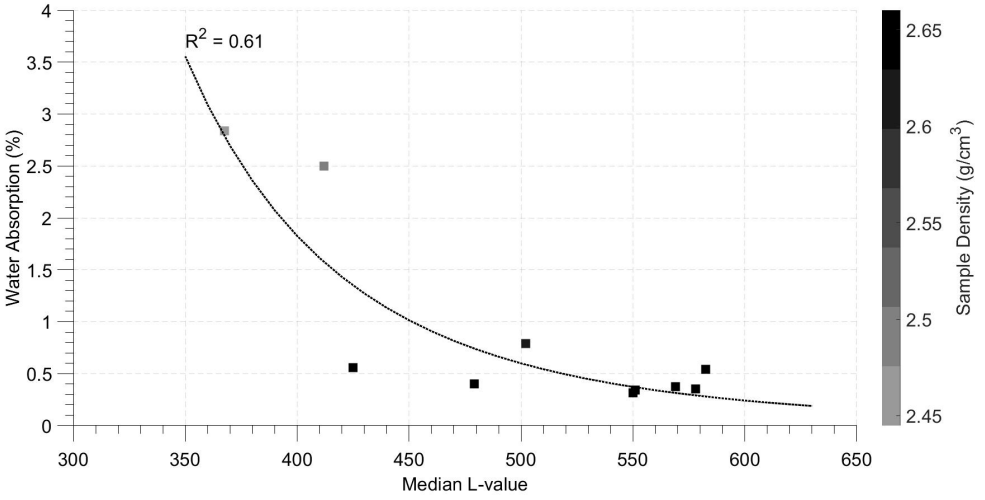

Figure J.9: Median Equotip type C L-value versus the WA of the untreatened limestone (Jen) aggregate pieces.

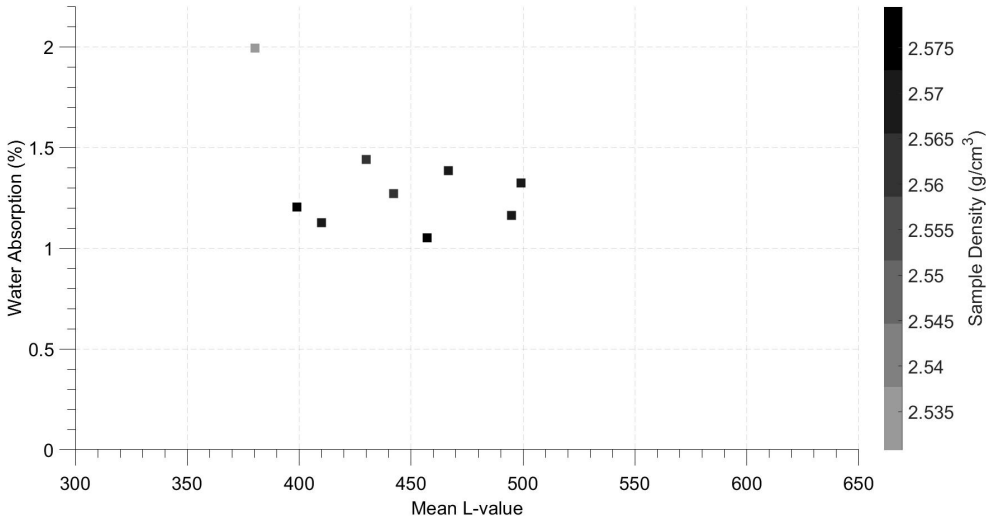

Figure J.10: Mean Equotip type D L-value versus the WA of the untreatened sandstone aggregate pieces with a density in the range 2.53 to 2.58 g/cm^3.

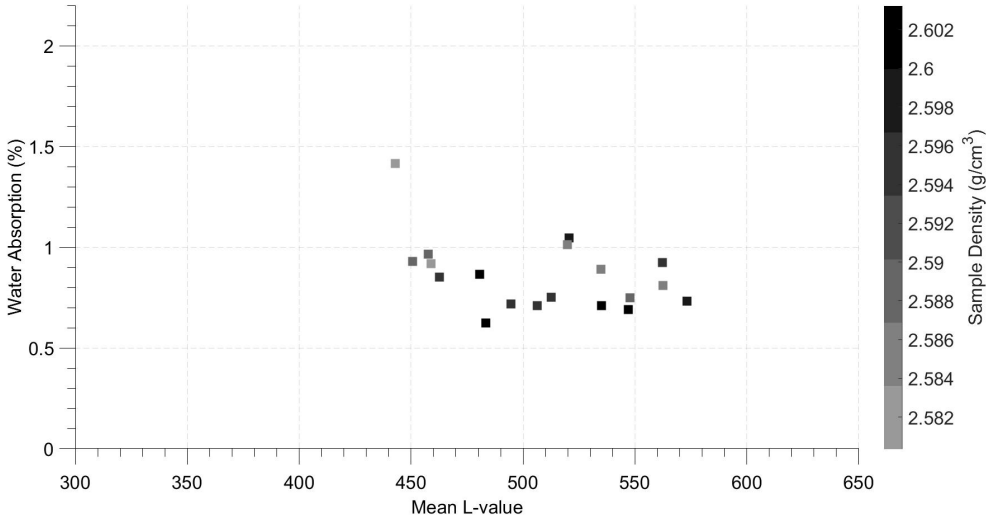

Figure J.11: Mean Equotip type D L-value versus the WA of the untreatened sandstone aggregate pieces with a density in the range 2.58 to 2.61 g/cm^3.

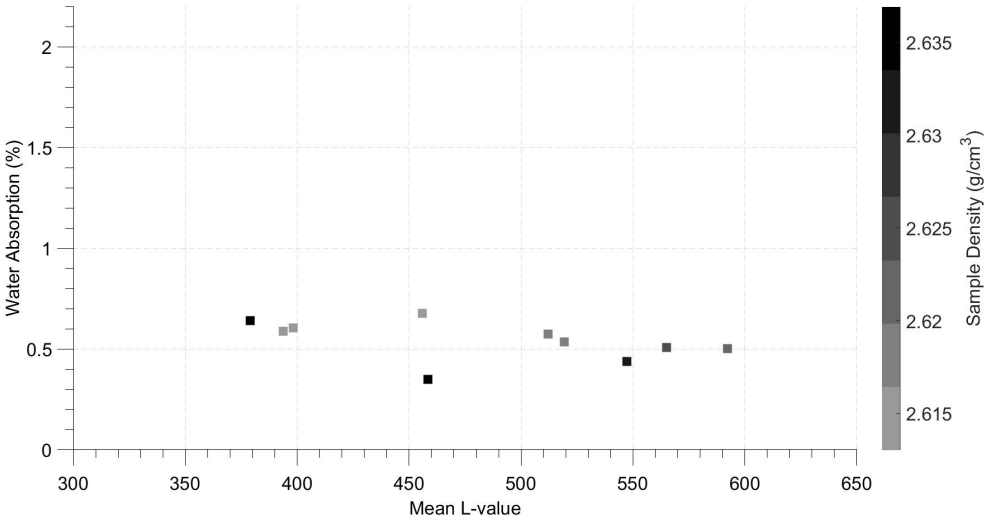

Figure J.12: Mean Equotip type D L-value versus the WA of the untreatened sandstone aggregate pieces with a density in the range 2.61 to 2.64 g/cm^3.

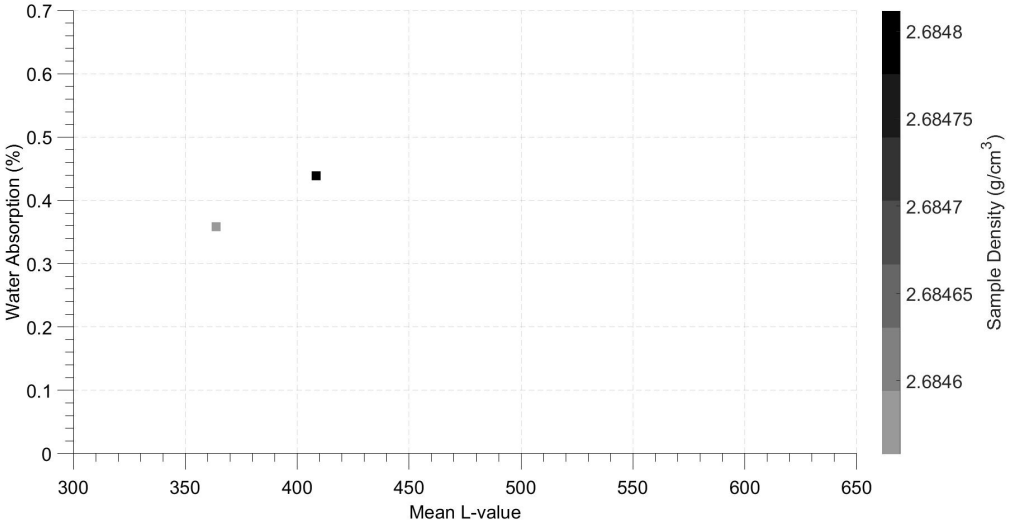

Figure J.13: Mean Equotip type D L-value versus the WA of the untreatened limestone (Lim) aggregate pieces with a density in the range 2.68 to 2.70 g/cm^3.

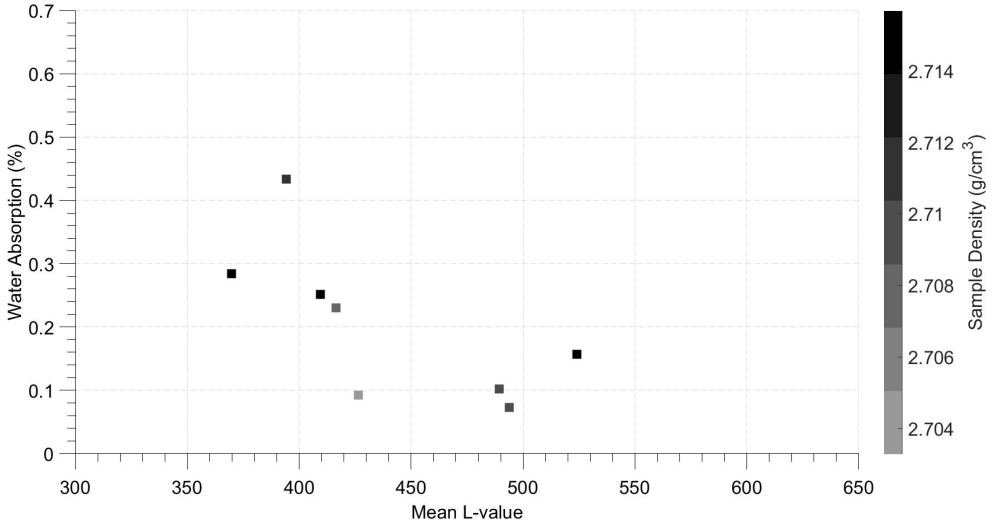

Figure J.14: Mean Equotip type D L-value versus the WA of the untreatened limestone (Lim) aggregate pieces with a density in the range 2.70 to 2.72 g/cm^3.

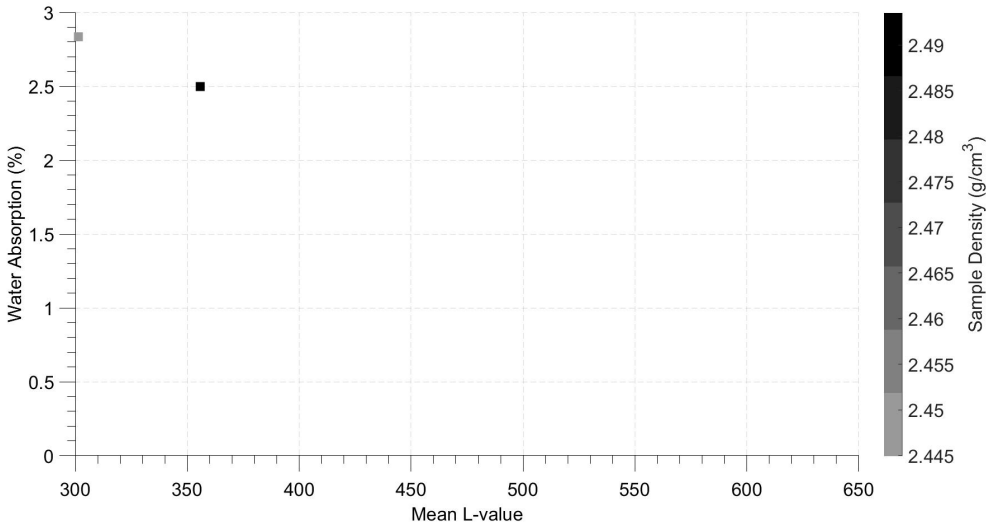

Figure J.15: Mean Equotip type D L-value versus the WA of the untreatened limestone (Jen) aggregate pieces with a density in the range 2.40 to 2.50 g/cm^3.

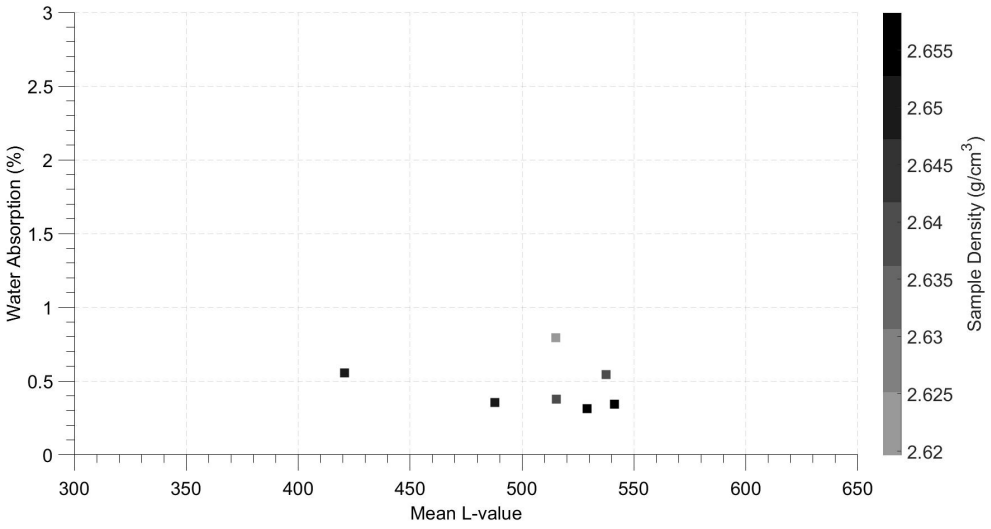

Figure J.16: Mean Equotip type D L-value versus the WA of the untreatened limestone (Jen) aggregate pieces with a density in the range 2.60 to 2.66 g/cm^3.

K

Equotip Core Data

Table K.1: UCS, Young's modulus and median rebound values of sandstone cores.

Sample	UCS (MPa)	E (GPa)	MEDIAN D-TYPE DRY	MEDIAN D-TYPE SATURATED	MEDIAN C-TYPE DRY	MEDIAN C-TYPE SATURATED
HA1	31.2	7.2	526	476.5	596	495.5
HA2	35.7	6.5	515.5	462.5	626.5	529
HA4	101.3	23.9	663	636	726.5	701.5
HA5	28.8	7.6	508	445.5	616	538.5
HA7	63.4	13.3	596	580	713	692.5
HA8	195.8	37.8	820	799	863.5	865
HA9	260.7	42.6	814	799	851.5	844.5
HA10	301.9	44.6	819	818.5	873	873
HA11	140.7	32.1	750.5	759.5	824	818
HA13	197.2	38.2	750	780	826.5	832
HA14	262.5	45.1	811	797.5	860.5	858

Table K.2: UCS, Young's modulus and median rebound values of limestone (Lim) cores.

Sample	UCS (MPa)	E (GPa)	MEDIAN D-TYPE DRY	MEDIAN D-TYPE SATURATED	MEDIAN C-TYPE DRY	MEDIAN C-TYPE SATURATED
LIM1	119.1	40.0	631	640	713	703.5
LIM2	166.7	44.3	609.5	607.5	710	691
LIM3	173.2	44.8	612.5	601.5	702.5	683.5
LIM4	198.1	46.2	626	623.5	711.5	712
LIM5	171.8	45.4	608.5	607	707.5	690
LIM6	192.6	45.2	617.5	625.5	715.5	699.5
LIM7	203.4	47.3	614.5	615.5	711.5	699
LIM8	158.8	44.0	614.5	614.5	719	705
LIM9	184.3	43.6	537	558	627.5	665
LIM10	173.7	42.5	616.5	616.5	708.5	689

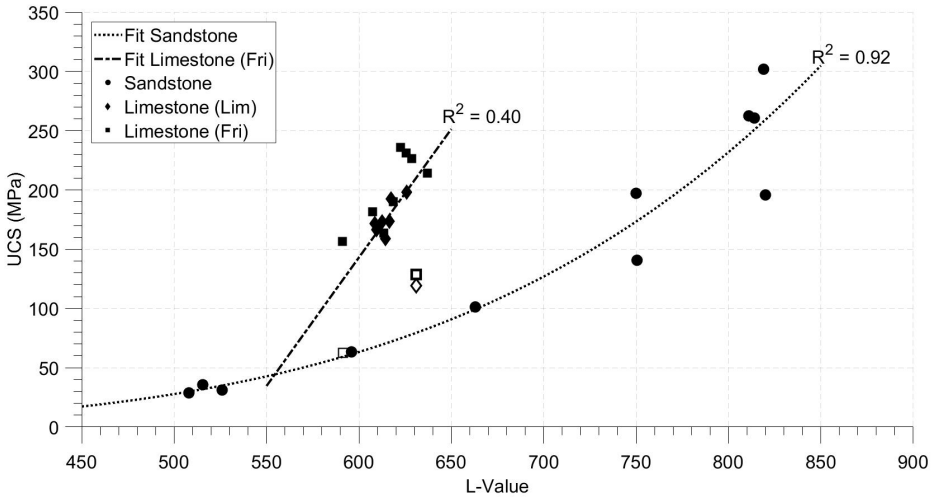

Figure K.1: The relation between the mean Equotip type D rebound value on saturated cores with a L/D of 1 and their UCS value. The horizontal bars represent the standard deviation of the Equotip measurements on the rock cores. The red shade is the theoretical range of expected UCS values based on the literature study shown in figure 2.6. The upper limit is the trend established by Kee (2010), while the lower limit is conform the trend observed by Aoki and Matsukura (2007); Verwaal and Mulder (1993).

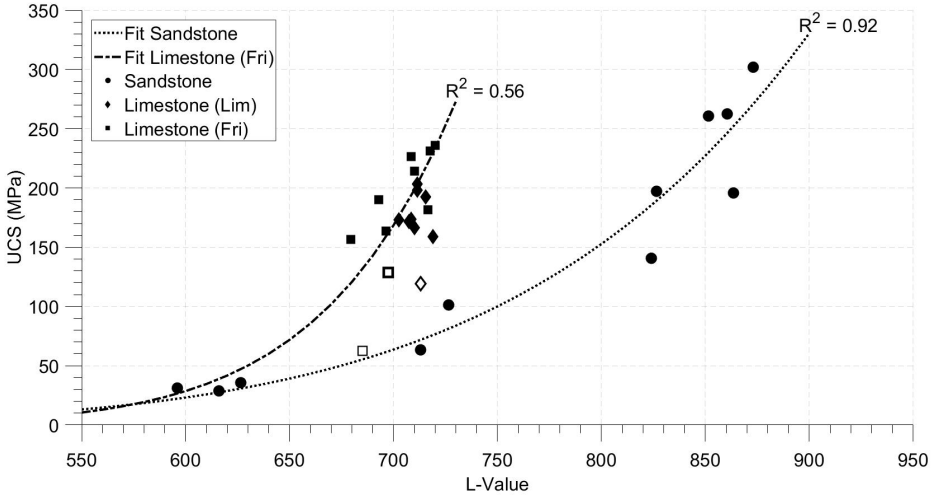

Figure K.2: The relation between the mean Equotip type D rebound value on saturated cores with a L/D of 1 and their UCS value. The horizontal bars represent the standard deviation of the Equotip measurements on the rock cores. The red shade is the theoretical range of expected UCS values based on the literature study shown in figure 2.6. The upper limit is the trend established by Kee (2010), while the lower limit is conform the trend observed by Aoki and Matsukura (2007); Verwaal and Mulder (1993).

Table K.3: UCS, Young's modulus and median rebound values of limestone (Fri) cores.

Sample	UCS (MPa)	E (GPa)	MEDIAN D-TYPE DRY	MEDIAN D-TYPE SATURATED	MEDIAN C-TYPE DRY	MEDIAN C-TYPE SATURATED
FRI1	62.5	20.0	591.5	568.5	685	680
FRI3	181.4	42.3	607.5	611	716.5	704
FRI5	235.9	47.7	622.5	623	720	722.5
FRI6	163.7	44.4	613.5	601	696.5	716.5
FRI7	231.3	47.9	625.5	624.5	717.5	721
FRI8	128.9	34.3	631	616	697.5	679.5
FRI9	156.8	44.2	591	592	679.5	669.5
FRI10	226.6	42.4	628.5	625	708.5	715
FRI11	190.0	44.9	618.5	631.5	693	717
FRI13	214.1	43.6	637	629	710	715.5

L

Photos of Aggregate Pieces

Figure L.1: Pictures of the sandstone aggregate pieces HA 1 to HA 10 from the Hartsteinwerke.

Figure L.2: Pictures of the limestone aggregate pieces LA 1 to LA 10 from Carrière des Limites.

Figure L.3: Pictures of the limestone aggregate pieces JA 1 to JA 10 from Carrière de Jenneret.